PRESSURE TRANSIENT TESTING OF U-SHAPED HORIZONTAL WELLS

BY

Abdallah Mubarak Al-Gahtani

ID # 198214320

A Dissertation Presented to the

DEANSHIP OF GRADUATE STUDIES

KING FAHD UNIVERSITY OF PETROLEUM & MINERALS

DHAHRAN, SAUDI ARABIA

In Partial Fulfillment of the

Requirements for the Degree of

DOCTOR OF PHILOSOPHY

In

PETROLEUM ENGINEERING

April 2014

KING FAHD UNIVERSITY OF PETROLEUM & MINERALS

DHAHRAN 31261, SAUDI ARABIA

DEANSHIP OF GRADUATE STUDIES

This thesis, written by **ABDALLAH MUBARAK AL-GAHTANI** under the direction of his thesis advisor and approved by his thesis committee, has been presented to and accepted by Dean of Graduate Studies, in partial fulfillment of the requirements for the degree of **DOCTOR OF PHILOSPHY IN PETROLEUM ENGINEERING.**

Thesis Committee

Dr. Hasan S. Al-Hashim
(Advisor, KFUPM)

Dr. Abdallah S. Al-Sultan
Department Chairman

Dr. Hasan Y. Al-Yousef
(Member, KFUPM)

21/5/14

Dr. Salam A. Zummo
Dean of Graduate Studies

Dr. Sidqi A. Abu-Khamsin
(Member, KFUPM)

Dr. Erdal Ozkan
(External member, CSM)

Dr. Hossein Kazemi
(External member, CSM)

ACKNOWLEDGEMENTS

I would like to express my sincere appreciation to my advisor, Dr. Hasan Al-Hashim, for his continuous support, guidance and patience, which has contributed significantly in the completion of this work. His dedication and enthusiasm to explore new research frontiers have always given me the courage to move forward in the research. In addition, his sincere advices to conduct genuine research with potential addition and impact to field's reality had inspired and motivated me to select him as my advisor.

I greatly acknowledge the help from Dr. Hasan Al Yousif and other committee members (Dr. Erdal Ozkan and Dr. Hossein Kazemi) for their valuable contribution, guidance and constructive suggestions. I am also grateful to Dr. Malikzadah for his support before leaving the department. Special thanks go to Dr. Sidgi Abu Khamsin for accepting to be a committee member.

I would like to thank the chairmen of the department Dr. Abduallh Sultan and the former chairman Dr. AbdulAziz Al Majed for their encouragement and support.

I would also like to express my deepest and most sincere gratitude to my family members. Special thanks go to my son engineer Mubarak for his instrumental help in the numerical side and coding of this research.

Finally, my greatest gratitude goes to my parents, wife, daughters and sons for their unconditional love and prayers through the course of completion of this research.

Table of Contents

LIST OF TABLES

LIST OF FIGURES

ABSTRACT ENGLISH

Student Name : Abdallah Mubarak Al Gahtani

Title of Study : Pressure Transient Testing of U-Shaped Horizontal Wells
Major Field : Petroleum Engineering

Date of Degree: April 2104

Over the past decade, drilling of long multilaterals and horizontal wells has been increasing steadily in the petroleum industry. This was supported by technological advancement in the areas of drilling and well completion in addition to the substantial rewards to maximize reservoir contact area and oil production rate at lower gas oil ratios. For these reasons, horizontal bore-hole lengths have grown rapidly and horizontal displacement have been extended to over 10,800 meters (35,770 feet). Even though long horizontal drain-holes may preclude or significantly delay the onset of production problems such as low production rates and low recovery efficiency, they are also facing many technical challenges that are hindering the full utilization of the bore-hole. Initially, it was believed that a horizontal well should be as long as possible. However, as the length increases, marginal gain in productivity becomes smaller and may not be enough to pay the cost of drilling the additional footage. This is due to the frictional losses in the wellbore. Not only this, but long horizontal wells were found to create non-uniform flux profiles due to the variation in formation damage caused by long time exposure to damaging drilling fluids in addition to frictional effects in the wellbore. Consequently,

the productivity of a long horizontal well is no longer proportional to the drilled well length.

In this research we propose to produce these long horizontal wells and laterals from the two ends (heel and toe) by using U-shape wells. The introduction of the U-shaped wells is driven by the need to maximize flow contribution from all drain-hole lengths and to have more uniform flux distribution along the horizontal drain-hole. The U-shape wells have additional advantages over the conventional horizontal wells enabling wellbore accessibility and better reservoir characterization. Not only this, but if they are planned ahead and half of the drain-hole length is drilled from one end and the other half is drilled from the other end, this will minimize the damage of the drain-hole.

The U-shape completion design for lateral drain-holes exists in the petroleum industry for well accessibility purposes, but not for production purposes and no pressure transient solution was developed for such setup. Solutions were developed for conventional horizontal wells and dual lateral and multilateral using a composite and holistic approach but not for two-way flow with discrete calculations to get the flow and pressure profiles along the horizontal drain-hole.

To achieve the objective of this study and support this idea, a semi-analytical model has been developed in this research for this U-shaped horizontal well. The well is assumed to be a finite-conductivity well which accounts for the impact of wellbore

frictional losses. The model includes the impact of wellbore hydraulics in the solution. The U-shaped wells can be produced from both ends at any desired constant rates or at any ratios to predict the pressures at the two ends (heel and toe). The developed model assumes a single phase flow and for a homogenous but an anisotropic reservoir. The reservoir is assumed to be an infinite acting reservoir. The developed model extends Ozkan's pressure transient analysis model for a single horizontal well. The developed solution based on collective science of transient reservoir response and wellbore steady flow models.

The developed semi-analytical model has been used to investigate the pressure transient behavior of this U-shaped horizontal well and evaluate the reservoir parameters by calculating the classical horizontal well performance and reservoir characteristics by measuring wellbore pressure at one or both wings. The model was also used to calculate the flow profile along the horizontal section under different constant rates and different ratios from both ends. The model can also be used as an optimization tool to maximize the benefits from long horizontal drain-hole as it allows producing the two wings at different flow rates at any ratios. Additionally, the developed model addresses the applicability of such well architecture and shows the merit of the U-shaped horizontal well from the production capacity and flow assurance point of view.

Finally, a comparison between the pressure transient behavior of the U-shaped horizontal well and the conventional single horizontal well is presented and discussed in

this dissertation. The results of this study confirm that the proposed production of long horizontal well through the U-shaped horizontal well is a viable solution not only for the non-contributing section of the drain-hole, but also result in a more uniform flux distribution along the entire length of the drain-hole. The U-shape wells can also be optimized to have more uniform flux distribution along the horizontal drain-hole in reservoirs subjected to water drive and/or gas cap drive.

ABSTRACT ARABIC

خلاصة الرساله

اسم الطالب : عبدالله مبارك القحطاني
عنوان الدراسه : تحليل تغير الضغط الوقتي للآبار الافقيه على شكل حرف U
التخصص : هندسة بترول
تاريخ الشهاده : ابريل 2104

على مدى العقد الماضي , أخذ حفر الأبار المتعددة الأطراف الطويلة والآبار الأفقية زيادة مطردة في الصناعة النفطية وساعد ذلك التقدم التكنولوجي في مجالات الحفر و استكمال الآبار بالاضافة إلى الفائدة الكبيرة للوصول لأقصى قدر من المنطقة المراد الاتصال بها بالمكامن و زيادة إنتاج النفط وانخفاض نسب الغاز المصاحب لأنتاج الزيت . و لهذه الأسباب , قد نمى الحفر الأفقي للآبار الطويلة بسرعة , وقد تم تمديد التمدد الأفقي إلى أكثر من 10.800 متر (35.770 قدم) . و على الرغم من أن حفر الأبار الأفقية الطويلة قد يمنع بشكل ملحوظ أو يؤخر ظهور بعض المشاكل المتعلقة بالأنتاج مثل معدلات الإنتاج المنخفضة وأنخفاض كفاءة أستخلاص الزيت , فإنها تواجه ايضا العديد من التحديات التقنية التي تعوق الأستفادة الكاملة من هذه الآبار الطول الكامل للبئر الأفقي المحفور .

في البداية , كان يعتقد أن الآبار الأفقية يجب أن تكون طويلة قدر الإمكان , و لكن أتضح أنه كلما زاد طول البئر الأفقي المحفور تكون الزيادة هامشية في الأنتاجية بعد طول معين و ربما لا تكون هذه الزيادة كافية لدفع تكاليف حفر الأقدام الأضافية . يرجع ذلك إلى زيادة الإحتكاك في هذه الآبار الطويلة , ليس هذا فحسب , ولكن تم التحقق من أن حفر الآبار الأفقية الطويلة يؤدي إلى تقليل قدرة التدفق غير المنتظم على طول البئر. و يعزى هذا التدفق الغير منتظم إلى التعرض لفترة طويلة لسوائل الحفر أثناء حفر الآبار الأفقية الطويلة بالإضافة إلى زيادة الأحتكاك في مجرى البئر . و بالتالي فإن إنتاجية هذه الآبار الطويلة لم يعد يتناسب مع أطوال هذه الآبار المحفورة .
في هذا البحث نقترح لإنتاج هذه الآبار الأفقية و الخطوط الفرعية الطويلة من طرفي البئر (كعب و اصبع القدم) بأستخدام الآبار على الشكل U . أن الدافع وراء إدخال الأبار على شكل حرف U هو الحاجة إلى رفع مساهمة

التدفق من جميع الأطوال المحفورة و أن يكون توزيع التدفق أكثر أتساقا على جميع الأبار المحفورة . هذا بألاضافة إلى أن الآبار على شكل U لها مزايا إضافية على الآبار الأفقية التقليدية وهو تمكين الوصول إلى أي موقع داخل البئر بسهولة مقارنه بالآبار الأفقية التقليدية . ليس هذا فحسب , بل يمكن تقليل مدة حفر هذه الآبار بالحفر من الجهتين و الأتصال في نفس الموقع المحفور لتقليل مخاطر الأضرار بمجرى هذه الآبار بسبب كثرة التعرض لسوائل الحفر .

لقد وجدت الآبار الأفقية على شكل حرف U في حقول النفط لاغراض الوصول إلى اماكن محددة داخل الآبار الأفقية ولم يكن لإنتاج أو لزيادة او تنظيم الأنتاج من الآبار الأفقية . وقد وضعت حلول للآبار الأفقية التقليدية و المزدوجة و المتعدده الأطراف الجانبية بأستخدام نهج شمولي مركب و لكن ليس لتدقيق الموائع في اتجاهين متعاكسين مع حسابات منفصلة للحصول على تدفق و ملامح الضغط الأفقي على طول الجانب الأفقي من البئر .

لتحقيق الهدف من هذه الدراسة ودعم هذه الفكرة , تم تطوير نموذج شبه تحليلي في هذا البحث لدراسة هذه الآبار الأفقية على شكل حرف U . و تفترض هذه الدراسة أن يكون البئر محدود الموصلية والتي تمثل تأثير الخسارة في الضغط نتيجة الاحتكاك بجوف البئر . يتضمن النموذج المطور آثار جوف البئر الهيدروليكية في الحل كما أن الآبار على شكل حرف U يمكن أن تنتج من كلا الطرفين حسب معدل التدفق المطلوب أو النسبة المطلوبة بين طرفي الأنتاج . النموذج المطور يفترض تدفق مرحلة واحدة و متجانسة لمكمن متباين الخواص . ومن المفترض أن يكون المكمن من المكامن التمثيل الأ نهائية . الحل المطور يكمن من حساب ضغط الآبار الوقتي لكل من طرفي الآبار على شكل الحرف -- . يعتمد النموذج المطورعلى أساسات حسابات الضغط الوقتية للمكامن و العمليات الحسابية المتطورة .

أو بأستحداث بئر عمودي يتقاطع مع هذه الآبار الافقية الطويلة في نقطة على شكل حرف -- صغيرة يتم تحديدها عبر طريقة مثلى .

وقد استخدم هذا النموذج للتحقق من سلوك الضغط الوقتي للبئر الأفقية على شكل حرف -- وتقييم خصائص و متغيرات المكامن عن طريق قياس ضغط البئر في طرف واحد أو كلا الطرفين و تم استخدام النموذج أيضا لحساب معدل التدفق على طول الجزء الأفقي تحت معدلات ثابتة ومختلفة بنسب مختلفة الأنتاج من الطرفين . ويمكن أيضا أن استخدام النموذج كأداة لتعزيز الفوائد من التدفق الأمثل الآبار الأفقية لأنها تتيح الأنتاج من الطرفين بمعدلات تدفق مختلفة و بأي نسبة . بالإضافة إلى ذلك ,يتناول النموذج المطور أثبات فاعلية تطبيق هذا التصميم من الآبار الأفقية على شكل حرف U لزيادة الطاقة الإنتاجية و ضمان التدفق بصورة امثل .

أخيرا , تم تقديم مقارنة بين سلوك ضغط البئر الأفقية الوقتي على شكل حرف U و كذلك البئر الأفقية التقليدية و مناقشتها في هذه الأطروحة و تؤكد نتائج هذه الدراسة ان طريقة الإنتاج المقترحة من الآبار الأفقية على شكل حرف -- وهو حل ناجح ليس فقط بالنسبة للأجزاء غير المنتجة من الأطوال الكلية المحفورة للآبار بل أيضا يؤدي إلى توزيع تدفق أكثر اتساقا على طول الجزء الأفقي . كما أنه يمثل حلول مثلى لأنتاج الآبار المحفورة في مكامن تحت دعم مائي من اسفل او غازي من اعلى .

درجة الدكتوراه في الفلسفه

جامعة الملك فهد للبترول والمعادن

الظهران، المملكه العربيه السعوديه

ابريل 2104

CHAPTER ONE

INTRODUCTION

In the last two decades, horizontal wells' drilling has gained wide acceptance due to the wide range of advantages they offer. The principal application of horizontal wells is to increase the well productivity via increased contact with the reservoir rock. The great contact area between horizontal wellbore and rock matrix allows reservoir fluids to flow in higher capacity to the wellbore. Hence, horizontal wells have added significant values to the petroleum industry in terms of increased deliverability, injectivity, and increased ultimate recovery. The idea of using horizontal wells to increase the area of contacted reservoir dates back to the early 1940's. Recent interest in horizontal wells has been accelerating because of improved drilling and completion technologies. Increases in oil production rate and improvement in ultimate recovery has been correlated to drilling long horizontal wells. Today, a worldwide acceptance exists in drilling horizontal wells to increase productivity as it becomes the standard well design after proving its rewards. However, it is more expensive to drill a horizontal well and therefore; it is of a paramount importance to determine the optimum horizontal section length that would make flow contribution along the whole section.

Business drivers of maximizing reservoir sweep, productivity and hence maximizing reward had driven in the evolution of the current horizontal well completion design. With the advancement of drilling technologies, the well completion design and size has drastically changed. The success stories in drilling and producing horizontal wells had inspired the reservoir engineers to stretch the need to drill multilateral wells to widen the exposure to the reservoir and maximize reservoir sweep efficiency. In addition, the evolution of drilling capability enabled drilling engineers to drill extended reach wells to offset the low productivity of the formation as in tight gas reservoirs. The journey of well completion spans from short horizontal well to more convoluted design of long horizontal wells with the treat of discrete control and monitoring systems. The introduction of such systems to the oil fields enabled more flexibility of sweeping reservoirs and more insight into reservoir characterization.

Lately, the drilling capability made it possible to intersect and connect wells for coal bed applications (2012) [47].

Horizontal wells are usually idealized as infinite-conductivity wellbores and this idealization is justified on the basis that the magnitude of the pressure drop in the wellbore is negligibly small. The infinite-conductivity idealization, however, rests on the assumption that the magnitude of the pressure drop in the wellbore is small when compared with the magnitude of the pressure drop in the reservoir. Then, given the fact that horizontal wells are often proposed and justified on the premise that high production rates can be obtained by small reservoir pressure drops, and the fact that, non-laminar flow that may develop at reasonably high production rates should cause increased wellbore pressure losses, the use of the infinite-conductivity assumption for horizontal wells deserves scrutiny. This goal can be achieved by the use of a comprehensive model that couples reservoir and wellbore hydraulics.

The inflow performance of a long, highly deviated or horizontal production drain-holes is generally more influenced by the pressure profile in the wellbore, being a function of frictional pressure loss and the skin due to prolong exposure to drilling fluids during the drilling operations. These effects will in general be more significant for dipping or vertically undulating wells especially in multi-phase flow. Flow regime-dependent flow conditions strongly affect the wellbore hydraulics and hence flow profile along the horizontal wellbores. Segregation and possible back flow of denser phases result in misinterpretation of the inflow distribution. To assess the downhole flow conditions more accurately, logging tools have been developed to overcome the flow regime related issues.

Horizontal wells have become the standard well architecture to be considered in the new field development. At the same time, it is well accepted that frictional pressure losses is an important factor that can impair well productivity and should be considered to drill the optimum well length. Early generation of wells were completed as barefoot wells or completed with liners. Al Qahtani et al. (1997) [25] presented the first formula to estimate the optimum horizontal well length beyond which the flow contribution along the wellbore is negligible and does not pay for the extra length to be drilled. Newer generations of horizontal wells are equipped with downhole flow choke systems; both active and passive, to offset the effect of

frictional pressure losses and equalize the flow along the horizontal section.

Pressure drop over horizontal wells causes unequal draw down along the well, thus reducing the effectiveness of the horizontal drain-hole section close to the toe of the well, and increasing the tendency for water and gas coning at the heel. Advanced well completion techniques have been designed using optimized number of Passive Inflow Control Devices, ICDs to control the flow from the different sections of the horizontal drain-hole to improve the contribution from the horizontal drain-hole and optimize well productivity (Dimitris et al. 2009 [42]). Furthermore ICD's can be tailored to follow any wanted flow profile, and is therefore an important tool for optimal reservoir management. Even though the use of ICDs are useful devices to optimize well productivity and reduce water production, they are very costly devices facing many challenges due to the additional pressure drop across them, and the costly workovers to replace them in case of failures. As drilling technology continues to exploit more complex and unconventional reservoirs, multi-stage fracturing techniques have emerged and implemented in many reservoirs to increase the productivity of these long horizontal wells. However, the problems associate with the pressure losses due to the additional production from these fractures are not resolved to maximize the full benefits from these massive multistage fracturing jobs.

Al Qahtani (1999) [32] presented a study to evaluate performance of horizontal wells utilizing coiled tubing production logging. The study revealed that some horizontal wells have small portion contributing to flow due to frictional pressure losses in the horizontal wellbore which impair the productivity of the wells. In addition, it highlighted the importance of using production logging and present field cases to evaluate horizontal well performance. Field data showed that even in relatively short wells, frictional pressure losses can impair productivity especially in wells drilled in high productive formations. Fig. 1 shows the flow and pressure profiles in a 1000-foot horizontal well. The production log indicated that the wellbore pressure is becoming close to the formation pressure and hindering the flow at the last portion of the section.

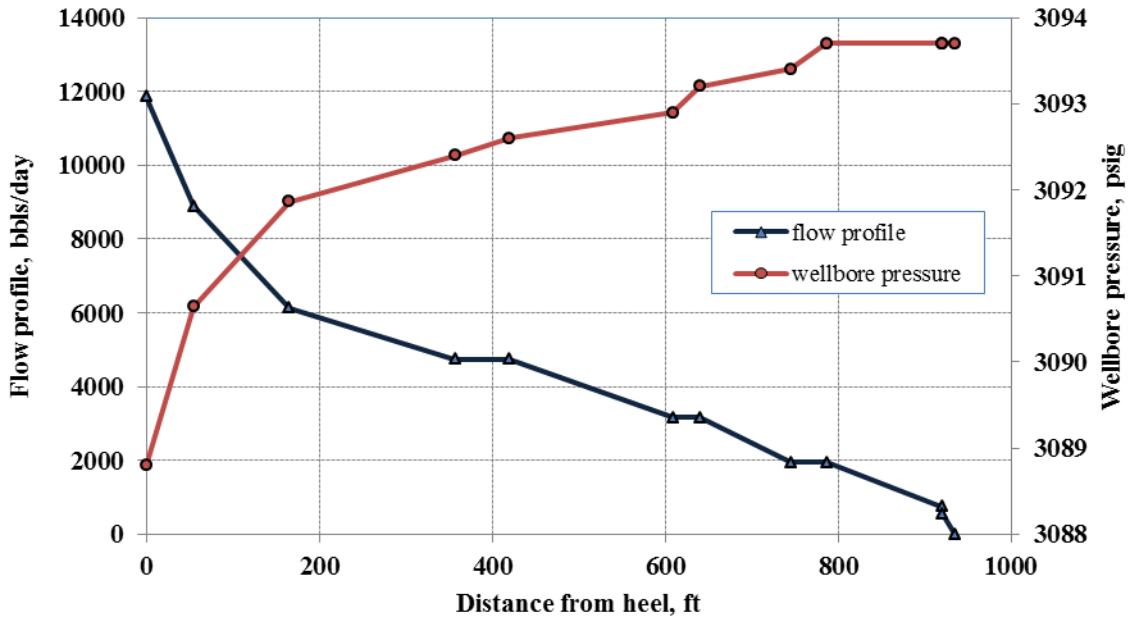

Fig. 1- Flow and pressure profiles in a 1000 foot horizontal well, Al Qahtani (1999).

The wellbore pressure and frictional pressure losses are shown in Fig.2 below. The total frictional pressure drop in the well is less than 5 psig. Although, the frictional pressure losses are small, it is hindering the potential of the well due to the high productivity of the well and hence the low pressure drawdown required to make that flow rate.

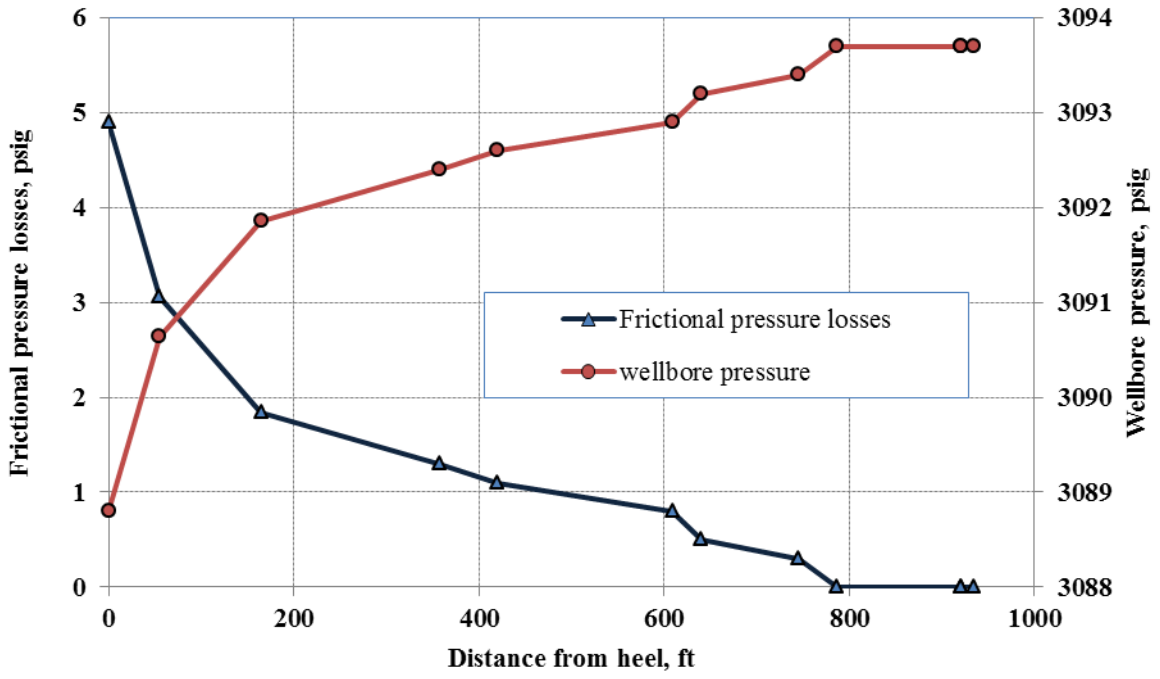

Fig. 2- Pressure and frictional pressure losses profiles in the same horizontal well, Al Qahtani (1999).

Horizontal wells have attracted a lot of attention in oil and gas fields not because they are the most rewarding design to be put in the ground that will pay off at a faster pace, but also due to the complication of production data during transient or steady-state flow conditions.

1.1 Background

Pressure Transient Testing In Of Horizontal Wells

Pressure transient well testing has undergone continuous development with respect to data acquisition and accuracy, as well as with respect to data analysis. In the early days, the objectives of well testing were simply to answer questions such as what was wrong with poorly performing wells and to determine if a well was due for stimulation job. Moreover, the recent acceleration of technological advances both in hardware and software is now revolutionizing well test design, data

acquisition, and interpretation. Improvements in equipment have led to more robust and accurate measurements of pressure and temperature, as well as the opportunity for more accurate control.

The complex flow geometry associated with horizontal wells makes well-test interpretation difficult. Interpretation of well tests from horizontal wells is much more difficult than interpretation of those from vertical wells because of a considerable wellbore storage effect, the 3D nature of the flow geometry and lack of radial symmetry, and strong correlations between certain parameters. Also, zonal variations of vertical permeability and shale distribution complicate well test interpretation.

In recent years, pressure-transient behavior of horizontal wells has received considerable attention because of the increase of the need to drill wells with more complex design adapted to challenging applications. The literatures on different subjects pertaining to transient tests cover different well completions and reservoir configurations. The literature on this subject spans the whole spectrum from response modeling and flow regime identification to field application.

The application of well testing is more complicated reservoir well/systems with challenging applications: heterogeneous, anisotropic, composite, layered and compounded with wellbore and near-wellbore flow characteristics. However, technological advances are associated with cost and complexity, and the need to assess both the quality and the value of the information obtained. All this leads to the need for evolving approach for commissioning, designing, execution, and interpretation of well tests.

The pressure behavior of new well design has brought about the need to come up with associated well test interpretation methodologies and software. The state of knowledge, however, is not complete for well test analysis. The problem lies in the evaluation of complex mathematical expression that describes the analytical solution of such systems and in the large number of possible solutions. The application of long horizontal wells adds to the challenge of transient testing especially for long horizontal wells with some portion of the section not contributing to the flow. Fig. 3 shows a typical horizontal well in a flat slab reservoir.

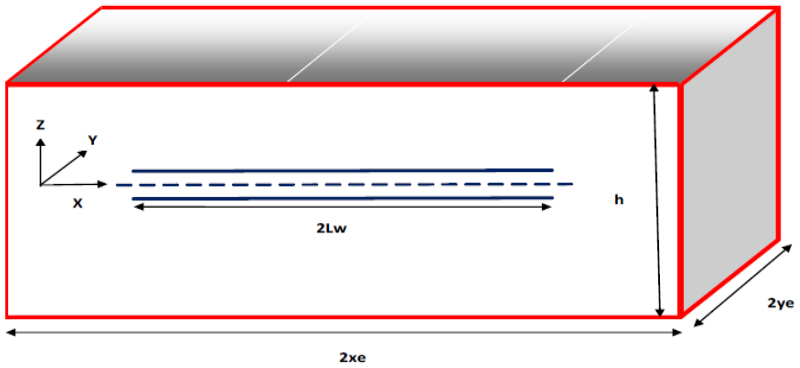

Fig. 3- A typical horizontal well in a flat slab reservoir

The main objective of this research is to develop a semi-analytical model for pressure transient testing of U-shaped long horizontal wells. That will enable characterizing well/rock parameters controlling fluid flow in porous media and hence total well productivity, with the consideration of formation damage in different sections of the wellbore. The appeal for this solution of such design is to enable reservoir engineers to utilize developed solution to maximize completion and sweep efficiencies, with new and more reservoir engineering monitoring knowledge.

1.2 Research Objectives

Evolving the design of well completion has been always to maximize recovery and optimizing production from oil formations. Transient pressure testing evolvement was driven by the need of the new solution for the emerging well completion designs. This solution development was brought about by the evolution of wells design, from vertical well solution to current well design with utmost complications of layering, compartmentalization, selective control and permanent downhole measurement.

The proposed extended-reach horizontally-intersected well or U-shaped wells was made possible because of advancement in drilling technology. This warrants having a new solution to analyze flow and reservoir parameters. The solution is deemed to offer more insight into reservoir performance and its utilization to maximize reservoir sweep efficiency.

The main objective of this research is to improve the productivity of long horizontal wells especially from the non-contributing sections due to the effect of wellbore hydraulics. The specific objectives are as follows;

1. Develop a semi-analytical model to investigate the pressure transient behavior of a U-shaped horizontal well.
2. To provide a viable and cost effective method to offset the frictional pressure losses on long horizontal drain-hole and hence maximize flow capacity of the horizontal well.
3. To investigate the impact of production rates from the two ends of the U-shaped horizontal well (toe to heel) on the flux distribution along the horizontal drain-hole.
4. To perform classical well test objectives of characterizing rock/well performance, namely, permeability, productivity index and potential skin damage.
5. To investigate the impact of potential skin damage and variation along the horizontal drain-hole.

Hereafter, the U-shaped well is referred to the horizontal well with two producing ends.

1.3 Research Methodology

The research approach will develop the solution in different steps to allow validations of results. The steps cover the following;

- Definition of the physical model that represents the well/reservoir configurations.
- Definition of boundary conditions and the number of unknown variables and the equations to be solved.
- Obtaining the mathematical model for the proposed U-shape horizontal wells.
- Single-layered horizontal well, with two production wings.
- Wellbore hydraulics will be considered

- The solution will utilize the pervious solutions of horizontal wells as a base case for mathematical formulation and model validation.
- Different mathematical solutions will be employed. These include the principle of superposition, convolution, and approximation.
- Program coding is written in FORTRAN language.
- Model validation against published studies of horizontal and extended reach wells in literature.
- Parametric study for parameters involved in the model.

1.4 Research Significance and Expected Results

Long horizontal wells are suffering from significant frictional pressure drops. The frictional pressure drops result in reducing the benefits from the full drilled horizontal drain-hole. In this study a new method is proposed to make full utilization of the long horizontal drain-hole by producing these long wells from both ends of the horizontal well (toe and heel). This new method is named as a U-shaped horizontal well. To support this idea and confirm its viability a semi-analytical pressure transient model has been developed and used to study the behavior of the U-shaped horizontal wells. The model accounts for the impact of the wellbore hydraulics and variable skin along the horizontal well. This model allows the production from both ends at the desired rate ratios and can be used to optimize the productivity of the well with a more uniform flux distribution along the horizontal drain-hole. The results of this study are expected to have significant impacts on the way those long horizontal wells are drilled, completed, and produced.

CHAPTER TWO

2.1 Literature Review

2.1.1 Horizontal Well Model

Reservoir response

During the last three decades, large body of publications and studies were presented on issues related to issues of pressure transient testing relevant to this study. Initially, the horizontal well was simplified to be line source or infinite conductivity pipe without considering pressure drop in it by many researchers. Based on the assumption, the productivity, and performance of horizontal wells were investigated. However, field reports indicated that the pressure drop had important impact for performance of horizontal well: the breakthrough of bottom water occurred near the heel end usually because of pressure drop along the well, which make the well section near the toe end no contribution for production. The coupled flow was applied to research influence of pressure drop by some researchers, in which pipe flow theory was used in horizontal well and seepage theory was used in reservoir.

There are other pertinent and important references on pressure transient testing. Interpretation of a horizontal well test is more difficult than for a vertical well test because of the 3D geometrical nature and the evolution into different flow regimes. Horizontal well test results will not only depend on the reservoir characteristics, but also on the well geometry and orientation. Even though a number of well-defined horizontal well pressure analyses have been reported in the literature [Daviau et al., 1988; Goode et al., 1987; Kuchuk et al., 1988; Matta and Santo, 1995], some of the issues are still not clearly resolved.

The transient-flow equation describes many flow problems in petroleum reservoirs. The pressure-transient solutions are derived using the source and Green's functions developed by Gringarten and Ramey (1973) [1] and introduced into petroleum engineering to solve unsteady-state flow problems in reservoirs.

Deviated wells with full or limited flow entry are very common, especially in offshore developments. The pressure transient behavior of fully penetrating deviated wells was investigated by Cinco et al (1975) [3] for homogeneous reservoirs.

Goode and Thambynayagam (1985) [5] presented an analytic solution for the pressure response during drawdown and buildup of a horizontal well. This method results from solving 3-D diffusivity equation with successive integral transform. Simplified solution for short, intermediate, and longtime was presented.

Clonts and Ramey (1986) [6] presented an analytical solution for pressure transient analysis for wells with horizontal drainholes. The solution presented was for the transient pressure response of a uniform flux horizontal drainhole in an anisotropic reservoir of finite thickness. The solution also applies for a reservoir with multiple drainholes in a vertical array. The solution shows that there are two possible types of transient pressure behavior depending on the length of the drainhole relative to the height of the reservoir. They also showed that the pressure transient response for multiple drainholes is identical to the single drainhole solution if dimensionless variables are defined relative to the number of drainholes. Consequently, the pressure response of a uniform flux vertical fracture can also be approximated by a vertical array of drainholes.

Kamal, Buhidma, SA Smith, and W.R. Jones (1993) [13] presented a pioneering a study on the influence of productivity variation along the horizontal section, due to heterogeneity or formation damage, on the pressure transient analysis. In the study, they showed the effects of using too long a production interval on the interpretation of test data by analyzing numerically simulated tests from wells that are only partially open to flow in the horizontal section. An analytical solution that allows for a well to consist of a number of segments of arbitrary length, strength, and skin was presented. The model was used to document the effect of neglecting the actual flux distribution and well length on the results of the well test interpretation. A new radial flow regime is identified from the results of the segmented horizontal well model. This analytical model is also useful in handling dual lateral completions.

Yildiz and Ozkan (1994) [15] investigated the transient pressure behavior of selectively completed horizontal wells. A new solution in Laplace space is presented and asymptotic approximations are derived. Computational issues are also addressed. Flow characteristics of sectionally completed

horizontal wells were discussed and the information that can be obtained from the analysis of pressure and derivative responses during various flow regimes was documented.

Kong, Xu and Lu (1996) [21] studied the pressure transient analysis for horizontal well and multi-branched horizontal wells. In this study the line source solution of multi-branched horizontal wells was presented. Analytical solutions for the transient pressure of horizontal wells near a fault or constant pressure boundary and multi-branched horizontal wells or horizontal well in pinch angle were developed. The solutions take into account with wellbore storage and skin in the Laplace transforms domain. Therefore the solutions of well bottom pressure in the physical space are easily obtained by the numerical inversion of the transforms. A table of Greens functions of transient pressures was prepared in this study for multi-branched horizontal wells and horizontal well in a wedge angle as well as horizontal wells near a fault or constant pressure boundary.

Kuchuk & Habashy (1997) [22] presented a new general method for solving the pressure diffusion equation in laterally composite reservoirs, where rock and fluid properties may change laterally as a function of y in the x-y plane. A general Green's function for a point source in 3D laterally composite systems is developed by using the reflection-transmission concept of electromagnetics to solve fluid-flow problems in 3D nonhomogeneous reservoirs,. The solutions in the Laplace transform domain are then developed from the Green's function for the pressure behavior of specific composite reservoirs. The solution method can also be applied to many different types of wells, such as vertical, fractured, and horizontal in composite reservoirs.

Ozkan, Yaldiz and Kuchuk (1997) [26] investigated the transient pressure behavior of dual-lateral wells. An analytical solution to compute the pressure responses of dual-lateral wells in the Laplace domain was presented, and the computational issues were addressed. The influence of the length, phase angle, and vertical and horizontal separations of die laterals were discussed. New flow regimes are identified and the conditions under which various flow regimes prevail were documented. Guidelines for the well test analysis of dual-lateral well responses are also presented.

Alkhonifer and Ershagi (1999) [29] presented a method to detect channel sands and vertical shale continuity using interference responses of parallel horizontal wells. Their method is based on integrating the responses at multiple isolated probing points along a horizontal observation well path, and mapping the permeability profiles from the application of a hybrid method that consists of deterministic and stochastic models.

Ozkan, Yildiz, and Raghavan (1999) [31] investigated the transient pressure behavior of perforated slant and horizontal wells and discussed the implications of perforations on the analysis of pressure and derivative responses. The results presented are derived from a 3D analytical model. In this model, it is possible to consider non-uniform distribution of perforations and each perforation may have different penetration length and skin factor. It was shown that convergent flow into perforations significantly influences the early-time flow characteristics. In addition to discussing transient behavior, the effect of perforations on productivity was also discussed.

Yildiz (2000) [33] presented a 3D analytical model to analyze the transient flow into multilateral horizontal wells. The model considers arbitrary phasing angle, selective lateral completion, non-uniform formation damage around each lateral, and areal and vertical permeability anisotropy. Using the model, transient pressure, derivative, and rate distribution characteristics of multilateral horizontal wells are investigated. Flow regimes are examined. A sensitivity study is carried out to identify the parameters controlling the transient pressure, derivative, and fractional rate responses. The sensitivity study included the impact of lateral length, orientation, and number, formation anisotropy, and the degree of formation damage around the laterals.

N. Mohannadi et al. (2003) [36] presented a solution for the pressure-transient responses of horizontal wells in anticlinal structures and curved wells in flat reservoirs. It was shown that, in the absence of gas cap, conventional horizontal-well models may be used to approximate the flow characteristics of the systems where the trajectory of the well does not conform to the curvature of the producing structure. If a gas cap is present, however, the unconformity of the well trajectory and producing layer manifests itself especially on derivative characteristics when the gas saturation increases around the well.

Fahem, Tiab, Sarfraz and Al Owayed (2003) [37] presented an analysis method of the transient pressure behavior of dual lateral wells. An infinite conductivity solution for dual lateral wells was developed by coupling both: the infinite conductivity horizontal well model and the superposition concepts. From the sensitivity analysts study, it was found that infinite conductivity solution for dual lateral wells is affected by the horizontal anisotropy, phasing of the lateral sections, dimensionless horizontal separation, mechanical skin and wellbore storage.

Yula et al. (2005) [39] presented a comprehensive semi-analytical model is built to investigate the effects of drilling/perforating damage and high-velocity flow on the performance of perforated

horizontal wells. The presented a semi-analytical model was for a completed horizontal well by coupling the 3D reservoir flow model and the wellbore-hydraulics model and discussed the pseudo-skin approach for clean perforated completion. In this paper, the additional pressure drop due to formation damage and high-velocity flow are addressed and incorporated into the previous semi-analytical model. The model considers the 3D convergent flow into individual perforations, flow through the damaged zone around the wellbore and the crushed zone around the perforation tunnels as well as the additional pressure drop due to non-Darcy flow in near wellbore region. Both oil and gas wells were discussed.

Medeiros, Ozkan, and Kazemi (2006) [41] presented a semi analytical model for the pressure-transient analysis of horizontal wells in composite, layered, and compartmentalized reservoirs. The model divides the reservoir into blocks that represent locally homogeneous substructures of the reservoir and couples the analytical, pressure-transient solutions at the block boundaries. This approach is consistent with the averaging effect of pressure transients and provides an alternative to full numerical modeling of horizontal-well pressure-transient responses in heterogeneous formations. The model can also be generalized for multiple wells of different geometry including multiple laterals.

M. Brown,and E. Ozkan, R. Raghavan, and H. Kazemi, (2009) [44] presented an analytical tri-linear flow solution to simulate the pressure transient and production behavior of fractured horizontal wells in unconventional reservoirs (Ozkan et al., 2009). The model was simple, but versatile enough to incorporate the fundamental petrophysical characteristics of unconventional reservoirs, including the intrinsic properties of the matrix and the natural fractures. This practical solution provided an excellent alternative to rigorous solutions, which are cumbersome to evaluate.

B.D. Poe Jr. and A. Erkal(2010) [45] presented the results of a study of the transient performance of a horizontal well that has been completed using Inflow Control Devices (ICD's) to modify the inflow profile along the wellbore to minimize the risk of premature gas or water breakthrough into the well. A realistic pressure and rate-transient design and interpretation computational model was developed and utilized in this study. The mathematical model has been used to evaluate the transient performance of a horizontal wellbore in single and dual porosity reservoirs.

P. Q. Lian1, L. S. Cheng and J. Y. Cui (2010) [46] presented A new computation model of fractured horizontal well coupling with reservoir. Pressure drop formula was derived for considering simultaneous production of fractures and horizontal wellbore in unsteady state. A reservoir/fractured

horizontal well coupling model were developed for finite conductivity condition that can be solved by the combination of quasi-Newton method and PSO (Particle Swarm Optimization) algorithm. The solution of a practical example showed that lots of factors can affect the productivity of the fractured horizontal well. The number of the fractures has an optimizing range and different fractures have different flow rates and the production in the central fracture is the lowest.

Zhijun, S., Yongzhe, Z., Hongjun, Q. and Jianlin, L. (2011) [47] presented a study on the research and planning required from the selection of location and targeted formation, casing design and execution practices and technologies required to drill the extended-reach horizontally-intersected wells or the U-shaped multilateral wells.

2.1.2 Wellbore flow and hydraulics

The intensive theoretical studies of horizontal wells over the last two decades have shown that the incorporation of horizontal wellbore hydraulics into the horizontal well model is a challenging issue. This section will review the relevant literature concerning the effect of hydraulics on horizontal well performance.

Dikken (1990) [10] was the first to incorporate the effect of frictional wellbore pressure drop in horizontal well productivity. He presented an approximate model to investigate the horizontal wellbore hydraulics. His model assumes sturdy flow in the reservoir and constant productivity index per unit of wellbore length. He developed a second order differential equation to determine the wellbore flow rate at any location in the wellbore. He then solved analytically the differential equation for the case of infinite wellbore length and numerically for the actual case. The result of these assumptions is an underestimated reservoir pressure drop and thus, for the most cases, Dikken's model magnifies the effect of wellbore hydraulics. In addition, the flow resistance term used in Dikken's model is a result of a specific correlation for the friction factor and the choices of unconventional dimensionless groups make it difficult to investigate the effect of individual variables.

Folefac et al. (1991) [11] described the equations on which the wellbore pressure drop model is based and presented an outline of a novel computational method which solves these equations by coupling a drift-flux model representing the multiphase flow inside the wellbore with reservoir flow equation to predict the productivity loss due to wellbore pressure drop. He showed that the inflow performance of

horizontal wells and hence their deliverability may be affected by pressure drop along the wellbore and the productivity index is no longer directly proportional to the well length. The study indicated that wellbore parameters such as well length, diameter and perforated interval have the most significant effect on the level of pressure drop in the wellbore. The consequence of ignoring this wellbore pressure drop is to over predict the well deliverability. It is also shown the wellbore pressure drop increases dramatically with increase in reservoir productivity.

Ozkan, Sarica and Raghavan (1993) [12] were the first to study the effect of wellbore hydraulics on horizontal-well transient pressure responses. The study investigated the effect of pressure drop within the horizontal section on horizontal-well responses. A general, semi-analytical model that couples wellbore and reservoir hydraulics was presented. Dimensionless groups are defined to correlate the effect of wellbore hydraulics on horizontal-well responses. The central new result of this study is a general semi analytical model that couples wellbore and reservoir hydraulics. Flux and pressure distributions along the length of the well are investigated and the validity of the infinite conductivity assumption is discussed. The model enables the rigorous evaluation of horizontal well productivity and can be used to determine optimum well length, wellbore diameter and production rate. A field example was presented to show that the consequences of the use of the infinite-conductivity well assumption cannot be ignored.

Su and Gudmundsson (1993) [14] developed the concept of perforation roughness to take into account the effect of holes or slots on wellbore pressure losses. They determined experimentally the various factors that contribute to the pressure drop in a perforated pipe. They concluded that the pressure drop is the sum of the pressure drop due to the wall friction, acceleration due to fluid flow, perforations roughness, and fluid mixing. They stated that the effect of the pressure drop due to perforations and the fluid mixing is an irreversible pressure drop and will cause a maximum reduction in the wellbore pressure of about 3% of the ordinary frictional pressure drop. They did not develop a correlation that could be used to determine the pressure drop.

Novy (1995) [16] extended Dikkin's work to gas wells. He generalized Dikken's model so that it can be applied to the recovery of gas. In the process, he found that the friction factor correlation used by Dikken gives friction factors that are too high for rough tubes. Novy performed extensive sensitivity studies and he concluded that if the ratio of well-bore pressure drop to drawdown at the producing end exceeds 10%, friction is apt to reduce productivity by 10% or more. He developed guidelines that

indicate whether wellbore friction can be neglected using a model of steady, single-phase flow and with particular values of the relevant physical parameters. These guidelines are based on well length, production rate, hole diameter, and roughness of the wellbore.

Ozkan et al. (1995) [18] extended the work by Serica et al. (1993) [12] and introduced the concept of horizontal well conductivity to model the effect of wellbore pressure drop in inflow performance and transient pressure behavior. The solution presented the details of the solution of horizontal-well flow-equation derived in the main text to account for wellbore hydraulics and the details of the procedure to compute the flux distribution and the wellbore pressure at the heel of a horizontal well.

Ouyang et al. (1996) [20] developed a model that includes the effect of friction, acceleration, and gravity on horizontal wellbore pressure. They concluded that acceleration may be as important as friction on the wellbore pressure drop, depending on the pipe geometry, fluid properties, and flow conditions.

Suzuki (1997) [27] studied the influence of wellbore hydraulics in horizontal section of wellbore on horizontal well pressure transient behavior. He developed a semi-analytical solution for finite conductivity horizontal well pressure-transient behavior assuming laminar to turbulent flow in the wellbore. Finite conductivity solution is obtained by semi analytical method, where turbulent flow of single phase fluid is assumed in wellbore. Based on the finite conductivity solution, finite conductivity pressure transients are presented in terms of type curves and derivatives, production distribution along wellbore, and pressure difference between the two ends of wellbore. Furthermore, quantified criteria for the approximation of infinite conductivity solution to finite conductivity solution is presented with respect to formation flow capacity, wellbore length, pipe roughness, and Reynold's number at the downstream end of wellbore. he concluded that finite conductivity pressure transients depends on the Reynolds number at the downstream end of the wellbore, a dimensionless reservoirs-wellbore constant, a relative pipe roughness of the wellbore, and dimensionless wellbore half length.

Ding (1999) [30] also studied the effect of wellbore hydraulics on horizontal-well transient pressure responses. In this study, the boundary integral equation, based on single layer heat potential, was used at the wellbore boundary to describe the transient phenomena in the presence of the pressure drop in the wellbore. The Galerkin type approach was used to solve the boundary integral equation. The proposed method can be used to study the pressure solution for any number of multilateral wells, as well as selectively perforated wells.

2.1.3 Formation damage

The skin factor effect and challenges it creates on performance of horizontal wells have been investigated in literature using different models and hypothesis and assuming increasing skim damage towards the heel of the well. Recent papers have expressed different viewpoints on the role of formation damage in the performance of horizontal wells. Some suggested that, as horizontal-well length, L, increases, the influence of formation damage on total pressure drop can become negligible, resulting in an additional advantage over vertical wells. Others indicated that the damaged zone may affect productivity more in horizontal wells than in vertical wells, and that skin damage sometimes can prevent horizontal-well projects from succeeding.

Renard et al. (1990) [9] studied the impact of formation damage on horizontal wells productivity. They derived the flow efficiency of horizontal wells assuming steady-state flow of an incompressible fluid in a homogeneous, anisotropic medium. A comparison between the flow efficiencies of vertical and horizontal wells indicated that permeability reduction around the wellbore is less detrimental to horizontal wells. They showed that the effect of damage around a horizontal wellbore is reduced slightly by increasing the well length. Conversely, if the vertical permeability is less than the horizontal permeability, the anisotropy ratio, k_H/k_V, magnifies the influence of formation damage near the horizontal wellbore.

Ozkan and Raghavan (1997) [22] discussed the performance of horizontal wells under the combined influences of wellbore friction and wellbore non-uniform damage. They showed that that wellbore damage may not be viewed merely as an additive pressure drop in the presence of friction. Wellbore hydraulics changes the flux distribution (inflow profile) along the wellbore, and, thus, results in additional pressure drop in the reservoir and across the skin zone. proper formulation of the wellbore model were developed to get the inflow profile along the well length (flux distribution) and the effect by wellbore hydraulics.

Furi and Hill (2002) [35] presented a new analytical model for formation damage skin factor and the resulting reservoir inflow that includes the effect of reservoir anisotropy and damage heterogeneity. The shape of the damaged region perpendicular to the wellbore is based on the pressure equation for an anisotropic medium, and is thus circular near the well and elliptical far from the well. The new model can be used for any distribution of damage along the well. The new skin factor model can be easily incorporated into any existing model of reservoir inflow for a horizontal well. They showed that

the effect of near well formation damage for a horizontal well completion is relatively small compared with vertical wells. However, if the reservoir thickness is large, radial flow becomes dominant and the impact of formation damage on a horizontal well is more significant, more like that of a vertical well.

Al-Khamis, Ozkan and Raghavan (2003) [38] developed a semi-analytical model that can be used to investigate the fundamental characteristics of horizontal interference well responses and to provide a means to calibrate numerical simulators. The model consists of the superposition of the responses of two finite-conductivity horizontal wells. The model presented was a semi-analytical model for interference tests of parallel and non-parallel horizontal wells. The models were used to investigate the general characteristics of interference test responses in horizontal wells. Their results indicated that the vertical interference well assumption is not valid for interference tests between two horizontal wells.

Al-Otaibi and Ozkan (2005) [40] Studied the effect of the non-uniform formation damage on horizontal performance. A synthetic pressure-transient response for different non-uniform skin distributions along a horizontal well and analyze these responses was generated by using the conventional tools that assume uniform distribution of skin. Skin estimates from well-test interpretation were then compared with the known skin distributions. The findings of this study showed that the pressure drop caused by skin depends on the flow regimes if the skin distribution is non-uniform. For most cases, the estimates of skin from early-time radial flow analysis represent the arithmetic average of the skin distribution which may be useful for stimulation decisions. The skin estimate from the pseudo-radial flow period corresponds to the skin pressure drop at the heel of the horizontal well, which represents the additional pressure drop to be considered in the productivity calculations. They demonstrated that the geometric interpretation of the non-uniform skin effect proposed in the literature is inaccurate and leads to significant errors in the calculation of horizontal well productivity.

2.2 Current-solutions shortcomings

The previous work pertaining to different aspects of horizontal wells' architecture and completion design provided a lot of insight into pressure transient response on issues related to the case of studies. Despite the large number of literature on different aspects of horizontal wells performance and pressure transient testing, the application of the extended-reach horizontally-intersected wells or the U-

shaped horizontal wells is new and no solution exists for pressure transient testing. The issue of the U-shaped horizontal wells was presented from the drilling technology ability but not from pressure transient behavior analysis and wells performance. This warrants to develop a solution to extend the solutions presented previously during the emergence of conventional horizontal wells to infer the reservoir and well characteristics as in classical well testing for the U-shaped wells.

CHAPTER THREE

3.1 Solution Development

The semi-analytical model developed in this research is based on previous analytical solutions for the diffusivity equation governing fluid flow in porous media. Using the Green's function, with source and sink concepts, to solve transient flow problems in homogenous porous media, the solution is to be obtained for this complex well-reservoir geometries and for the boundary conditions in this model. This chapter deals with the development of the model that can adequately describe the pressure-transient of a horizontal well producing from both the heel and toe and passing through a homogenous reservoir. We also assumed that the center of the well length to be at equilibrium, hence both producing ends have a common pressure point at that point. We will first discuss the physical model and subsequently develop the semi-analytical model that describes the physical model.

3.2 Physical Model

The proposed work is to develop solution for U-shaped wells. The solution is to offer more insight into reservoir performance and its utilization to maximize reservoir sweep efficiency by developing a semi-analytical solution of pressure transient testing of U-shaped multilateral wells, with flexibility to have general solution for U-shaped horizontal wells.

The well-reservoir physical model is shown in Fig.4. For a U-shaped well in a reservoir with anisotropic but a homogenous layer of uniform thickness, h. An isothermal and a single-phase flow of fluid of constant compressibility and viscosity are considered. The initial reservoir pressure is assumed uniform.

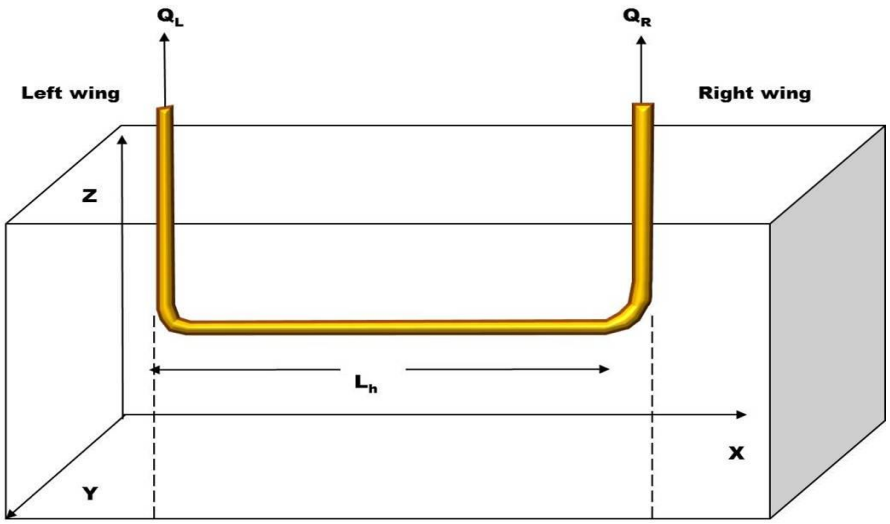

Fig. 4- A U-Shaped Multilateral well

The solution assumes the following conditions;

- The reservoir is a flat slab reservoir, homogenous, anisotropic, having constant and uniform thickness with two impermeable layers at the top and bottom of the formation.
- The pressure at the outer boundaries of the reservoir is assumed to be constant and equal to the initial reservoir pressure, infinite acting reservoir.
- Constant porosity and permeability in each direction, but the formation is anisotropic.
- Gravitational effect is negligible.
- The well is extending in the midpoint of the formation height (symmetrical).
- An isothermal and a single-phase flow of fluid of constant compressibility and viscosity, and formation volume factor are considered.
- The well is of finite conductivity wellbore
- A U-shape well with flexible production ratio from both wings

3.3 Mathematical Model Formulations

3.3.1 Transient flow in porous media

Single-phase fluid flow in porous media is governed by the diffusivity equation, which is derived from the continuity equation and Darcy's law.

Consider a horizontal well in a parallelepiped drainage volume under the following constraints;

• The reservoir is homogeneous but anisotropic, with the coordinates aligned with the principal permeability directions.

• The reservoir has dimensions of X_e, Y_e, and Z_e in the X, Y, and Z directions, respectively.

• The outer boundaries of the reservoir are at constant potential.

• Formation properties are independent of pressure.

• Reservoir fluid is single-phase and slightly compressible with a constant compressibility.

Using these assumptions, the diffusivity equation can be made in the familiar three-dimensional, Cartesian form as follows

$$\eta_x \frac{\partial^2 p(M,t)}{\partial x^2} + \eta_y \frac{\partial^2 p(M,t)}{\partial y^2} + \eta_z \frac{\partial^2 p(M,t)}{\partial z^2} = \frac{\partial p(M,t)}{\partial t} \qquad (1)$$

Where η_j is the diffusivity constant given by $\eta_j = 2.637x10^{-4} \frac{k_j}{\phi \mu c_t} \qquad j = x,y,z$

The assumptions implied by the diffusivity equation are: slightly compressible fluid, homogeneous and anisotropic porous media, constant permeabilities, porosity and fluid viscosity, small pressure gradient, and negligible gravity effect.

The diffusivity equation can be solved by the sink/source technique. Because the diffusivity equation is in the same format as the heat conduction problems, we can directly apply the sink/source technique

to solve the flow in porous media. The solution from this technique applies to different state in the flow period, both transient flow and stabilized flow. The boundary condition of the reservoir is constant pressure, no-flow boundary or mixed, which makes the model practical to a wide range of flow problems in petroleum engineering.

The work of Gringarten and Ramey (1973) is an early application of the Green's (source) function for the problem of unsteady-state fluid flow in a reservoir. The mathematical solution was based on Green's function solution of the three-dimensional diffusivity equation for fluid flow in isotropic and homogeneous porous media. The Green's function is defined as the pressure response at (x, y, z) at time t due to an instantaneous point source of unit strength generated at point (x', y', z') at time τ with the reservoir being initially at a constant pressure P_e , and the boundary being kept without flow or at the same constant pressure P_e. Any no-flow or constant-pressure boundaries are modeled by using appropriate Green's functions as the reservoir well/shape configuration demands. The basic principle of this method is to find the Green's function of the partial differential equation under the prescribed boundary conditions, and then the solution for such a boundary is derived. Laplace transformation, presented by Churchill (1944), has been useful in solving transient problems described by linear differential equations. When the transformation is applied to an ordinary differential equation it reduces the original problem to an algebraic problem. A partial differential equation can be reduced to an ordinary differential equation in Laplace space. Once the transformed problem is solved, in many cases the real time solution may be found directly from tables of Laplace transforms. The Laplace transformation is one of the most powerful tools in mathematics. However, the analytical inversion of a function in the Laplace field to the real field may sometimes be very difficult, or impossible. Stehfest (1970) presented an algorithm to invert numerically these Laplace-field functions.

In a simpler term, Green's function is a cause-effect two point function, $G(M, M'; t, \tau)$ is the effect at the field point M due to a unit source applied at the source point M' and at time τ with unit strength and zero initial pressure and uniform boundary conditions.

The instantaneous point source solution was expressed by Gringarten and Ramey (1973):

$$\Delta p(M',M,t) = \frac{q}{8\phi c_t (\pi\eta t)^{3/2}} \exp\left[-\frac{(M',M)^2}{4\eta t} \right] \qquad (2)$$

3.3.2 Pressure in term of Green's function

Green's function has the following boundary properties. For the pressure prescribed boundary B, $G(M,M';t,\tau)$ it vanishes on B. For the flux prescribed boundary B, the normal derivative of Green's function vanishes on B. if domain Ω is of infinite extent, $G(M,M';t,\tau)$ become zero when M is at infinity.

The pressure drop is obtained by integrating Greens function with respect to the volume of source and with respect to time. Gringarten and Ramey (1973) presented a list of example source function for common transient flow problems. For a uniform initial pressure reservoir, the pressure drop due to continuous withdrawal of fluid from a volume source in Ω, can be expressed by the following Green's function representation (Gringarten and Ramey, 1973)

$$\Delta p(M,t) = P_i - P(M,t)$$

$$= \frac{1}{\phi c_t} \int_0^t \int_\Omega q(M',\tau)\, G(M,M';t,\tau)\, dM'\, d\tau' - \eta \int_0^t \int_B \left[G(M,M';t,\tau) \frac{\partial p}{\partial n_B} - p(M',\tau) \frac{\partial G(M,M',t-\tau)}{\partial n_B} \right]_{M' \in B} d\Omega\, d\tau \qquad (3)$$

The second term vanishes when the reservoir domain is infinite or the outer boundary condition is that of zero flux and zero pressure. For infinite reservoir or finite reservoir with impermeable boundaries,

$$\Delta p(M,t) = \frac{1}{\phi c_t} \int_0^t \int_\Omega q(M',\tau)\, G(M,M';t,\tau)\, dM'\, d\tau' \qquad (4)$$

For a uniform flux source,

$$\Delta p(M,t) = \frac{1}{\phi c_t} \int_0^t q(M',\tau)\, S(M,t)\, d\tau \qquad (5)$$

Where $S(M;t,\tau)$ is the source function given by;

$$S(M,t) = \int_{\Omega} G(M,M';t-\tau)\, dM' \tag{6}$$

If the pressure is to be calculated at the wellbore (source), then

$$\Delta p(M,t) = \frac{1}{\phi c_t} \int_0^t q(M_w,\tau)\, S(M;t-\tau)\, d\tau \tag{7}$$

And

$$S(M,t) = \int_{D_w} G(M,M_w;t-\tau)\, dM_w d\tau \tag{8}$$

Where,

$q(M_w,\tau)$: The flow rate per unit length

$S(M,t)$: The instantaneous uniform-flux source function for the particular source-reservoir system.

M_w: a dummy point in the source

$G(M,M_w;t-\tau)$: the instantaneous Green's function

For a three-dimensional model with the same coordinate system, equation (5) becomes

$$\Delta p(x,y,z,t) = \frac{1}{\phi c_t} \int_0^t q(\tau)\, S(x,y,z;t-\tau)\, d\tau \tag{9}$$

Where $S(x,y,z;t-\tau)$ is the total source function in the three-dimensional space.

Using Newman's product rule, this total source function maybe defined as the product of the three one-dimensional instantaneous source functions

$$S(x,y,z;t-\tau) = S(x,t)\, S(y,t)\, S(z,t) \tag{10}$$

The total flow rate is per unit volume of the source. If the flow rate is assumed constant, then it can be removed from the integral. The $q(M_w,\tau)$ is the fluid withdrawal per unit surface area per unit time and can be expressed as

$$q(M_w,\tau) = Q\,2l_w$$

Then equation (9) becomes

$$\Delta p(x,y,z,t) = \frac{q(\tau)}{\phi c_t}\int_0^t S(x,t)\,S(y,t)\,S(z,t)\,d\tau \qquad (11)$$

A continuous source function is obtained by integrating the right-hand side of the equation with respect to time.

3.4 Horizontal Well Flow Model Solution

3.4.1 Transient Reservoir response

The solution to the pressure transient response of horizontal drainholes was derived using instantaneous source and Green's functions together with Newman product method. The drainhole is represented as a constant rate line source of length 2L in a reservoir of height h with impermeable upper and lower boundaries. The reservoir is infinite in the x and y directions with dimensional permeabilities of K_x, K_y, and K_z . The drainhole is located at X_w & Y_w, the distance from the origin in the X and Y directions respectively.

Considering a horizontal well having wellbore length of $2L_w$, extends in an infinite reservoir,
The unsteady state pressure drop created by production from the wellbore at any point in the reservoir (x,y,z) is given by equation (11) (Gringarten and Ramey, 1973) as

$$\Delta p(x,y,z,t) = \frac{q(\tau)}{\phi c_t}\int_0^t S(x,t)\,S(y,t)\,S(z,t)\,d\tau \qquad (12)$$

The horizontal well model was based on the assumption of the solid bar source reservoir as the intersection of the three one-dimensional instantaneous source of infinite slabs in an infinite acting reservoir in the X, Y, and Z directions. By the principle of the Newman's product method, the instantaneous source function for a horizontal well system is given as the product of the three individual source functions in the X, Y, and Z directions. After substituting and for isotropic reservoir, equation (12) becomes as presented by Colnts & Ramey (1986)

$$\Delta P(x,y,z,t) =$$

$$\frac{q(\tau)}{\phi c_t}\int_0^t \left\{\frac{1}{2}\left[erf\left(\frac{\frac{l}{2}+(x-x_w)}{2\sqrt{\eta\, t}}\right)+erf\left(\frac{\frac{l}{2}-(x-x_w)}{2\sqrt{\eta\, t}}\right)\right]\times\frac{\exp\left[\frac{-(y-y_w)^2}{4\eta\, t}\right]}{2\sqrt{\pi\eta t}}\times\frac{1}{h}\left[1+2\sum_{n=1}^{\infty}\exp\left(-\frac{\eta^2\pi^2 t}{h^2}\right)\cos\left(\eta\pi\frac{z_w}{h}\right)\cos\left(\eta\pi\frac{z_w}{h}\right)\right]\right\}dt$$

(13)

In dimensionless form and for a typical horizontal well as shown in the Fig.5 (ZwD=0.5). The calculations of P_{wD} vs. t_D are based on Ozkan's work (1987) [8].

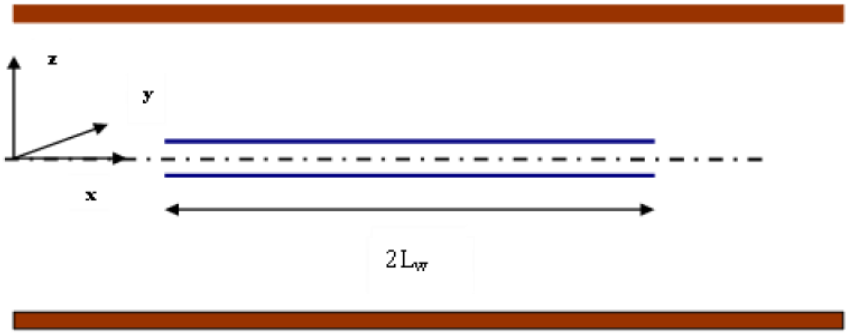

Fig. 5- Schematic of the Horizontal Well-Reservoir System

The reservoir response for a horizontal well is given by Ozkan et al. (1987) as

$$P_D(x_D,y_D,z_D;Z_{wD},L_D,t_D)=\frac{\sqrt{\pi}}{4}\sqrt{\frac{k}{k_y}}\int_0^{\tau_D}\exp\left[\frac{-y^2{}_D}{4t_D}\right].\left[erf\frac{\left(\sqrt{\frac{k}{k_x}}+x_D\right)}{2\sqrt{t_D}}+erf\frac{\left(\sqrt{\frac{k}{k_x}}-x_D\right)}{2\sqrt{t_D}}\right]$$

$$\times\left\{1+2\sum_{n=1}^{\infty}\exp\left(-n^2\pi^2L^2{}_Dt_D\right)\cos n\pi z_{wD}\cos n\pi z_D\right\}\frac{dt_D}{\sqrt{t_D}} \qquad (14)$$

The pressure derivative with respect to the logarithm of the dimensionless time is given by;

$$t_D P'_D(x_D, y_D, z_D; Z_{wD}, L_D, t_D) = \frac{\delta P_D}{\delta \ln t_D} = \frac{\sqrt{\pi}}{4}\sqrt{\frac{k}{k_y}}\left[erf\frac{\left(\sqrt{\frac{k}{k_x}} + x_D\right)}{2\sqrt{t_D}} + erf\frac{\left(\sqrt{\frac{k}{k_x}} - x_D\right)}{2\sqrt{t_D}}\right]\exp\left[\frac{-y^2{}_D}{4t_D}\right]$$

$$\times\left\{1 + 2\sum_{n=1}^{\infty}\exp\left(-n^2\pi^2 L^2{}_D t_D\right)\cos n\pi z_{wD}\cos n\pi z_D\right\}\sqrt{t_D} \qquad (15)$$

The dimensionless pressure response for a horizontal well expressed using the Green's function is given by

$$P_D(x_D, r_{wD}, t_D) = \int_0^{t_D}\int_x q_{hD}(x'_D; t'_D)\, G_{\mathrm{D}}(x_D - x'_D, t_D - t'_D)\, dx'_D dt'_D \qquad (16)$$

Where $G_{\mathrm{D}}(x_D, t_D)$ is the instantaneous point-source function given by

$$G_{\mathrm{D}}(x_D, y_D, z_D, t_D) = \frac{\eta}{2L^2 t_D}\sqrt{\frac{k_z}{k}}\exp\left(\frac{x_D{}^2 + y_D{}^2}{4t_D}\right)\left[1 + 2\sum_{n=1}^{\infty}\exp\left(-\frac{\eta^2\pi^2 t_D}{h_D{}^2}\right)\cos\left(\eta\pi\frac{z_D}{h_D}\right)\cos\left(\eta\pi\frac{z_{wD}}{h_D}\right)\right] \qquad (17)$$

Where η is the diffusivity constant given by

$$\eta = 2.637\ \mathrm{x}10^{.4}\frac{k}{\mu\phi c_t} \qquad (18)$$

The following dimensionless groups are used to express the dependent (i.e. the pressure) and independent (i.e. the other parameters) variables of the solution as follows;

$$P_D = \frac{kh}{141.2q\mu B}\Delta P \qquad (19)$$

$$t_D = \frac{2.637x10^{-4}kt}{\mu\phi c_t L} \qquad (20)$$

Where; time, *t* is in hours,

Length, L is the horizontal wellbore length

The uniform permeability, *k*, corresponds to the equivalent isotropic-system permeability defined by

$$k = \sqrt[3]{k_x\, k_y\, k_z} \tag{21}$$

Several other dimensionless variables used in this work are as follows:

$$x_D = \frac{2x}{L}\sqrt{\frac{k}{k_x}} \tag{22}$$

$$x_{wD} = \frac{2x_w}{L}\sqrt{\frac{k}{k_x}} \tag{23}$$

$$y_D = \frac{2y}{L}\sqrt{\frac{k}{k_x}} \tag{24}$$

$$y_{wD} = \frac{2y_w}{L}\sqrt{\frac{k}{k_x}} \tag{25}$$

$$z_D = \frac{z}{h}, \tag{26}$$

$$z_{wD} = \frac{z_w}{h}, \tag{27}$$

$$L_D = \frac{L}{2h}\sqrt{\frac{k_z}{k}} \tag{28}$$

The dimensionless formation thickness and dimensionless wellbore radius are given by

$$h_D = \frac{2h}{L}\sqrt{\frac{k}{k_z}} \tag{29}$$

and

$$r_{wD} = \frac{r_{we}}{h} \tag{30}$$

Where r_{we} is the equivalent wellbore radius for an anisotropic reservoir given by:

$$r_{we} = \frac{r_w}{2}\left[\left(\frac{\sqrt{k_x k_y}}{k_z}\right)^{0.25} + \left(\frac{k_z}{\sqrt{k_x k_y}}\right)^{0.25}\right], \tag{31}$$

The dimensionless flux in the well is given as:

$$q_{hD} = \frac{q_h L}{qB}\sqrt{\frac{k_x}{k}}, \qquad \text{where} \quad q_h(x) \text{ is the flux along the wellbore sandface} \tag{32}$$

For short-term approximation of eq. 14 can be obtained by Ozkan et al. (1987) as ;

$$P_D(x_D, y_D, z_D; z_{wD}, L_D, t_D) = -\frac{\beta}{8L_D} E_i\left[-\frac{(z_D - z_{wD})^2 / L^2{}_D + y^2{}_D}{4t_D}\right] \tag{33}$$

Where

$$\beta = \begin{Bmatrix} 2 & for\ |x_D| < \sqrt{\frac{k}{k_x}} \\ 1 & for\ |x_D| = \sqrt{\frac{k}{k_x}} \\ 0 & for\ |x_D| > \sqrt{\frac{k}{k_x}} \end{Bmatrix} \tag{34}$$

The duration of initial radial flow periods are given by:

$$t_D \le \min\begin{Bmatrix} \beta_D{}^2 / 20 \\ (z_D + z_{wD})^2 / (20L^2{}_D) \\ (z_D + z_{wD} - 2)^2 / (20L^2{}_D) \end{Bmatrix} \tag{35}$$

For long-term approximation of eq. 14 can be obtained by;

$$P_D(x_D, y_D, z_D; z_{wD}, L_D, t_D) = \frac{1}{2}(Ln\, t_D + 2.80907) + \sigma(x_D, y_D) + F(x_D, y_D, z_D; z_{wD}, L_D, t_D) \tag{36}$$

Where $\sigma(x_D, y_D)$ and $F(x_D, y_D, z_D; z_{wD}, L_D, t_D)$ are given by;

$$\sigma(x_D, y_D) = 0.25\left\{\begin{array}{l}\left(x_D - \sqrt{\frac{k}{k_x}}\right).Ln\left[\left(x_D - \sqrt{\frac{k}{k_x}}\right)^2 + y^2{}_D\right] \\ -\left(x_D + \sqrt{\frac{k}{k_x}}\right).Ln\left[\left(x_D - \sqrt{\frac{k}{k_x}}\right)^2 + y^2{}_D\right] \\ -2y_D \arctan\left[2y_D \Big/ \left(x^2{}_D + y^2{}_D - \sqrt{\frac{k}{k_x}}\right)\right]\end{array}\right\} \tag{37}$$

And

$$F(x_D, y_D, z_D; z_{wD}, L_D, t_D) = \sum_{n=1}^{\infty} \cos n\pi z_D \cos n\pi z_{wD} \int_{-1}^{+1} K_0(\tilde{r}_D L_D n\pi) d\alpha \tag{38}$$

And

$$\tilde{r}_D = \left(x_D - \alpha\sqrt{\frac{k}{k_x}}\right)^2 + y^2{}_D \tag{39}$$

A typical horizontal well transient response for an infinite conductivity well (no wellbore hydraulics effects considered) and for different values of L_D's is shown in fig.6.

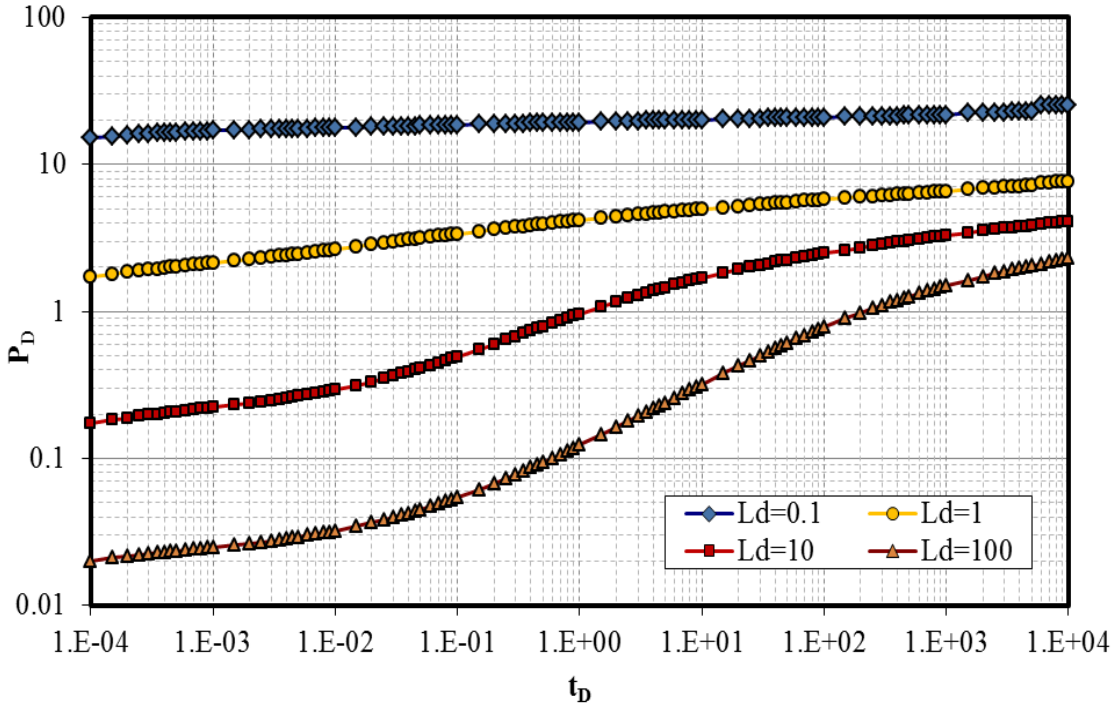

Fig. 6- Typical horizontal well pressure transient response, P_{wd} vs. t_D for different L_d values.

More detailed presentation of mathematical formulation of horizontal wells response in an infinite-acting reservoirs is shown in appendix-A.

3.4.2 Wellbore flow hydraulics

Wellbore Pressure Drop Equations

The wellbore pressure in horizontal wells is one of the important factors in well performance evaluation. The infinite conductivity wellbore assumption is valid only in cases when the pressure drop in the wellbore is very small compared to the drawdown in the reservoir. Since the lateral length is relatively long, pressure drop inside the lateral is sometimes significant. Realizing the importance of wellbore pressure drop, several analytical or experimental studies have been conducted to investigate the different aspects of horizontal wellbore flow behavior, and some analytical wellbore models for single-phase flow have been developed. The pressure drop along a horizontal wellbore can be high

because of the frictional pressure drop term. The frictional pressure drop along the wellbore depends mainly on the flow rate, the length of the well, fluid properties, and well hydraulic conductivity. Thus for a long horizontal well with high flow rate and/or small wellbore diameter, the pressure drop along the wellbore can be significant and will affect the performance of horizontal wells. For better understanding of horizontal well behavior, a good estimate of the pressure drop within the horizontal portion of the well is needed. This estimation can help reservoir engineers in optimizing an individual completion and/or optimizing the depletion plan for a reservoir.

Horizontal wellbore model

In most of available models, the wellbore hydraulics of horizontal wells is simulated to that of horizontal pipe. This is because of the geometrical similarities between a horizontal well and a horizontal pipe. With this assumption, the basic pipe flow equation can be derived from the equations of continuity, momentum, and energy, as

$$\frac{dp}{\partial x} = \left(\frac{dp}{\partial x}\right)_{gravity} + \left(\frac{dp}{\partial x}\right)_{acceleration} + \left(\frac{dp}{\partial x}\right)_{friction} \tag{40}$$

Assuming a single-phase flow of an incompressible Newtonian fluid under isothermal conditions with no heat transfer, the frictional pressure drop is estimated by

$$\Delta P_f = 2\frac{f\rho v^2}{g_c D} L \tag{41}$$

If we convert the unit in eq. 41 to oil field unit shown as,

$$v = \frac{q}{A} = \frac{4q}{\pi D^2}\frac{bbl}{day}\frac{5.615\,ft^3}{bbl}\frac{day}{86400s}\frac{1}{ft^2} = 8.2758\times10^{-5}\frac{q}{D^2} \tag{42}$$

$$\Delta P_f = 2\frac{f\rho L}{32.17D}\left(8.2758\times10^{-5}\frac{q}{D^2}\right)^2\frac{ft^2}{144in^2} \tag{43}$$

$$\Delta P_f = 2.9569 \times 10^{-12} \frac{f \rho L q^2}{D^5} \tag{44}$$

Under the current convention of the flow into the heel of the horizontal section at x=0, the flow rate at some point x in the wellbore q_{hc}, is related to the flux from the reservoir, q_h, by

$$\left(\frac{\partial q_{hc}}{\partial x} \right)_x = -q_h(x) \tag{45}$$

If we reverse the direction toward the toe of the well by inducing a pressure sink point, where flow increases with increasing x, then the flow rate at some point x in the wellbore q_{hc} become,

$$\left(\frac{\partial q_{hc}}{\partial x} \right)_x = +q_h(x) \tag{46}$$

Under the assumptions of flow, the steady state momentum equation for the flow in the horizontal wellbore for the flow toward the heel is given by

$$\frac{dP_h}{dx} = E\ f\ q_{hc}^2 \tag{47}$$

For production wells, the friction factor is given by the following correlations;
For laminar flow;

$$f = \frac{64}{N_{\mathrm{Re}}} \left(1 + 0.04304\, N_{\mathrm{Re}}{}^{0.6142} \right) \tag{48}$$

Turbulent

$$f = f_0 \left(1 - 0.0153\, N_{\mathrm{Re}}{}^{0.3978} \right) \tag{49}$$

The value of f_0 can be obtained by Colebrook-White correlation (1937) [1].

For laminar flow regime (N_{Re}<2300)

$$f_m = \frac{64}{N_{\mathrm{Re}}} \tag{50}$$

Turbulent (N_{Re}>2300)

$$\frac{1}{\sqrt{f_m}} = 1.74 - 2\log\left(\frac{2\varepsilon_D}{d} + \frac{18.7}{N_{\mathrm{Re}}\sqrt{f}}\right) \tag{51}$$

Or simplified by Jain (1976) [4]

$$\frac{1}{\sqrt{f_m}} = 1.14 - 2\log\left(\frac{\varepsilon_D}{d} + \frac{21.25}{N_{\mathrm{Re}}{}^{0.9}}\right) \tag{52}$$

The Colebrook-White correlation (1937) [1] will be used to compute the friction factor, f , as a function of the Reynolds number, N_{Re} , and the relative well surface roughness, ε_D.

$$\frac{1}{\sqrt{f}} = -4\log\left(.269\,\varepsilon_D + \frac{1.255}{N_{\mathrm{Re}}\sqrt{f}}\right) \tag{53}$$

3.4.3 Wellbore and Reservoir coupling: infinite-conductivity model

Coupling the reservoir transient response to the wellbore requires segmenting the wellbore into equal segment and calculating the reservoir response in that section and coupling that to the wellbore flow.
For infinite-conductivity horizontal wells, the wellbore hydraulics is ignored, which is not in line with reality in the field and fluid flow mechanics.

The calculation of the reservoir response is based on solution for infinite-conductivity model is achieved by applying Green's function and the product solution method with source function, presented by Gringarten and Ramey (1973).
The dimensionless pressure response for a horizontal well can be expressed using the method of source and sinks and Green's function as;

$$P_D(x_D, r_{wD}, t_D) = \int_0^{t_D} \int_x q_{hD}(x'_D, t'_D) G_{Di}(x_D - x'_D, t_D - t'_D) dx'_D dt'_D \quad (54)$$

Where

$G_{Di}(x_D, t_D)$ is the instantaneous point-source function given by

$$G_{Di}(x_D, y_D, z_D; x_{wD}, y_{wD}, z_{wD}, t_D) = \frac{\eta}{2L^2 t_D} \sqrt{\frac{k_Z}{k}} \exp\left[\frac{-\left(x_D{}^2 - y_{wD}{}^2\right)}{4t_D}\right]$$

$$\left\{1 + 2\sum_{n=1}^{\infty} \exp\left[\frac{-n^2\pi^2 t_D}{h_D^2}\right] \cos n\pi z_{wD} \cos n\pi z_D\right\} \quad (55)$$

To obtain the infinite-conductivity horizontal well solution, eq. 54 is discretized in space and time. The horizontal section is divided into M segments with an equal length. The equation was given by Ozkan et al. (1995) [17] as

$$P_D(x_{Dj}, r_{wD}, t_D) = \int_0^{t_D} \sum_{i=1}^{M} q_{hDi}(t'_D) G_{Di}(x_{Dj}, t_D - t'_D) dt'_D \quad (56)$$

And the $G_{Di}(x_D, t_D)$ becomes

$$G_{Di}(x_{Dj}, t_D) = \frac{\sqrt{\pi}}{4} \left(\begin{array}{l} \left[erf\left(\frac{x_{Dj} - \frac{2i-2}{M}}{2\sqrt{t_D}} \right) - erf\left(\frac{x_{Dj} - \frac{2i}{M}}{2\sqrt{t_D}} \right) \right] \\ \left\{1 + 2\sum_{n=1}^{\infty} \exp\left(-n^2\pi^2 L^2{}_D t_D\right) \cos n\pi\left(z_{wD} + r_{wD}\right) \cos n\pi z_{wD}\right\} \frac{1}{\sqrt{t_D}} \end{array} \right) \quad (57)$$

Where

$x_{Di} = \frac{2i-1}{M}$ is the dimensionless distance along the horizontal wellbore.

Eq. 56 can be discretized in time as follows:

$$P_D(x_{Dj}, r_{wD}, t_D) = \sum_{k=1}^{N} \int_{k=1}^{Dk} \sum_{i=1}^{M} q_{hDi}(t'_D) G_{Di}(x_{Dj}, t_D - t'_D) dt'_D \quad (58)$$

Where N is the number of time points.

If q_{hDi} is assumed to be constant during the time steps $\left(t_{Dk} - t_{Dk-1}\right)$ then it becomes:

$$P_D(x_{Dj}, r_{wD}, t_D) = \widehat{P}_D(x_{Dj}, r_{wD}, t_{DN}) + \sum_{i=1}^{M} q_{hDi}(t_{DN}) \int_0^{t_{DN}-t_{Dk}} G_{Di}(x_{Dj}, t_D - t'_D) dt'_D \quad (59)$$

Where

$$\widehat{P}_D(x_{Dj}, r_{wD}, t_{DN}) = \sum_{k=1}^{N-1} \sum_{i=1}^{M} q_{hDi}(t_{Dk}) \left[\int_0^{t_{DN}-t_{Dk-1}} G_{Di}(x_{Dj}, t'_D) dt'_D - \int_0^{t_{DN}-t_{Dk}} G_{Di}(x_{Dj}, t'_D) dt'_D \right] \quad (60)$$

For infinite-conductivity well, the wellbore pressure is;

$$P_{wD}(t_{DN}) - \widehat{P}_D(x_{Dj}, r_{wD}, t_{DN}) = \sum_{i=1}^{M} q_{hDi}(t_{DN}) \int_0^{t_{DN}-t_{Dk}} G_{Di}(x_{Dj}, t_D - t'_D) dt'_D \quad (61)$$

Then

$$P_{wD}(t_{DN}) - \sum_{k=1}^{N-1} \sum_{i=1}^{M} q_{hDi}(t_{Dk}) \left[\int_0^{t_{DN}-t_{Dk-1}} G_{Di}(x_{Dj}, t'_D) dt'_D - \int_0^{t_{DN}-t_{Dk}} G_{Di}(x_{Dj}, t'_D) dt'_D \right]$$
$$= \sum_{i=1}^{M} q_{hDi}(t_{DN}) \int_0^{t_{DN}-t_{Dk}} G_{Di}(x_{Dj}, t_D - t'_D) dt'_D \quad (62)$$

Eq. 62 is evaluated at the center of each segment, which results in a set of M equations in M+ 1 unknown. Unknowns are $q_{hDi}(t_{DN})$ for i=1,2,….,M, and $P_{wD}(t_{DN})$. An additional equation is required to solve this set of equations can be obtained by setting the total flux entering the wellbore is equal to the sum of the fluxes entering each segment.

Or

$$\sum_{i=1}^{M} q_{hi}(t) = q_t \text{ or } \sum_{i=1}^{M} q_{hDi}(t_{DN}) = M \quad (63)$$

The mechanical skin factor along the horizontal section in each segment can be incorporated into eq. 63 then the equation was given by Al-Otaibi et al. (2005) [39] as

$$P_{wD}(t_{DN}) - \sum_{k=1}^{N-1} \sum_{i=1}^{M} q_{hDi}(t_{Dk}) \left[\int_0^{t_{DN}-t_{Dk-1}} G_{Di}(x_{Dj}, t'_D) dt'_D - \int_0^{t_{DN}-t_{Dk}} G_{Di}(x_{Dj}, t'_D) dt'_D \right]$$
$$= \sum_{i=1}^{M} q_{hDi}(t_{DN}) \int_0^{t_{DN}-t_{DN-1}} G_{Di}(x_{Dj}, t_D - t'_D) dt'_D + q_{hDi}(t_{DN}) S_{hmj} \quad (64)$$

The equation can be solved in forward manner in time, which requires a solution of the following matrix;

$$\begin{Bmatrix} 1 & A_{11} & A_{21} & A_{31} & A_{41} & A_{51} & -- & -- & A_{m-1,1} & A_{m1} \\ 1 & A_{12} & A_{22} & A_{32} & A_{42} & A_{52} & -- & -- & A_{m-1,2} & A_{m2} \\ 1 & A_{13} & A_{23} & A_{33} & A_{43} & A_{53} & -- & -- & A_{m-1,3} & A_{m3} \\ 1 & A_{14} & A_{24} & A_{34} & A_{44} & A_{54} & -- & -- & A_{m-1,4} & A_{m4} \\ 1 & A_{15} & A_{25} & A_{35} & A_{45} & A_{55} & -- & -- & A_{m-1,5} & A_{m5} \\ 1 & -- & -- & -- & -- & -- & -- & -- & -- & -- \\ 1 & -- & -- & -- & -- & -- & -- & -- & -- & -- \\ 1 & A_{1,m-1} & A_{2,m-1} & A_{3,m-1} & & -- & & & A_{m-1,m-1} & A_{m,m-1} \\ 1 & A_{1,m} & A_{2,m} & A_{3,m} & & -- & -- & & A_{m-1,m} & A_{m,m} \\ 0 & 1 & 1 & 1 & 1 & 1 & -- & -- & 1 & 1 \end{Bmatrix} \begin{Bmatrix} P_{wD} \\ q_{hD1} \\ q_{hD2} \\ q_{hD3} \\ q_{hD4} \\ q_{hD5} \\ .... \\ .... \\ q_{hDM-1} \\ q_{hDM} \end{Bmatrix} = \begin{Bmatrix} B_1 \\ B_2 \\ B_3 \\ B_4 \\ B_5 \\ B_6 \\ .... \\ B_{M-1} \\ B_M \\ M \end{Bmatrix} \tag{65}$$

Where matrix coefficients, $A_{i,j}$, are given by

$$A_{i,j} = -\left(\int_0^{t_{DN}-t_{DN-1}} G_{Di}(x_{Dj}, t_D - t'_D) dt'_D + q_{hDi}(t_{DN}) S_{hmj} \right) \tag{66}$$

Where the skin is only calculated when i=j. The right-hand vector B_j is obtained by evaluating the following expression at the center of each segment, x_{Dj};

The computation of the right-hand side vector B_j given by

$$B_j = \sum_{k=1}^{N-1} \sum_{i=1}^{M} q_{hDi}(t_{Dk}) \left[\int_0^{t_{DN}-t_{Dk-1}} G_{Di}(x_{Dj}, t'_D) dt'_D - \int_0^{t_{DN}-t_{Dk}} G_{Di}(x_{Dj}, t'_D) dt'_D \right] \tag{67}$$

And

$$G_{Di}(x_{Dj}, t_D) = \frac{\sqrt{\pi}}{4} \left(\left[erf\left(\frac{x_{Dj} - \frac{2i-2}{M}}{2\sqrt{t_D}} \right) - erf\left(\frac{x_D j - \frac{2i}{M}}{2\sqrt{t_D}} \right) \right] \left\{ 1 + 2\sum_{n=1}^{\infty} \exp\left(-n^2 \pi^2 L^2{}_D t_D\right) \cos n\pi\left(z_{wD} + r_{wD}\right) \cos n\pi z_{wD} \right\} \frac{1}{\sqrt{t_D}} \right) \tag{68}$$

$$P_D(x_D, y_D, z_D; z_{wD}, L_D, t_D) = -\frac{\beta}{8L_D} E_i\left[-\frac{(z_D - z_{wD})^2 / L^2{}_D + y^2{}_D}{4t_D}\right] \quad (69)$$

Where

$$\beta = \begin{Bmatrix} 2 & for\ |x_D| < \sqrt{\frac{k}{k_x}} \\ 1 & for\ |x_D| = \sqrt{\frac{k}{k_x}} \\ 0 & for\ |x_D| > \sqrt{\frac{k}{k_x}} \end{Bmatrix} \quad (70)$$

Where the horizontal well skin factor is defined by Ozkan and Raghavan (1997) as:

$$S_{hm} = \frac{P_{hi}(r_w, x, t) - P_s(r_w + \Delta r_{ws}, x, t)}{\frac{Lk_{\tilde{r}}}{kh}\left(\tilde{r}\frac{\partial P}{\partial \tilde{r}}\right)_{\tilde{r}=r_w, x}} = \frac{\frac{kh}{141.2qB\mu}\Delta P_s}{\tilde{q}_{hDi}} = \frac{h}{2L_H}\frac{k}{k_{\tilde{r}}}\left(\frac{k_{\tilde{r}}}{k_s} - 1\right)\ln\frac{\tilde{r}_s}{r_w} \quad (71)$$

The dimensionless flux profile in an infinite-conductivity well for the example published in literature by Ozkan et al. (1993), at early and late times, t_D's, are shown in Fig.7.

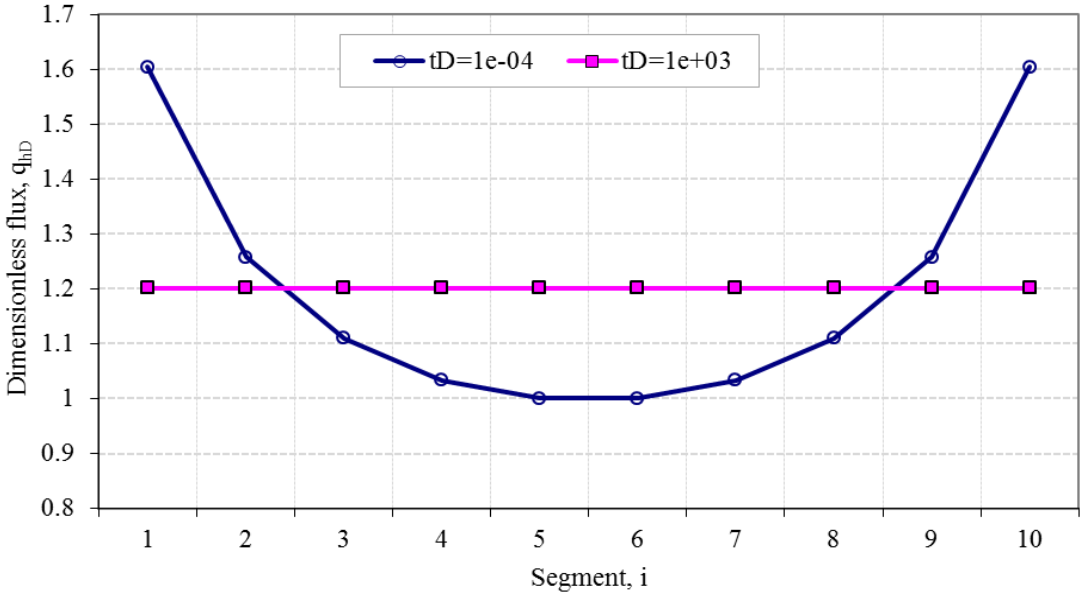

Fig. 7- Dimensionless flux profile in an infinite-conductivity at early and late times.

The pressure response and pressure derivative for the infinite-conductivity horizontal well is shown in Fig.8.

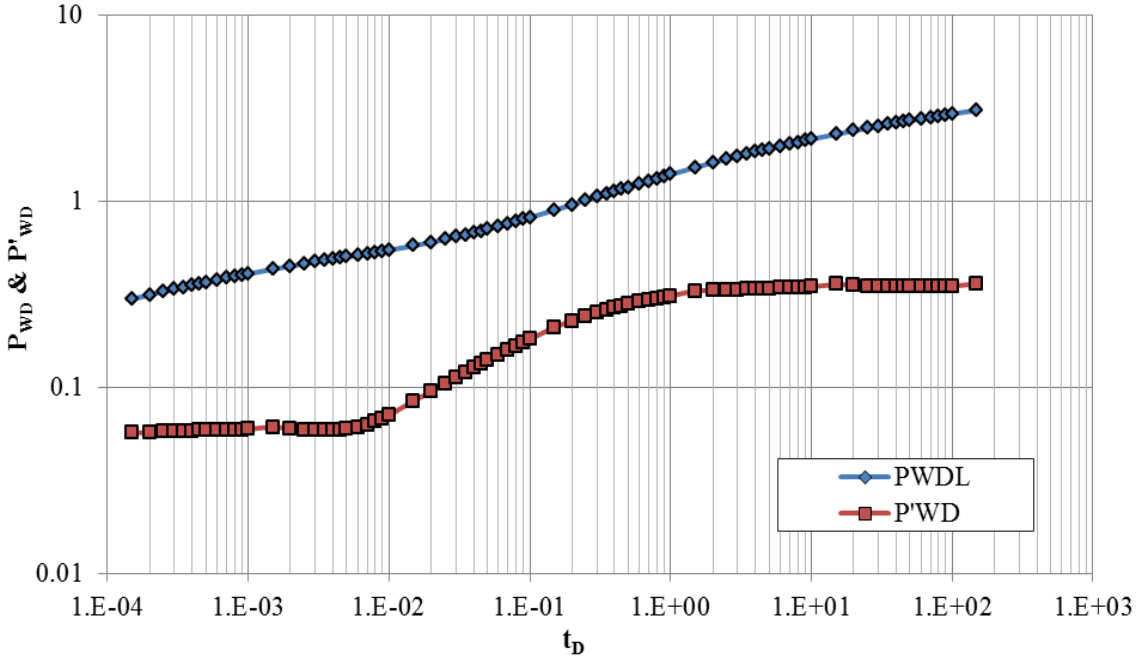

Fig. 8- Pressure response and pressure derivative for the infinite-conductivity horizontal well

3.4.4 Wellbore and Reservoir coupling: finite-conductivity model

The solution for the finite-conductivity horizontal well solution is the same as the solution for the infinite conductivity well but with the wellbore hydraulics considered in calculations. The wellbore hydraulics effect adds a pressure drop to the pressure formula analogous to the mechanical skin factor but function of the flow rate. The wellbore hydraulics is not a linear function of flow rate. This nonlinear function makes it more complicated to solve and warrants using nonlinear regression or solution to find best estimates as the solutions will be based on estimation of flow rates which are function of the empirical correlation of the friction factor.

Wellbore Hydraulics Formulations

Considering a single-phase liquid flow in wellbore, the wellbore hydraulics can be assimilated into calculation of the wellbore pressure.

Let $q_h(x)$ be the flux along the wellbore sandface. The total flow rate at the heel end $(x=0)$, q_t can be expressed as the integration of flux with respect to x' from $x=0$ to $x=L_h$

$$q_t = \int_0^{L_h} q_h\,(x')dx' \tag{72}$$

The flow rate at any point (x) inside the wellbore, $q_{hc}(x)$ is calculated by

$$q_{hc}(x) = \int_x^{L_h} q_h\,(x')dx' \tag{73}$$

Thus

$$\left(\frac{\partial q_{hc}}{\partial x}\right)_x = -q_h(x) \tag{74}$$

And

$$\left(\frac{\partial^2 q_{hc}}{\partial x^2}\right)_x = -\frac{\partial q_h}{\partial x} \tag{75}$$

From the above equations, the wellbore flow rate and pressure at a given point are dependent on flux distribution (wellbore hydraulics).

For a single-phase liquid flow, the pressure gradient in a horizontal wellbore is mainly due frictional pressure losses, which can be expressed by

$$\frac{dP_h}{dx} = 2\frac{f\rho v^2}{144 g_c d} \tag{76}$$

Where f is the Fanning friction factor.

For any location with local flow rate of $q_{hc}(x)$

$$\frac{dP_h}{dx} = E\ f\ q_{hc}^2 \tag{77}$$

Where

$$E = 9.117 \times 10^{-13} \frac{\rho}{\pi^2 r^5{}_w} \tag{78}$$

Pressure gradient can be expressed in terms of Reynolds number, $N_{\mathrm{Re}t}$ is given by;

$$N_{\mathrm{Re}t} = 6.166x10^{-2} \frac{\rho q_{hc}}{r_w \mu} \tag{79}$$

Horizontal well conductivity

Horizontal well conductivity is used to describe the significance of pressure gradient inside horizontal wellbores.

$$C_{hD} = 3.66x10^{13} \frac{r_w{}^4}{khL/2} \tag{80}$$

Differentiating equation 77,

$$\frac{d^2 P_h}{dx^2} = E\left(q_{hc}^2 \frac{\partial f}{\partial x} + 2 f q_{hc} q_h \right) \tag{81}$$

Using $\left(\frac{\partial q_{hc}}{\partial x} \right)_x = -q_h(x)$ and integrating twice,

$$\left(\frac{dP_h}{dx} \right)_{x=0} = E\ f\ q^2 \tag{82}$$

$$\frac{dP_h}{dx}(x) - \frac{dP_h}{dx}(0) = \frac{dP_h}{dx}(x) - Ef_t\ q_t^2 = E \int_0^x \left(q_{hc}^2 \frac{\partial f}{\partial x'} - 2 f q_{hc} q_h \right) dx_1 \tag{83}$$

Integrating using boundary conditions yields, Ozkan et al. (1995)[17]

$$P_h(x,t) - P_{wf}(t) = Ef_t\, q_t^2(x - x_0) + E\int_0^x \int_0^{x'} \left(q_{hc}^2 \frac{\partial f}{\partial x''} - 2 f q_{hc} q_h \right) dx'' dx' \quad (84)$$

Where f_t is the apparent friction factor at the total flow rate q_t.

Using the definition of hydraulic conductivity of a horizontal well, to describe the pressure gradient inside wellbore using pseudo-permeability, k_w, by analogy to Darcy's law,

$$C_{hD} = 7.395x10^{13} \frac{r_w^{\ 4}}{khL_h} \quad (85)$$

And multiplying by a factor of $\frac{kh}{(141.2q_t\mu)}$, equation 84 becomes,

$$\frac{kh}{(141.2q_t\mu)}\left[P_h(x,t) - P_{wf}(t)\right] = \frac{4\pi}{C_{hD}L_h}\left[x + \frac{1}{f_t\, q_t^2}\int_0^x \int_0^{x'} \left(q_{hc}^2 \frac{\partial f}{\partial x''} - 2 f q_{hc} q_h \right) dx'' dx' \right] \quad (86)$$

Incorporating the parameter of Reynolds's number and simplifying,

$$\frac{kh}{(141.2q_t\mu)}\left[P_h(x,t) - P_{wf}(t)\right] = \frac{4\pi}{C_{hD}L_h}\left[x - \frac{1}{L_h}\int_0^x \int_0^{x'} \left(\frac{D_f}{N_{\mathrm{Re}} f_t} \right) q_{hD} dx'' dx' \right] \quad (87)$$

In dimensionless form, we have

$$P_{wD}(t_D) - P_D(x_D, t_D) = \frac{N_{\mathrm{Re}t} f_t}{16} \frac{\pi}{C_{hD}} \left(2x_D - \int_0^x \int_0^{x'} \left(\frac{D_f}{N_{\mathrm{Re}t} f_t} \right) q_{hD} dx'' dx' \right) \quad (88)$$

Where,

$$D_f = N_{\mathrm{Re}}^{\ 2} \frac{df}{dN_{\mathrm{Re}}} + 2N_{\mathrm{Re}} f \quad (89)$$

The local friction factor, f, is determined as a function of N_{Re} and ε_D. N_{Re} and f_t on the other hand, are known from the given fluid and well data and the production rate. For production wells, the friction factor is given by the following correlations (Ouyang et al.(1996) [18]);

$$f = \begin{cases} \dfrac{64}{N_{\mathrm{Re}}}\left(1 + 0.04304\, N_{\mathrm{Re}}{}^{0.6142}\right) & \text{for laminar flow } (N_{\mathrm{Re}} < 2300) \\ \dfrac{1}{\left(1.17 - 2\log\left(\dfrac{\varepsilon}{d}\dfrac{21.25}{N_{\mathrm{Re}}{}^{0.9}}\right)^{2}\right)}\left(1 - 0.0153\, N_{\mathrm{Re}}{}^{0.3978}\right) & \text{for turnlent flow } (N_{\mathrm{Re}} \rangle 2300) \end{cases} \quad (90)$$

Coupling and Solution Approach

Based on the continuity of the pressure and flux along the sand face, P_D and q_{hD} are the same for both reservoir side and wellbore side. Hence, using the appropriate solution for P_D under any arbitrary flux distribution, q_{hD}, can obtain the coupling equation.

The coupling of the reservoir model with the wellbore model is to systematically investigate the effects of finite wellbore conductivity and different configurations of the well on the productivity of horizontal wells. From the results of previous sections, a linear system was developed including N+2M equations, in which N+M equations are from the reservoir model and M from the wellbore model. At the same time, they are N+2M unknowns which include inflow flux and pressure at each of M nodes over wellbore, and pressures or influxes on N outer boundary nodes.

The reservoir model and wellbore model should be solved simultaneously to determine the unknown pressures and influxes. However, since the wellbore model is nonlinear, the coefficients in the equation are functions of unknown influxes), the approach of Newton-Raphson is often used to solve this type of problem.

For pseudo-radial flow in a slab reservoir, and using Ozkan & Raghvan solutions (1993) using the method of source and sinks and Green's function the dimensionless reservoir pressure can be expressed as;

$$P_D(x_D, r_{wD}, t_D) = \int_0^{t_D}\int_x q_{hD}(x'_D, t'_D) G_{Di}(x_D - x'_D, t_D - t'_D)\, dx'_D dt'_D \quad (91)$$

Where

$G_{Di}(x_D, t_D)$ is the instantaneous point-source function given by

$$G_{Di}(x_D, y_D, z_D; x_{wD}, y_{wD}, z_{wD}, t_D) = \frac{\eta}{2L^2 t_D}\sqrt{\frac{k_Z}{k}}\exp\left[\frac{-\left({x_D}^2 - {y_{wD}}^2\right)}{4t_D}\right]$$

$$\times\left\{1 + 2\sum_{n=1}^{\infty}\exp\left[\frac{-n^2\pi^2 t_D}{h_D^2}\right]\cos n\pi z_{wD}\cos n\pi z_D\right\} \quad (92)$$

Putting this into coupling formula to get the wellbore pressure, P_{wD} for a finite-conductivity horizontal well (wellbore hydraulics effect included) well at any location along the horizontal section and any time, as in eq. (88), yields

$$P_{wD}(t_D) - P_D(x_D, r_{wD}, t_D) = \frac{N_{\mathrm{Re}t} f_t}{16}\frac{\pi}{C_{hD}}\left(2x_D - \int_0^{\mathrm{x}}\int_0^{x'}\left(\frac{D_f}{N_{\mathrm{Re}t} f_t}\right) q_{hD} dx'' dx'\right) \quad (93)$$

The horizontal well flow equation for finite-conductivity model can be solved by discretizing both in space and time. To discretize eq. (93) in space, we divide the horizontal section of the well into M equal segments and denoting the center of each segment as x_{Dj}. The double integral on the right side of the equation can be discretized as follows;

$$\int_{x_{wD}}^{x_D}\int^{x_D'} Dq_{hD} dx_D'' dx_D' = \sum_{i=1}^{j-1}\left(x_{Dj} - i\Delta x_D + \frac{\Delta x_D}{2}\right)\Delta x_D D_i q_{hDi} + \frac{\Delta x_D^2}{8} D_j q_{hDj} \quad (94)$$

In equation (93), Di and q_{hDi} are evaluated at the center of the i^{th} segment and x_{Dj} is located at the center of the j^{th} segment. This yield,

$$P_{wD}(t_D) - P_D(x_D, t_D) = \frac{N_{\mathrm{Re}t} f_t}{16}\frac{\pi}{C_{hD}}\left(2x_D - \sum_{i=1}^{j-1}\left(x_{Dj} - i\Delta x_{Di} + \frac{\Delta x_D}{2}\right)\Delta x_{Di} D q_{hDi} + \frac{\Delta x_{Di}^2}{8} D_j q_{hDj}\right) \quad (95)$$

Similarly, the expression given in eq. (95) for the dimensionless reservoir pressure $P_D(x_D, r_{wD}, t_D)$ can be discretized as follows;

$$P_D(x_{Dj}, r_{wD}, t_D) = \int_0^{t_D} \sum_{i=1}^{M} q_{hDi}(t'_D) G_{Di}(x_{Dj}, t_D - t'_D) dt'_D \tag{96}$$

Where

$$G_{Di}(x_{Dj}, t_D) = \frac{\sqrt{\pi}}{4} \left(\left[erf\left(\frac{x_{Dj} - \frac{2i-2}{M}}{2\sqrt{t_D}} \right) - erf\left(\frac{x_{Dj} - \frac{2i}{M}}{2\sqrt{t_D}} \right) \right] \left\{ 1 + 2\sum_{n=1}^{\infty} \exp\left(-n^2\pi^2 L^2{}_D t_D\right) \cos n\pi\left(z_{wD} + r_{wD}\right) \cos n\pi z_{wD} \right\} \right) \tag{97}$$

Discretizing eq. (95) in time,

$$P_D(x_{Dj}, r_{wD}, t_D) = \sum_{k=1}^{N} \int_{k=1}^{Dk} \sum_{i=1}^{M} q_{hDi}(t'_D) G_{Di}(x_{Dj}, t_D - t'_D) dt'_D \tag{98}$$

Where N is the number of time points.

If q_{hDi} is assumed to be constant during the time steps $\left(t_{Dk} - t_{Dk-1}\right)$ then it becomes:

$$P_D(x_{Dj}, r_{wD}, t_D) = \widehat{P}_D(x_{Dj}, r_{wD}, t_{DN}) + \sum_{i=1}^{M} q_{hDi}(t_{DN}) \int_0^{t_{DN} - t_{Dk}} G_{Di}(x_{Dj}, t_D - t'_D) dt'_D \tag{99}$$

where

$$\widehat{P}_D(x_{Dj}, r_{wD}, t_{DN}) = \sum_{k=1}^{N-1} \sum_{i=1}^{M} q_{hDi}(t_{Dk}) \left[\int_0^{t_{DN} - t_{Dk-1}} G_{Di}(x_{Dj}, t'_D) dt'_D - \int_0^{t_{DN} - t_{Dk}} G_{Di}(x_{Dj}, t'_D) dt'_D \right] \tag{100}$$

Then, the finite-conductivity horizontal well, the wellbore pressure becomes;

$$P_{wD}(t_{DN}) - \widehat{P}_D(x_{Dj}, r_{wD}, t_{DN}) - \sum_{i=1}^{M} q_{hDi}(t_{DN}) \int_0^{t_{DN} - t_{Dk}} G_{Di}(x_{Dj}, t_D - t'_D) dt'_D =$$
$$\frac{N_{\mathrm{Re}t} f_t}{16} \frac{\pi}{C_{hD}} \left(2x_{Dj} - \sum_{i=1}^{j-1} \left(x_{Dj} - i\Delta x_{Di} + \frac{\Delta x_{Di}}{2} \right) \Delta x_{Di} D q_{hDi} + \frac{\Delta x_{Di}^2}{8} D_j q_{hDj} \right) \tag{101}$$

Eq. (101) is evaluated at the center of each segment, which results in a set of M equations in M+ 1 unknowns. Unknowns are $q_{hDi}(t_{DN})$ for i=1,2,….,M, and $P_{wD}(t_{DN})$. The additional equation is required to solve this set of equations can be obtained by setting the total flux entering the wellbore is equal to the sum of the fluxes entering each segment, that is

$$\sum_{i=1}^{M} q_{hDi}(t_{DN}) = M \tag{102}$$

By dividing the wellbore into M segments, and assuming the segment sequential number starts from the heel end to the toe end. The dimensionless x-coordinate for an observation point at the center of the jth segment is given by

$$x_{Dj} = \frac{(2j-1)}{M} \tag{103}$$

The summation of the dimensionless flux as stated earlier is M. That is

$$\int_0^1 q_{hD}\, dx'_D = \sum_{i=1}^{M} \int_{\frac{i-1}{M}}^{i/M} q_{hD}(i)\, dx'_D \cong \sum_{i=1}^{M} q_{hD}(i)\frac{1}{M} \tag{104}$$

And

$$\sum_{i=1}^{M} q_{hD}(i)\frac{1}{M} = M \tag{105}$$

Then, the discrete form for the pressure response equation for the jth segment is given by Ozkan et al. (1995)[18];

$$P_{wD}(t_{DN}) - \widehat{P}_D(x_{Dj}, r_{wD}, t_{DN}) - \sum_{i=1}^{M} q_{hDi}(t_{DN}) \int_0^{t_{DN}-t_{Dk}} G_{Di}(x_{Dj}, t_D - t'_D) dt'_D =$$
$$\frac{N_{\mathrm{Re}t} f_t}{16} \frac{\pi}{C_{hD}} \left(2x_{Dj} - \sum_{i=1}^{j-1} \left(x_{Dj} - i\Delta x_D + \frac{\Delta x_D}{2} \right) \Delta x_D D_i q_{hDi} + \frac{\Delta x_D^2}{8} D_j q_{hDj} \right) \tag{106}$$

Or

$$P_{wD}(t_{DN}) - \widehat{P}_D(x_{Dj}, r_{wD}, t_{DN}) - \sum_{i=1}^{M} q_{hDi}(t_{DN}) \int_0^{t_{DN}-t_{Dk}} G_{Di}(x_{Dj}, t_D - t'_D) dt'_D =$$
$$\frac{N_{\mathrm{Re}t} f_t}{8} \frac{\pi}{C_{hD}} \left(\frac{2j-1}{M} \right) - \frac{\pi}{16 C_{hD}} \left(\sum_{i=1}^{j-1} \left(\frac{j-i}{M^2} \right) D_i q_{hDi} + \frac{D_j q_{hDj}}{8M^2} \right) \tag{107}$$

Where

$$C_{hD} = 7.395x10^{13} \frac{r_w^{\ 4}}{khL_h} \tag{108}$$

Eq. (107) can be written in this form,

$$P_{wD}(t_{DN}) - \sum_{i=1}^{M} q_{hDi}(t_{DN}) \int_0^{t_{DN}-t_{Dk}} G_{Di}(x_{Dj}, t_D - t'_D) dt'_D + \frac{\pi}{16 C_{hD}} \left(\sum_{i=1}^{j-1} \left(\frac{j-i}{M^2} \right) D_i q_{hDi} + \frac{D_j q_{hDj}}{8M^2} \right) =$$
$$\frac{N_{\mathrm{Re}t} f_t}{8} \frac{\pi}{C_{hD}} \left(\frac{2j-1}{M} \right) + \widehat{P}_D(x_{Dj}, r_{wD}, t_{DN}) \tag{109}$$

If the integral $\int_0^{t_{DN}-t_{Dk}} G_{Di}(x_{Dj}, t_D - t'_D) dt'_D$ is made to be defined as variable $\tilde{s}_{ij}$

Then eq. (109) becomes

$$P_{wD}(t_{DN}) - \sum_{i=1}^{M} q_{hDi}(t_{DN}) . \tilde{s}_{ij} + \frac{\pi}{16 C_{hD}} \left(\sum_{i=1}^{j-1} \left(\frac{j-i}{M^2} \right) D_i q_{hDi} + \frac{D_j q_{hDj}}{8M^2} \right) =$$
$$\frac{N_{\mathrm{Re}t} f_t}{8} \frac{\pi}{C_{hD}} \left(\frac{2j-1}{M} \right) + \widehat{P}_D(x_{Dj}, r_{wD}, t_{DN}) \tag{110}$$

Further simplifying,

$$P_{wD}(t_{DN}) - \sum_{i=1}^{j-1} q_{hDi}(t_{DN}).\tilde{s}_{ij} - \sum_{i=j+1}^{M} q_{hDi}(t_{DN}).\tilde{s}_{ij} + \frac{\pi}{16\,C_{hD}}\left(\sum_{i=1}^{j-1}\left(\frac{j-i}{M^2}\right)D_i q_{hDi} + \frac{D_j q_{hDj}}{8M^2}\right) = \frac{N_{\mathrm{Re}t}\, f_t}{8}\frac{\pi}{C_{hD}}\left(\frac{2j-1}{M}\right) + \hat{P}_D(x_{Dj}, r_{wD}, t_{DN}) \quad (111)$$

Or

$$P_{wD}(t_{DN}) - \sum_{i=1}^{j-1}\left[\tilde{s}_{ij} - \frac{\pi}{16\,C_{hD}}\left(\frac{j-i}{M^2}\right)D_i\right]q_{hDi}(t_{DN}). - \sum_{i=j+1}^{M} q_{hDi}(t_{DN}).\tilde{s}_{ij} + \frac{\pi}{16\,C_{hD}}\left(\frac{D_j q_{hDj}}{8M^2}\right) = \frac{N_{\mathrm{Re}t}\, f_t}{8}\frac{\pi}{C_{hD}}\left(\frac{2j-1}{M}\right) + \hat{P}_D(x_{Dj}, r_{wD}, t_{DN}) \quad (112)$$

Eq. (112) can be written in the form of

$$P_{wD}(t_{DN}) - \sum_{i=1}^{M} q_{hDi}(t_{DN}).\left[H_{ji} - A_{ji}\right] = B_j,\ j = 1,....,M \quad (113)$$

Where

From eq. (113),

$$H_{ji} = \begin{cases} \frac{\pi}{16C_{hD}}\left(\frac{j-i}{M^2}\right)D_i & \text{for } i = 1,2,..., \text{j-1} \\ \frac{\pi}{16C_{hD}}\left(\frac{1}{8M^2}\right)D_i & \text{for } i = j \\ 0 & \text{for } i \rangle j \end{cases} \quad (114)$$

And

$$A_{ji} = \tilde{s}_{ij}\ ,\ j = 1,2,...,M$$

$$B_j = \frac{N_{\mathrm{Re}t} f_t}{8} \frac{\pi}{C_{hD}} \left(\frac{2j-1}{M} \right) + \hat{P}_D(x_{Dj}, r_{wD}, t_{DN}) \, , \; j = 1,2,...,M \tag{115}$$

Introducing the variable Q_i as follows;

$$Q_i = \begin{Bmatrix} \tilde{P}_{wD}(\mathrm{t_D}) & \text{for} \;\; i = 1 \\ q_{hDi} & \text{for} \;\; 1 \langle i \le M \end{Bmatrix} \tag{116}$$

This is to calculate the unknowns in this solution.

M+1 unknowns $\left(P_{wD}(t_{DN}) \text{ and } q_{hDi}(t_{DN}) \, i = 1,....,M \right)$

And M+1 equations

The equations can be written in a matrix form as follows;

$$\sum_{i=1}^{M+1} G_{ji} Q_i - B_j = 0 \qquad \text{for } 1 \le j \le M+1 \tag{117}$$

Where

$$G_{ji} = \begin{Bmatrix} 1 & \text{for} \;\; j \le M \;\; \& \;\; i = 1 \\ \left[H_{ji-1} - A_{ji-1} \right] & \text{for} \;\; j \le M \;\; \& \;\; i = 2,....,M \\ 1 & \text{for} \;\; j = M+1 \;\; \& \;\; 2 \le i \le M+1 \\ 0 & \text{for} \;\; j = M+1 \;\; \& \;\; i = 1 \end{Bmatrix} \tag{118}$$

Or

$$\begin{Bmatrix} 1 & G_{12} & -- & -- & G_{1\,m+1} \\ 1 & G_{22} & -- & -- & G_{2\,m+1} \\ 1 & - & - & - & - \\ 1 & - & - & - & - \\ 1 & G_{m2} & -- & -- & G_{m\,m+1} \\ 0 & 1 & -- & -- & 1 \end{Bmatrix} \begin{Bmatrix} P_{wD} \\ q_{hD1} \\ .... \\ .... \\ q_{hDM-1} \\ q_{hDM} \end{Bmatrix} = \begin{Bmatrix} B_1 \\ B_2 \\ .... \\ B_{M-1} \\ B_M \\ M \end{Bmatrix} \tag{119}$$

Where G_{ij} is a function of the flux distribution H_{ji} and other potential factors.

This nonlinear equation is solved by;

$$F(G_{ij}) = G(Q).Q - B \tag{120}$$

Or $$F_j = \sum_{i=1}^{M+1} G_{ij} Q_i - B_j \qquad \text{for } j = 1,....,M+1 \tag{121}$$

Where $F(G_{ij})$ is a (M+1) x1 vector in the form of

$$F(G_{ij}) = \begin{Bmatrix} F_1 \\ F_2 \\ F_3 \\ .. \\ .. \\ F_{M+1} \end{Bmatrix} \tag{122}$$

And $G(Q)$ is a square matrix with a dimension of (M+1) as defined on the left-hand side of eq. (121). B is a (M+1) x 1 vector as defined on the right-hand side of equation 120. Q is given in eq. (121). Using Newton-Raphson's iteration method the solution is obtained by iteration for the non-linear matrix problem.

$$\Delta Q^k = Q^{k+1} - Q^k \tag{123}$$

And

$$J(Q^k).\Delta Q^k = -F(Q^k) \tag{124}$$

Where $J(Q^k)$ is the Jacobian matrix which is defined as follows;

$$J(Q^k)=\begin{Bmatrix} \frac{\partial F_1}{\partial Q_1} \frac{\partial F_1}{\partial Q_2} \_ \_ \_ \_ \frac{\partial F_1}{\partial Q_M} \frac{\partial F_1}{\partial Q_{M+1}} \\ \frac{\partial F_2}{\partial Q_1} \frac{\partial F_2}{\partial Q_2} \_ \_ \_ \_ \frac{\partial F_1}{\partial Q_M} \frac{\partial F_1}{\partial Q_{M+1}} \\ \_ \_ \_ \_ \_ \_ \_ \_ \_ \_ \_ \_ \_ \_ \_ \_ \_ \_ \\ \_ \_ \_ \_ \_ \_ \_ \_ \_ \_ \_ \_ \_ \_ \_ \_ \_ \_ \\ \frac{\partial F_M}{\partial Q_1} \frac{\partial F_M}{\partial Q_2} \_ \_ \_ \_ \frac{\partial F_M}{\partial Q_M} \frac{\partial F_M}{\partial Q_{M+1}} \\ \frac{\partial F_{M+1}}{\partial Q_1} \frac{\partial F_{M+1}}{\partial Q_2} \_ \_ \frac{\partial F_{M+1}}{\partial Q_M} \frac{\partial F_{M+1}}{\partial Q_{M+1}} \end{Bmatrix} \tag{125}$$

From eq. (121) and using the chain rule for the derivative, given by Yula Tang et al. (2005) [38] as

$$\frac{\partial F_j}{\partial Q_i}=\sum_{i=1}^{M+1}\left[\frac{\partial G_{jl}}{\partial Q_i}Q_l+G_{jl}\frac{\partial Q_l}{\partial Q_i}\right] \tag{126}$$

Since $\frac{\partial G_{jl}}{\partial Q_i}=\frac{\partial H_{jl-1}}{\partial Q_i}$ and from eq. (114),

$$\frac{\partial G_{jl}}{\partial Q_i}=\frac{\partial H_{jl-1}}{\partial Q_i}=\begin{Bmatrix} \frac{\pi}{16C_{hD}}\left(\frac{j-(L-1)}{M^2}\right)\frac{\partial D_{l-1}}{\partial Q_i} & \text{for } i=1,2,...,\text{j-1} \\ \frac{\pi}{16C_{hD}}\left(\frac{1}{8M^2}\right)\frac{\partial D_{l-1}}{\partial Q_i}-\frac{\partial D_{l-1}}{\partial Q_i}D_i & \text{for } l\text{-}1=j \\ 0 & \text{for } l\text{-}1\rangle j \end{Bmatrix} \tag{127}$$

From eq. (121), $\frac{\partial Q_l}{\partial Q_i}=\begin{cases}\mathbf{0} & if\ L\neq i\\ \mathbf{1} & if\ L=i\end{cases}$ (128)

Since

$$D_L=N_{\mathrm{Re}}^2\frac{\partial f}{\partial N_{\mathrm{Re}}}+2N_{\mathrm{Re}}\ f\big|_l \tag{129}$$

Then

$$\frac{\partial D_L}{\partial Q_i} = 2N_{\mathrm{Re}} \frac{\partial N_{\mathrm{Re}}}{\partial Q_i} \left. \frac{df}{dN_{\mathrm{Re}}} \right|_l + N_{\mathrm{Re}}^2 \frac{\partial}{\partial Q_i} \left(\frac{\partial f}{\partial N_{\mathrm{Re}}} \right) + 2 \frac{\partial N_{\mathrm{Re}l}}{\partial Q_i} \left. f \right|_l + 2N_{\mathrm{Re}l} \left(\frac{\partial f}{\partial Q_i} \right) \quad (130)$$

Or

$$\frac{\partial D_L}{\partial Q_i} = \frac{\partial N_{\mathrm{Re}}}{\partial Q_i} \left\{ 4N_{\mathrm{Re}} \left. \frac{df}{dN_{\mathrm{Re}}} \right|_l + N_{\mathrm{Re}}^2 \left(\frac{\partial^2 f}{\partial N_{\mathrm{Re}}^2} \right) + 2 \left. f \right|_l \right\} \quad (131)$$

If the Reynolds number at the Lth segment is

$$N_{\mathrm{Re}} = N_{\mathrm{Re}i} \frac{\sum_{l+1}^{M+1} Q_i}{M} \quad (132)$$

Then,

$$\frac{\partial N_{\mathrm{Re}l}}{\partial Q_i} = \begin{cases} \mathbf{0} & if \quad i \le l \\ \dfrac{N_{\mathrm{Re}t}}{M} & if \quad i \rangle l \end{cases} \quad (133)$$

The computation of the Jacobian matrix involves the evaluation of the first and the second derivative of the friction factor with respect to Reynolds umber.

The procedure is setup to calculate the function, by Yula Tang et al. (2005) [38] as

$$Q_i = \begin{Bmatrix} \widetilde{P}_{wD}(\mathrm{t_D}) \\ q_{hDi} \end{Bmatrix} \text{ For } i = 1,2,...,\mathrm{M} \quad (134)$$

Where q_{hDi}'s & $\widetilde{P}_{wD}(\mathrm{t_D})$'s are part of the calculated function Q_i and interdependent variables.

Detailed procedure for calculating parameters for nonlinear model is shown in appendix-B.

Similar results are calculated for the finite-conductivity well as shown in Fig. 9 for different times.

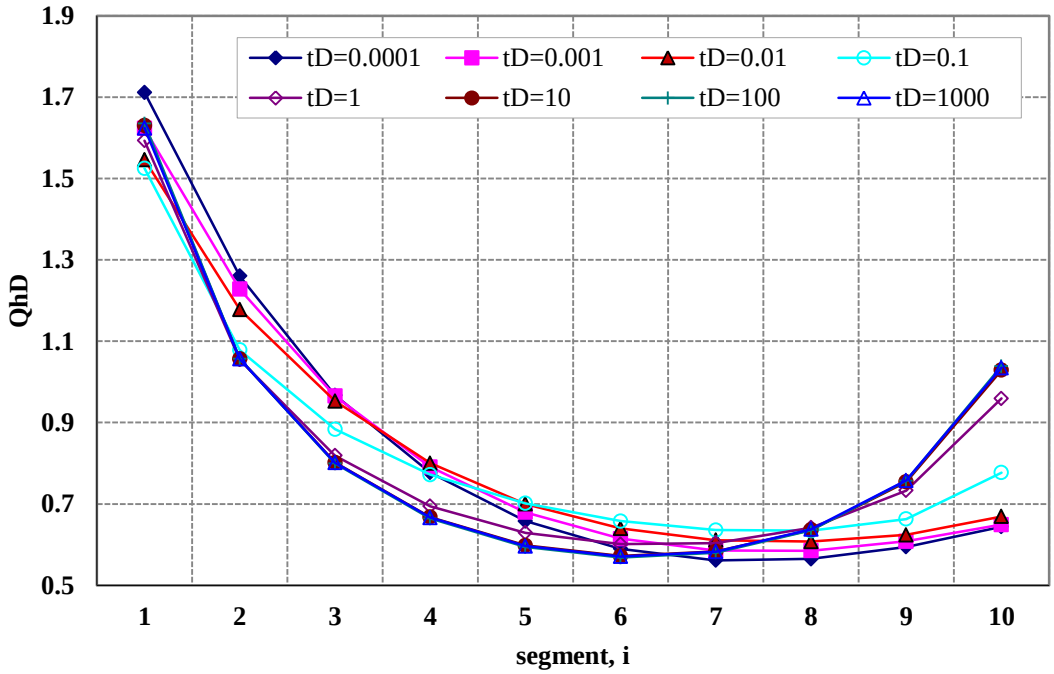

Fig. 9- Dimensionless influx profile for the finite-conductivity horizontal wells case

The pressure and pressure derivative are shown in Fig. 10.

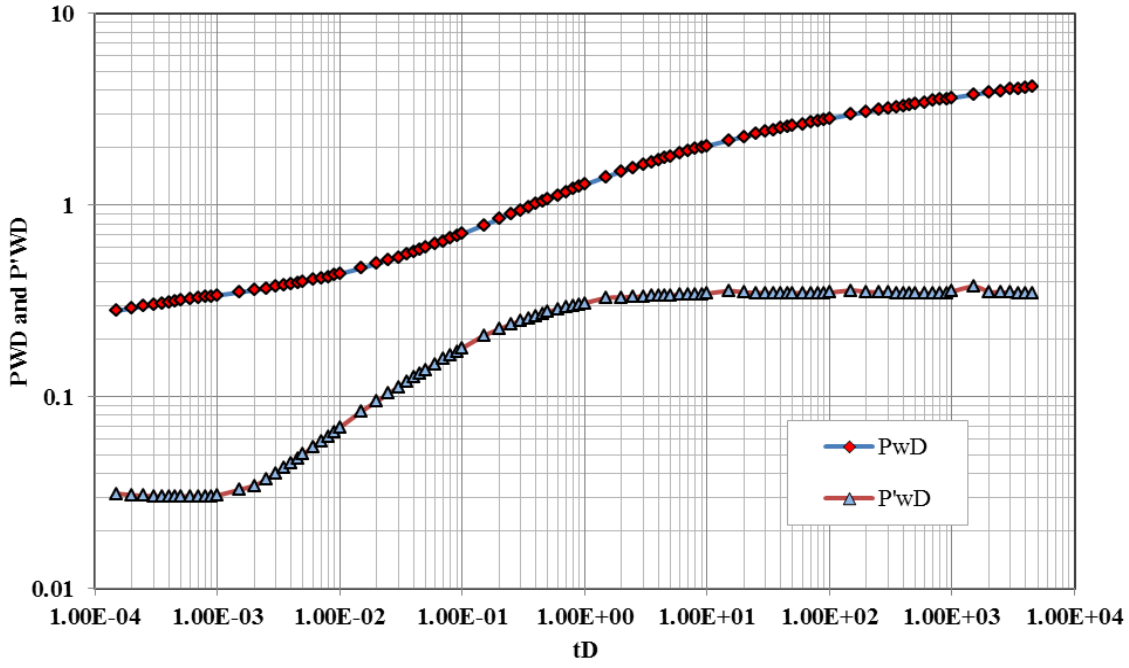

Fig. 10- pressure response and pressure derivative for the finite-conductivity horizontal well

Comparing the infinite and finite cases is shown in Fig. 11. The dimensionless pressure for both cases differs at early time due to the effect of wellbore hydraulics but vanishes when the reservoir response dominates.

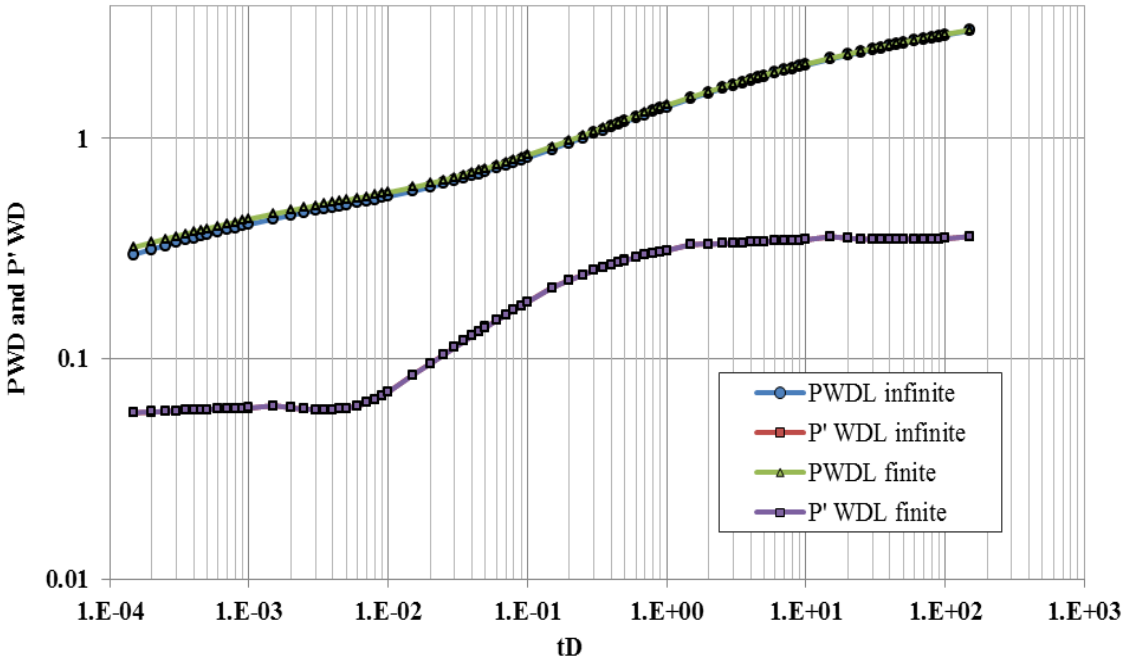

Fig. 11- Pressure response and pressure derivative for the infinite and finite conductivity horizontal wells.

3.4.5 Model Validation and Comparison

The model is validated against the results by Ozkan and Khamis (2003) for finite-conductivity horizontal well.

The well data is as follows;

Q, STBD=	2000
L, ft =	2000
r_w, ft =	0.165
h, ft =	100
K_x, md =	50
K_y, md =	100
K_z, md =	25
X, ft =	1000
Y, ft =	3000
Z, ft =	50

Table 3.1 Ozkan case data

The results for the flux distribution along the finite-conductivity horizontal well in the example are shown in Fig. 12 for two time periods and compared with results by Ozkan & Khamis (2003) for the same case for model validation.

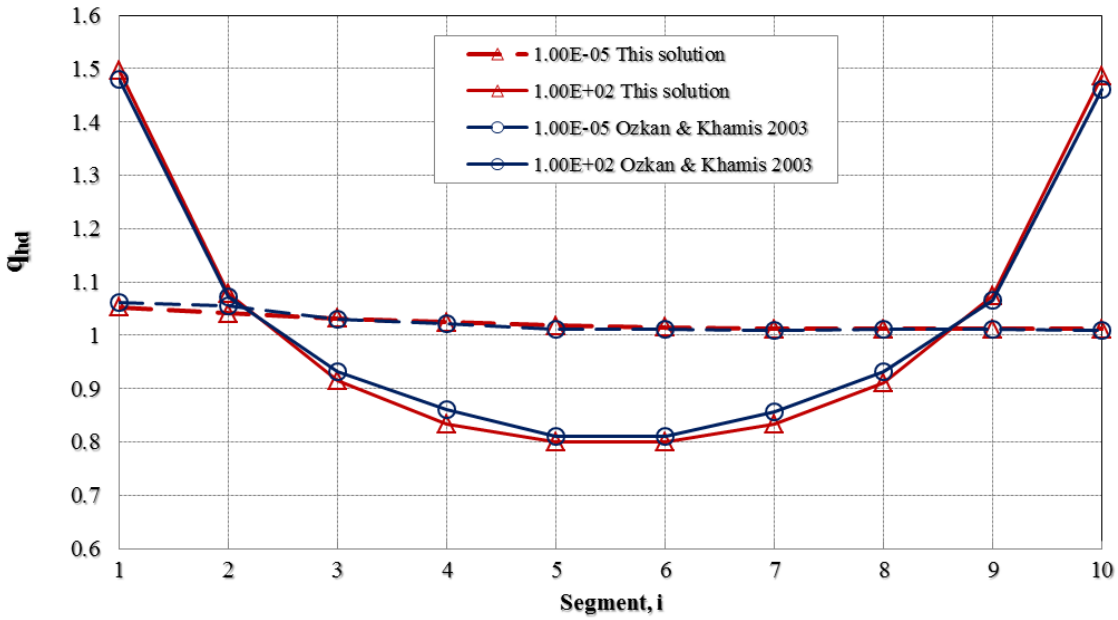

Fig. 12- Dimensionless flux profile for finite-conductivity horizontal well example by Ozkan(2003)

Similarly for the transient pressure response of the well is shown with the pressure derivative curve in Fig. 13. The two plots indicated a good comparison of the two results for both pressure and derivative, and the flux values.

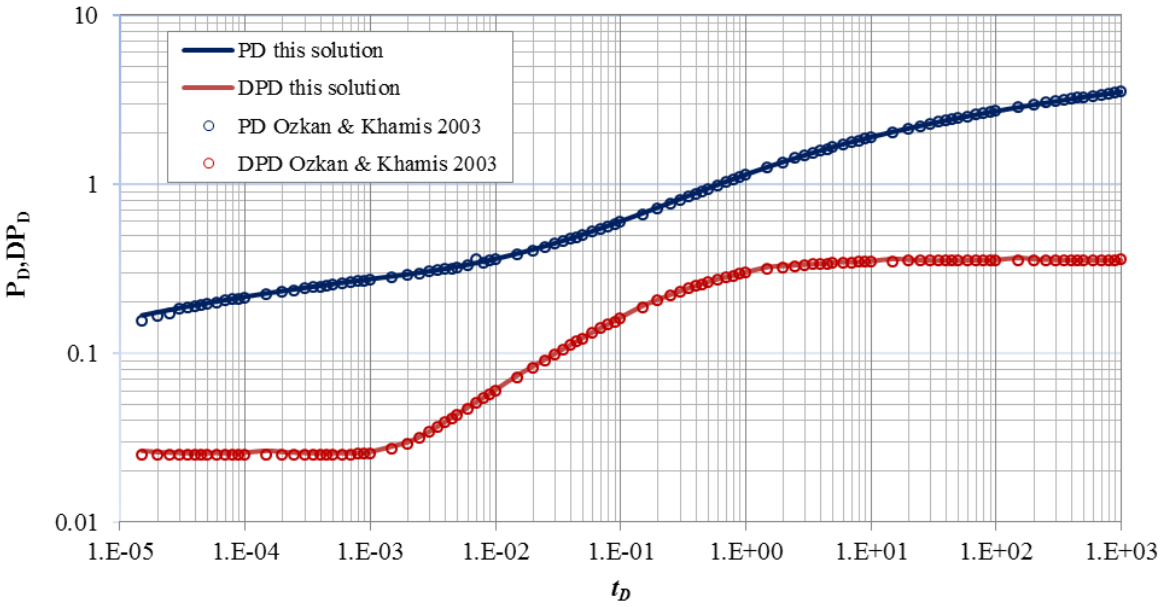

Fig. 13- Pressure response and pressure derivative for the infinite and finite conductivity horizontal wells

3.5 Semi analytical Model for the U-shaped Well

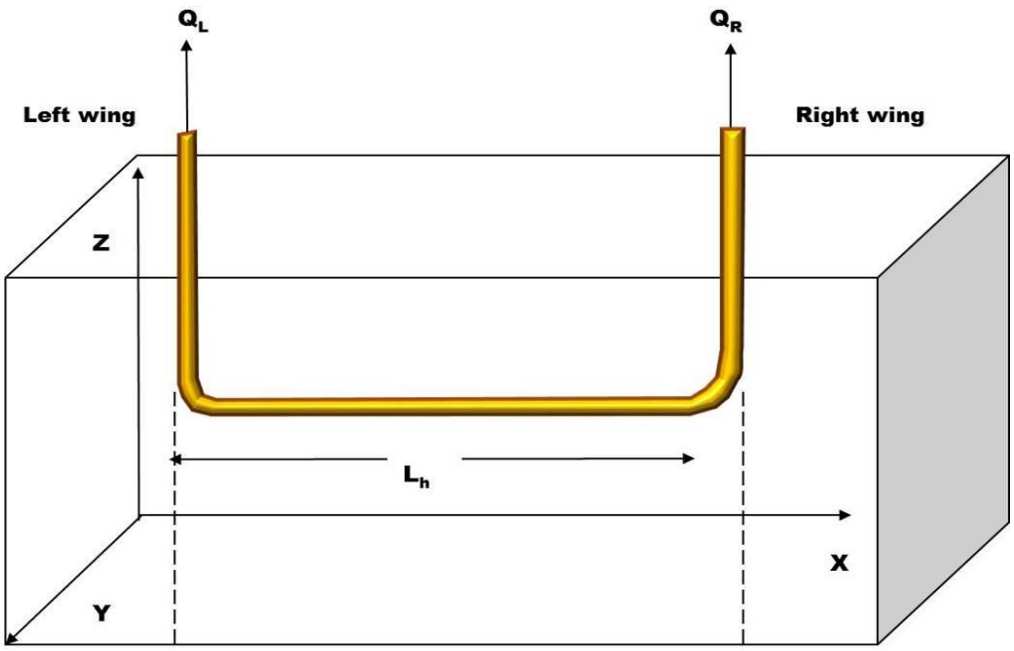

Fig. 14- A U-shaped horizontal well schematic

In well testing, it is generally assume that the reservoir is at uniform pressure P_i before production. So, the initial condition is

$$p(R,t) = p_i \qquad R \in \Omega,\ t = 0 \tag{135}$$

The boundary conditions involved can be classified as follows:

For outer boundaries:

1. Constant pressure boundary condition (Dirichlet boundary)

$$p(R,t) = p_i \qquad on\ S_i,\ t \rangle 0 \tag{136}$$

2. No-flow boundary condition (Neumann boundary)

$$\frac{\partial p}{\partial \eta_i} = 0 \quad on\ S_i,\ t\rangle 0 \tag{137}$$

3. Infinite reservoir

$$p(R,t) = p_i \qquad R \to \infty \tag{138}$$

For practical problems, boundary conditions may be a combination of three types of boundary conditions discussed above.

For the inner boundary:

1. Constant pressure boundary condition

$$p(R,t) = p_w \qquad R \text{ on wellbore },\ t\rangle 0 \tag{139}$$

Where P_w is a specified pressure.

2. Constant flow rate boundary condition

$$q_t = \frac{\kappa}{B\mu}\int \frac{\partial p}{\partial \eta_i} d\mathrm{s} = \text{const} \qquad R \text{ on wellbore},\ t\rangle 0 \tag{140}$$

Where k_a is the geometric average permeability in the plane normal to the direction of wellbore, B is the formation volume factor, and q_t is the total flow rate from the well.

3.5.1 Coupling Solution for Different Flow Directions

The semi-analytical solution of the U-shaped wells lie in the development of analytical formulation for the fluid flow in both directions with a split point taking place at any point along the horizontal section. The position of that point is determined by the well/reservoir flow characteristics and dictated by the ratio of the flow from both ends.

The solution comprise both analytical and numerical solution, as in the case with a single well, but the point of split will be iteratively found that will ensure that the pressure gradient of both side of that point is increasing toward the point of production at the two ends.

The solution is based on the mathematical formulation of flow towards the two directions of the well, namely left wing and right wing. The solution was based on foundational work by Ozkan (2003) [33] and adapted to the two directions of flow and reservoir response. The solution couples the wellbore flow to the transient response of the reservoir as detailed in the other sections. This would warrant the reformulation of both reservoir response and the wellbore hydraulics for left and right flows. The reservoir response is basically dependent on the Green's function and the point source solution.
The equations are to be calculated by putting together in a matrix form but due to the nonlinearity nature of the equations, we will adopt Newton-Raphson approach of creating the Jacobian matrix and calculating the error residuals of the parameters of interest using iterative procedure.
The computational algorithm for the coupled solution of the equations using Newton-Raphson Method is summarized as:

1. Initialize variables;

2. Calculate residuals;

3. Build the Jacobian matrix;

4. Solve the linear system J x = -R;

5. Update variables: $x = x_o + x$;

6. If solution has not converged go to step 2;

7. Update variables from previous time step;

8. If it has not reached final time or error set point go to step 2.

To solve a system of nonlinear equations using Newton-Raphson method, primary variable are made q_{hDij} for i=2,3,…n. The system of the nonlinear equations is shown in matrix form,

$$J\delta q = R \qquad (141)$$

Where J denotes the Jacobian matrix, δq denotes the solution vector, and R denotes the residual vector. Elements of these matrices and vectors are given by

$$J_{j,k-1} = \frac{\partial f_{jm}}{\partial q_{Dkm}} \quad \text{for j=1, …, M-1 and i=2, …,M} \tag{142}$$

Green's function for right wing:

Assume that a finite quantity of fluid (Q bbl.) is removed at time $t = \tau$ from a plane located at $x = x'$ in a 1D infinite reservoir. This is called instantaneous plane source is

$$\Delta p(x,t) = \frac{\psi}{\sqrt{4\pi\eta_x(t-\tau)}} \exp\left\{-\frac{(x-x')^2}{4\eta_x(t-\tau)}\right\} \tag{143}$$

Where x is the distance in the x direction to the calculation point and x' is the distance in the x direction to the source point. ψ is called the source strength and

$$\psi = \frac{5.615Q(bbl)}{\phi c_t A_{yz}} \tag{144}$$

Where A_{yz} is the cross-sectional area in the $y-z$ plane.

Applying the Newman's product method to the 1D plane source, we obtain the following instantaneous point source solution (3D) for infinite reservoir

$$\Delta p(x,t) = \frac{5.615Q(bbl)}{\phi c_t} \frac{1}{8\left[\pi(t-\tau)^{3/2}\right]\sqrt{\eta_x\eta_y\eta_z}} \exp\left\{-\left[\frac{(x-x')^2}{4\eta_x(t-\tau)} + \frac{(y-y')^2}{4\eta_y(t-\tau)} + \frac{(z-z')^2}{4\eta_z(t-\tau)}\right]\right\} \tag{145}$$

The instantaneous uniform flux source function for an infinite slab source in the x-direction Green's function for a plane source is obtained by spatial integration of the point source solution. The solution for a source of width l is obtained by integrating equation (143) from $-½$ to $+½$ which yields

$$S(x,\tau) = \frac{1}{2l}\left[erf\frac{l/2 + (x-x')}{4\eta_x(t-\tau)} + erf\frac{l/2 - (x-x')}{4\eta_x(t-\tau)}\right] \tag{146}$$

Where l is the width of the source in the x-direction.

In order to obtain the solution for the opposite direction in the x-direction and since it is function of the spatial difference and integration of the point source, the solution for a source of width l is obtained by integrating equation (143) from $+½$ to $-½$ which yields

$$S(x,\tau)=\frac{1}{2l}\left[erf\,\frac{l/2-(x-x')}{4\eta_x(t-\tau)}+erf\,\frac{l/2+(x-x')}{4\eta_x(t-\tau)}\right] \tag{147}$$

Since Green's function is obtained by integrating function on spatial difference, the solution mathematically should be the same as the left wing for the infinite-acting reservoir.

The Green's function can also be derived for wings that are not intersecting at the same angle. The Green's function for the tilted wing can be adapted as follows;

$$G(x,y,t-\tau)=\frac{1}{2\sqrt{4\pi\eta_x\eta_y\eta_z(t-\tau)}}\exp\left\{-\frac{(-x\sin\alpha+y\cos\alpha)^2}{4\eta_x(t-\tau)}\right\}$$
$$.\left[\mathrm{erf}\left[\frac{l/2+(x\cos\alpha+y\sin\alpha-lw)}{\sqrt{4\eta_x(t-\tau)}}\right]\right]+\mathrm{erf}\left[\frac{l/2-(x\cos\alpha+y\sin\alpha-lw)}{\sqrt{4\eta_x(t-\tau)}}\right] \tag{148}$$

Where Z coordinates is the same, and changes are in the X & Y coordinates. α is the angle of deviation of the wing at intersection.

Then the transient pressure response can be calculated by;

$$\Delta p(x,t)=\frac{5.615Q(bbl)}{\phi C_t}\frac{1}{2\sqrt{4\pi\eta_x\eta_y\eta_z(t-\tau)}}\exp\left\{-\frac{(-x\sin\alpha+y\cos\alpha)^2}{4\eta_x(t-\tau)}\right\}$$
$$.\left[\mathrm{erf}\left[\frac{l/2+(x\cos\alpha+y\sin\alpha-lw)}{\sqrt{4\eta_x(t-\tau)}}\right]\right]+\mathrm{erf}\left[\frac{l/2-(x\cos\alpha+y\sin\alpha-lw)}{\sqrt{4\eta_x(t-\tau)}}\right] \tag{149}$$

The general pressure transient solution for horizontal wells is usually derived using the method of sources and sinks and Green's functions. The dimensionless pressure response for a horizontal well is given by

$$P_D(x_D, r_{wD}, t_D) = \int_0^{t_D} \int_x q_{hD}(x'_D; t'_D)\, G_D(x_D - x'_D, t_D - t'_D)\, dx'_D dt'_D \tag{150}$$

For the wellbore hydraulics effect, similar formulations for the flow towards the toe of the section is to be developed

$$\frac{dP_h}{dx} = E\ f\ q_{hc}^2$$

Differentiating previous equation,

$$\frac{d^2 P_h}{dx^2} = E\left(q_{hc}^2 \frac{\partial f}{\partial x} + 2 f q_{hc} q_h \right) \tag{151}$$

For the flow towards the toe, where flow rate increases as x increases;

$$\left(\frac{\partial q_{hc}}{\partial x} \right)_x = q_h(x) \tag{152}$$

$$\left(\frac{dP_h}{dx} \right)_{x=0} = E\ f\ q^2 \tag{153}$$

$$\frac{dP_h}{dx}(x) - \frac{dP_h}{dx}(0) = \frac{dP_h}{dx}(x) - E f_t\ q_t^2 = E \int_0^x \left(q_{hc}^2 \frac{\partial f}{\partial x'} + 2 f q_{hc} q_h \right) dx_1 \tag{154}$$

Integrating using boundary conditions at toe yields

$$P_h(x,t) - P_{wf}(t) = E f_t\ q_t^2 x + E \int_0^x \int_0^{x'} \left(q_{hc}^2 \frac{\partial f}{\partial x''} + 2 f q_{hc} q_h \right) dx'' dx' \tag{155}$$

Where f_t is the apparent friction factor at the total flow rate of q_t.

Multiplying by $\frac{kh}{141.2 q_t \mu}$ yields

$$\frac{kh}{(141.2 q_t \mu)} \left[P_h(x,t) - P_{wf}(t) \right] = \frac{4\pi}{C_{hD} L_h} \left[x + \frac{1}{f_t\ q_t^2} \int_0^x \int_0^{x'} \left(q_{hc}^2 \frac{\partial f}{\partial x''} - 2 f q_{hc} q_h \right) dx'' dx' \right] \tag{156}$$

In dimensionless form,

$$P_{wD}(t_D) - P_D(x_D, t_D) = \frac{N_{\mathrm{Re}t} f_t}{16} \frac{\pi}{C_{hD}} \left(2 x_D + \int_0^x \int_0^{x'} \left(\frac{D_f}{N_{\mathrm{Re}t} f_t} \right) q_{hD} dx'' dx' \right) \tag{157}$$

Where D is given by the following expression

$$D = N_{\mathrm{Re}}^2 \frac{df}{dN_{\mathrm{Re}}} + 2N_{\mathrm{Re}} f \tag{158}$$

The wellbore pressure for both wings wellbore hydraulics in both directions together with the reservoir response and assuming for convenience, that the center of the coordinates axis in x-y plane is at the heel of the well, so that $X_w = Y_w = 0$, then equation (157) yields;

$$P_{wDl}(t_D) - P_D(x_D, t_D) = \left(\frac{N_{\mathrm{Ret}} f_t}{16} \frac{\pi}{C_{hD}} \left(2x_D - \int_0^x \int_0^{x'} \left(\frac{D_f}{N_{\mathrm{Ret}} f_t} \right) q_{hD} dx'' dx' \right) \right) \tag{159}$$

$$P_{wDR}(t_D) - P_D(x_D, t_D) = \left(\frac{N_{\mathrm{Ret}} f_t}{16} \frac{\pi}{C_{hD}} \left(2x_D + \int_0^x \int_0^{x'} \left(\frac{D_f}{N_{\mathrm{Ret}} f_t} \right) q_{hD} dx'' dx' \right) \right) \tag{160}$$

Considering the wellbore hydraulics for two dimensionless times, results are shown below in Fig. 15.

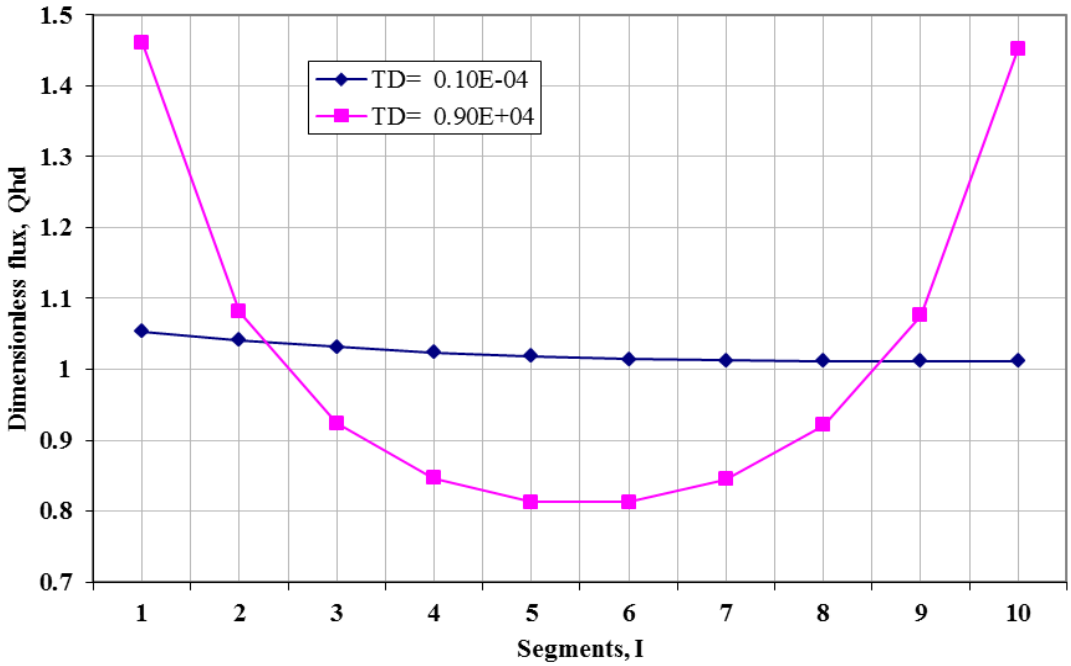

Fig. 15- Dimensionless flux along the finite-conductivity horizontal well at different time steps, lift wing only

Calculating the same results for the flow towards the toe, as the well is reversed in the x-coordinates, times, results are shown below in Fig. 16.

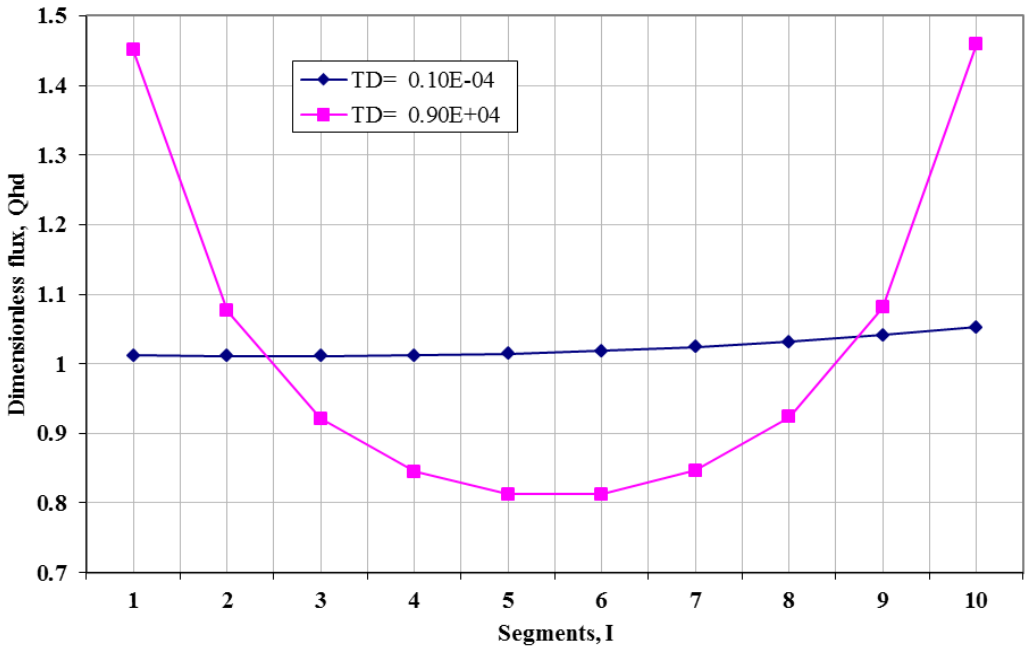

Fig. 16- Dimensionless flux along the finite-conductivity horizontal well at different time steps, right wing only

Both solutions were augmented in the U-shaped flow solution to account for the flow in both directions.

Extended reach wells

Calculating the dimensionless flux along the horizontal section for different well length namely 2000’ and 6000’, the dimensionless flux is lower for the 6000’ well as expected with more rate of depreciation. Shown in Fig. 17 are the runs for the two scenarios where it is expected to show some difference in both scenarios and different rate of pressure drop along the section as shown in the plots. Results were obtained at early time where the reservoir response has not made effect of the well fluxes at the toe and heel.

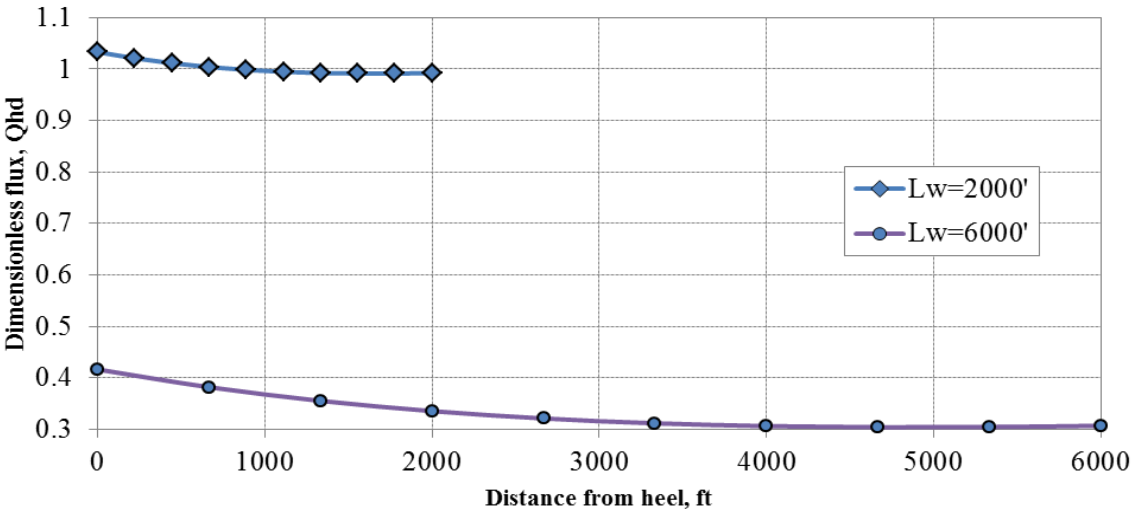

Fig. 17- Dimensionless flux along the finite-conductivity horizontal section for different well length

Looking at the wellbore pressure at the heel, PwD, the PwD in 2000’ well is higher because of the lower productivity of the well as expected.

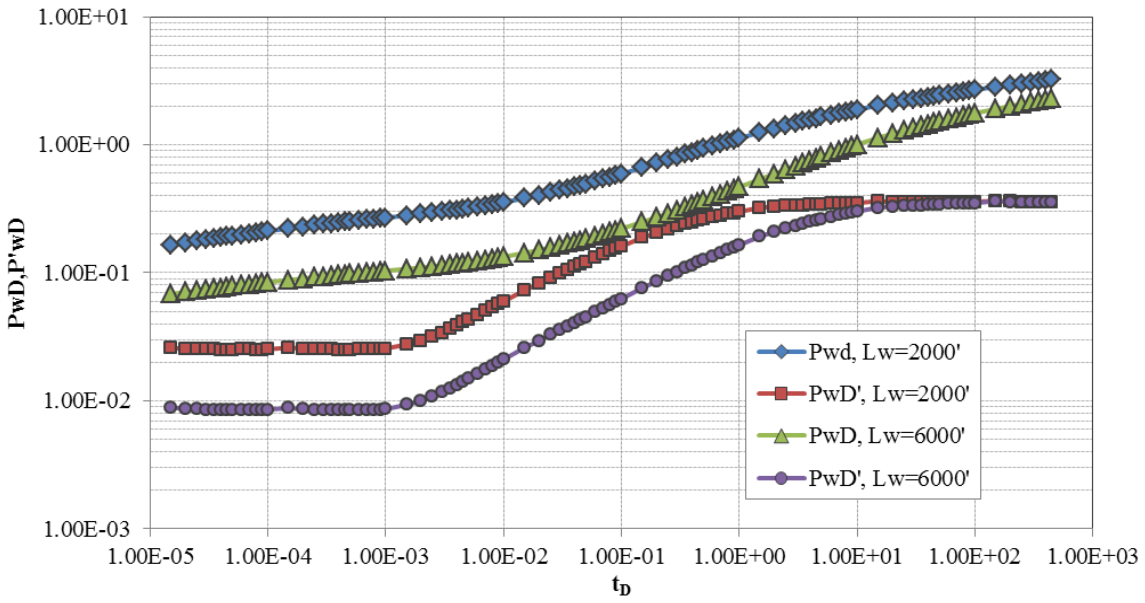

Fig. 18- pressure derivative for the different scenarios for different well length

The difference in P_{wD} and rate of change was evident in the derivative curves of both wells as shown in Fig. 18. Comparing the pressure derivative of both wells;

- There is a shift in the two curves because of the difference and rate of change in P_{wD} curves.
- The length of early radial is the same in two wells since it has to do with vertical permeability

3.5.2 U-shaped Horizontal well Flow Model

In the U-shaped horizontal wells and producing from both sides, a point of split of flow will take place along the horizontal section that will depend on the flow rates and well/reservoir interaction.
For that to happen, a continuity of wellbore and sand face pressure have to take place. This means that at the point of split one would expect to have an equal flux in both sides as shown in Fig. 19.

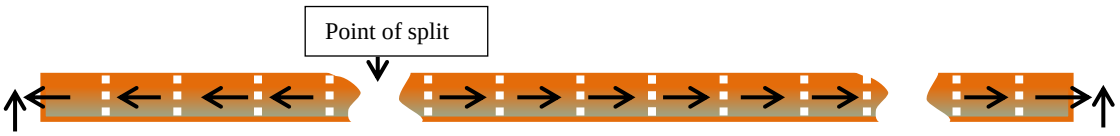

Fig. 19- Flow split schematic in the U-shaped horizontal well.

The mathematical formulation will be used to construct the solution matrix considering the point of split of flow. The point of flow split is found by iterative solution to satisfy the conditions of continuity of pressure at the wellbore and reservoir at the point of split of flow. The matrix is solved using Newton's method to find the wellbore pressures at the two ends and flow flux profile along the horizontal well.
The generic matrix is setup to solve the flux variables like the same approach of discretizing both sections into M segments. The section to the left of the split point is subscripted by L while the section to the right of the split point is subscripted by R.

By dividing the wellbore into M segments, and assuming the segment sequential number starts from the heel end to the toe end. The dimensionless x-coordinate for an observation point at the center of the j-th segment is given by

$$x_{jD} = \frac{(2j-1)}{M} \qquad (169)$$

We can obtain the discrete form for the pressure response equation for the j-th segment by

$$P_{wD}(t_D) - P_D(J,t_D) = \frac{N_{\mathrm{Re}t} f_t}{8} \frac{\pi x_{D,J}}{C_{hD}} - \frac{\pi}{16 C_{hD}} \left(\sum_{i=1}^{j-1} \left(\frac{(2j-1)}{M} - \frac{(2i-1)}{M} \right) \frac{1}{M} D_{f,i} q_{hD,i} + \frac{D_{f,j} q_{hD,j}}{2M^2} \right) \tag{170}$$

Or the wellbore pressure profile can be calculated at any location x along the section by

$$P_D(J,t_D) = P_{wD}(t_D) - \frac{N_{\mathrm{Re}t} f_t}{8} \frac{\pi x_{D,J}}{C_{hD}} + \frac{\pi}{16 C_{hD}} \left(\sum_{i=1}^{j-1} \left(\frac{(2j-1)}{M} - \frac{(2i-1)}{M} \right) \frac{1}{M} D_{f,i} q_{hD,i} + \frac{D_{f,j} q_{hD,j}}{2M^2} \right) \tag{171}$$

Where

$$C_{hD} = 7.395 x 10^{13} \frac{r_w^{\ 4}}{khL_h} \tag{172}$$

The equation becomes

$$P_D(J,t_D) = P_{wD}(t_D) - \frac{\pi N_{\mathrm{Re}t} f_t}{8 C_{hD}} \frac{(2j-1)}{M} + \frac{\pi}{16 C_{hD}} \left(\sum_{i=1}^{j-1} \left(2 \left(\frac{j-i}{M^2} \right) \right) \frac{1}{M} D_{f,i} q_{hD,i} + \frac{D_{f,j} q_{hD,j}}{2M^2} \right) \tag{173}$$

Using new variables to conform to other computations

$$x_{kDj} = \tilde{L}_{Dk} \frac{2j-1}{M} \tag{174}$$

$$\Delta x_{kD} = \tilde{L}_{Dk} \frac{1}{M} \tag{175}$$

$$\tilde{L}_{Dk} = L_{Dk} h_D \sqrt{\frac{k}{k_x}} \tag{176}$$

$$P_D(J,t_D) = P_{wD}(t_{DN}) + \frac{2\pi \tilde{L}_D}{16 C_{hD}} \left[\sum_{i=1}^{j-1} \left(\frac{j-i}{M^2} \right) D_i q_{hDi} + \frac{1}{2M^2} D_j q_{hDj} \right] - \frac{\pi N_{\mathrm{Re}t} f_t}{8 C_{hD}} \frac{(2j-1)}{M} \tag{177}$$

Since this equation will be computed to construct the matrix of wellbore effect, the computation will be done for diagonal and no-diagonal elements of the matrix. The elements of the matrix H will be as follows

$$H_{ji}=\begin{Bmatrix}\dfrac{\pi\,\tilde{L}_D}{8C_{hD}}\left(\dfrac{j-i}{M^2}\right)D_i\,q_{hDi}-\dfrac{\pi N_{\mathrm{Re}t}\,f_t}{8C_{hD}}\dfrac{(2j-1)}{M} & \text{for } j\le M \;\; i\le j-1\\ \dfrac{\pi\,\tilde{L}_D}{8C_{hD}}\left(\dfrac{1}{2M^2}\right)D_j q_{hDj}-\dfrac{\pi N_{\mathrm{Re}t}\,f_t}{8C_{hD}}\dfrac{(2j-1)}{M} & \text{for } j\le M \;\; i=j\\ 0 & \text{for } j\le M \;\; i\rangle j\end{Bmatrix} \text{ for } 1\le i\le M \;\&\; 1\le j\le M$$

(178)

For the u-shaped well, formulation of the flow toward the toe was presented where the change of direction of flow will change the sign of pressure gradient. Since solution is based on numerical scheme using the point of split of flow, then the two pressure gradient solutions are put in the solution matrix where the point of split is at segment M_s and the remaining segments of the wellbore where the flow will go to the right wing is for the segments $M_R = M - M_s$.

Equation (177) can be written as follows to describe flow where the flow is split at segment Msp.

$$\begin{aligned}&P_{wD}(t_{DN})-\left[\sum_{i=Msp+1}^{M}q_{hDi}(t_{DN})\,G_{ij}-q_{hDj}(t_{DN})\,S_j\right]_{FTL}-\left[\sum_{i=1}^{Msp}q_{hDi}(t_{DN})\,G_{ij}-q_{hDj}(t_{DN})\,S_j\right]_{FTR}\\&+\left(\frac{2\pi\,\tilde{L}_D}{16C_{hD}}\left[\sum_{i=1}^{j-1}\left(\frac{j-i}{Msp^2}\right)D_i q_{hDi}+\frac{1}{2Msp^2}D_j q_{hDj}\right]-\frac{\pi N_{\mathrm{Re}t}\,f_t}{8C_{hD}}\frac{(2j-1)}{Msp}\right)_{FTL}\\&-\left(\frac{2\pi\,\tilde{L}_D}{16C_{hD}}\left[\sum_{i=Msp+1}^{j-1}\left(\frac{j-i}{(M-Msp)^2}\right)D_i q_{hDi}-\frac{1}{2(M-Msp)^2}D_j q_{hDj}\right]-\frac{\pi N_{\mathrm{Re}t}\,f_t}{8C_{hD}}\frac{(2j-1)}{(M-Msp)}\right)_{FTL}\\&=\tilde{P}_{DHj}+\tilde{P}_{DTj}\end{aligned}$$

(179)

For the flow towards the heel,

$$P_{wDL}(t_{DN}) - \sum_{i=1}^{M} q_{hDi}\left(\tilde{S}_{ij} - \left(\frac{\pi \tilde{L}_D}{8C_{hD}}\left(\frac{j-i}{Msp^2}\right)D_i\right)_{FTL}\right) - q_{hDj}\left(S_j - \left(\frac{\pi \tilde{L}_D}{8C_{hD}}\frac{1}{2Msp^2}D_j\right)_{FTL}\right)$$

For the flow towards the toe,

$$= \tilde{P}_{Dj} + \left(\frac{\pi N_{Ret} f_t}{8C_{hD}}\frac{(2j-1)}{Msp}\right)_{FTL}$$

$$P_{wDR}(t_{DN}) - \sum_{i=1}^{M} q_{hDi}\left(\tilde{S}_{ij} - \left(\frac{\pi \tilde{L}_D}{8C_{hD}}\left(\frac{j-i}{(M-Msp)^2}\right)D_i\right)_{FRT}\right) - q_{hDj}\left(S_j - \left(\frac{\pi \tilde{L}_D}{8C_{hD}}\frac{1}{2(M-Msp)^2}D_j\right)_{FRT}\right)$$

$$= \tilde{P}_{Dj} + \left(\frac{\pi N_{Ret} f_t}{8C_{hD}}\frac{(2j-1)}{(M-Msp)}\right)_{FTR} \tag{180}$$

And hence, the elements of the matrix H will be as follows

$$H_{ji} = \begin{cases} \frac{\pi \tilde{L}_D}{8C_{hD}}\left(\frac{j-i}{Ms^2}\right)D_i\, q_{hDi} - \frac{\pi N_{Ret} f_t}{8C_{hD}}\frac{(2j-1)}{Ms} & \text{for } j \le Ms \;\; i \le j-1 \\ \frac{\pi \tilde{L}_D}{8C_{hD}}\left(\frac{1}{2Ms^2}\right)D_j q_{hDj} - \frac{\pi N_{Ret} f_t}{8C_{hD}}\frac{(2j-1)}{Ms} & \text{for } j \le Ms \;\; i = j \\ 0 & \text{for } j \le Ms \;\; i \rangle j \\ 0 & \text{for } j \le Ms \;\; i \le j \\ \frac{\pi \tilde{L}_D}{8C_{hD}}\left(\frac{j-i}{MR^2}\right)D_i\, q_{hDi} - \frac{\pi N_{Ret} f_t}{8C_{hD}}\frac{(2j-1)}{MR} & \text{for } j \le MR \;\; i \le j-1 \\ \frac{\pi \tilde{L}_D}{8C_{hD}}\left(\frac{1}{2MR^2}\right)D_j q_{hDj} - \frac{\pi N_{Ret} f_t}{8C_{hD}}\frac{(2j-1)}{MR} & \text{for } j \le MR \;\; i = j \\ 0 & \text{for } j \rangle Ms \;\; i \rangle j \end{cases} \text{for } 1 \le i \le M \;\&\; 1 \le j \le M$$

(181)

From eq. 180,

$$R_{ji} = -S_{ji} + H_{ji} \tag{182}$$

And

$$\sum_{i=1}^{2M+2} G_{ji} Q_i - B_j = 0 \tag{183}$$

Where

$$G_{ji} = -R_{ji} = H_{ji} - S_{ji} \tag{184}$$

And

$$G_{ji} = \begin{Bmatrix} 1 & G_{l11} & G_{l21} & G_{l31} \ldots G_{lm1} & 0 \ldots . & 0 & 0 & 0 & 0 \\ 1 & G_{l12} & G_{l22} & G_{l32} \ldots G_{lm2} & 0 \ldots . & 0 & 0 & 0 & 0 \\ 1 & \ldots \ldots \ldots \ldots & & & 0 \ldots . & 0 & 0 & 0 & 0 \\ 1 & G_{lm1} & G_{lm2} & G_{lm3} \ldots G_{lm,m} & 0 \ldots . & 0 & 0 & 0 & 0 \\ 0 & 1 & 1 & 1 \ldots . 1 & 0 \ldots . & 0 & 0 & 0 & 0 \\ 0 & 0 & 0 & 0 & 0 & 1 \ldots & 1 & 1 & 1 & 0 \\ 0 & 0 & 0 & 0 & 0 & G_{Rm,m} \ldots G_{Rm3} G_{Rm2} G_{Rm1} & & & & 1 \\ 0 & 0 & 0 & 0 & 0 & \ldots \ldots \ldots \ldots & & & & 1 \\ 0 & 0 & 0 & 0 & 0 & G_{Rm,m} \ldots G_{Rm3} G_{Rm2} G_{Rm1} & & & & 1 \\ 0 & 0 & 0 & 0 & 0 & G_{Rm,m} \ldots G_{Rm3} G_{Rm2} G_{Rm1} & & & & 1 \end{Bmatrix} \tag{185}$$

Then the calculated variables Q_I as follows

$Q_1 = P_{wDl}(t_D)$ and $Q_{M+2} = P_{wDR}(t_D)$ for left & right wings respectively

$$Q_I = q_{hD,I}\ , I = 1, M \tag{186}$$

And noting that

$$\sum_{I=1}^{Ms} Q_{I+1} = \sum_{I=1}^{Ms} q_{hD,I} = Ms \qquad \text{for left wing} \tag{187}$$

$$\sum_{I=Ms}^{M} Q_{I+1} = \sum_{I=Ms}^{M} q_{hD,I} = M - Ms \qquad \text{for right wing} \tag{188}$$

We have (M+2) unknowns (P_{wD} & $q_{hD}\ , I = 1, M$). We also have (M+2) equations by evaluating the equation at the J[th] segment, J=1,…M, and the additional equations 187 and 188. The (M+1) equations can now be written in a matrix form as follows:

$$\sum_{I=1}^{M+2} Q_I . G_{J,I} = B_j \qquad J=1, \ldots, M+2 \tag{189}$$

Where

$$\begin{Bmatrix} 1 & G_{l11} & G_{l21} & G_{l31}\ldots G_{lm1} & 0 & \ldots. & 0 & 0 & 0 & 0 \\ 1 & G_{l12} & G_{l22} & G_{l32}\ldots G_{lm2} & 0 & \ldots.. & 0 & 0 & 0 & 0 \\ 1 & \ldots\ldots\ldots\ldots\ldots & & & 0 & \ldots. & 0 & 0 & 0 & 0 \\ 1 & G_{lm1} & G_{lm2} & G_{lm3}\ldots G_{lm,m} & 0 & \ldots. & 0 & 0 & 0 & 0 \\ 0 & 1 & 1 & 1\ldots\ldots 1 & & 0\ldots.. & 0 & 0 & 0 & 0 \\ 0 & 0 & 0 & 0 & 0 & 1\ldots & 1 & 1 & 1 & 0 \\ 0 & 0 & 0 & 0 & 0 & G_{Rm,m}\ldots G_{Rm3}G_{Rm2}G_{Rm1} & & & & 1 \\ 0 & 0 & 0 & 0 & 0 & \ldots\ldots\ldots\ldots\ldots\ldots & & & & 1 \\ 0 & 0 & 0 & 0 & 0 & G_{Rm,m}\ldots G_{Rm3}G_{Rm2}G_{Rm1} & & & & 1 \\ 0 & 0 & 0 & 0 & 0 & G_{Rm,m}\ldots G_{Rm3}G_{Rm2}G_{Rm1} & & & & 1 \end{Bmatrix} \begin{Bmatrix} P_{wDl} \\ q_{hDl1} \\ q_{hDl2} \\ q_{hDl3} \\ \ldots. \\ q_{hDlm} \\ q_{hDRm} \\ \ldots.. \\ q_{hDl3} \\ q_{hDR2} \\ q_{hDR1} \\ P_{wDR} \end{Bmatrix} = \begin{Bmatrix} B_{l1} \\ B_{l2} \\ B_{l3} \\ B_{l4} \\ \ldots \\ M_L \\ M_R \\ \ldots \\ B_{l4} \\ B_{R3} \\ B_{R2} \\ B_{R1} \end{Bmatrix} \qquad (190)$$

This is a nonlinear system of equations. The nonlinear system is solved by Newton-Raphson method. Let

$$F(Q) = G(Q).Q - B \qquad (191)$$

Where

$F(Q)$ is a (M+2)x1 vector in the form of

$$F(Q) = \begin{bmatrix} F_1 \\ F_2 \\ F_3 \\ \vdots \\ F_{M+1} \end{bmatrix} \qquad (192)$$

And $G(Q)$ is a square matrix with a dimension of (M+2) as defined in the left-hand side of eq. 189.

B is a (M+2)x1 vector as defined on the right-hand-side of eq. 189.

Using Newton's iteration method, we get the solution of the $(k+1)^{th}$ iteration for the non-linear matrix problem.

$$Q^{k+1} = Q^k + \Delta Q^k \qquad (193)$$

Where

$$J\left(Q^k\right).\Delta Q^k = -F\left(Q^k\right) \qquad (194)$$

And

$J\left(Q^k\right)$ is the Jacobian matrix

The Jacobian matrix is defined as

$$J\left(Q^k\right)=\begin{bmatrix} \frac{\partial F_1}{\partial Q_1} & \frac{\partial F_1}{\partial Q_2} & \frac{\partial F_1}{\partial Q_3} & \cdots & \frac{\partial F_1}{\partial Q_{M+2}} \\ \frac{\partial F_2}{\partial Q_1} & \frac{\partial F_2}{\partial Q_2} & \frac{\partial F_2}{\partial Q_3} & \cdots & \frac{\partial F_2}{\partial Q_{M+2}} \\ \vdots & & & & \\ \frac{\partial F_{M+2}}{\partial Q_1} & \frac{\partial F_{M+2}}{\partial Q_2} & \frac{\partial F_{M+2}}{\partial Q_3} & .... & \frac{\partial F_{M+2}}{\partial Q_{M+2}} \end{bmatrix} \qquad (195)$$

The computation of the Jacobian involves the evaluation of the first and second derivative of friction factor with respect to Reynolds number.

From eq. (191) and using the chain rule for the derivative,

$$\frac{\partial F_j}{\partial Q_i} = \sum_{i=1}^{M+1}\left[\frac{\partial G_{jl}}{\partial Q_i}Q_l + G_{jl}\frac{\partial Q_l}{\partial Q_i}\right] \qquad (196)$$

Since $\frac{\partial G_{jl}}{\partial Q_i} = \frac{\partial H_{jl-1}}{\partial Q_i}$ and from eq. 191,

$$\frac{\partial G_{jl}}{\partial Q_i}=\frac{\partial H_{jl-1}}{\partial Q_i}=\begin{Bmatrix}\dfrac{\pi\,\tilde{L}_D}{8C_{hD}}\left(\dfrac{j-i}{M_s{}^2}\right)D_i\dfrac{\partial D_{l-1}}{\partial Q_i} & \text{for } j\le M_s \;\; i\le j-1\\ \dfrac{\pi\,\tilde{L}_D}{8C_{hD}}\left(\dfrac{1}{2M_s{}^2}\right)D_j\dfrac{\partial D_{l-1}}{\partial Q_i} & \text{for } j\le M_s \;\; i=j\\ 0 & \text{for } j\le M_s \;\; i\rangle j\\ 0 & \text{for } j\le M_s \;\; i\le j\\ \dfrac{\pi\,\tilde{L}_D}{8C_{hD}}\left(\dfrac{j-i}{M_R{}^2}\right)D_i\dfrac{\partial D_{l-1}}{\partial Q_i} & \text{for } j\le M_R \;\; i\le j-1\\ \dfrac{\pi\,\tilde{L}_D}{8C_{hD}}\left(\dfrac{1}{2M_R{}^2}\right)D_j\dfrac{\partial D_{l-1}}{\partial Q_i} & \text{for } j\le M_R \;\; i=j\\ 0 & \text{for } j\rangle M_s \;\; i\rangle j\end{Bmatrix} \tag{197}$$

Where $M_R = M - Ms$

From eq. (191), $\dfrac{\partial Q_l}{\partial Q_i}=\begin{cases}\mathbf{0} & if\;\; L\neq i\\ \mathbf{1} & if\;\; L=i\end{cases}$ (198)

Since

$$D_L = N_{\mathrm{Re}}^2\frac{\partial f}{\partial N_{\mathrm{Re}}}+2N_{\mathrm{Re}}\;f\big|_l \tag{199}$$

Then

$$\frac{\partial D_L}{\partial Q_i}=2N_{\mathrm{Re}}\frac{\partial N_{\mathrm{Re}}}{\partial Q_i}\frac{df}{dN_{\mathrm{Re}}}\bigg|_l+N_{\mathrm{Re}}^2\frac{\partial}{\partial Q_i}\left(\frac{\partial f}{\partial N_{\mathrm{Re}}}\right)+2\frac{\partial N_{\mathrm{Re}l}}{\partial Q_i}\;f\big|_l+2N_{\mathrm{Re}l}\left(\frac{\partial f}{\partial Q_i}\right) \tag{200}$$

Or

$$\frac{\partial D_L}{\partial Q_i}=\frac{\partial N_{\mathrm{Re}}}{\partial Q_i}\left\{4N_{\mathrm{Re}}\frac{df}{dN_{\mathrm{Re}}}\bigg|_l+N_{\mathrm{Re}}^2\left(\frac{\partial^2 f}{\partial N_{\mathrm{Re}}^{\;2}}\right)+2\;f\big|_l\right\} \tag{201}$$

If the Reynolds number at the Lth segment is

$$N_{\mathrm{Re}} = N_{\mathrm{Re}i}\frac{\sum_{l+1}^{M+1} Q_i}{M} \tag{202}$$

Then,

$$\frac{\partial N_{\mathrm{Re}l}}{\partial Q_i} = \begin{cases} \mathbf{0} & if \quad i \le l \\ \dfrac{N_{\mathrm{Re}t}}{M} & if \quad i \rangle l \end{cases} \tag{203}$$

The computation of the Jacobian matrix involves the evaluation of the first and the second derivative of the friction factor with respect to Reynolds umber.

The procedure is setup to calculate the function,

$$Q_i = \left\{ \begin{matrix} \tilde{P}_{wD}(\mathrm{t_D}) \\ q_{hDi}(\mathrm{t_D}) \end{matrix} \right\} \text{ For } i = 1,2,...,\mathrm{M}+2 \tag{204}$$

Where q_{hDi}'s & $\tilde{P}_{wD}(\mathrm{t_D})$'s are part of the calculated function Q_i and interdependent variables.

3.5.3 U-Shaped Horizontal Well Results

Dimensionless Flux Calculations

Figure 20 shows the fluxes of an infinite conductivity well. The well is segmented into 16 segments with equal flow rate and the split of the flow became at the middle of the wellbore. Due to the large size of each segment, the split of the flow is spans in the middle two segments.

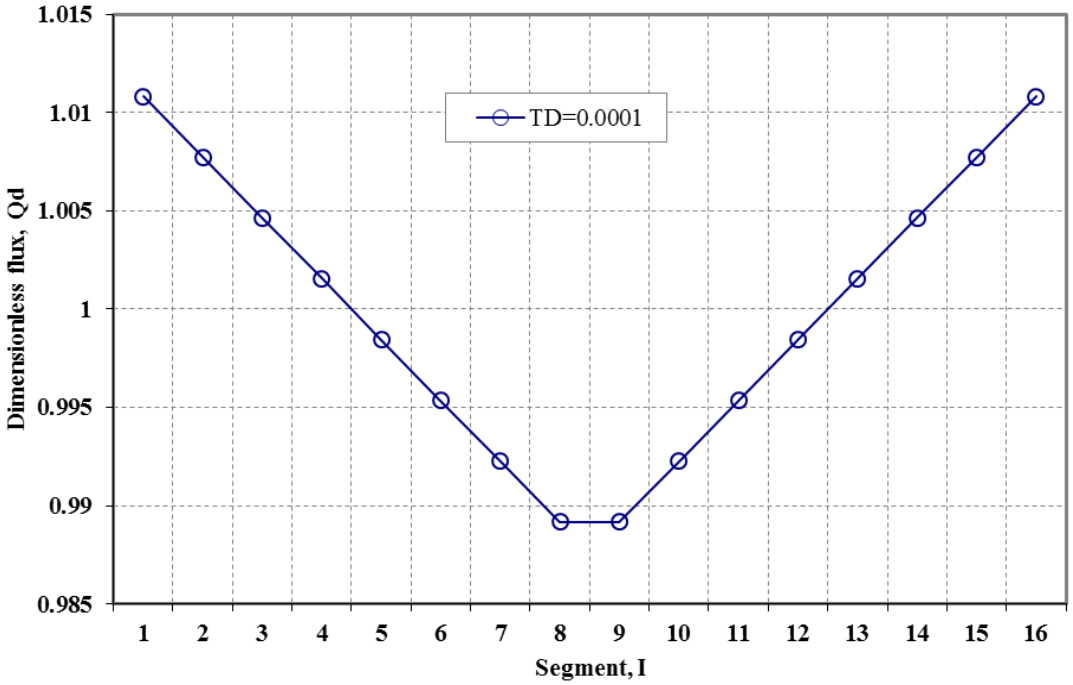

Fig. 20 Dimensionless flux along the horizontal section at different time steps, U-shape infinite conductivity well

Figure 21 presents the pressures and pressure derivatives of the two wells, P_{WDL}, P'_{WDL}, P_{WDR}, and P'_{WDR}. The wellbore pressures are identical as expected, similarly for the pressure derivatives.

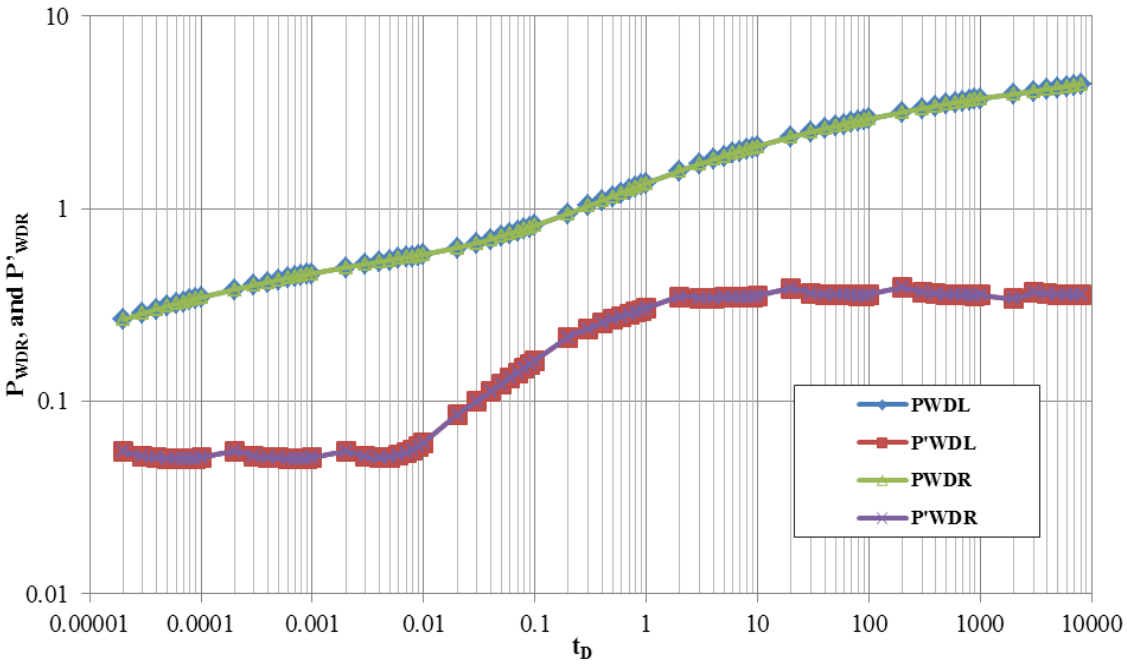

Fig. 21- Pressure and pressure derivative, U-shape infinite conductivity well

Considering the wellbore hydraulics effect for the same well conditions, Fig. 22 shows the flow influxes for the well segments.

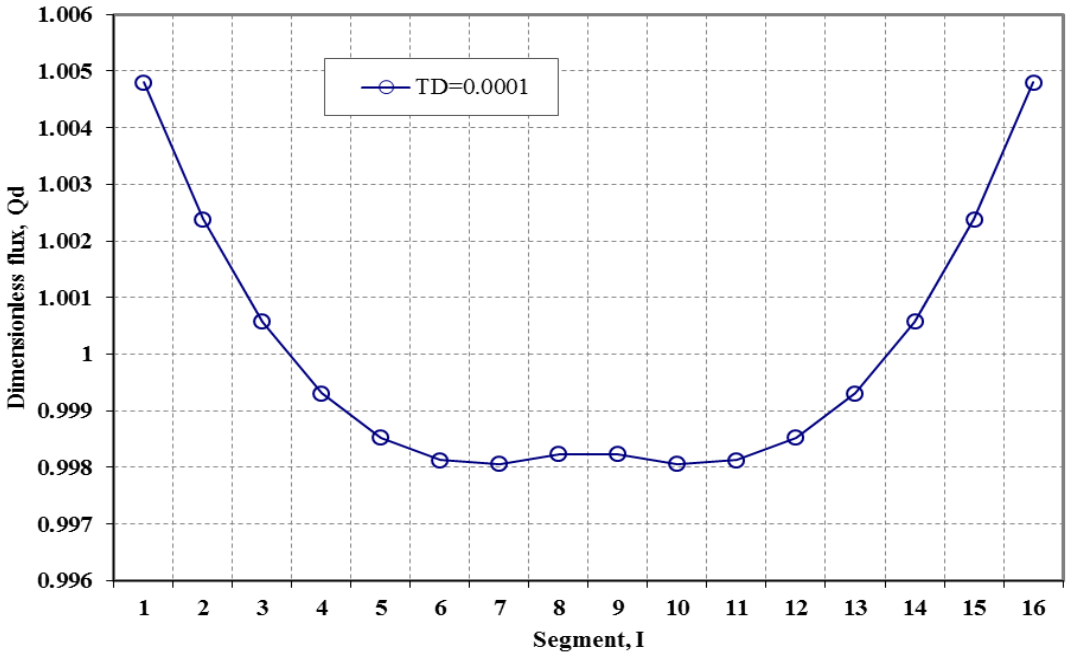

Fig. 22- Dimensionless flux along the horizontal section, U-shape finite conductivity well

Figure 23 presents the pressures and pressure derivatives of the two wells, P_{WDL}, P'_{WDL}, P_{WDR}, and P'_{WDR} for the same case of considering the wellbore hydraulics. The wellbore pressures are identical as expected, similarly for the pressure derivatives.

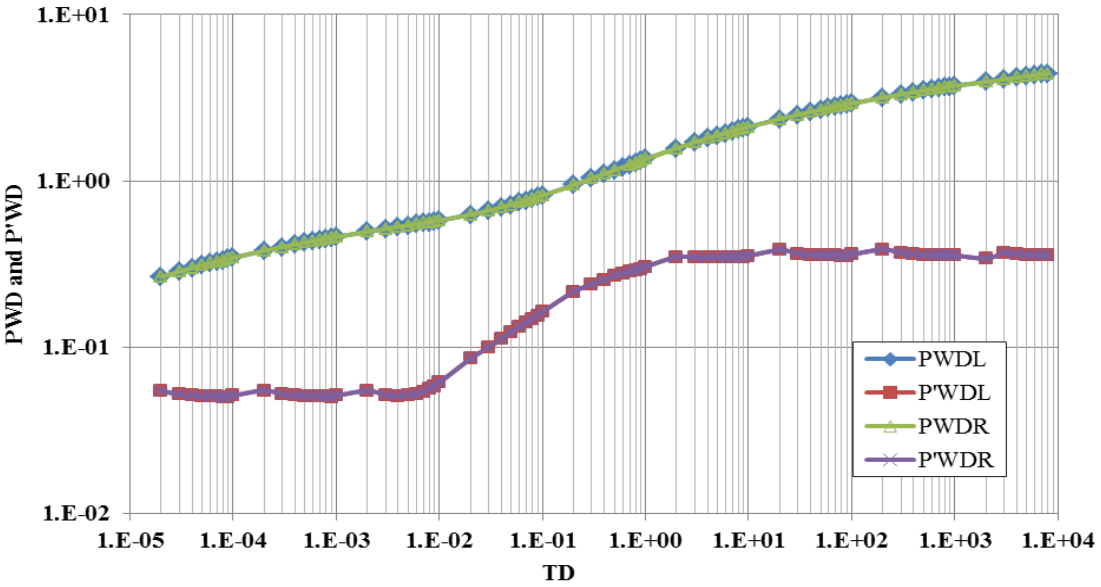

Fig. 23- Pressure and pressure derivative, U-shape finite conductivity well

Flow ratio change effects

With changing flow rate in either wing, the flow influxes will change accordingly. Considering the changes in the right wing for comparison, intuitively, the flow split will change towards the left wing as the right wing will draw most of the flow.

Figures 24 to 29 present the results for the three cases of different flow rate ratios, Qr of 1.7, 2.2, and 3.

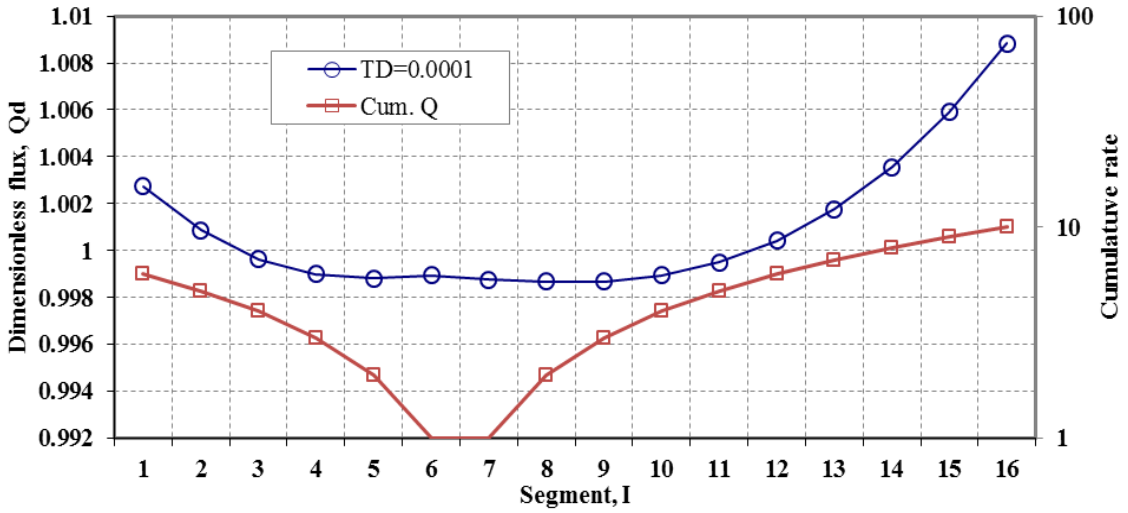

Fig. 24- Dimensionless flux profile along the U-shape finite conductivity well (Qr=1.7 QL)

Shown with circles are the fluxes of each segment while the red squares are the cumulative flow rate for each segment at the right Y axis. The ratio of the two ratios is 1.7.

Figure 25 shows the pressures and pressure derivatives of the two wells, P_{WDL}, P'_{WDL}, P_{WDR}, and P'_{WDR} for the same case of considering the wellbore hydraulics. Unlike previous cases, the wellbore pressures are not identical as expected. However, the pressure derivatives are identical.

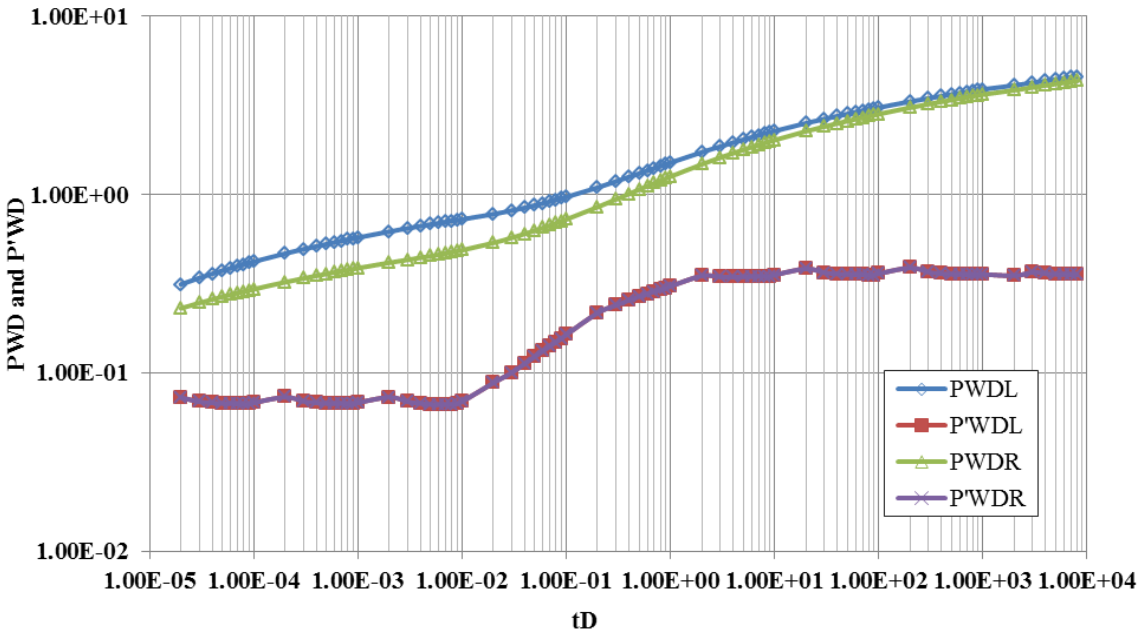

Fig. 25- Pressure and derivative of left and right wings, (Qr=1.7 QL)

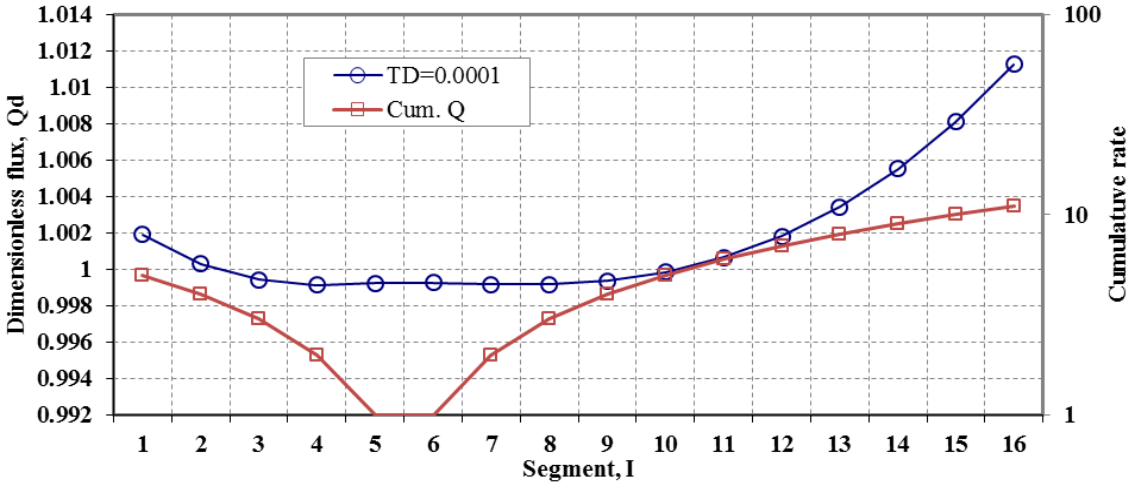

Fig. 26- Dimensionless flux profile along the U-shape finite conductivity well (Qr=2.2 QL)

Shown with circles are the fluxes of each segment while the red squares are the cumulative flow rate of each segment at the right Y axis. The ratio of the two ratios is 2.2.

Figure 27 shows the pressures and pressure derivatives of the two wells, P_{WDL}, P'_{WDL}, P_{WDR}, and P'_{WDR} for the same case of considering the wellbore hydraulics. Unlike previous cases, the wellbore pressures are not identical as expected and parted more in this case. However, the pressure derivatives are identical.

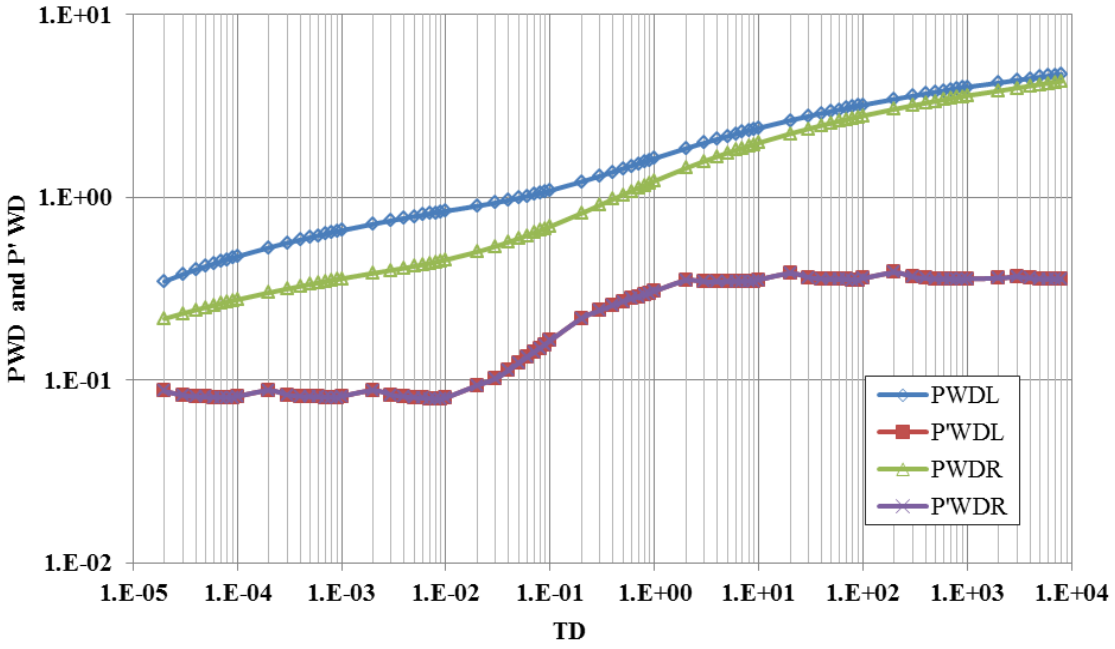

Fig. 27- Pressure and derivative of left and right wings, rate are not similar (Qr=2.2 QL)

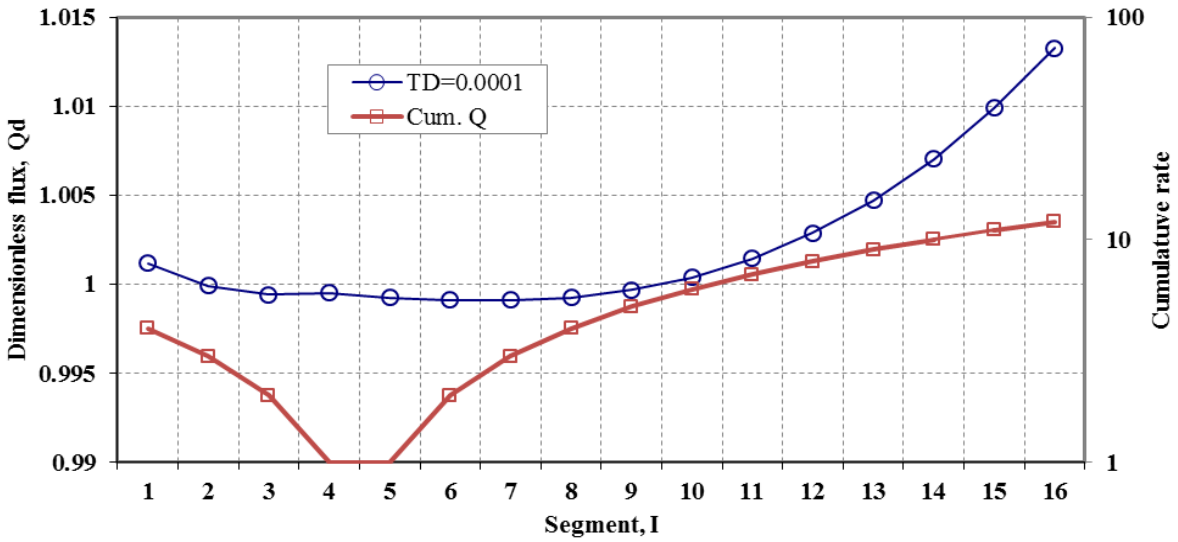

Fig. 28- Dimensionless flux profile along the U-shape finite conductivity well (Qr=3 QL)

Shown with circles are the fluxes of each segment while the red squares are the cumulative flow rate of each segment at the right Y axis. The ratio of the two ratios is 3.

Fig 29 shows the pressures and pressure derivatives of the two wells, P_{WDL}, P'_{WDL}, P_{WDR}, and P'_{WDR} for the same case of considering the wellbore hydraulics. Unlike previous cases, the wellbore pressures are not identical as expected and parted more in this case. However, the pressure derivatives are identical.

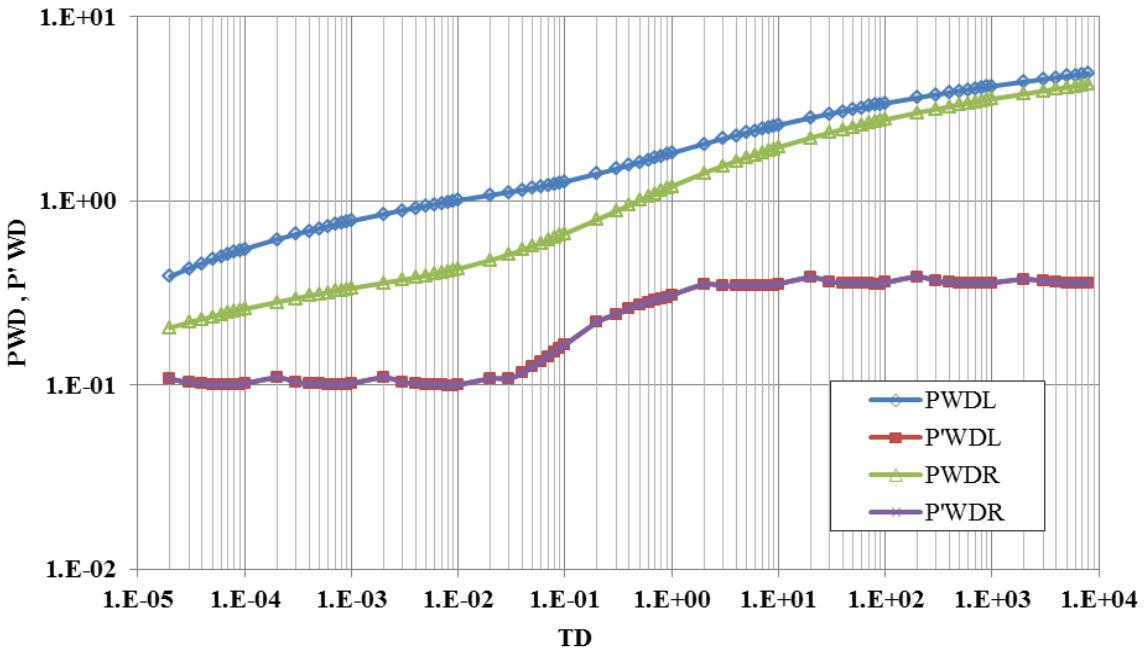

Fig. 29- Pressure and derivative of left and right wings, rate are not similar (Qr=3 QL)

Considering the same case but for larger number of segments (80), times, results are shown in fig's. 30 and 31.

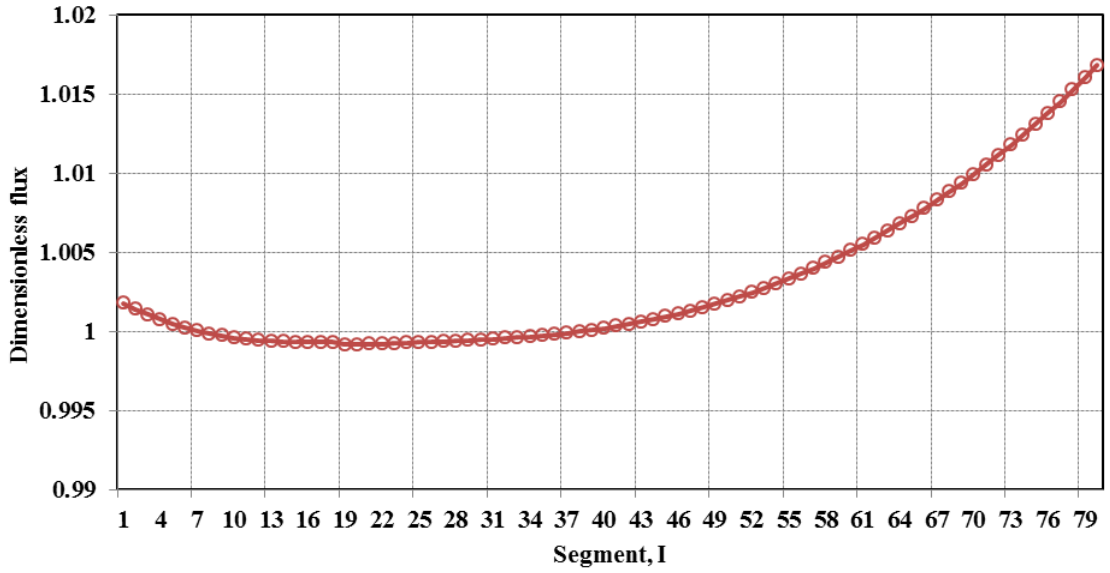

Fig. 30- Dimensionless flux profile along the U-shape finite conductivity well (Qr=3 QL)

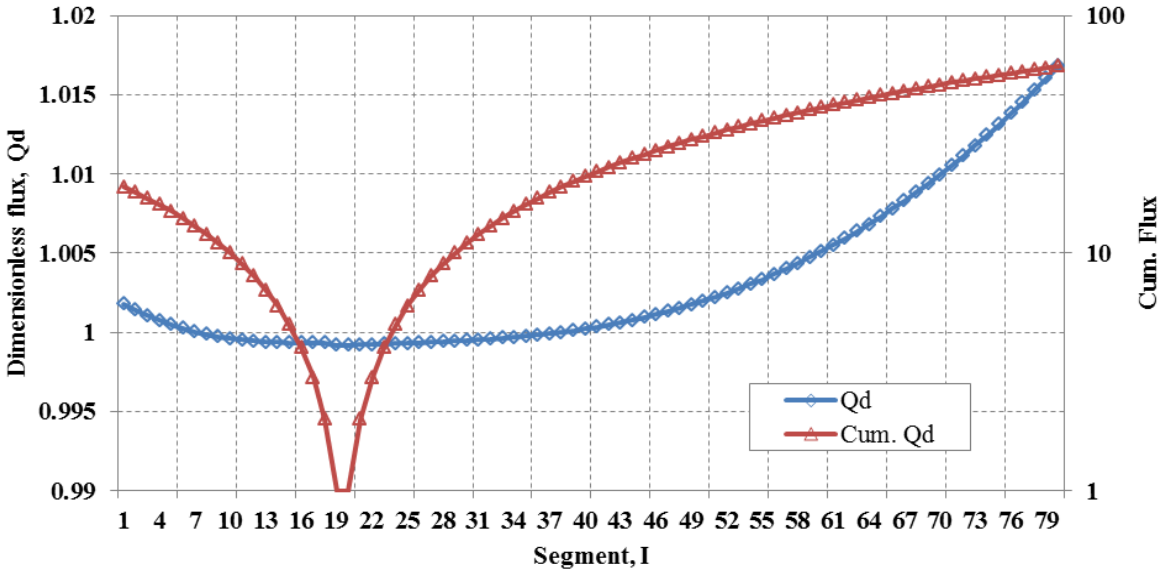

Fig. 31- Dimensionless flux and cumulative profiles along the U-shape finite conductivity well (Qr=3 QL)

Changing the flow rate ratio of the right wing compared to the left wing, for flow ratio from 0.11 to 5.02 times the rate of the left wing. The triangle marker in each line represents the point of split. Results are shown below in Fig. 32.

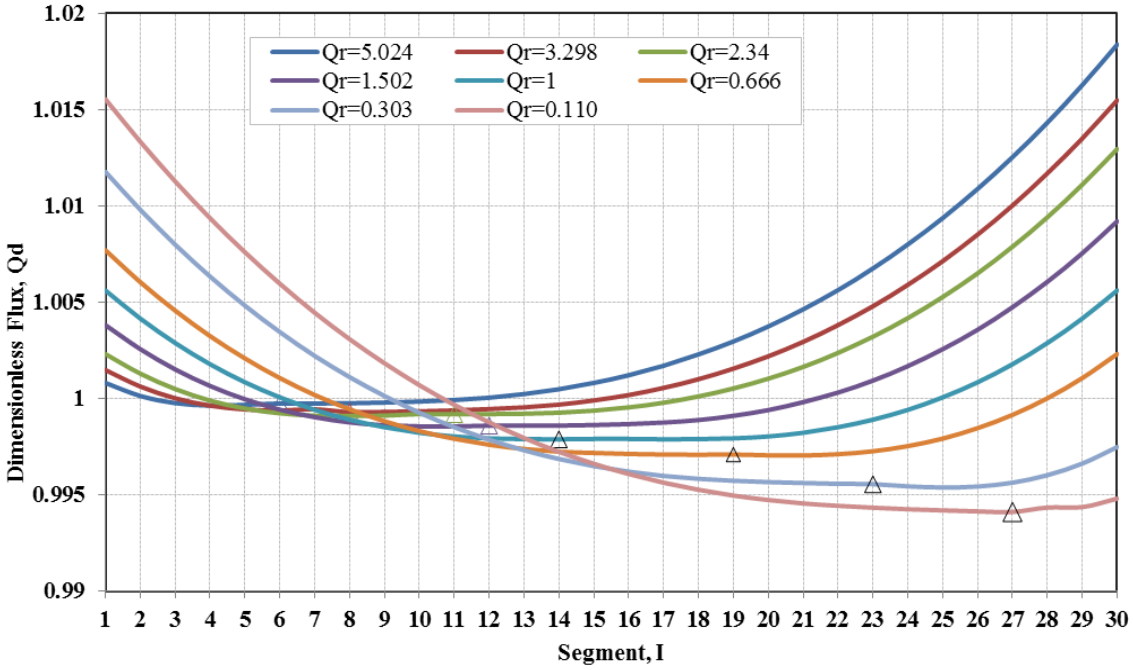

Fig. 32- Dimensionless flux profile along the U-shape finite conductivity well (varying right wing rate)

3.5.4 Wellbore Pressure Gradient Calculations

By dividing the wellbore into M segments, and assuming the segment sequential number starts from the heel end to the toe end. The dimensionless x-coordinate for an observation point at the center of the j-th segment is given by

$$x_{jD} = \frac{(2j-1)}{M} \tag{205}$$

We can obtain the discrete form for the pressure response equation for the j-th segment by

$$P_{wD}(t_D) - P_D(J,t_D) = \frac{N_{\mathrm{Re}t} f_t}{8} \frac{\pi x_{D,J}}{C_{hD}} - \frac{\pi}{16 C_{hD}} \left(\sum_{i=1}^{j-1} \left(\frac{(2j-1)}{M} - \frac{(2i-1)}{M} \right) \frac{1}{M} D_{f,i} q_{hD,i} + \frac{D_{f,j} q_{hD,j}}{2M^2} \right) \tag{206}$$

Or the wellbore pressure profile can be calculated at any location x along the section by

$$P_D(J,t_D) = P_{wD}(t_D) - \frac{N_{\mathrm{Re}t} f_t}{8} \frac{\pi x_{D,J}}{C_{hD}} + \frac{\pi}{16 C_{hD}} \left(\sum_{i=1}^{j-1} \left(\frac{(2j-1)}{M} - \frac{(2i-1)}{M} \right) \frac{1}{M} D_{f,i} q_{hD,i} + \frac{D_{f,j} q_{hD,j}}{2M^2} \right) \tag{207}$$

Where

$$C_{hD} = 7.395x10^{13} \frac{r_w^{\ 4}}{khL_h} \tag{208}$$

The equation becomes

$$P_D(J,t_D) = P_{wD}(t_D) - \frac{\pi N_{\mathrm{Re}t} f_t}{8 C_{hD}} \frac{(2j-1)}{M} + \frac{\pi}{16 C_{hD}} \left(\sum_{i=1}^{j-1} \left(2 \left(\frac{j-i}{M^2} \right) \right) \frac{1}{M} D_{f,i} q_{hD,i} + \frac{D_{f,j} q_{hD,j}}{2M^2} \right) \tag{209}$$

Using new variables to conform to other computations

$$x_{kDj} = \tilde{L}_{Dk} \frac{2j-1}{M} \tag{210}$$

$$\Delta x_{kD} = \tilde{L}_{Dk} \frac{1}{M} \tag{211}$$

$$\tilde{L}_{Dk} = L_{Dk} h_D \sqrt{\frac{k}{k_x}} \tag{212}$$

$$P_D(J, t_D) = P_{wD}(t_{DN}) + \frac{2\pi \tilde{L}_D}{16 C_{hD}} \left[\sum_{i=1}^{j-1} \left(\frac{j-i}{M^2} \right) D_i q_{hDi} + \frac{1}{2M^2} D_j q_{hDj} \right] - \frac{\pi N_{Ret} f_t}{8 C_{hD}} \frac{(2j-1)}{M} \tag{213}$$

Since this equation will be computed to construct the matrix of wellbore effect, the computation will be done for diagonal and no-diagonal elements of the matrix. The elements of the matrix HB will be as in eq. 178.

$$HB_{ji} = \left\{ \begin{array}{ll} \frac{\pi \tilde{L}_D}{8 C_{hD}} \left(\frac{j-i}{M^2} \right) D_i \, q_{hDi} - \frac{\pi N_{Ret} f_t}{8 C_{hD}} \frac{(2j-1)}{M} & \text{for } j \le M \;\; i \le j-1 \\ \frac{\pi \tilde{L}_D}{8 C_{hD}} \left(\frac{1}{2M^2} \right) D_j q_{hDj} - \frac{\pi N_{Ret} f_t}{8 C_{hD}} \frac{(2j-1)}{M} & \text{for } j \le M \;\; i = j \\ 0 \qquad\qquad\qquad\qquad\qquad\qquad\qquad\qquad & \text{for } j \le M \;\; i \rangle j \end{array} \right\} \text{for } 1 \le i \le M \;\&\; 1 \le j \le M \tag{214}$$

So, the pressure profile is calculated by

$$P_D(J, t_D) = P_{wD}(t_{DN}) + HB_j(t_D) \tag{215}$$

For the u-shaped well, formulation of the flow toward the toe was presented where the change of direction of flow will change the sign of pressure gradient. Since solution is based on numerical scheme using the point of split of flow, then the two pressure gradient solutions are put in the solution matrix where the point of split is at segment M_s and the remaining segments of the wellbore where the flow will go to the right wing is for the segments $M_R = M - M_s$, as in eq. 181 ,

$$HB_{ji}=\begin{Bmatrix}\frac{\pi\,\widetilde{L}_D}{8C_{hD}}\left(\frac{j-i}{{M_s}^2}\right)D_i\,q_{hDi}-\frac{\pi N_{\mathrm{Re}t}\,f_t}{8C_{hD}}\frac{(2j-1)}{M_s} & \text{for } j\le M_s \;\; i\le j-1\\ \frac{\pi\,\widetilde{L}_D}{8C_{hD}}\left(\frac{1}{2{M_s}^2}\right)D_j q_{hDj}-\frac{\pi N_{\mathrm{Re}t}\,f_t}{8C_{hD}}\frac{(2j-1)}{M_s} & \text{for } j\le M_s \;\; i=j\\ 0 & \text{for } j\le M_s \;\; i\rangle j\\ 0 & \text{for } j\le M_s \;\; i\le j\\ \frac{\pi\,\widetilde{L}_D}{8C_{hD}}\left(\frac{j-i}{{M_R}^2}\right)D_i\,q_{hDi}-\frac{\pi N_{\mathrm{Re}t}\,f_t}{8C_{hD}}\frac{(2j-1)}{M_R} & \text{for } j\le M_R \;\; i\le j-1\\ \frac{\pi\,\widetilde{L}_D}{8C_{hD}}\left(\frac{1}{2{M_R}^2}\right)D_j q_{hDj}-\frac{\pi N_{\mathrm{Re}t}\,f_t}{8C_{hD}}\frac{(2j-1)}{M_R} & \text{for } j\le M_R \;\; i=j\\ 0 & \text{for } j\rangle M_s \;\; i\rangle j\end{Bmatrix}\quad \text{for } 1\le i\le M \;\&\; 1\le j\le M \tag{216}$$

And hence, the pressure profile is calculated by two equations for both sides

$$P_{DL}\left(J,t_D\right)=P_{wDL}(t_{DN})+HB_{Lj}\left(t_D\right) \tag{217}$$

$$P_{DR}\left(J,t_D\right)=P_{wDR}(t_{DN})+HB_{Rj}\left(t_D\right) \tag{218}$$

The calculations of pressure profile are made for two scenarios; equal flow and double flow. Results are shown figures 33 to 38.

Equal flow results;

As expected, the dimensionless flux along the wellbore is symmetrical with the split of the flow at the middle. The results are shown in Fig. 33.

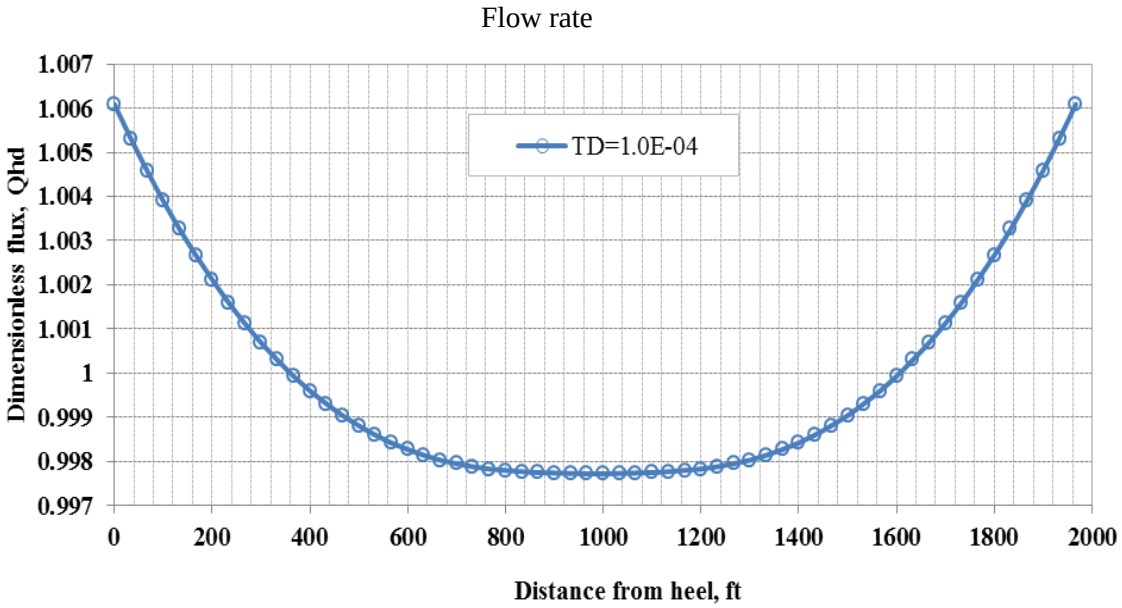

Fig. 33- Dimensionless flux profile along the U-shape finite conductivity well (QL=QR)

Similarly, the pressure profiles are symmetrical with gradient reaching lowest at the middle and changing towards the two ends of the well. The results are shown in Fig. 34.

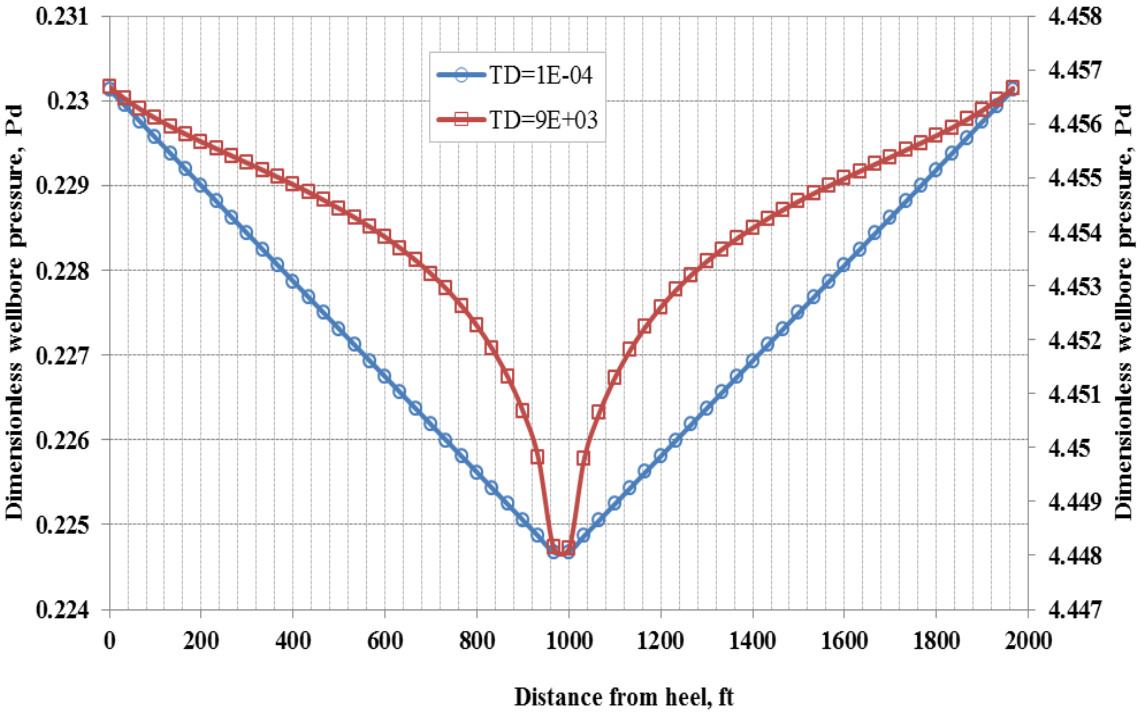

Fig. 34- Wellbore pressure profile along the U-shape finite conductivity well (QL=QR)

Double flow results

Unlike the equal flow rates, the dimensionless flux along the wellbore is not symmetrical with the split of the flow shifted to the left wing. The results are shown in Fig. 35.

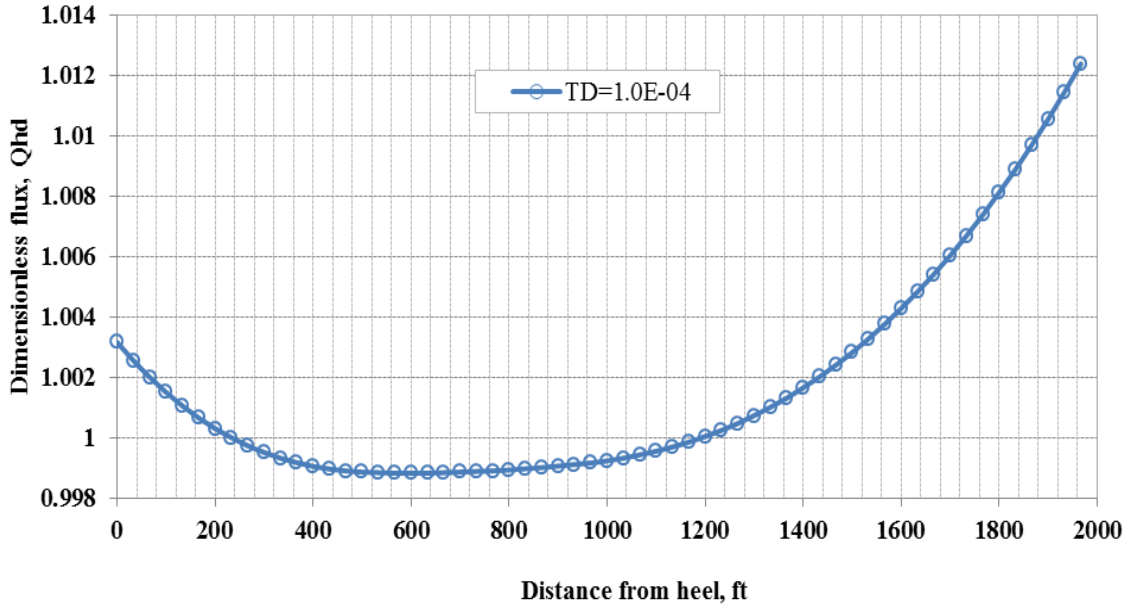

Fig. 35- Dimensionless flux profile along the U-shape finite conductivity well (QL=0.5 QR)

Similarly, the pressure profiles are not symmetrical with gradient reaching lowest at the split point and changing towards the two ends of the well. The results are shown in Fig. 36.

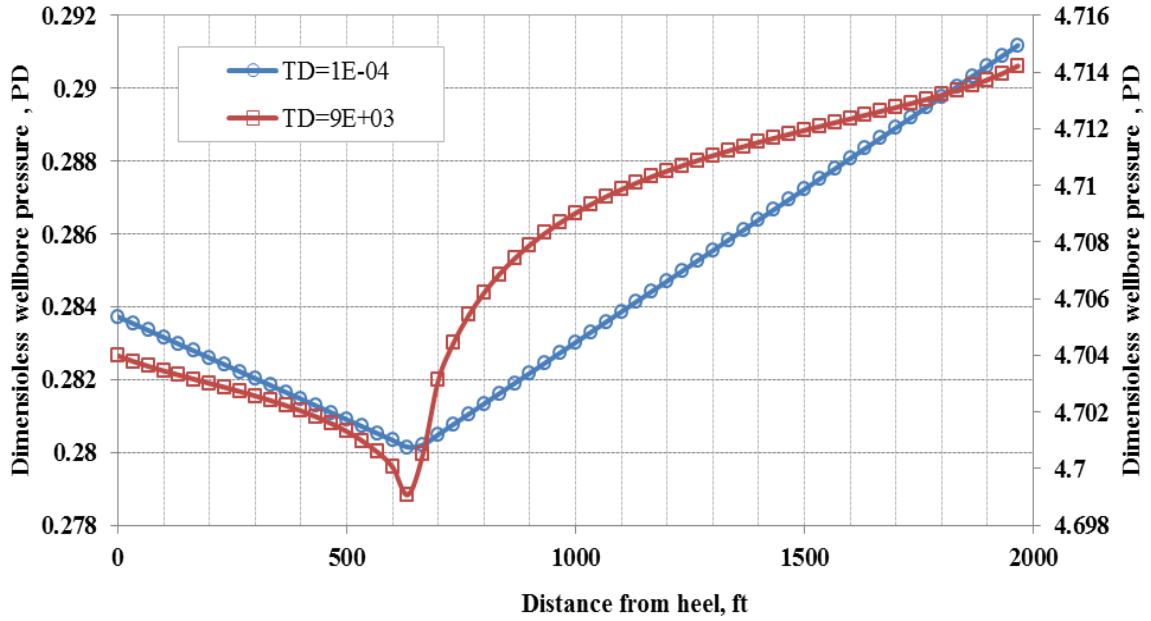

Fig. 36- Wellbore pressure profile along the U-shape finite conductivity well (QL=0.5QR)

If the well is assumed an infinite- conductivity well, which means that wellbore hydraulics are not considered, then the wellbore pressure will be equal to the sandface pressure.

The dimensionless pressure at the sand face, P_{oD}, is plotted for the same case and same time steps.

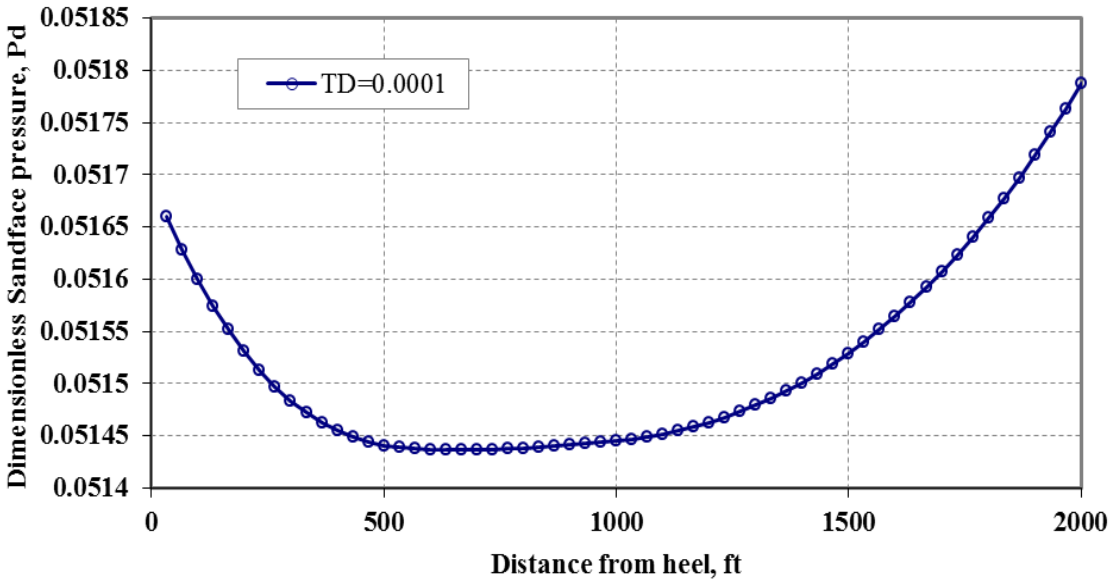

Fig. 37- Dimensionless pressure at sandface at early time, t_D=1E-04, U-shape finite conductivity well (QL=0.5QR)

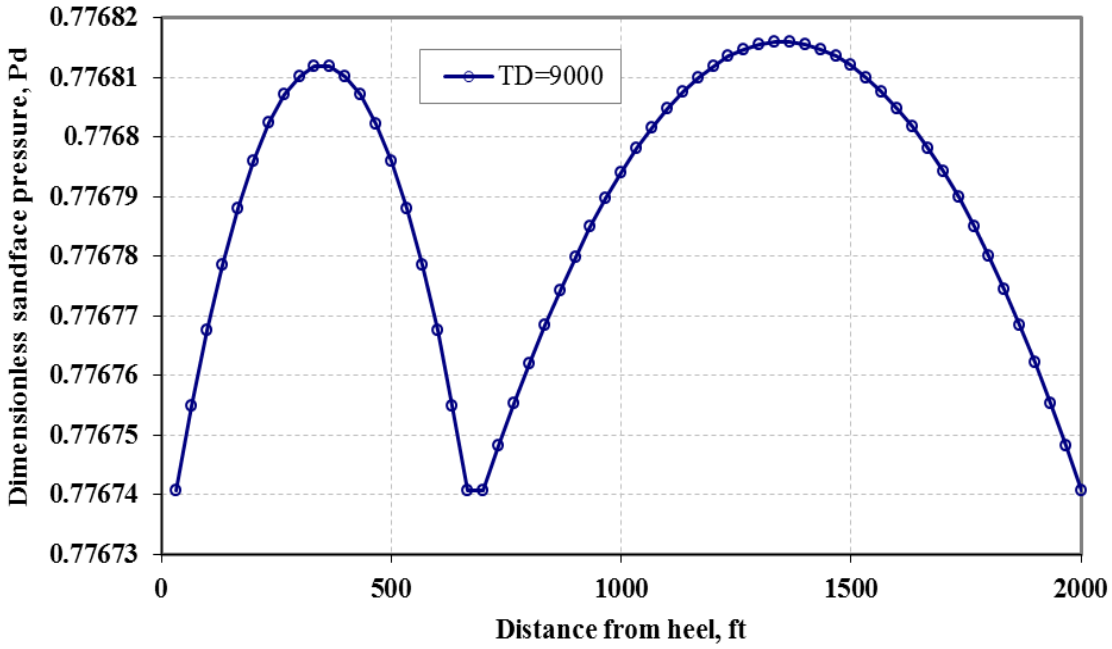

Fig. 38- Dimensionless pressure at sandface at early time, t_D =9.0E03, U-shape finite conductivity well (QL=0.5QR)

3.5.5 Specific Transient Productivity Index

The specific productivity index was addressed in literature for vertical wells for numerical simulation to get the transient productivity of a cell. In horizontal wells, the specific index addressed was for a steady-state condition and was not for was addressed in literature for transient pressure case.

Here, we calculate the transient productivity index for horizontal wells and for the U-shaped horizontal wells using the formulation and methodology developed.

From the previous equations for calculating the reservoir response, the general expression defining the pressure drop at time t, and point M due to continuous source is obtained by integrating the instantaneous point-source function with respect to time from 0 to t. For a uniform initial pressure reservoir with infinite or impermeable boundaries, the pressure response can be presented as:

$$\Delta P(M,t) = \frac{1}{\mu\phi c_t}\int_{\Omega} q(\tau)\, s(M, t-\tau)\, d\tau \qquad (219)$$

Where $s(M, t-\tau)$ is the instantaneous infinite slab source function (Green's function).

The general pressure transient solution for horizontal wells is usually derived using the method of sources and sinks of Green's functions. The dimensionless pressure response for a horizontal well is given by

$$P_D(x_D, r_{wD}, t_D) = \int_0^{t_D}\int_x q_{hD}(x'_D; t'_D)\, G_{\mathrm{D}}(x_D - x'_D, t_D - t'_D)\, dx'_D dt'_D \qquad (220)$$

Where $G_{\mathrm{D}}(x_D, t_D)$ is the instantaneous point-source function given by

$$G_{\mathrm{D}}(x_D, y_D, z_D, t_D) = \frac{\eta}{2L^2 t_D}\sqrt{\frac{k_z}{k}}\exp\left(\frac{{x_D}^2 + {y_D}^2}{4t_D}\right)\left[1 + 2\sum_{n=1}^{\infty}\exp\left(-\frac{\eta^2\pi^2 t_D}{{h_D}^2}\right)\cos\left(\eta\pi\frac{z_D}{h_D}\right)\cos\left(\eta\pi\frac{z_{wD}}{h_D}\right)\right] \qquad (221)$$

Where η is the diffusivity constant given by

$$\eta = 2.637\ \mathrm{x}10^{-4}\,\frac{k}{\mu\phi c_t} \qquad (222)$$

Where the uniform permeability, k, corresponds to the equivalent isotropic-system permeability defined by

$$k = \sqrt[3]{k_x\, k_y\, k_z} \qquad (223)$$

The dimensionless flux in the well is given as:

$$q_{hD} = \frac{q_h L}{qB}\sqrt{\frac{k_x}{k}}, \qquad \text{where} \quad q_h(x) \text{ is the flux along the wellbore sandface} \qquad (224)$$

In order to use such analytical solution in computational procedures, equations are to be discretized in space and time. The horizontal section is divided into M segments with an equal length of L, equation (184) becomes

$$P_D(x_D, r_{wD}, t_D) = \int_0^{t_D} \sum_{i=1}^{M} q_{hD}(t'_D)\, G_{Di}(x_{Dj}, t_D - t'_D)\, dt_D' \qquad (225)$$

Where

$$G_{Di}(x_D, y_D, z_D; x_{wD}, y_{wD}, z_{wD}, t_D) = \frac{\sqrt{\pi}}{4}\sqrt{\frac{k^2}{k_x k_y}}\int_0^{\tau_D} \exp\left[\frac{-(y_D - y_{wD})^2}{4t_D}\right]$$

$$\left[erf\left(\frac{x_D - x_{wD} - \frac{i-1}{M} L_D h_D \sqrt{\frac{k}{k_x}}}{2\sqrt{t_D}}\right) - erf\left(\frac{x_D - x_{wD} - \frac{i}{M} L_D h_D \sqrt{\frac{k}{k_x}}}{2\sqrt{t_D}}\right)\right]$$

$$\left\{1 + 2\sum_{n=1}^{\infty} \exp\left[\frac{-n^2\pi^2 t_D}{h_D^2}\right] \cos n\pi z_{wD} \cos n\pi z_D\right\} \frac{dt_D}{\sqrt{t_D}} \qquad (226)$$

We may now write P_D as follows:

$$P_D(x_{Dj}, y_D, z_D; x_{wD}, y_{wD}, z_{wD}, t_D) = \int_0^{t_D} \sum_{i=1}^{M} q_{hD}(\tau_D) G_{Di}(x_{Dj}, y_D, z_D; x_{wD}, y_{wD}, z_{wD}, t_D - \tau_D) d\tau_D$$

(227)

Where we shall divide the well into M equal segments to obtain the dimensionless Green's function for the well as:

If we discretize equation (191) in time domain, we obtain

$$P_D(x_{Dj}, y_D, z_D; x_{wD}, y_{wD}, z_{wD}, t_D) = \sum_{l=1}^{N} \int_{t_{Dl-1}}^{t_{Dl}} \sum_{i=1}^{M} q_{hDi}(\tau_D) G_{Di}(x_{Dj}, y_D, z_D; x_{wD}, y_{wD}, z_{wD}, t_D - \tau_D) d\tau_D$$

(228)

If we assume q_{hDi} to be constant in each time interval (t_{Dl}, t_{Dl-1}), then we obtain;

$$P_D(x_{Dj}, y_D, z_D; x_{wD}, y_{wD}, z_{wD}, t_D) = \tilde{P}_D(x_{Dj}, y_D, z_D; x_{wD}, y_{wD}, z_{wD}, t_D) + \sum_{i=1}^{M} q_{hDi}(\tau_{DN}) \int_0^{t_{DN}-t_{DN-1}} G_{Di}(x_{Dj}, y_D, z_D; x_{wD}, y_{wD}, z_{wD}, t_D - \tau_D) d\tau_D \quad (229)$$

In equation (193), we have used

$$\tilde{P}_D(x_{Dj}, y_D, z_D; x_{wD}, y_{wD}, z_{wD}, t_D) = \sum_{l=1}^{N-1} \sum_{i=1}^{M} q_{hDi}(t_{Dl}) \left[\int_0^{t_{DN}-t_{Dl-1}} G_{Di}(x_{Dj}, y_D, z_D; x_{wD}, y_{wD}, z_{wD}, \tau_D) d\tau_D - \int_0^{t_{DN}-t_{Dl}} G_{Di}(x_{Dj}, y_D, z_D; x_{wD}, y_{wD}, z_{wD}, \tau_D) d\tau_D \right] \quad (230)$$

Where the source function in the equation $G_{\mathrm{D}i}$ is given by

$$G_{\mathrm{D}i}(x_{Dj}, t_D) = \frac{\sqrt{\pi}}{4} \left(\left[erf\left(\frac{x_{Dj} - \frac{2i-2}{M}}{2\sqrt{t_D}} \right) - erf\left(\frac{x_{Dj} - \frac{2i}{M}}{2\sqrt{t_D}} \right) \right] \left(1 + 2\sum_{n=1}^{\infty} \exp\left(-\eta^2 \pi^2 {l_D}^2 t_D\right) \cos\left(\eta\pi(z_{wD} + r_{wD})\right) \cos\left(\eta\pi z_{wD}\right) \right) \frac{1}{\sqrt{t_D}} \right) \quad (231)$$

Or discretizing in time,

$$P_D(x_{Dj}, r_{wD}, t_D) = \sum_{k=1}^{N} \int_{t_{Dk-1}}^{t_{Dk}} \sum_{i=1}^{M} q_{hD_i}(t'_D)\, G_{\mathrm{D}_i}(x_{Dj}, t_D - t'_D)\, dt'_D \quad (232)$$

Where N is the number of points. If we assume that the flux, q_{hD} , is constant, during the time step $\left(t_{Dk} - t_{Dk-1}\right)$, then equation become

$$P_D(x_{Dj}, r_{wD}, t_D) = \widetilde{P}_D(x_{Dj}, r_{wD}, t_{DN}) + \sum_{i=1}^{M} q_{hDi}(t_{DN}) \int_0^{t_{DN}-t_{Dk}} G_{D_i}(x_{Dj}, t_D - t'_D)\, dt'_D \quad (233)$$

Where

$$\widetilde{P}_D(x_{Dj}, r_{wD}, t_{DN}) = \sum_{k=1}^{N-1} \sum_{i=1}^{M} q_{hDi}(t_{Dk}) \left[\int_0^{t_{DN}-t_{Dk-1}} G_{D_i}(x_{Dj}, t'_D)\, dt'_D - \int_0^{t_{DN}-t_{Dk}} G_{D_i}(x_{Dj}, t'_D)\, dt'_D \right] \quad (234)$$

In order to compute the specific transient productivity index along the horizontal well, the Greens function is obtained from t=0 to the time of interest and the theoretical index for segment i is obtained in dimensionless form by

$$PI_D(i, t_D) = q_{hDj}(t_{DN}) / P_D(t_{DN}) \quad (235)$$

The actual index is obtained by incorporating the mechanical skin along the horizontal well as follows

$$PI_D(i, t_D) = q_{hDj}(t_{DN}) / \left(P_D(t_{DN}) + S(i)\right) \quad (236)$$

Where $S(i)$ is the mechanical skin at the segment of study.

We may also incorporate the wellbore hydraulics effect in the formula and consider as a pseudo skin effect

$$PI_D(i, t_D) = q_{hDj}(t_{DN}) / \left(P_D(t_{DN}) + S(i) + \Delta P_f(i)\right) \quad (237)$$

The total dimensionless transient productivity index is basically the summation of the productivity indices along the horizontal well length as agreed upon in literature.

$$PI_{Dt}(i, t_D) = \sum_{i=1}^{M} PI_D(i, t_D) \quad (238)$$

The calculated specific transient productivity index along the horizontal well at different time steps for equal flow rates from both segments and double rates respectively are shown in figures 37 and 38. The results show that the values are the same for equal rate while they are double at the double rate at initial time which changes to be equal at later time for both wings and both production scenarios which signify the domination of reservoir response.

These calculations can be repeated if the skin factor is to be considered.

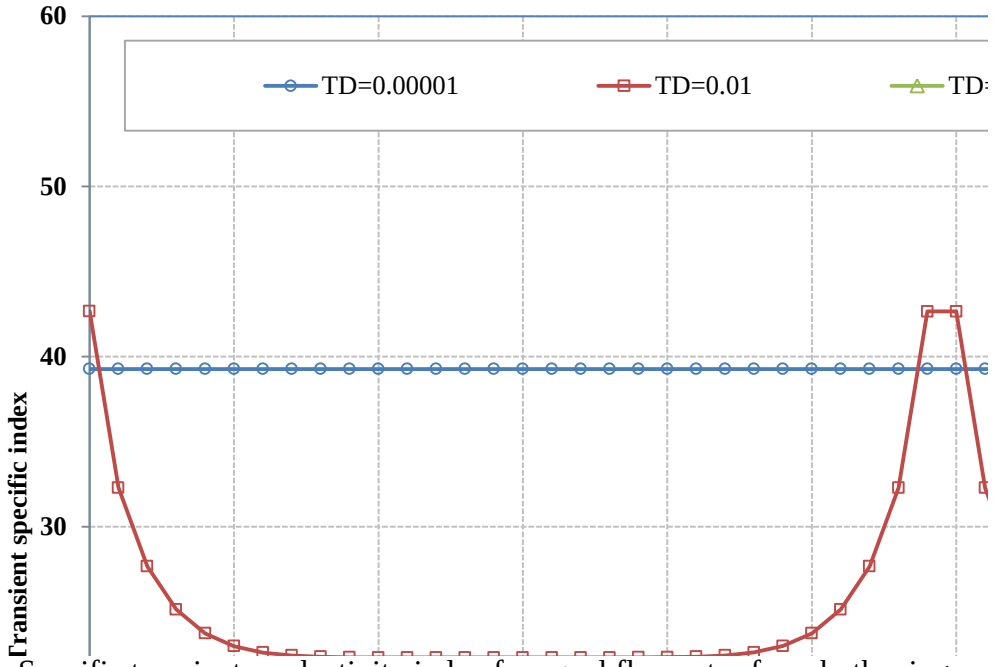

Fig. 39- Specific transient productivity index for equal flow rates from both wings

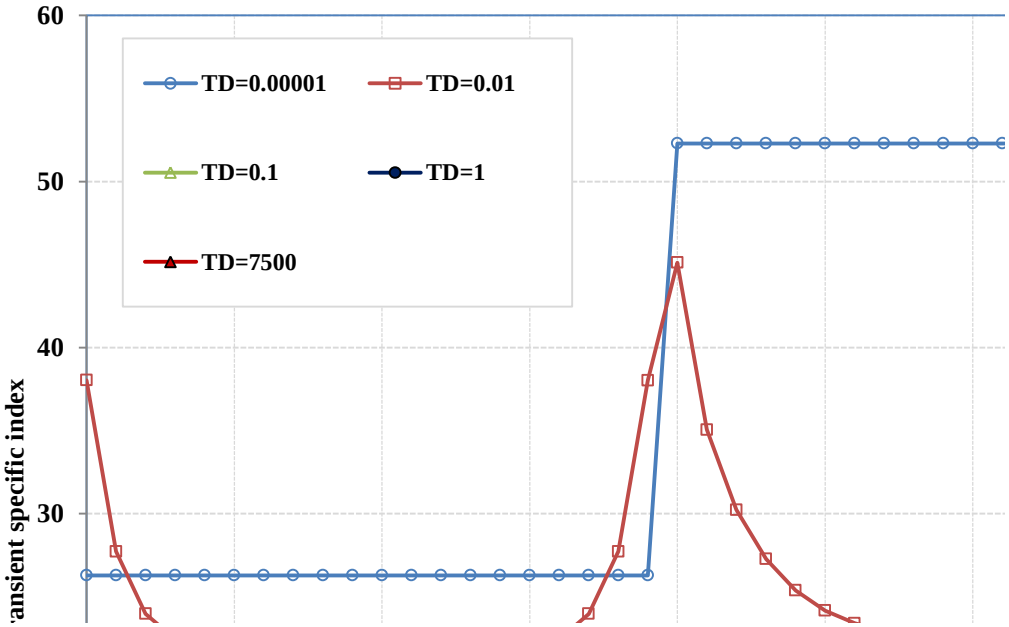

Fig. 40- Specific transient productivity index for double flow rate from right wing.

3.5.6 Skin Consideration in Transient Pressure Calculations

Since long time, the skin damage and its effect has been considered by reservoir engineers. The skin effect occurs in a region of altered permeability adjacent to the wellbore. The skin factor effect and challenges it creates on performance of horizontal wells have been investigated in literature using different models and hypothesis and assuming increasing skin damage towards the heel of the well [Renard et al. (1990) [7], Ozkan and Raghavan (1997) [22]].

The pressure drop between the skin boundary and wellbore at some point is:

$$P_s(r_s, x, t) - P_s(r_w, x, t) = \frac{141.2\,\mu}{K_s} q_{hs}(x, t) \ln \frac{r_s}{r_w} \qquad (239)$$

Similarly, if the permeability of the skin zone were the same as that of the reservoir (no skin damage), then the pressure drop across the skin zone would be:

$$P_s(r_s, x, t) - P(r_w, x, t) = \frac{141.2\,\mu}{K_r} q_{hs}(x, t) \ln \frac{r_s}{r_w} \tag{240}$$

Then the additional pressure drop at the wellbore because of the skin region is given by:

$$\Delta P_s(r_s, x, t) = \Delta P_s(r_s, x, t) + \frac{141.2\,\mu}{K_s} q_{hs}(x, t) S_m(x, t) \tag{241}$$

Where

$$\Delta P_s(r, x, t) = P(r, x, t) - P_s(r_s, x, t) \tag{242}$$

And

The dimensionless mechanical skin factor can be expressed in terms of the flux distribution by

$$S_m(x, t) = \frac{P_f(r_w, x, t) - P_s(r_w, x, t)}{\frac{LK_r}{hK}\left(r\frac{dP}{dr}\right)_{r=rw,\,x}} = \frac{\frac{kh}{141.2qB\mu}}{q_{hsD}} \tag{243}$$

Where

$$qhs_D = \frac{q_h(x, t)L}{q} = \frac{Lk_r}{141.2qB\,\mu}\left[r\frac{dP}{dr}\right]_{r=rw,\,x} \tag{244}$$

The pressure drop in dimensionless form at some point in the reservoir (any point in the well), using the reservoir response and considering the effect of skin factor, is given by:

$$P_{hDi}(x_{Di}, t_D) = P_{Di}(x_{Di}, y_{wDi}, z_{wDi} + r_{wDi}; x_{wDi}, y_{wDi}, z_{wDi}, t_D) + q_{hDi}(x_{Di}, t_D) S(x_{Di}) \tag{245}$$

Where q_{hDi} is for the flow at the point

$S(x_{Di})$ is the mechanical skin around the well at point x_{Di}.

The dimensionless pressure drop due to skin has been given as:

$$P_{Ds} = q_{hDi} L_{Di} h_{Di} S_{hm} \sqrt{\frac{k}{k_x}} \tag{246}$$

Where the horizontal well skin factor is defined by Ozkan and Raghavan (1997) as:

$$S_{hm} = \frac{P_{hi}(r_w, x, t) - P_s(r_w + \Delta r_{ws}, x, t)}{\frac{Lk_{\tilde{r}}}{kh}\left(\tilde{r}\frac{\partial P}{\partial \tilde{r}}\right)_{\tilde{r}=r_w, x}} = \frac{\frac{kh}{141.2qB\mu}\Delta P_s}{\tilde{q}_{hDi}} = \frac{h}{2L_H}\frac{k}{k_{\tilde{r}}}\left(\frac{k_{\tilde{r}}}{k_s} - 1\right)\ln\frac{\tilde{r}_s}{r_w} \tag{247}$$

The mechanical skin factor, $S_{hm}(x_D)$ is related to the skin effect by the following equation

$$S(x_D) = q_{hD}(x_D)S(x_D) = \frac{kh}{141.2qB\mu}\Delta P_s \tag{248}$$

And using this coordinate center, equation (209) can be written as:

$$P_{hD}(x_D, t_D) = P_D(x_D, 0, z_{wD} + r_{wD}; 0, 0, z_{wD}, t_D) + q_{hD}(x_D, t_D)S(x_D) \tag{248}$$

The wellbore flow rate and pressure at a given point are dependent on flux distribution (wellbore hydraulics). The wellbore pressure, hence, affects the flux distribution which requires understanding the relation of reservoir performance and wellbore hydraulics.

And incorporating the wellbore hydraulics, the wellbore pressure is obtained by

$$P_{wD}(t_D) = P_D(x_D, t_D) - \frac{N_{\mathrm{Re}t} f_t}{16}\frac{\pi}{C_{hD}}\left(2x_D - \int_0^x \int_0^{x'}\left(\frac{D_f}{N_{\mathrm{Re}t} f_t}\right) q_{hD} dx'' dx'\right) \tag{249}$$

If we divide the total length of the wellbore into equal M segments and denoting the center of each segment as x_{Dj}, we may write the double integral in equation (214) as:

$$\int_{x_{wD}}^{x_D}\int^{x_D'} D q_{hD} dx_D'' dx_D' = \sum_{i=1}^{j-1}\left(x_{Dj} - i\Delta x_{D1} + \frac{\Delta x_{D1}}{2}\right)\Delta x_{D1} D q_{hDi} + \frac{\Delta x_{D1}^2}{8} D_j q_{hDj} \tag{250}$$

In equation 250, D_i and q_{hDi} are evaluated at the center of the i^{th} interval.

$$P_{wD}(t_D) = P_D(J, t_D) - \frac{\pi N_{\mathrm{Re}t} f_t}{8 C_{hD}} \frac{(2j-1)}{M} + \frac{\pi}{16 C_{hD}} \left(\sum_{i=1}^{j-1} \left(2 \left(\frac{j-i}{M^2} \right) \right) \frac{1}{M} D_{f,i} q_{hD,i} + \frac{D_{f,j} q_{hD,j}}{2M^2} \right)$$

(251)

The mechanical skin factor along the horizontal section in each segment can be incorporated into eq. 251, then the equation becomes

$$P_{wD}(t_{DN}) - \sum_{k=1}^{N-1} \sum_{i=1}^{M} q_{hDi}(t_{Dk}) \left[\int_0^{t_{DN}-t_{Dk-1}} G_{Di}(x_{Dj}, t'_D) dt'_D - \int_0^{t_{DN}-t_{Dk}} G_{Di}(x_{Dj}, t'_D) dt'_D \right]$$
$$= \sum_{i=1}^{M} q_{hDi}(t_{DN}) \int_0^{t_{DN}-t_{DN-1}} G_{Di}(x_{Dj}, t_D - t'_D) dt'_D + q_{hDj}(t_{DN}) S_{hmj} \qquad (252)$$

And eq. 252 becomes

$$P_{wD}(t_{DN}) - \sum_{i=1}^{j-1} \left[\tilde{s}_{ij} - \frac{\pi}{16 C_{hD}} \left(\frac{j-i}{M^2} \right) D_i \right] q_{hDi}(t_{DN}). - \sum_{i=j+1}^{M} q_{hDi}(t_{DN}). \tilde{s}_{ij} + \frac{\pi}{16 C_{hD}} \left(\frac{D_j q_{hDj}}{8M^2} \right) =$$
$$\frac{N_{\mathrm{Re}t} f_t}{8} \frac{\pi}{C_{hD}} \left(\frac{2j-1}{M} \right) + \hat{P}_D(x_{Dj}, r_{wD}, t_{DN}) + q_{hDj}(t_{DN}) S_{hmj}$$

(253)

Rearranging,

$$P_{wD}(t_{DN}) - \sum_{i=1}^{j-1} \left[\tilde{s}_{ij} - \frac{\pi}{16 C_{hD}} \left(\frac{j-i}{M^2} \right) D_i \right] q_{hDi}(t_{DN}). - \left[S_{hmj} + \tilde{s}_{jj} - \frac{\pi}{16 C_{hD}} \left(\frac{D_j q_{hDj}}{8M^2} \right) \right] q_{hDj}(t_{DN}) - \sum_{i=j+1}^{M} q_{hDi}(t_{DN}). \tilde{s}_{ij} =$$
$$\frac{N_{\mathrm{Re}t} f_t}{8} \frac{\pi}{C_{hD}} \left(\frac{2j-1}{M} \right) + \hat{P}_D(x_{Dj}, r_{wD}, t_{DN})$$

(254)

Using eq. 254 and the previous solution approach, the dimensionless flux and wellbore pressure can be calculated.

If we assume a conical shape skin factor as more accepted in literature, with a skin value ranging from 0.1 to 0.01 in the conventional flow to left and from to 0.01 to 0.1 in the case with flow to the right.

Results for flow towards the left are shown in Fig's 41 and 42.

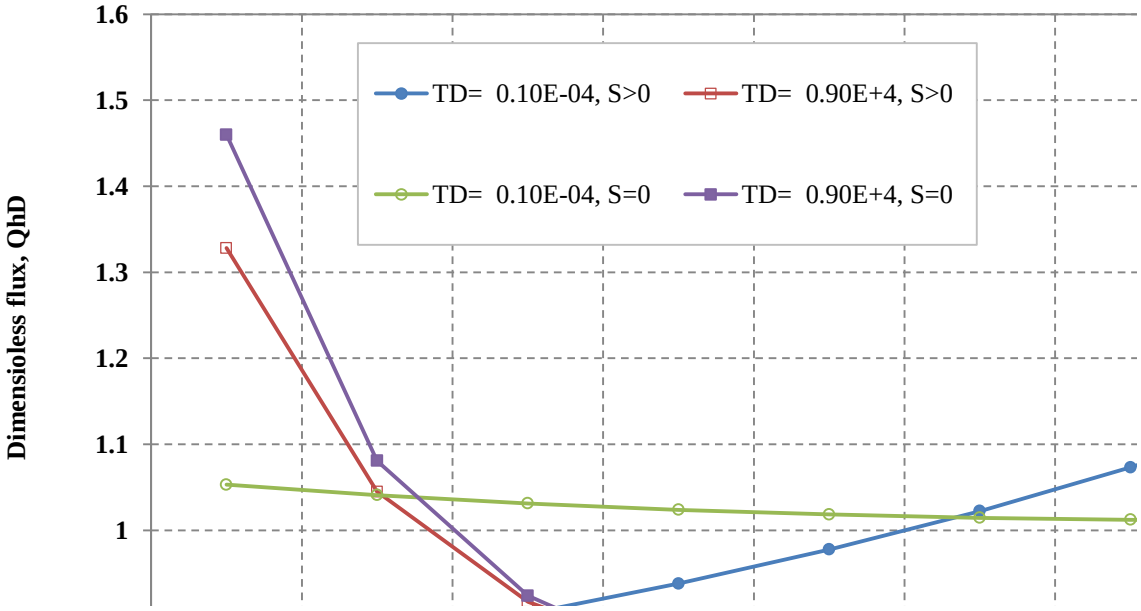

Fig. 41- Dimensionless flux profile along the U-shape finite conductivity well (increasing skin value towards the heel, left flow)

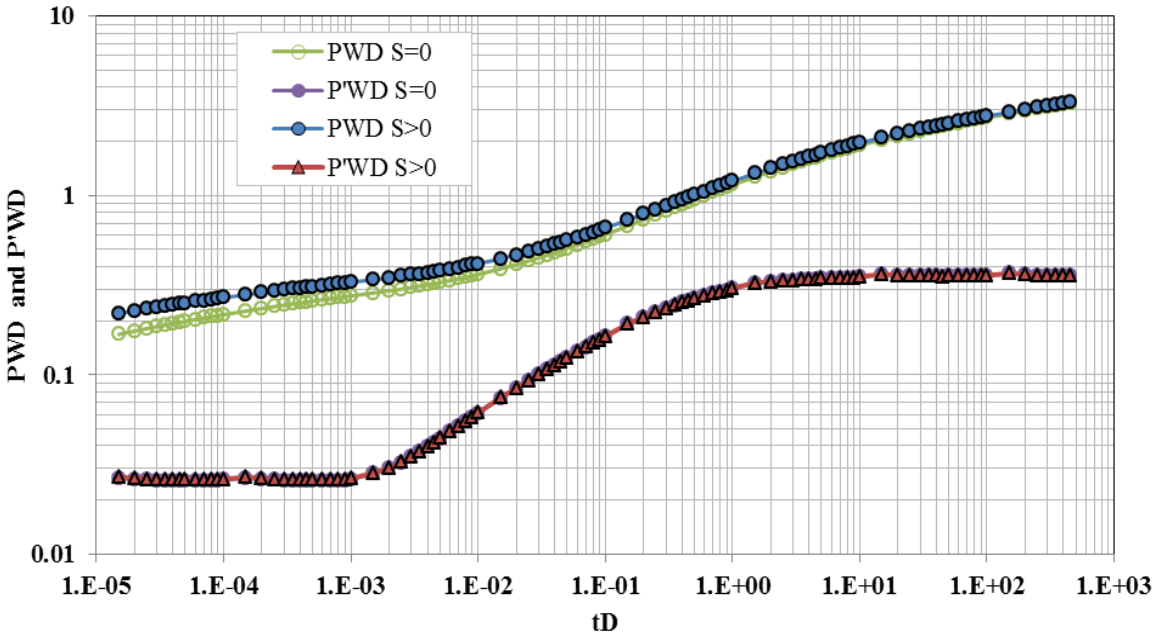

Fig. 42- Dimensionless pressure and derivative of the U-shape finite conductivity well (increasing skin value towards the heel, left flow)

Similarly, for the flow towards the right, Results for flow towards the left are shown in Fig's 43 and 44.

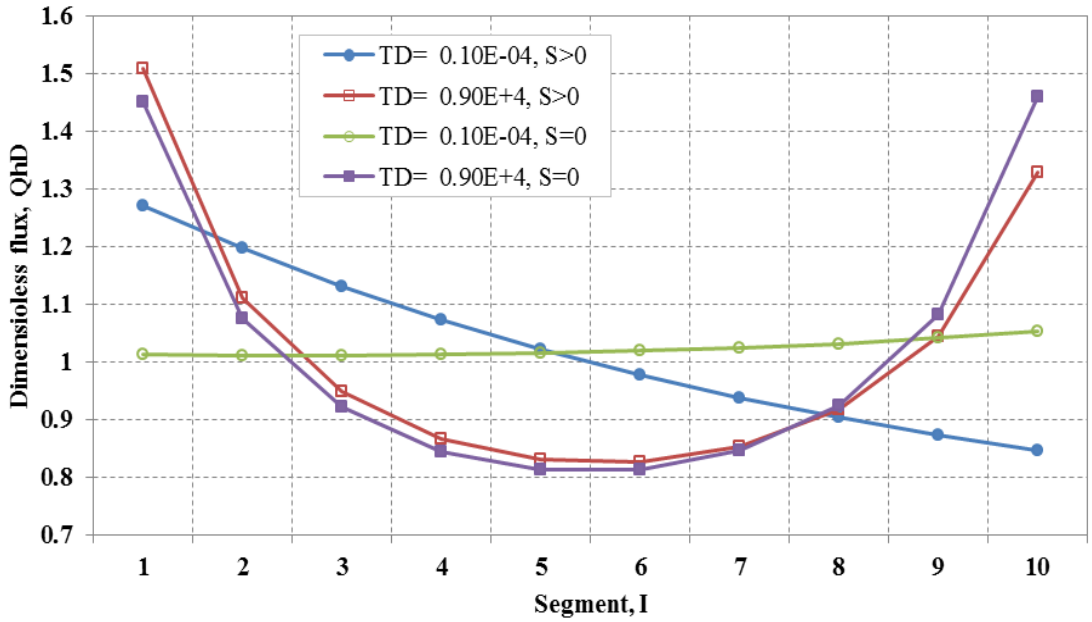

Fig. 43- Dimensionless flux profile along the U-shape finite conductivity well (increasing skin value towards the toe, left flow)

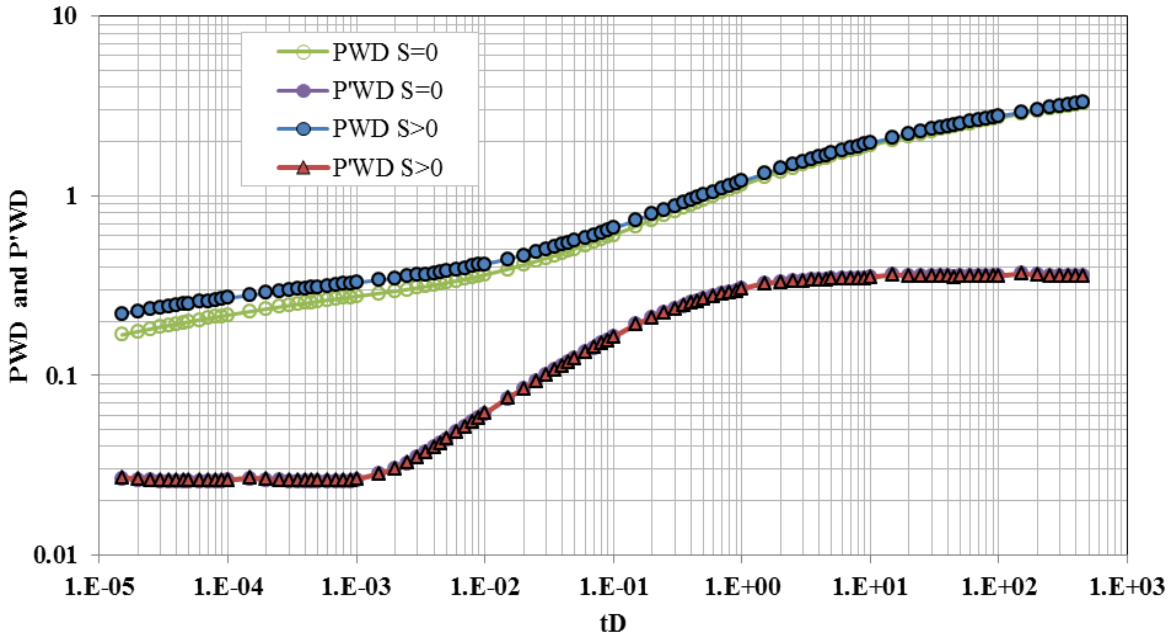

Fig. 44- Dimensionless pressure and derivative of the U-shape finite conductivity well (increasing skin value towards the toe, left flow)

To investigate the performance of horizontal wells under the combined influence of wellbore friction and formation damage, a new model is used for the U-shaped well which couples wellbore, reservoir, and non-uniform skin along the wellbore. For the U-shaped well with flow in both directions, equation 179 is modified to describe flow where the flow is split at segment Msp.

$$P_{wD}(t_{DN}) - \left[\sum_{i=Msp+1}^{M} q_{hDi}(t_{DN})\,G_{ij} - q_{hDj}(t_{DN})\,S_j\right]_{FTL} - \left[\sum_{i=1}^{Msp} q_{hDi}(t_{DN})\,G_{ij} - q_{hDj}(t_{DN})\,S_j\right]_{FTR}$$
$$+\left(\frac{2\pi\,\tilde{L}_D}{16C_{hD}}\left[\sum_{i=1}^{j-1}\left(\frac{j-i}{Msp^2}\right)D_i q_{hDi} + \frac{1}{2Msp^2}D_j q_{hDj}\right] - \frac{\pi N_{Ret} f_t}{8C_{hD}}\frac{(2j-1)}{Msp}\right)_{FTL}$$
$$-\left(\frac{2\pi\,\tilde{L}_D}{16C_{hD}}\left[\sum_{i=Msp+1}^{j-1}\left(\frac{j-i}{(M-Msp)^2}\right)D_i q_{hDi} - \frac{1}{2(M-Msp)^2}D_j q_{hDj}\right] - \frac{\pi N_{Ret} f_t}{8C_{hD}}\frac{(2j-1)}{(M-Msp)}\right)_{FTL}$$
$$= \tilde{P}_{DHj} + \tilde{P}_{DTj} \qquad (255)$$

Where FTR & FTL are the flow towards right and left respectively.

Incorporating the skin effect into the calculation, shown in Fig.'s 47 to 48 are the plots for different scenarios for skin values of 0, 0.1, 1, and 10 at early time (t_D=0.10E-04) and late time (t_D=0.75E+04) for both constant skin value and varying values along the horizontal section.

For constant skin values, results are shown in Fig.45.

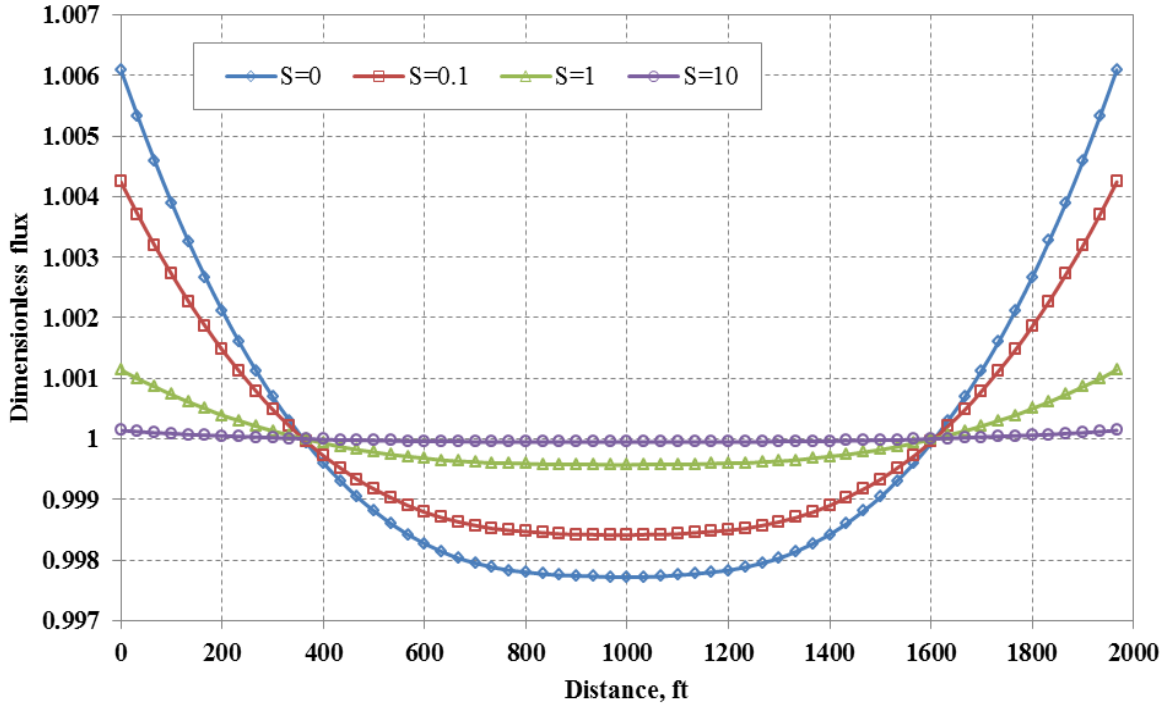

Fig.45- Dimensionless flux for different skin values at early time (t_D=0.10E-04)

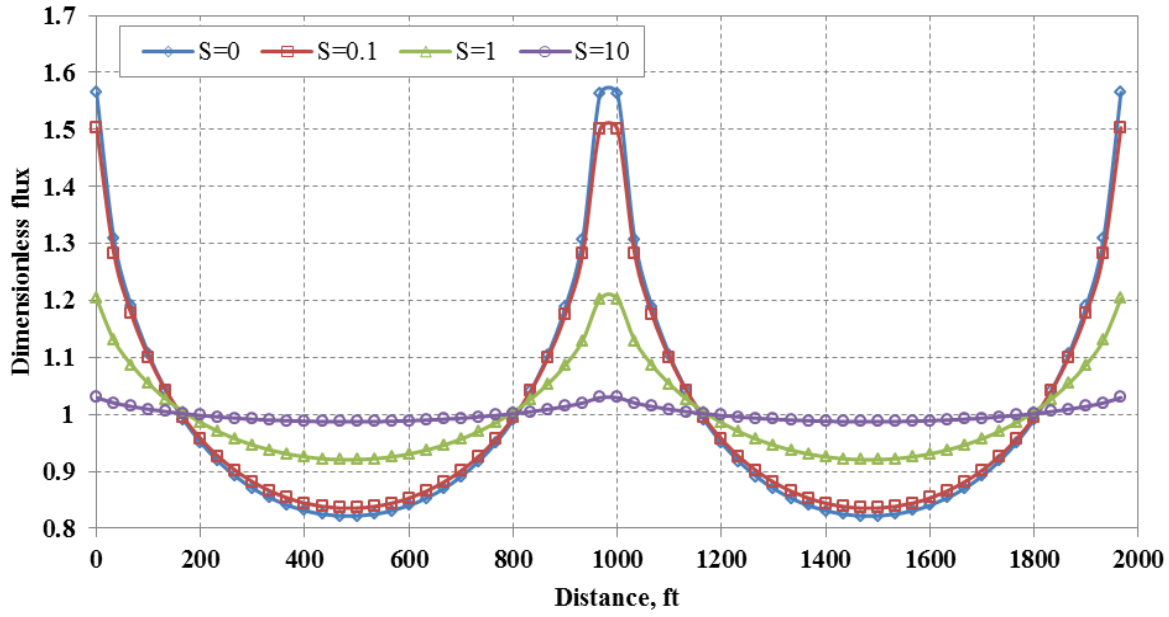

Fig.46- Dimensionless flux for different skin values at early time (t_D=0.75E+04)

For varying skin values, with increasing skin value from the toe of each wing, results are shown in Fig. 47.

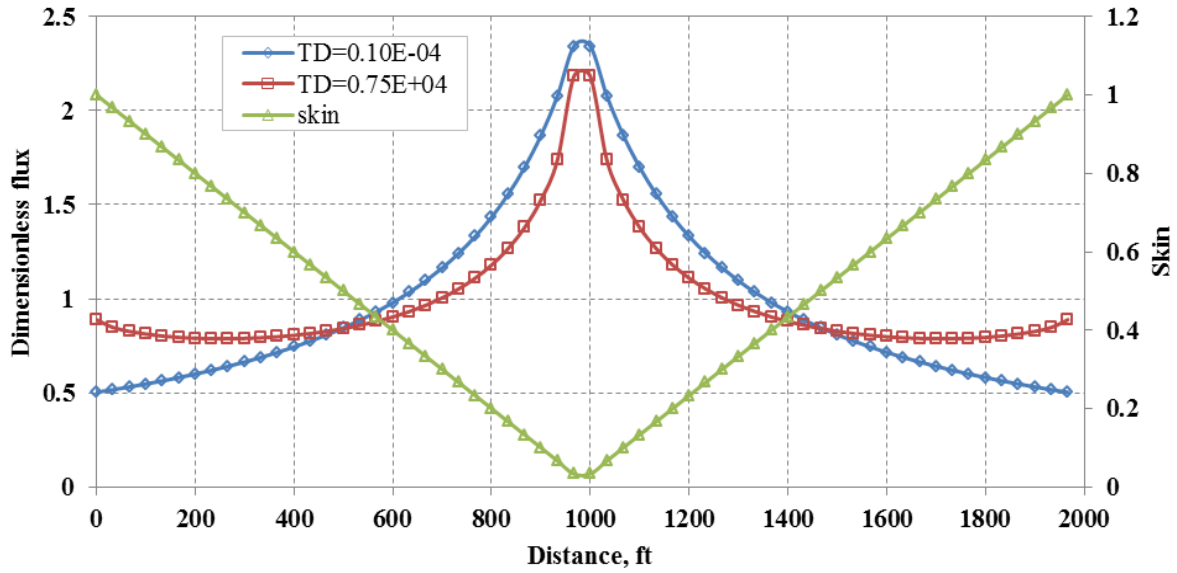

Fig.47- Dimensionless flux for decreasing skin value at middle for different times.

For varying skin values, with decreasing skin value from the toe of each wing, results are shown in Fig. 48.

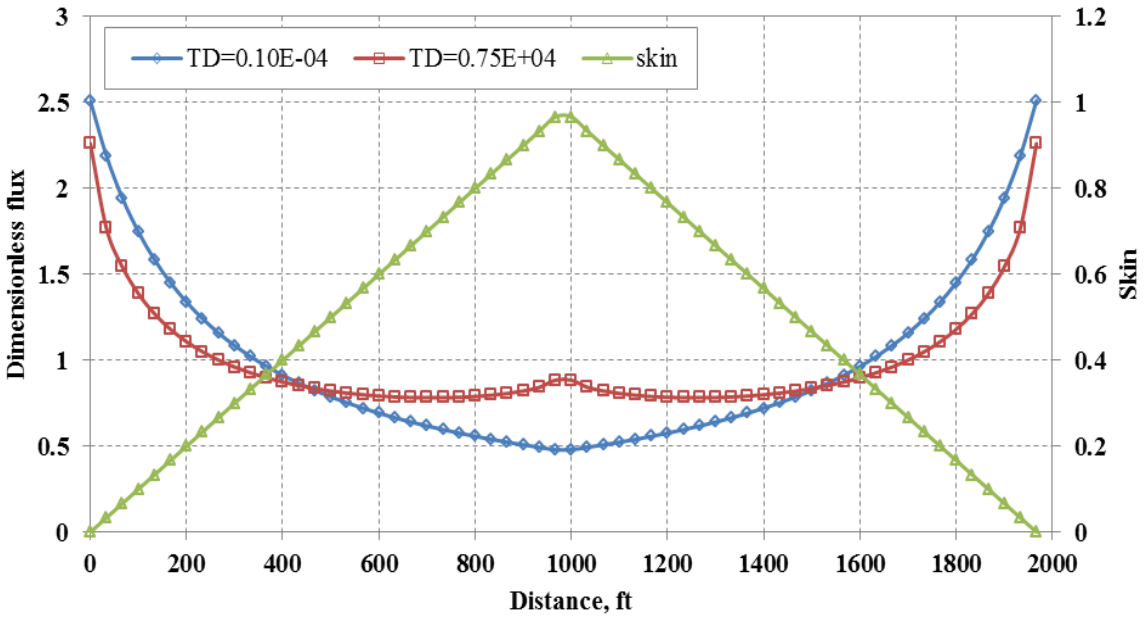

Fig.48- Dimensionless flux for increasing skin value at middle for different times

If we need to evaluate the skin effect on a well if the choice is to drill a classical horizontal well or a U-shaped well, then the skin damage at the toe of both scenarios are assumed to be the same (in this example S=0.039) and increase linearly with the same rate of 0.01. The distribution of assumed skin is shown in Fig. 49.

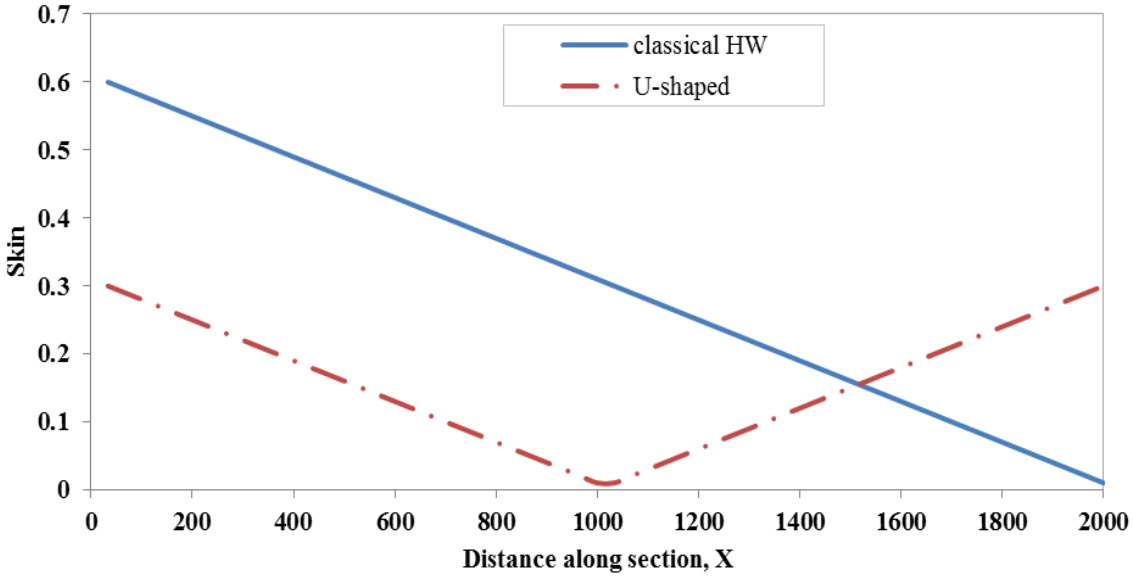

Fig.49- Assumed skin value profile for two well designs

The calculated impact of the skin distribution is shown in Fig.50.

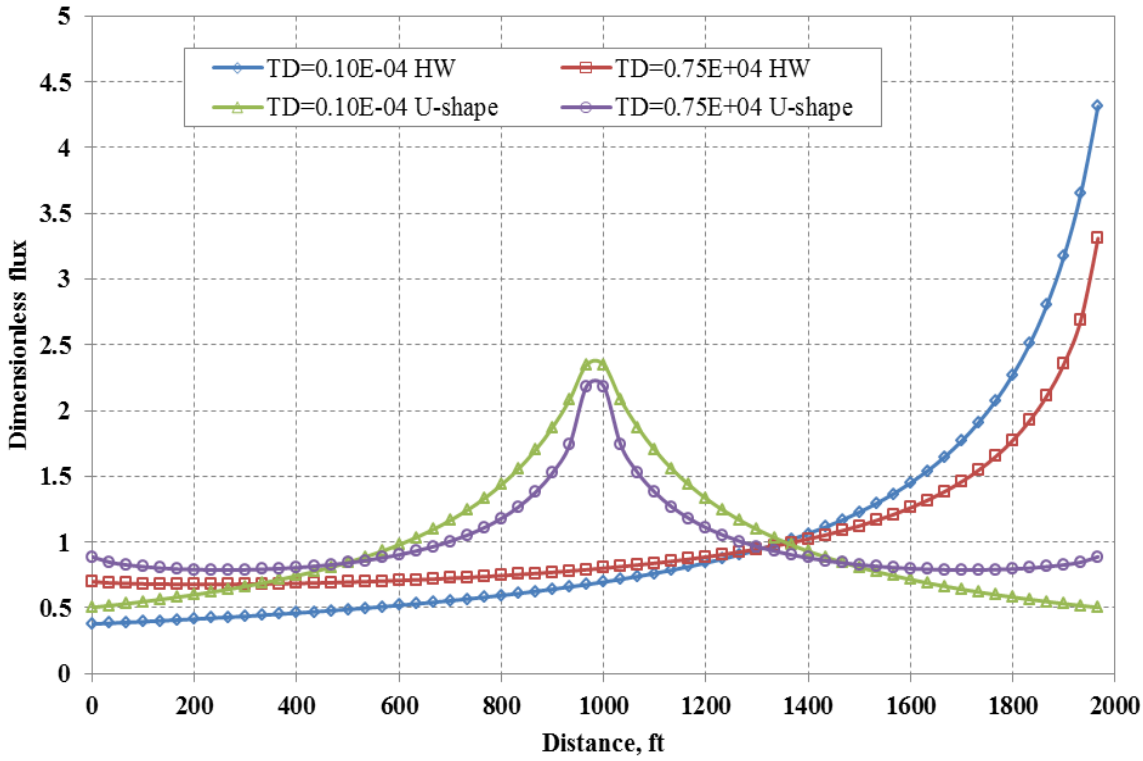

Fig. 50- Dimensionless flux for different well design

Results showed that skin factor does impact the flux profile along the horizontal well and it is a function of the combination of reservoir flow characteristics and well conductivity. Hence, it is an important factor that cannot be overlooked. The U-shaped design is a way to improve well performance by reducing mechanical damage during drilling and permanent effect of wellbore hydraulics. In addition, the wellbore damage may not be viewed merely as an additive pressure drop due to skin in the presence of friction inside the long horizontal section of the well. Wellbore hydraulics changes the flux distribution (inflow profile) along the wellbore and, thus, results in additional pressure drop in the reservoir and across the skin zone. Horizontal wells, for a number of reasons, are unlikely to have smooth distributions of damage along their trajectories. Thus, segmented well testing would be an ideal tool to estimate the skin, Si, of each segment especially in the zone where more severe damage is expected, because it delivers a detailed picture of the skin distribution along an extended horizontal well.

CHAPTER 4

4.1 Application of U-Shaped Horizontal Well

Simulating the field case presented in fig. 51 to calculate the flow profile along the horizontal well bore, the wellbore/flow profile were calculated by a steady-state model, similar to the previous calculations, assuming a pipe-flow model with a modified friction factors for the wellbore wall friction. The wellbore section composes of perforated (open to flow) and non-perforated sections (no flow). The non-perforated sections are treated as pipe flow model where in the other sections the flow contribution from the reservoir is augmented in calculations of wellbore hydraulics. The simulated runs utilized calculated values for the specific productivity index for perforated sections to get a good match the field case. The unit PI values for the perforated zones were assumed to get a good match. The calculated values of the PI increase at the heel and toe of the well as expected. The composite PI value of the well match the actual PI obtained from the production log.

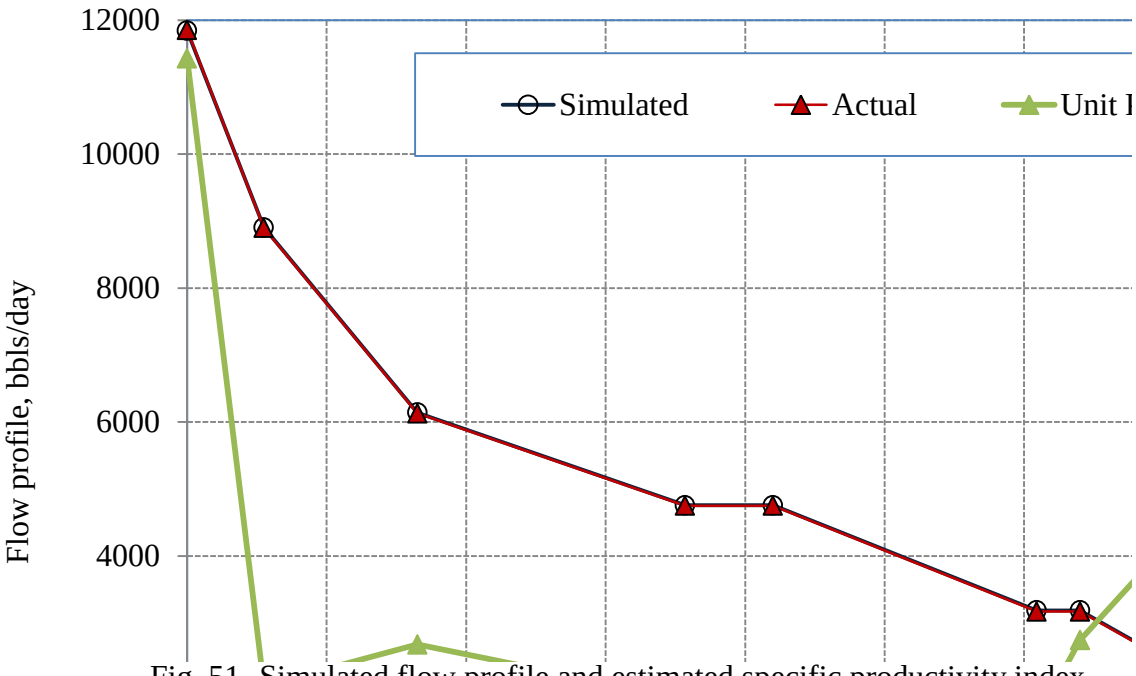

Fig. 51- Simulated flow profile and estimated specific productivity index.

The application of U-shaped horizontal well design will add lots of advantages to the use of horizontal wells. Aside from wellbore accessibility and reduction of exposure to drilling fluid, hence less potential of damage, the split of flow to both directions is a way to reduce the fluid travel distance and hence reduce the impact of frictional pressure losses.

4.2 U-shaped Horizontal Well Flow Simulation

The flow simulation of horizontal well performance to show the merit of having the U-shaped well design was done for a 4000 foot horizontal well and for two well productivity indices (1000 and 2000 STB/D/psi), for the well data shown in table 1. The flow simulations in such wells have shown that these wells will be far restricted by the outflow performance, i.e. wellbore hydraulics and not the inflow performance or the flow capacity of the reservoir.

Figure 52 shows a comparison of the flow profiles considering the two PI values. The results show that the high PI well will suffer from effect of the frictional pressure losses in the wellbore and some portion of the section will yield no contribution.

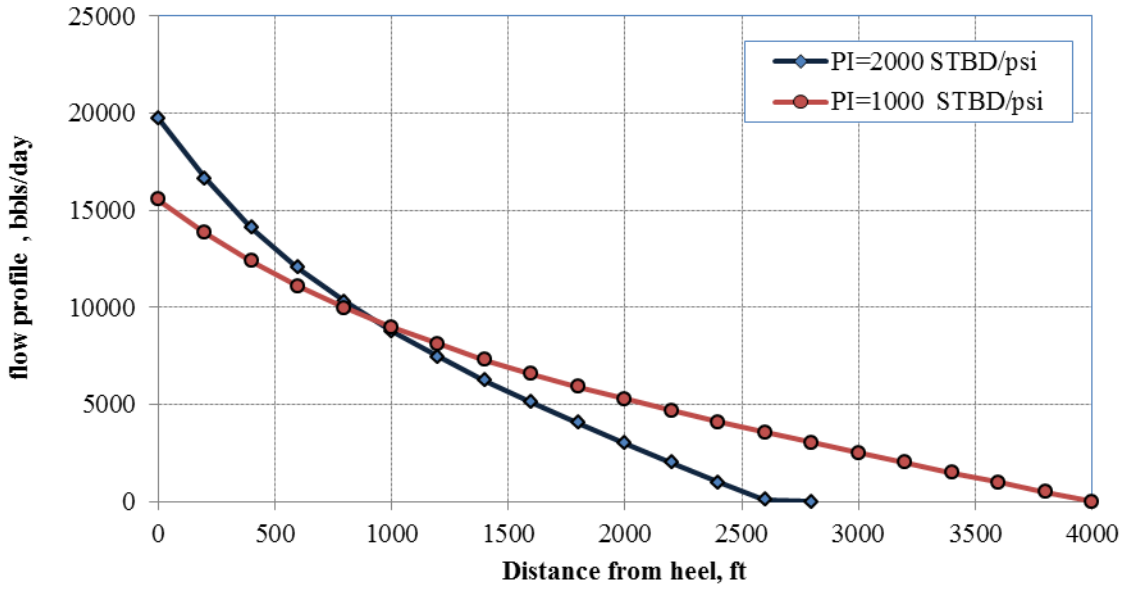

Fig. 52- Flow profiles considering the two PI values.

Looking at the pressure profiles in both cases of PI values, Fig. 53 shows a comparison of the flow profiles where the wellbore pressure reaches a constant value faster in the high PI case and hence less contribution from the rest of the section.

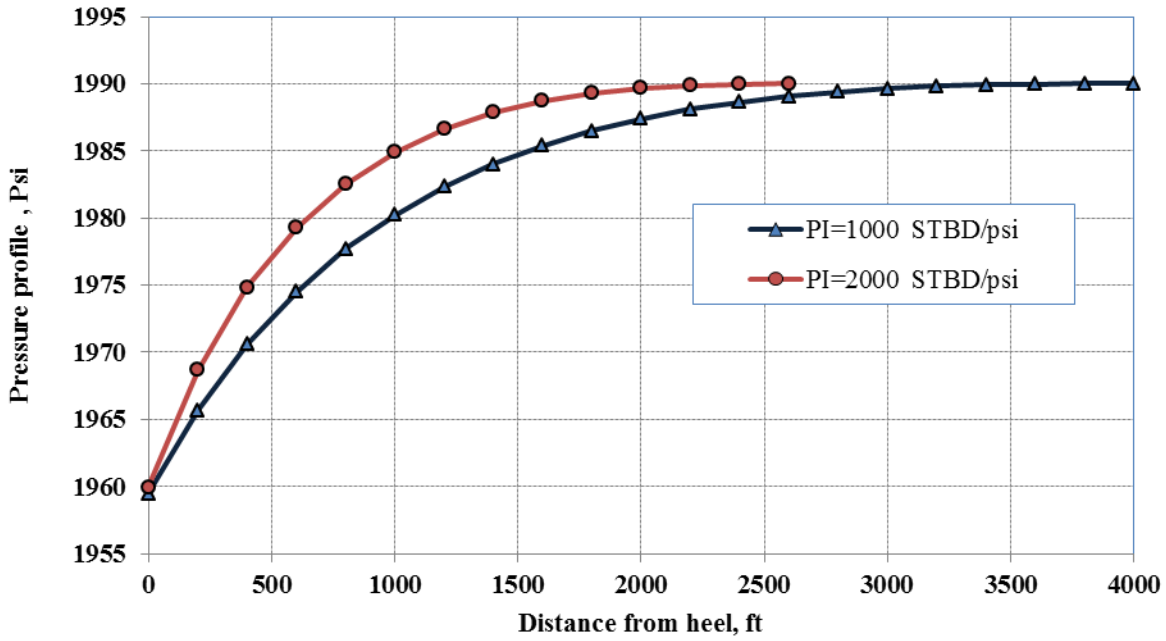

Fig. 53- Pressure profiles considering the two PI values.

Calculating the frictional pressure loses in both scenarios, as shown in Fig. 54, the frictional pressure losses in the 2000 PI well are more as expected for the same pressure drawdown of 10.32 psi at the toe of the wells.

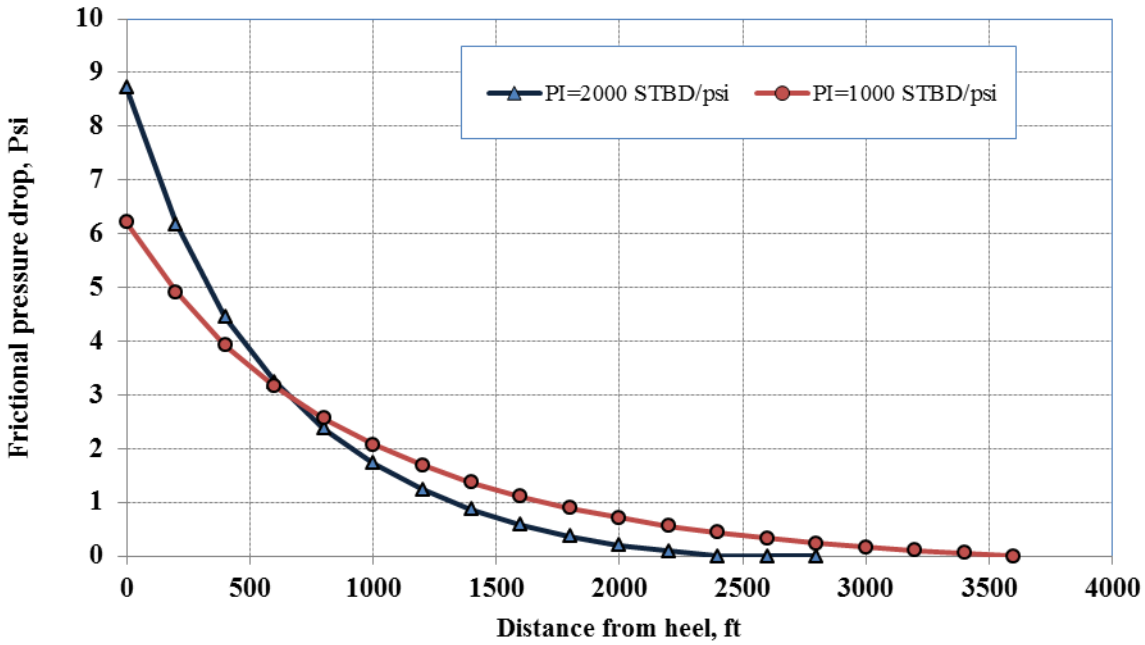

Fig. 54- Frictional pressure losses considering the two PI values.

Using the same well data and applying the U-shape design, flow simulation indicated less flow restriction from the effect of friction as flow travel will be split into half reducing the frictional losses by half. Figure 55 shows the simulation of the U-shaped well with flow production from both sides. Simulations indicated that each wing can produce almost as the full length conventional well. In addition, it shows the pressure profiles in both wings.

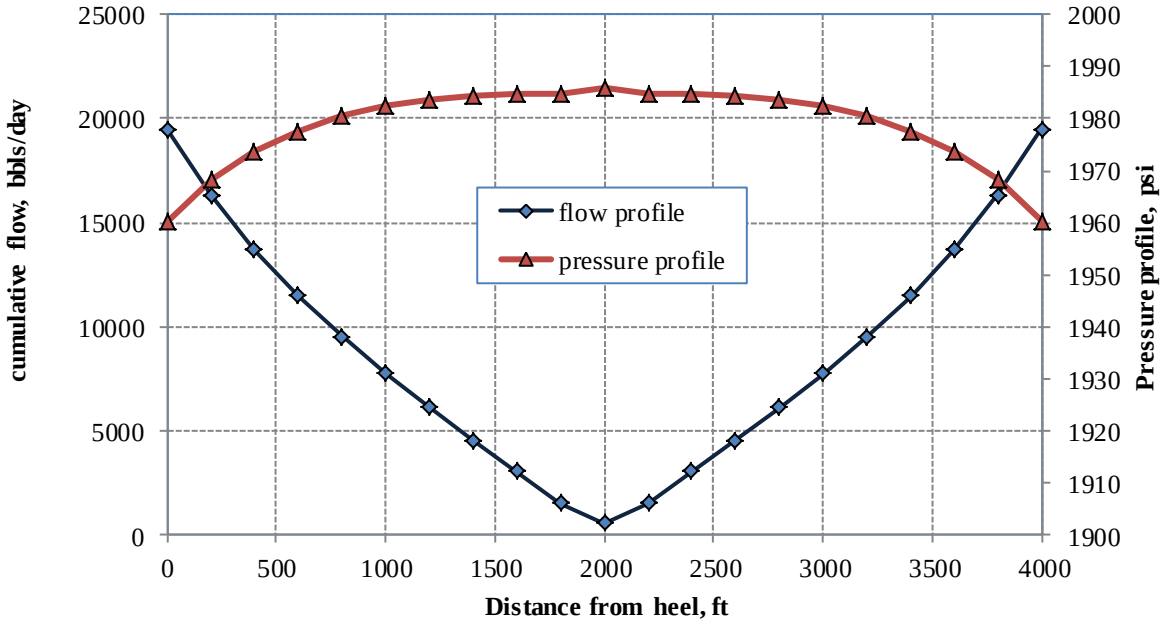

Fig. 55- Flow and pressure profiles of the U-shaped horizontal well.

Calculating the frictional pressure for the U-shaped well, as shown in Fig. 56 below, the frictional pressure losses is less which makes the pressure drawdown at the middle around 15 psi yielding high flow into the wellbore.

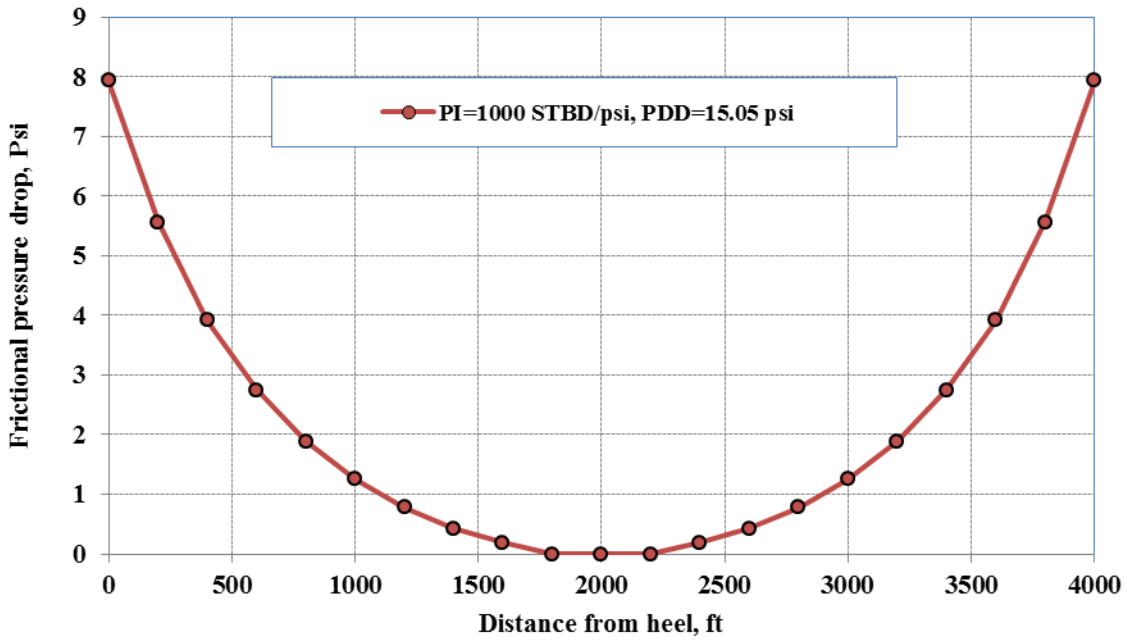

Fig. 56- Frictional pressure losses considering the U-shaped well.

Table1: well data for the cases in study

API	**27**	
Sol. GOR	**300**	**SCF/STB**
Gas gravity	**0.78**	
B_o	**1.09**	**RB/STB**
Diameter	**5**	**in**
Viscosity	**1**	**cp**
P_e	**2000**	**psi**
P_{wf}	**1960**	**psi**
L_w	**4000**	**feet**

CHAPTER 5

CONCLUSIONS AND RECOMMENDATIONS

5.1 CONCLUSIONS

Flow simulation supported by the reality in the field in producing horizontal wells showed that wellbore hydraulics impact the flow profile and influxes along the horizontal wellbore. This effect is exacerbated by conditions in the section with the presence of multiphase flow and undulation of the section that create liquid flow back and accumulation of fluids. Alleviating the impact of wellbore hydraulics and associated flow conditions will help enhance flow capacity. The U-shaped flow setup could optimize the flow efficiency of the system by mitigating/alleviating those flow hinders. The right wing location could be optimized by being at any position along the horizontal wellbore to ensure optimum flow and flow assurance.

Another way to offset the impact of wellbore hydraulics is to maximize flow efficiency from non/low contributing sections is by enhancing their productivities by any method like hydraulic fracturing.

A semi-analytical solution to predict the performance of a U-shaped horizontal well and its pressure transient responses at both ends was developed. The model was developed for a single phase flow and for a homogenous but an anisotropic reservoir. The reservoir is assumed to be an infinite acting reservoir. The well is assumed to be a finite-conductivity well which account for the impact of wellbore frictional losses. The solution assumes a U-shaped horizontal well with flexibility to produce from both ends at any desired rate ratio. Based on the results of this study the following conclusions can be derived:

1. The proposed U-shaped horizontal well has been found to be a viable solution for the non-contributing section of the horizontal drain-hole.

2. The results show that a split of flow occurs along the horizontal section. The position of this split is found to be function of the rate ratio of the production from both ends, skin damage, and frictional pressure loss. Not only this but, the results indicated an appreciable impact that show the merit of drilling the U-shape horizontal well and producing from both ends, which will reduce the frictional losses effect and hence maximize well performance.

3. The U-shaped horizontal well shows that the application of such well design will be a key enabler for flow assurance of long horizontal wells as it maximize flow capacity by alleviating the effect of wellbore hydraulics on flow influx into wellbore.

4. A new solution to calculate the transient specific productivity index along the horizontal section has been developed. The solution predicts the specific productivity as function of time along the horizontal drain-hole.

5.2 Recommendations for Future Works

1. Perform full-field reservoir simulation studies utilizing the U-shaped horizontal wells (both producers and injectors) and optimize the production from these reservoirs under different drive mechanisms.

2. Extend the existing model to handle multiphase flow.

3. Extend the existing model to predict the performance of multi-stage fractured horizontal wells.

APPENDIX A

A.1 Pressure Solutions of Diffusivity Equation

In deriving the diffusivity equation for radial flow toward a well in a circular reservoir, the isothermal flow of fluid with small and constant compressibility is assumed. The pressure gradient is assumed to be very small and the reservoir is assumed to be homogeneous and isotropic. All parameters of rock and fluid properties are assumed to be constant. By combining the conservation of mass and Darcy's law, the diffusivity equation in dimensionless form can be written as follows (Lee, 1982):

$$\frac{\partial^2 p_D}{\partial r_D{}^2} + \frac{1}{r_D}\frac{\partial p_D}{\partial r_D} = \frac{\partial p_D}{\partial t_D} \tag{A-1}$$

where

$$P_D = \frac{kh}{141.2 q \mu B}\Delta P, \tag{A-2}$$

And

$$t_D = \frac{0.0002637\, k\, t}{\phi \mu\, \mathrm{C_t}\, \mathrm{r_w}^2} \tag{A-3}$$

By giving initial and boundary conditions, the solution of the diffusivity equation can be derived analytically, semi-analytically, or numerically. These solutions include the van Everdingen and Hurst solution (van Everdingen and Hurst, 1949), the Theis solution (Theis, 1935), and the log approximation solution (Lee, 1982). In addition, the solutions of the diffusivity equation can also be solved using known source functions and flow rates (Gringarten and Ramey, 1973).

A.2 Source Function Solutions and Convolution

Some of the solutions of the diffusivity equation, or the pressure response function $P_D(t_D)$ can be derived by convolving source functions $S(t_D)$ with flow rates q_D (t_D) (Gringarten and Ramey, 1973; Raghavan, 1993):

$$P_D(t_D) = \int_0^{t_D} q_D(\tau)\, S(t_D - \tau)\, d\tau \qquad \text{(A-4)}$$

Where $S(t_D)$ is the instantaneous uniform-flux source function for the particular source-reservoir system.

A.3 Horizontal well in an infinite reservoir

Consider a horizontal well, such as in Fig. (1), producing slightly compressible petroleum fluids from an infinite-acting reservoir at a constant rate. To simulate the transient pressure response of this well, an analytical model should be used for this purpose. The following assumptions are very important for the selection of this model:

1- The reservoir is homogenous and having constant and uniform thickness with two impermeable layers at the top and bottom of the formation.

2- Constant porosity and permeability in each direction, but the formation is anisotropic.

3- Gravitational and frictional effects are negligible.

4- No-flow boundaries.

The solution to the diffusivity equation based on the above conditions can be obtained using different techniques which are applicable for the transient flow of fluid in the porous media. Gringarten, A. C. and Ramey, H. J. (1973) were the first to introduce the use of the source and Green's function in solving unsteady state flow problems in the reservoirs. They stated that the infinite line source can be visualized as the intersection of two perpendicular infinite plane sources normal to two of the three principal axes of permeability while the point source can be visualized as the intersection of three perpendicular infinite plane sources normal to the principal axes of permeability. Ozkan, E. (1988) introduced new source solutions to the diffusivity equation using the Laplace space to overcome the difficulties that might result when we apply the Gringarten and Ramey's source solution in complex geometrical configurations such as dual-porosity and dual-permeability porous media. Spivak, D. (1988) presented the same solution considering the infinite line source as a result of the integrating process for any point from ($-\infty$ to $+\infty$) and the pressure drop distribution created by a continuous source of any shape can be obtained by the principal of the superposition in time and space. Therefore

a line or a plane source can be generated by superposing an infinite number of point source along the line or plane. The mathematical model can be used to simulate the pressure behavior created by the constant production of a horizontal well having a known length and extending in the midpoint of an infinite formation having a known height is (Daviau et al 1988):

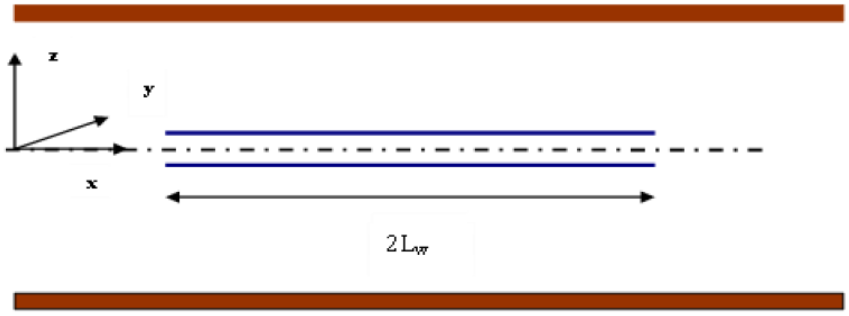

Fig. (57), Horizontal well acting in an infinite reservoir.

$$\Delta P(x,y,z,t)=\frac{q(\tau)}{\phi c_t}\int_0^t\left\{\frac{1}{2}\left[erf\left(\frac{\frac{l}{2}+(x-x_w)}{2\sqrt{\eta\, t}}\right)+erf\left(\frac{\frac{l}{2}-(x-x_w)}{2\sqrt{\eta\, t}}\right)\right]\times\frac{\exp\left[\frac{-(y-y_w)^2}{4\eta\, t}\right]}{2\sqrt{\pi\eta t}}\times\frac{1}{h}\left[1+2\sum_{n=1}^{\infty}\exp\left(-\frac{\eta^2\pi^2 t}{h^2}\right)\cos\left(\eta\pi\frac{z_w}{h}\right)\cos\left(\eta\pi\frac{z_w}{h}\right)\right]\right\}dt$$

(A-5)

In dimensionless form and for a typical horizontal well as shown in the figure below (ZwD=0.5). The calculations of PwD vs. tD are based on Ozkan's work in SPE paper 16378.

The reservoir response for a horizontal well is given by

$$P_D(x_D, y_D, z_D; z_{wD}, L_D, t_D) = \frac{\sqrt{\pi}}{4}\sqrt{\frac{k}{k_y}}\int_0^{\tau_D}\exp\left[\frac{-y^2{}_D}{4t_D}\right].\left[erf\frac{\left(\sqrt{\frac{k}{k_x}}+x_D\right)}{2\sqrt{t_D}}+erf\frac{\left(\sqrt{\frac{k}{k_x}}-x_D\right)}{2\sqrt{t_D}}\right]$$

$$\times\left\{1+2\sum_{n=1}^{\infty}\exp\left(-n^2\pi^2L^2{}_Dt_D\right)\cos n\pi z_{wD}\cos n\pi z_D\right\}\frac{dt_D}{\sqrt{t_D}} \qquad \text{(A-6)}$$

where the dimensionless parameters in the above model are defined as follows:

$$\eta = 2.637\ \text{x}10^{-4}\frac{k}{\mu\phi c_t} \qquad \text{(A-7)}$$

$$P_D(x_D, y_D, z_D; z_{wD}, L_D, t_D) = \frac{kh}{141.2q\mu B}\Delta P, \qquad \text{(A-8)}$$

$$t_D = \frac{2.637x10^{-4}kt}{\mu\phi c_t L} \qquad \text{(A-9)}$$

$$k = \sqrt[3]{k_x\,k_y\,k_z} \qquad \text{(A-10)}$$

$$x_D = \frac{2x}{L}\sqrt{\frac{k}{k_x}} \qquad \text{(A-11)}$$

$$x_{wD} = \frac{2x_w}{L}\sqrt{\frac{k}{k_x}} \qquad \text{(A-12)}$$

$$y_D = \frac{2y}{L}\sqrt{\frac{k}{k_x}} \tag{A-13}$$

$$y_{wD} = \frac{2y_w}{L}\sqrt{\frac{k}{k_x}} \tag{A-14}$$

$$z_D = \frac{z}{h}, \tag{A-15}$$

$$z_{wD} = \frac{z_w}{h}, \tag{A-16}$$

$$L_D = \frac{L}{2h}\sqrt{\frac{k_z}{k}} \tag{A-17}$$

$$h_D = \frac{2h}{L}\sqrt{\frac{k}{k_z}} \tag{A-18}$$

$$r_{wD} = \frac{r_{we}}{h} \tag{A-19}$$

$$r_{we} = \frac{r_w}{2}\left[\left(\frac{\sqrt{k_x k_y}}{k_z}\right)^{0.25} + \left(\frac{k_z}{\sqrt{k_x k_y}}\right)^{0.25}\right], \tag{A-20}$$

$$q_{hD} = \frac{q_h L}{qB}\sqrt{\frac{k_x}{k}}, \quad \text{where } q_h(x) \text{ be the flux along the wellbore sandface} \tag{A-21}$$

The above model consists of three instantaneous source functions which are S(x, t), S(y, t), and S(z, t). S(x, t) represents the infinite slab source in an infinite reservoir and S(y, t) represents the infinite plane source in an infinite reservoir while S(z, t) represents the infinite plane source in an infinite slab reservoir. To solve the above model, two approximations should be done for the three functions based on the fluid flow dynamic and flow regimes in early and late time.

A.4 Short-time approximation

At early time, it is known that there is no flow in the reservoir beyond the tips of the well. Therefore short-time approximation can be obtained by considering the asymptotic behavior of the three instantaneous source functions that are involved in the model. The first instantaneous function S(x, t) =1 when the monitoring point is located inside the well as the time approaches zero (Spivak 1988):

$$S(x_D, t_D) = \frac{1}{2\sqrt{\pi\eta_x t}} e^{-\frac{(x-x_w)^2}{4\eta_x t}} = 1 \qquad \text{(A-22)}$$

and the proper time limit for the above equation to be applied as determined by Gringarten and Ramey (1973) is:

$$t_D = \frac{(1-x_D)^2}{20} \qquad \text{(A-23)}$$

The second instantaneous function S(z, t) has the following formula:

$$S(z_D, t_D) = \frac{1}{2\sqrt{\pi\eta_x t}} e^{-\frac{(z-z_w)^2}{4\eta_x t}} = \frac{1}{2\sqrt{\pi\eta_x L_w}} \sqrt{\frac{k_x}{k_z}} e^{-\frac{(z_D)^2}{4t_D}} \qquad \text{(A-24)}$$

Since this function deals with the infinite plane source in an infinite slab reservoir, there is a time at which the upper or lower boundary starts to affect the pressure behavior. This time can be estimated by:

$$t_D \le \min\left[\begin{array}{c}\dfrac{\left[\left(\bar{z}_D + 2z_{wD}\right)/L_D\right]^2}{20} \\ \dfrac{\left[\left(\bar{z}_D + 2z_{wD} - 2\right)/L_D\right]^2}{20}\end{array}\right] \tag{A-25}$$

While the third instantaneous function S(y, t) has the following formula for the short time approximation:

$$S(y_D, t_D) = \frac{1}{2\sqrt{\pi\eta_y t}} e^{-\frac{(y-y_w)^2}{4\eta_x t}} = \frac{1}{2\sqrt{\pi\, t_D L_w}} \sqrt{\frac{\eta_x}{\eta_y}} e^{-\frac{(y_D)^2}{4t_D}} \tag{A-26}$$

and the proper time for this approximation to be applicable is:

$$t_D = \frac{{y_D}^2}{20} \tag{A-27}$$

Based on the short time approximations for the above three functions, the short time approximation for Eq. (261) can be written as the product of the three approximations:

$$P_D(x_D, y_D, z_D, z_{wD}, L_D, t_D) = \frac{1}{4L_D} \int_0^{\tau_D} \frac{1}{t_D} \exp\left[\frac{-({y_D}^2 + {z_D}^2)}{4t_D}\right] dt_D = \frac{1}{4L_D} E_i\left[\frac{-({y_D}^2 + {z_D}^2)}{4t_D}\right] \tag{A-28}$$

When $E_i\left[\dfrac{-({y_D}^2 + {z_D}^2)}{4t_D}\right] \le 0.01$,

$$P_D(x_D, y_D, z_D, L_D, t_D) = \frac{1}{4L_D}\left(\ln\left(\frac{t_D}{{y_D}^2 + {z_D}^2}\right) + 0.80907\right) \quad \text{(A-29)}$$

A.5 Long-time approximation

At late time, the pressure behavior of horizontal wells starts to be affected by the pseudo-steady state flow. Therefore the long time approximation of Eq. (261) takes into consideration this fact. The first instantaneous function which represents the infinite slab source in an infinite reservoir is approximated as follows (Spivak 1988):

$$S(x_D, t_D) = \frac{1}{2\sqrt{\pi\eta_x t}} e^{-\frac{(x-x_w)^2}{4\eta_x t}} = \frac{1}{\sqrt{\pi t_D}} \quad \text{(A-30)}$$

and the long limit of the time so that the pseudo steady state will take place is:

$$t_D = \frac{25(1-x_D)^2}{3} \quad \text{(A-31)}$$

The approximation for the second source function and the time limit are:

$$S(y_D, t_D) = \frac{1}{2\sqrt{\pi\, t_D L_w}} \sqrt{\frac{\eta_x}{\eta_y}} \quad \text{(A-32)}$$

$$t_D = 25{y_D}^2$$

while the approximation and the time limit for the third function are:

$$S(z_D, t_D) = \frac{1}{h} \tag{A-33}$$

$$t_D = \frac{5}{\pi^2 L_D{}^2} \tag{A-34}$$

Therefore the long time approximation of Eq. (261) can be written as follows:

$$P_D(x_D, y_D, z_D, z_{wD}, L_D, t_D) = \frac{q(\tau_D)}{2L_w \phi \mu} \int_0^{t_{D1}} S(x_D, t_D)\, S(y_D, t_D)\, S(z_D, t_D)\, d\tau_D + \frac{1}{2} \int_{t_{D1}}^{t_D} \frac{1}{\tau_D}\, d\tau_D$$

$$P_D(x_D, y_D, z_D, z_{wD}, L_D, t_D) = P_D(x_D, y_D, z_D, z_{wD}, L_D, t_{D1}) + \frac{1}{2} \ln\left(\frac{t_D}{t_{D1}}\right) \tag{A-35}$$

Where

$$t_{D1} \geq \max\begin{bmatrix} \frac{25}{3}(1 - x_D)^2 \\ 25 y_D{}^2 \\ \frac{5}{\pi^2 L_D{}^2} \end{bmatrix} \tag{A-36}$$

APPENDIX-B

PARAMETER ESTIMATION

The fundamental concept of parameter estimation is to determine optimal values of parameters for a numerical model that predicts dependent variable outputs of a function, process or phenomenon based on observations of independent variable inputs.

LEAST SQUARES METHODS

The least squares optimality criterion minimizes the sum of squares of residuals between actual observed outputs and output values of the numerical model that are predicted from input observations. The Newton-Raphson Algorithm is a method used to solve nonlinear least squares problems because it performs well and is easy to implement.

LINEAR MODELS

Many processes exhibit true linear behavior. Many others operate over such small excursions of input variable values that the output behavior appears linear.

The classic least squares problem is to fit a model with an input x's and output y's using parameters b and m as shown in Equation B-1. Multiple data observations may be concatenated as shown in Equation B-2 and represented in matrix form per Equation B-3. Even for optimal estimates of model parameters {β}, each data observation will have some residual error e_i between the observed output y_i and the predicted model output as shown in Equations B-4 and B-5.

$$y = b + m\,x = [\ x\ ]\begin{Bmatrix} b \\ m \end{Bmatrix} \tag{B-1}$$

$$\begin{Bmatrix} y_1 \\ y_2 \\ \vdots \\ y_{nobs} \end{Bmatrix} \approx \begin{bmatrix} 1 & x_1 \\ 1 & x_2 \\ \vdots & \vdots \\ 1 & x_{nobs} \end{bmatrix} \begin{Bmatrix} b \\ m \end{Bmatrix} \tag{B-2}$$

$$\{Y\} \approx [X]\ \{\beta\} \qquad \text{for } \underset{nobs\,x\,1}{\{Y\}} = \begin{Bmatrix} y_1 \\ y_2 \\ \vdots \\ y_{nobs} \end{Bmatrix} \qquad \underset{nobs\,x\,2}{[X]} = \begin{bmatrix} 1 & x_1 \\ 1 & x_2 \\ \vdots & \vdots \\ 1 & x_{nobs} \end{bmatrix} \qquad \underset{2\,x\,1}{\{\beta\}} = \begin{Bmatrix} b \\ m \end{Bmatrix} \tag{B-3}$$

$$\begin{Bmatrix} e_1 \\ e_2 \\ \vdots \\ e_{nobs} \end{Bmatrix} = \begin{Bmatrix} y_1 \\ y_2 \\ \vdots \\ y_{nobs} \end{Bmatrix} - \begin{bmatrix} 1 & x_1 \\ 1 & x_2 \\ \vdots & \vdots \\ 1 & x_{nobs} \end{bmatrix} \begin{Bmatrix} b \\ m \end{Bmatrix} \tag{B-4}$$

$$\{e\} = \{Y\} - [X]\ \{\beta\} \qquad \text{for } \underset{nobs\,x\,1}{\{e\}} = \begin{Bmatrix} e_1 \\ e_2 \\ \vdots \\ e_{nobs} \end{Bmatrix} \tag{B-5}$$

The scalar sum of squares SSQ of residual errors is shown in Equation B-6. To minimize the sum of squares, one may set the partial derivative of the sum of squares with respect to the model parameters

{β} equal to zero as shown in Equation B-7. Rearranging these terms provides a linear matrix solution for optimal model parameters per Equation B-8.

$$SSQ = \{e\}^T\{e\} = \{Y\}^T\{Y\} - 2\{\beta\}^T[X]^T\{Y\} + \{\beta\}^T[X]^T[X]\{\beta\} \quad \text{(B-6)}$$

$$\partial SSQ / \partial\{\beta\} = -2[X]^T\{Y\} + 2[X]^T[X]\{\beta\} = 0 \quad \text{(B-7)}$$

$$\underset{2\,x\,1}{\{\beta\}} = (\underset{2\,x\,nobs}{[X]^T}\ \underset{nobs\,x\,2}{[X]})^{-1}\ \underset{2\,x\,nobs}{[X]^T}\ \underset{nobs\,x\,1}{\{Y\}} \quad \text{(B-8)}$$

MULTIPLE DEPENDENT VARIABLES

Multiple simultaneous linear outputs for each input data observation may be modeled using this methodology as shown in Equation B-9. Note that the number of data observations *nobs* must be greater than or equal to the number of parameters *npar* (not *npar* times *nout*) to prevent singularity of the symmetric matrix ($[X]^T[X]$).

$$\underset{npar\,x\,nout}{\{\beta\}} = (\underset{npar\,x\,nobs}{[X]^T}\ \underset{nobs\,x\,npar}{[X]})^{-1}\ \underset{npar\,x\,nobs}{[X]^T}\ \underset{nobs\,x\,nout}{[Y]} \quad \text{(B-9)}$$

NON-LINEAR MODELS

It is often tempting to linearize models of nonlinear phenomena in an effort to arrive at estimates for parameters. One should exercise caution however in that linear least squares solutions for linearized models minimize the sum of squares of residuals for nonlinear forms of the dependent variables rather than residuals of those dependent variables themselves.

LEVENBERG-MARQUARDT

The Levenberg-Marquardt algorithm iteratively adjusts estimates of nonlinear model parameters {β} to minimize residuals between measured dependent variable outputs {y} and predictions from a numerical model f(.) based on independent variable inputs {x} as shown in Equation B-10. For a given set of model parameters $\{\beta\}_k$ at iteration *k* each measured training pair $\{x\}_i$ and $\{y\}_i$ will have residuals $\{e\}_{i,k}$ as shown in Equation B-11. For parameter updates {Δβ} shown in Equation B-12, the Taylor series expansion for residuals at iteration *k+1* may be written as shown in Equation B-13 using the Jacobian [J] of the numerical model with respect to model parameters in Equation B-14.

$$\underset{\text{noutx 1}}{\{y\}} = f\left(\underset{\text{ninpx 1}}{\{x\}}, \underset{\text{nparx 1}}{\{\beta\}} \right) \tag{B-10}$$

$$\{e\}_{i,k} = \{y\}_i - f\left(\{x\}_i, \{\beta\}_k\right) \tag{B-11}$$

$$\{\beta\}_{k+1} = \{\beta\}_k + \{\Delta\beta\} \tag{B-12}$$

$$\underset{\text{noutx 1}}{\{e\}_{i,k+1}} = \underset{\text{noutx 1}}{\{e\}_{i,k}} - \underset{\text{noutx npar}}{[J]_{i,k}} \quad \underset{\text{nparx 1}}{\{\Delta\beta\}} \tag{B-13}$$

$$[J]_{i,k} = \begin{bmatrix} \frac{\partial f_1}{\partial \beta_1} & \frac{\partial f_1}{\partial \beta_2} & \cdots & \frac{\partial f_1}{\partial \beta_{npar}} \\ \frac{\partial f_2}{\partial \beta_1} & \frac{\partial f_2}{\partial \beta_2} & \cdots & \frac{\partial f_2}{\partial \beta_{npar}} \\ \vdots & \vdots & \ddots & \vdots \\ \frac{\partial f_{nout}}{\partial \beta_1} & \frac{\partial f_{nout}}{\partial \beta_2} & \cdots & \frac{\partial f_{nout}}{\partial \beta_{npar}} \end{bmatrix} \quad \text{evaluated for } \{x\}_i \tag{B-14}$$

If only one training pair is available and the number of dependent variable outputs is equal to the number of parameters (*nobs*=1 and *nout=npar*), Equation B-13 is deterministic and one can try to

drive all *nout* residuals $\{e\}_{i,k+1}$ to zero using Equation B-15. This provides the classical Newton-Raphson root finding algorithm shown in Equation B-16.

$$\{\Delta\beta\} = [J]^{-1}_{i,k} \{e\}_{i,k} \tag{B-15}$$

$$\{\Delta\beta\} = -[J]^{-1}_{i,k} \quad f(\{x\}_i, \{\beta\}_k) \qquad \text{for } \{y\}_i = \{0\} \tag{B-6}$$

If only one training pair is available and the number of dependent variable outputs is larger than the number of parameters (*nobs*=1 and *nout*>*npar*), residuals $\{e\}_{i,k+1}$ at iteration *k+1* can be minimized by the standard linear least squares solution shown in Equation B-17.

$$\underset{npar\,x\,1}{\{\Delta\beta\}} = \left(\underset{npar\,x\,nout}{[J]^T_{i,k}} \quad \underset{nout\,x\,npar}{[J]_{i,k}} \right)^{-1} \left(\underset{npar\,x\,nout}{[J]^T_{i,k}} \quad \underset{nout\,x\,1}{\{e\}_{i,k}} \right) \tag{B-17}$$

However, if the number of parameters is greater than the number of dependent variable outputs, Equation B-17 is row insufficient and multiple training pairs are required (*nobs*>1 for *nout*<*npar*). Residuals from all training pairs at iteration *k* shown in Equation B-11 may be concatenated as shown in Equation B-18 providing an aggregate sum of squares SSQ over all observations. Similarly all residuals predicted at iteration *k+1* for update $\{\Delta\beta\}$ in Equation B-13 may be concatenated as shown Equation B-19. The linear least squares solution for parameter updates that will minimize the predicted aggregate SSQ after at iteration *k+1* is then shown in Equations B-20 and B-21.

$$SSQ_k = \begin{Bmatrix} \{e\}_{1,k} \\ \{e\}_{2,k} \\ \vdots \\ \{e\}_{nobs,k} \end{Bmatrix}^T \begin{Bmatrix} \{e\}_{1,k} \\ \{e\}_{2,k} \\ \vdots \\ \{e\}_{nobs,k} \end{Bmatrix} = \sum_{i=1}^{nobs} \left(\{e\}^T_{i,k} \{e\}_{i,k} \right) \tag{B-18}$$

$$\begin{Bmatrix} \{e\}_{1,k+1} \\ \{e\}_{2,k+1} \\ \vdots \\ \{e\}_{nobs,k+1} \end{Bmatrix} = \begin{Bmatrix} \{e\}_{1,k} \\ \{e\}_{2,k} \\ \vdots \\ \{e\}_{nobs,k} \end{Bmatrix} - \begin{bmatrix} [J]_{1,k} \\ [J]_{2,k} \\ \vdots \\ [J]_{nobs,k} \end{bmatrix} \{\Delta\beta\} \tag{B-19}$$

$$\{\Delta\beta\} = \left(\begin{bmatrix} [J]_{1,k} \\ [J]_{2,k} \\ \vdots \\ [J]_{nobs,k} \end{bmatrix}^T \begin{bmatrix} [J]_{1,k} \\ [J]_{2,k} \\ \vdots \\ [J]_{nobs,k} \end{bmatrix} \right)^{-1} \left(\begin{bmatrix} [J]_{1,k} \\ [J]_{2,k} \\ \vdots \\ [J]_{nobs,k} \end{bmatrix}^T \begin{Bmatrix} \{e\}_{1,k} \\ \{e\}_{2,k} \\ \vdots \\ \{e\}_{nobs,k} \end{Bmatrix} \right) \tag{B-20}$$

$$\{\Delta\beta\} = \left(\sum_{i=1}^{nobs} \left([J]_{i,k}^T [J]_{i,k} \right) \right)^{-1} \left(\sum_{i=1}^{nobs} \left([J]_{i,k}^T \{e\}_{i,k} \right) \right) \tag{B-21}$$

Equation B-21 provides rapid second order Newtonian convergence but can become unstable if the square Jacobian summation is nearly singular. Levenberg and Marquardt showed that a positive factor λ added to the diagonal elements of the square Jacobian summation matrix as shown in Equation B-22 can provide both rapid and stable convergence. For very small values of λ, this provides Newtonian convergence similar to Equation B-21. For larger values of λ, this provides small but stable steps along the gradient shown in Equation B-23.

$$\{\Delta\beta\} = \left(\sum_{i=1}^{nobs} \left([J]_{i,k}^T [J]_{i,k} \right) + \lambda \underset{npar\,x\,npar}{[I]} \right)^{-1} \left(\sum_{i=1}^{nobs} \left([J]_{i,k}^T \{e\}_{i,k} \right) \right) \tag{B-22}$$

$$\{\Delta\beta\} = \frac{1}{\lambda} \left(\sum_{i=1}^{nobs} \left([J]_{i,k}^T \{e\}_{i,k} \right) \right) \tag{B-23}$$

If parameter updates provide a stable step with smaller aggregate SSQ than prior iterations, factor λ is reduced in preparation for the next iteration. If parameter updates provide an unstable step with larger aggregate SSQ than prior iterations, those updates are rejected, factor λ is increased and the process is

repeated. Typically λ is started at a value of 0.1, is reduced by a factor of 10 for stable steps, and is increased by a factor of 10 for unstable steps.

Convergence may be assessed by observing when absolute values of parameter updates are small while the aggregate SSQ approaches the expected standard deviation of residuals. Observing the progression of factor λ can also help indicate convergence.

The algorithm may be summarized as follows.

1) Postulate initial estimates for parameters $\{\beta\}$
2) Evaluate aggregate SSQ over all training pairs for initial parameter estimates (Equation B-18)
3) Set factor $\lambda = 0.1$
4) Proceed through all training pairs
    a) Evaluate all residuals $\{e\}_{i,k}$ (Equation B-11)
    b) Evaluate all Jacobians $[J]_{i.k}$ (Equation B-14)
    c) Accumulate summations $\sum_{i=1}^{nobs}\left([J]_{i,k}^{T} [J]_{i,k} \right)$ and $\sum_{i=1}^{nobs}\left([J]_{i,k}^{T} \{e\}_{i,k} \right)$ (Equation B-23)
5) Add factor λ to diagonal and compute parameter updates $\{\Delta\beta\}$ (Equation B-22)
6) Update parameters $\{\beta\}_{k+1}$ (Equation B-12)
7) Evaluate aggregate SSQ over all training pairs for new parameter estimates (Equation B-18)
8) If aggregate SSQ has been reduced:
    a) Reduce factor $\lambda_{NEW} = \lambda_{OLD} / 10$
    b) Proceed with the next iteration at step 4)
9) If aggregate SSQ has increased:

a) Discard the new parameter estimates and use immediate prior values

b) Increasee factor $\lambda_{NEW} = \lambda_{OLD} * 10$

c) Proceed with the next iteration at step 5)

Because of its robust performance, Levenberg-Marquardt method is often used with finite difference numerical approximations for the Jacobian [J] of the numerical model with respect to model parameters. Note that this Jacobian must be re-evaluated for each training pair for each iteration whether analytically or numerically.

Penalty functions may be added to residuals to impose explicit or implicit inequality constraints on parameters. However as with any gradient technique, convergence may dither across constraint boundaries if the minimum SSQ is at a constraint boundary.

Levenberg, K. "A Method for the Solution of Certain Problems in Least Squares." *Quart. Appl. Math.* **2**, 164-168, 1944.

Marquardt, D. "An Algorithm for Least-Squares Estimation of Nonlinear Parameters." *SIAM J. Appl. Math.* **11**, 431-441, 1963.

APPENDIX-C

Table C-1 data for Fig.1

	flow profile	wellbore pressure
0	11855	3088.8
55	8900	3090.64
165	6130	3091.86
357	4750	3092.4
420	4750	3092.6
609	3170	3092.9
640	3170	3093.2
745	1944	3093.4
787	1944	3093.7
920	750	3093.7
921	550	3093.7
935	0	3093.7

Table C-2 data for Fig. 2

	Frictional losses	wellbore pressure
0	4.9	3088.8
55	3.06	3090.64
165	1.84	3091.86
357	1.3	3092.4
420	1.1	3092.6
609	0.8	3092.9
640	0.5	3093.2
745	0.3	3093.4
787	0	3093.7
920	0	3093.7
921	0	3093.7
935	0	3093.7

Table C-3 data for Fig.6

td	Ld=0.1	Ld=1	Ld=5	Ld=10	Ld=50	Ld=100	Ld=200
1.E-04	15.1679	1.705517	0.34519	0.174181	3.73E-02	2.02E-02	1.15E-02
2.E-04	15.59674	1.785889	0.362069	0.182621	3.90E-02	2.10E-02	1.20E-02
2.E-04	15.86536	1.842218	0.374044	0.18861	4.02E-02	2.16E-02	1.23E-02
3.E-04	16.05402	1.885454	0.38333	0.193255	4.12E-02	2.21E-02	1.25E-02
3.E-04	16.19594	1.920454	0.390912	0.19705	4.19E-02	2.25E-02	1.27E-02
4.E-04	16.30771	1.949795	0.397318	0.20026	4.26E-02	2.28E-02	1.29E-02
4.E-04	16.39871	1.975014	0.402862	0.203039	4.31E-02	2.31E-02	1.30E-02
5.E-04	16.47466	1.997097	0.407746	0.205491	4.36E-02	2.33E-02	1.31E-02
5.E-04	16.53931	2.016715	0.41211	0.207685	4.40E-02	2.35E-02	1.32E-02
6.E-04	16.64421	2.050336	0.419649	0.211481	4.48E-02	2.39E-02	1.34E-02
7.E-04	16.72634	2.07844	0.42601	0.214692	4.54E-02	2.43E-02	1.36E-02
8.E-04	16.79298	2.102547	0.431512	0.217476	4.60E-02	2.45E-02	1.37E-02
9.E-04	16.84854	2.123643	0.436366	0.219938	4.65E-02	2.48E-02	1.39E-02
1.E-03	16.89587	2.142403	0.440715	0.222149	4.69E-02	2.50E-02	1.40E-02
2.E-03	17.06094	2.214328	0.45773	0.230841	4.87E-02	2.59E-02	1.44E-02
2.E-03	17.1667	2.266755	0.47051	0.23741	5.00E-02	2.65E-02	1.47E-02
3.E-03	17.24541	2.309461	0.481206	0.24293	5.11E-02	2.71E-02	1.50E-02
3.E-03	17.30872	2.346232	0.490651	0.247817	5.21E-02	2.76E-02	1.53E-02
4.E-03	17.36196	2.378857	0.499231	0.252267	5.30E-02	2.80E-02	1.55E-02
4.E-03	17.40801	2.40833	0.507156	0.256385	5.38E-02	2.85E-02	1.57E-02
5.E-03	17.44862	2.435282	0.514558	0.260238	5.46E-02	2.89E-02	1.59E-02
5.E-03	17.48495	2.460148	0.521527	0.263872	5.54E-02	2.92E-02	1.61E-02
6.E-03	17.5479	2.504817	0.534407	0.270604	5.68E-02	2.99E-02	1.65E-02
7.E-03	17.60112	2.544184	0.546162	0.276768	5.80E-02	3.06E-02	1.68E-02
8.E-03	17.64725	2.57941	0.557028	0.282484	5.92E-02	3.12E-02	1.71E-02
9.E-03	17.68796	2.611305	0.567166	0.287833	6.03E-02	3.17E-02	1.74E-02
1.E-02	17.72438	2.640458	0.576696	0.292876	6.14E-02	3.22E-02	1.76E-02
2.E-02	17.86462	2.757528	0.617728	0.314775	6.60E-02	3.45E-02	1.88E-02
2.E-02	17.96421	2.844728	0.651472	0.333009	6.99E-02	3.65E-02	1.98E-02
3.E-02	18.04147	2.914284	0.680562	0.348903	7.33E-02	3.82E-02	2.06E-02
3.E-02	18.10462	2.972163	0.706349	0.363134	7.64E-02	3.97E-02	2.14E-02
4.E-02	18.15802	3.021734	0.729635	0.376106	7.92E-02	4.12E-02	2.21E-02
4.E-02	18.20428	3.065088	0.750944	0.388081	8.18E-02	4.25E-02	2.28E-02
5.E-02	18.24509	3.103613	0.77064	0.399241	8.43E-02	4.37E-02	2.34E-02
5.E-02	18.28159	3.13828	0.788987	0.40972	8.66E-02	4.49E-02	2.40E-02
6.E-02	18.34475	3.198674	0.822371	0.429004	9.10E-02	4.71E-02	2.51E-02
7.E-02	18.39817	3.250089	0.852262	0.446507	9.50E-02	4.91E-02	2.61E-02
8.E-02	18.44444	3.294853	0.879398	0.462604	9.87E-02	5.10E-02	2.70E-02

9.E-02	**18.48526**	**3.334492**	**0.904295**	**0.477552**	**0.102122**	**5.27E-02**	**2.79E-02**
0.1	**18.52178**	**3.37006**	**0.927325**	**0.491538**	**0.105388**	**5.44E-02**	**2.87E-02**
0.15	**18.66231**	**3.510054**	**1.02229**	**0.55096**	**0.119601**	**6.17E-02**	**3.24E-02**
0.2	**18.76203**	**3.608331**	**1.095817**	**0.598982**	**0.131474**	**6.78E-02**	**3.55E-02**
0.25	**18.83938**	**3.684813**	**1.156043**	**0.639748**	**0.141857**	**7.31E-02**	**3.82E-02**
0.3	**18.90259**	**3.747434**	**1.207138**	**0.675391**	**0.151182**	**7.80E-02**	**4.06E-02**
0.35	**18.95602**	**3.800456**	**1.251551**	**0.707179**	**0.159707**	**8.24E-02**	**4.29E-02**
0.4	**19.00231**	**3.846434**	**1.290849**	**0.735937**	**0.167598**	**8.65E-02**	**4.50E-02**
0.45	**19.04314**	**3.887022**	**1.326103**	**0.762239**	**0.174971**	**9.04E-02**	**4.69E-02**
0.5	**19.07967**	**3.923352**	**1.358074**	**0.786503**	**0.18191**	**9.40E-02**	**4.88E-02**
0.6	**19.14288**	**3.983944**	**1.414256**	**0.830031**	**0.194727**	**0.100721**	**5.22E-02**
0.7	**19.19632**	**4.037175**	**1.462577**	**0.868422**	**0.20641**	**0.106882**	**5.54E-02**
0.8	**19.24261**	**4.08331**	**1.504966**	**0.902793**	**0.217197**	**0.112593**	**5.83E-02**
0.9	**19.28344**	**4.12402**	**1.542722**	**0.933934**	**0.227252**	**0.117937**	**6.11E-02**
1	**19.31997**	**4.160448**	**1.576762**	**0.962418**	**0.236693**	**0.122973**	**6.37E-02**
1.5	**19.46053**	**4.300722**	**1.709703**	**1.076911**	**0.277212**	**0.144823**	**7.50E-02**
2	**19.56027**	**4.400309**	**1.80557**	**1.162604**	**0.310425**	**0.162989**	**8.46E-02**
2.5	**19.63763**	**4.47758**	**1.880586**	**1.231154**	**0.33898**	**0.178801**	**9.29E-02**
3	**19.70083**	**4.540729**	**1.942222**	**1.288313**	**0.364238**	**0.192941**	**0.100346**
3.5	**19.75427**	**4.594128**	**1.994535**	**1.337343**	**0.387004**	**0.205815**	**0.107188**
4	**19.80057**	**4.640389**	**2.03998**	**1.380277**	**0.407806**	**0.217686**	**0.113528**
4.5	**19.8414**	**4.681198**	**2.080151**	**1.418467**	**0.427008**	**0.228738**	**0.119457**
5	**19.87793**	**4.717705**	**2.116148**	**1.45286**	**0.444877**	**0.239105**	**0.125043**
6	**19.94114**	**4.780884**	**2.178558**	**1.512817**	**0.477332**	**0.258158**	**0.135374**
7	**19.99458**	**4.834304**	**2.231429**	**1.563926**	**0.506367**	**0.27543**	**0.144809**
8	**20.04087**	**4.880581**	**2.277294**	**1.608459**	**0.532709**	**0.291295**	**0.153533**
9	**20.08171**	**4.921402**	**2.317794**	**1.647916**	**0.556866**	**0.306011**	**0.161677**
10	**20.11823**	**4.957919**	**2.354054**	**1.683338**	**0.579206**	**0.319769**	**0.169336**
15	**20.25878**	**5.098455**	**2.493822**	**1.820555**	**0.671233**	**0.378064**	**0.202337**
20	**20.35851**	**5.198175**	**2.593155**	**1.918613**	**0.742675**	**0.425089**	**0.22953**
25	**20.43587**	**5.275526**	**2.670274**	**1.994963**	**0.801323**	**0.464958**	**0.253018**
30	**20.49908**	**5.338728**	**2.733322**	**2.057496**	**0.851183**	**0.49979**	**0.27388**
35	**20.55252**	**5.392165**	**2.786648**	**2.110454**	**0.894604**	**0.530841**	**0.292757**
40	**20.59881**	**5.438455**	**2.832855**	**2.156385**	**0.933089**	**0.558929**	**0.310066**
45	**20.63965**	**5.479286**	**2.873621**	**2.196936**	**0.967664**	**0.584618**	**0.326097**
50	**20.67617**	**5.515811**	**2.910094**	**2.233237**	**0.999059**	**0.60832**	**0.341062**
60	**20.73895**	**5.578973**	**2.973214**	**2.296101**	**1.0543**	**0.650844**	**0.368366**
70	**20.79239**	**5.632412**	**3.026598**	**2.3493**	**1.101917**	**0.688386**	**0.392923**
80	**20.83868**	**5.678703**	**3.072847**	**2.395411**	**1.143755**	**0.722025**	**0.415313**

90	**20.87952**	**5.719536**	**3.113647**	**2.436103**	**1.181069**	**0.752529**	**0.435939**
100	**20.91605**	**5.756062**	**3.150147**	**2.472517**	**1.214744**	**0.780452**	**0.455097**
150	**21.00227**	**5.891244**	**3.289511**	**2.612157**	**1.346378**	**0.892797**	**0.534862**
200	**21.10201**	**5.990977**	**3.389206**	**2.711722**	**1.44165**	**0.977245**	**0.597767**
250	**21.17937**	**6.068336**	**3.466542**	**2.78898**	**1.516304**	**1.044958**	**0.650064**
300	**21.24257**	**6.131544**	**3.529733**	**2.85212**	**1.577694**	**1.101515**	**0.694988**
350	**21.29602**	**6.184985**	**3.583163**	**2.905512**	**1.629831**	**1.150092**	**0.73445**
400	**21.34231**	**6.231278**	**3.629448**	**2.951769**	**1.675142**	**1.192672**	**0.769684**
450	**21.38314**	**6.272111**	**3.670274**	**2.992574**	**1.71521**	**1.230579**	**0.801538**
500	**21.41967**	**6.308637**	**3.706796**	**3.029078**	**1.751122**	**1.264739**	**0.830622**
600	**21.38187**	**6.361838**	**3.76794**	**3.091191**	**1.813174**	**1.324217**	**0.882075**
700	**21.43531**	**6.41528**	**3.821375**	**3.144607**	**1.865954**	**1.375063**	**0.926819**
800	**21.4816**	**6.461572**	**3.867664**	**3.190882**	**1.911751**	**1.419396**	**0.966379**
900	**21.52244**	**6.502406**	**3.908494**	**3.231702**	**1.952199**	**1.458698**	**1.001841**
1000	**21.55896**	**6.538933**	**3.945018**	**3.268217**	**1.988416**	**1.493993**	**1.033982**
1500	**22.39435**	**6.748723**	**4.099835**	**3.416135**	**2.129669**	**1.631639**	**1.161145**
2000	**22.49409**	**6.848457**	**4.199565**	**3.515852**	**2.228942**	**1.729509**	**1.253796**
2500	**22.57145**	**6.925818**	**4.276923**	**3.593202**	**2.306024**	**1.805745**	**1.326819**
3000	**22.63466**	**6.989026**	**4.34013**	**3.656404**	**2.369047**	**1.868201**	**1.387098**
3500	**22.6881**	**7.042467**	**4.39357**	**3.70984**	**2.422355**	**1.921105**	**1.438428**
4000	**22.73439**	**7.08876**	**4.439862**	**3.75613**	**2.468549**	**1.966995**	**1.483127**
4500	**22.77523**	**7.129594**	**4.480695**	**3.79696**	**2.509305**	**2.007514**	**1.522715**
5000	**22.81176**	**7.16612**	**4.517221**	**3.833485**	**2.54577**	**2.043789**	**1.558241**
6000	**25.188**	**7.459268**	**4.627636**	**3.921078**	**2.614235**	**2.109356**	**1.621306**
7000	**25.24144**	**7.512709**	**4.681077**	**3.974517**	**2.667613**	**2.162534**	**1.67368**
8000	**25.28773**	**7.559003**	**4.72737**	**4.020808**	**2.713857**	**2.208627**	**1.719166**
9000	**25.32857**	**7.599836**	**4.768203**	**4.061641**	**2.754652**	**2.249304**	**1.759371**
10000	**25.36509**	**7.636363**	**4.80473**	**4.098166**	**2.791149**	**2.285706**	**1.795393**
15000	**50.74495**	**10.29145**	**5.455855**	**4.500006**	**2.988855**	**2.455491**	**1.949527**
20000	**50.84468**	**10.39119**	**5.55559**	**4.59974**	**3.08855**	**2.555051**	**2.048533**
25000	**50.92204**	**10.46855**	**5.63295**	**4.677099**	**3.165884**	**2.632304**	**2.125449**
30000	**50.98525**	**10.53176**	**5.696158**	**4.740306**	**3.229075**	**2.695439**	**2.188359**
35000	**51.0387**	**10.5852**	**5.749599**	**4.793747**	**3.282504**	**2.748828**	**2.241587**
40000	**51.08499**	**10.63149**	**5.795892**	**4.84004**	**3.328787**	**2.795082**	**2.287719**
45000	**51.12583**	**10.67233**	**5.836725**	**4.880873**	**3.369613**	**2.835885**	**2.328428**
50000	**51.16235**	**10.70885**	**5.873252**	**4.9174**	**3.406134**	**2.872387**	**2.364854**
60000	**85.22641**	**14.16559**	**6.619211**	**5.326086**	**3.543854**	**2.974389**	**2.447966**
70000	**85.27986**	**14.21903**	**6.672652**	**5.379527**	**3.597292**	**3.027812**	**2.501318**
80000	**85.32615**	**14.26532**	**6.718945**	**5.42582**	**3.643581**	**3.074087**	**2.547537**

90000	85.36699	14.30616	6.759779	5.466654	3.684411	3.114907	2.588311
100000	85.40352	14.34268	6.796306	5.503181	3.720935	3.151422	2.62479
150000	365.2069	42.41879	12.52957	8.447137	4.439782	3.5906	2.920628
200000	365.3066	42.51852	12.6293	8.546872	4.539515	3.690324	3.02031
250000	365.384	42.59588	12.70666	8.624232	4.616873	3.767675	3.097633
300000	365.4472	42.65909	12.76987	8.68744	4.68008	3.830877	3.160816
350000	365.5007	42.71253	12.82331	8.740881	4.73352	3.884315	3.214239
400000	365.547	42.75883	12.86961	8.787174	4.779812	3.930604	3.260518
450000	365.5878	42.79966	12.91044	8.828008	4.820645	3.971435	3.30134
500000	365.6243	42.83619	12.94697	8.864535	4.857171	4.00796	3.337858
600000	717.8217	78.08877	20.04899	12.44852	5.630434	4.431528	3.586376
700000	717.8752	78.14221	20.10243	12.50196	5.683876	4.484968	3.639814
800000	717.9215	78.1885	20.14873	12.54825	5.730168	4.53126	3.686101
900000	717.9623	78.22934	20.18956	12.58909	5.771002	4.572093	3.72693
1000000	717.9989	78.26586	20.22609	12.62561	5.807528	4.608619	3.763453
1500000	3542.499	360.7438	76.83354	41.00085	11.60156	7.583825	5.332188
2000000	3542.598	360.8435	76.93327	41.10058	11.7013	7.683559	5.431918
2500000	3542.676	360.9209	77.01063	41.17794	11.77866	7.760918	5.509276
3000000	3542.739	360.9841	77.07384	41.24115	11.84187	7.824126	5.572482
3500000	3542.792	361.0375	77.12728	41.29459	11.89531	7.877567	5.625921
4000000	3542.839	361.0838	77.17358	41.34089	11.9416	7.92386	5.672213
4500000	3542.88	361.1246	77.21441	41.38172	11.98243	7.964693	5.713046
5000000	3542.916	361.1612	77.25094	41.41825	12.01896	8.00122	5.749572
6000000	7075.603	714.4184	147.9516	76.80037	19.14693	11.59822	7.582153
7000000	7075.656	714.4719	148.0051	76.85381	19.20037	11.65166	7.635594
8000000	7075.702	714.5182	148.0514	76.9001	19.24666	11.69796	7.681886
9000000	7075.743	714.559	148.0922	76.94094	19.2875	11.73879	7.722719

Table C-4 data for Fig. 7

tD=1e-04	tD=1e+03
1.60383	1.20115
1.25767	1.20115
1.11039	1.20115
1.03373	1.20115
1.0001	1.20115
1.0001	1.20115
1.03373	1.20115
1.11039	1.20115
1.25767	1.20115

1.60383	**1.20115**

Table C-5 data for Fig. 8

TD	P_{WD}	P'_{WD}
1.50E-04	**0.297821**	**5.69E-02**
2.00E-04	**0.31383**	**5.73E-02**
2.50E-04	**0.326456**	**5.76E-02**
3.00E-04	**0.336883**	**5.79E-02**
3.50E-04	**0.345763**	**5.81E-02**
4.00E-04	**0.353497**	**5.83E-02**
4.50E-04	**0.360345**	**5.85E-02**
5.00E-04	**0.36649**	**5.87E-02**
6.00E-04	**0.377158**	**5.91E-02**
7.00E-04	**0.386204**	**5.91E-02**
8.00E-04	**0.394053**	**5.91E-02**
9.00E-04	**0.400984**	**5.91E-02**
1.00E-03	**0.407185**	**5.96E-02**
1.50E-03	**0.431037**	**6.11E-02**
2.00E-03	**0.447905**	**5.98E-02**
2.50E-03	**0.46094**	**5.91E-02**
3.00E-03	**0.471559**	**5.88E-02**
3.50E-03	**0.480526**	**5.86E-02**
4.00E-03	**0.488303**	**5.87E-02**
4.50E-03	**0.495191**	**5.89E-02**
5.00E-03	**0.501397**	**5.96E-02**
6.00E-03	**0.512306**	**6.12E-02**
7.00E-03	**0.521799**	**6.30E-02**
8.00E-03	**0.530311**	**6.52E-02**
9.00E-03	**0.538107**	**6.77E-02**
1.00E-02	**0.545353**	**7.07E-02**
1.50E-02	**0.576246**	**8.45E-02**
2.00E-02	**0.601687**	**9.50E-02**
2.50E-02	**0.623752**	**0.104358**
3.00E-02	**0.64343**	**0.112644**
3.50E-02	**0.6613**	**0.120083**

4.00E-02	**0.677739**	**0.126839**
4.50E-02	**0.69301**	**0.133033**
5.00E-02	**0.707302**	**0.138921**
6.00E-02	**0.733485**	**0.149461**
7.00E-02	**0.757122**	**0.158417**
8.00E-02	**0.778747**	**0.166425**
9.00E-02	**0.798729**	**0.173657**
0.1	**0.817337**	**0.181099**
0.15	**0.895419**	**0.209986**
0.2	**0.957328**	**0.227196**
0.25	**1.009017**	**0.240559**
0.3	**1.053552**	**0.251211**
0.35	**1.092754**	**0.259901**
0.4	**1.12781**	**0.267131**
0.45	**1.159537**	**0.273242**
0.5	**1.18853**	**0.278984**
0.6	**1.239949**	**0.288304**
0.7	**1.284632**	**0.294715**
0.8	**1.324153**	**0.299838**
0.9	**1.359591**	**0.304039**
1	**1.391717**	**0.309983**
1.5	**1.518515**	**0.329146**
2	**1.611148**	**0.331292**
2.5	**1.684161**	**0.333212**
3	**1.744433**	**0.334792**
3.5	**1.795758**	**0.336074**
4	**1.840454**	**0.337122**
4.5	**1.880038**	**0.33799**
5	**1.915562**	**0.339649**
6	**1.977256**	**0.342156**
7	**2.029614**	**0.34243**
8	**2.075093**	**0.342711**
9	**2.115292**	**0.342977**
10	**2.15131**	**0.346495**
15	**2.290341**	**0.356999**
20	**2.389309**	**0.351735**
25	**2.466209**	**0.3495**
30	**2.529109**	**0.348367**
35	**2.582331**	**0.347724**

40	**2.628459**	**0.347332**
45	**2.669164**	**0.34708**
50	**2.705588**	**0.347906**
60	**2.768636**	**0.349138**
70	**2.821967**	**0.348395**
80	**2.868178**	**0.347919**
90	**2.908947**	**0.347601**
100	**2.945422**	**0.350503**
150	**3.085048**	**0.358925**
200	**3.184705**	**0.353942**
250	**3.262019**	**0.351227**
300	**3.325196**	**0.349789**
350	**3.378615**	**0.348935**
400	**3.424892**	**0.348388**
450	**3.465712**	**0.348015**
500	**3.502229**	**0.346298**
600	**3.563942**	**0.345432**
700	**3.617373**	**0.349002**
800	**3.663657**	**0.348448**
900	**3.704485**	**0.34807**
1000	**3.741006**	**0.354615**
1500	**3.891813**	**0.3758**
2000	**3.99154**	**0.354165**
2500	**4.068895**	**0.351401**
3000	**4.1321**	**0.349933**
3500	**4.185539**	**0.349057**
4000	**4.231831**	**0.348494**
4500	**4.272663**	**0.34811**
5000	**4.309188**	**0.405559**
6000	**4.406421**	**0.452019**
7000	**4.459861**	**0.349064**
8000	**4.506154**	**0.348501**
9000	**4.546987**	**0.348117**
10000	**4.583513**	**0.474262**
15000	**5.093142**	**0.914044**
20000	**5.192876**	**0.354187**
25000	**5.270235**	**0.351419**
30000	**5.333443**	**0.349947**
35000	**5.386885**	**0.34907**

40000	5.433177	0.348505
45000	5.474011	0.348119
50000	5.510537	1.171418
60000	6.067282	1.830556
70000	6.120723	0.34907
80000	6.167016	0.348507
90000	6.207849	0.348122
100000	6.244376	1.69691
150000	10.42194	6.415946

Table C-6 data for Fig.9

	tD=0.0001	tD=0.001	tD=0.01	tD=0.1	tD=1	tD=10	tD=100	tD=1000	tD=10000	tD=100000	tD=1000000
1	1.71123	1.6229	1.54599	1.52478	1.59297	1.62994	1.63503	1.62391	1.41337	0.98336	0.85077
2	1.2602	1.22798	1.17785	1.07847	1.05462	1.05639	1.05665	1.05624	1.03319	0.9026	0.84175
3	0.96716	0.96509	0.95288	0.88348	0.81859	0.80171	0.79949	0.80142	0.83394	0.84824	0.83527
4	0.77699	0.79094	0.80014	0.77197	0.6946	0.66757	0.664	0.66653	0.71912	0.8114	0.83068
5	0.65762	0.67945	0.70002	0.70154	0.62897	0.59805	0.59395	0.5966	0.65599	0.78832	0.82768
6	0.5898	0.61441	0.63983	0.65794	0.60104	0.572	0.5681	0.57076	0.63056	0.77698	0.82611
7	0.56157	0.58533	0.61101	0.6357	0.6041	0.58314	0.58024	0.58276	0.63797	0.77637	0.82589
8	0.56507	0.58505	0.60737	0.63425	0.64156	0.63626	0.63539	0.63757	0.6804	0.78636	0.82697
9	0.59446	0.60805	0.62401	0.66308	0.73281	0.75421	0.75692	0.75794	0.77032	0.8081	0.82944
10	0.64418	0.64906	0.66919	0.77706	0.95903	1.02901	1.0385	1.03455	0.95341	0.84653	0.83373

Table C-7 data for Fig.12

	1.00E-05 This solution	1.00E+02 This solution	1.00E-05 Ozkan & Khamis 2003	1.00E+02 Ozkan & Khamis 2003
1	1.05297	1.49699	1.061	1.481
2	1.04093	1.07913	1.056	1.071
3	1.03129	0.91411	1.031	0.931
4	1.02384	0.83405	1.021	0.861
5	1.01833	0.79987	1.011	0.811
6	1.01455	0.7994	1.011	0.811
7	1.01228	0.83255	1.009	0.856
8	1.01126	0.91125	1.011	0.931
9	1.01126	1.07411	1.011	1.066
10	1.01201	1.48728	1.009	1.461

Table C-8 data for Fig.15

	TD= 0.10E-04	TD= 0.90E+04
1	1.05297	1.45989
2	1.04093	1.08077
3	1.03129	0.92388
4	1.02384	0.8463
5	1.01833	0.81287
6	1.01455	0.8124
7	1.01228	0.84482
8	1.01126	0.92109
9	1.01126	1.07591
10	1.01201	1.45079

Table C-9 data for Fig.16

	TD= 0.10E-04	TD= 0.90E+04
1	1.01201	1.45079
2	1.01126	1.07591
3	1.01126	0.92109
4	1.01228	0.84482
5	1.01455	0.8124
6	1.01833	0.81287
7	1.02384	0.8463
8	1.03129	0.92388
9	1.04093	1.08077
10	1.05297	1.45989

Table C-10 data for Fig.20

	TD=0.0001
1	1.01083
2	1.00773
3	1.00464
4	1.00155
5	0.99845
6	0.99536
7	0.99227
8	0.98917
9	0.98917
10	0.99227

11	**0.99536**
12	**0.99845**
13	**1.00155**
14	**1.00464**
15	**1.00773**
16	**1.01083**

Table C-11 data for Fig.21

	TD=0.0001
1	**1.01083**
2	**1.00773**
3	**1.00464**
4	**1.00155**
5	**0.99845**
6	**0.99536**
7	**0.99227**
8	**0.98917**
9	**0.98917**
10	**0.99227**
11	**0.99536**
12	**0.99845**
13	**1.00155**
14	**1.00464**
15	**1.00773**
16	**1.01083**

Table C-12 data for Fig.22

	TD=0.0001
1	**1.0048**
2	**1.00238**
3	**1.00057**
4	**0.99931**
5	**0.99852**
6	**0.99813**
7	**0.99806**
8	**0.99823**
9	**0.99823**
10	**0.99806**
11	**0.99813**

12	0.99852
13	0.99931
14	1.00057
15	1.00238
16	1.0048

Table C-13 data for Fig.24

qr=1.0 ql	qr=1.7 ql	qr=2.2 ql	qr=3 ql
1.0048	1.00274	1.0019	1.00117
1.00238	1.00086	1.0003	0.99991
1.00057	0.99964	0.99943	0.99942
0.99931	0.999	0.99913	0.9995
0.99852	0.99881	0.99924	0.99925
0.99813	0.99895	0.99927	0.99913
0.99806	0.99875	0.99917	0.9991
0.99823	0.99867	0.99916	0.99926
0.99823	0.99868	0.99936	0.99967
0.99806	0.99893	0.99983	1.00038
0.99813	0.99949	1.00064	1.00143
0.99852	1.00041	1.00182	1.00286
0.99931	1.00176	1.00343	1.00472
1.00057	1.00357	1.0055	1.00705
1.00238	1.00591	1.00809	1.00988
1.0048	1.00882	1.01124	1.01326

Table C-14 data for Fig.30

	Qhd
0	0.05166
33.33333	0.051629
66.66667	0.0516
100	0.051574
133.3333	0.051551
166.6667	0.051531
200	0.051513
233.3333	0.051497
266.6667	0.051484
300	0.051472
333.3333	0.051463

Table C-15 data for Fig. 31

0	0.28373	4.703988
33.33333	0.283541	4.703788
66.66667	0.283352	4.703612
100	0.283163	4.703452
133.3333	0.282975	4.703302
166.6667	0.282786	4.703157
200	0.282598	4.703015
233.3333	0.282409	4.702871
266.6667	0.282221	4.702723
300	0.282033	4.70257
333.3333	0.281845	4.702407

366.6667	0.051455
400	0.051449
433.3333	0.051444
466.6667	0.051441
500	0.051439
533.3333	0.051437
566.6667	0.051437
600	0.051436
633.3333	0.051437
666.6667	0.051437
700	0.051437
733.3333	0.051438
766.6667	0.051438
800	0.051439
833.3333	0.05144
866.6667	0.051441
900	0.051442
933.3333	0.051444
966.6667	0.051445
1000	0.051447
1033.333	0.051449
1066.667	0.051452
1100	0.051455
1133.333	0.051459
1166.667	0.051463
1200	0.051468
1233.333	0.051473
1266.667	0.051479
1300	0.051486
1333.333	0.051493
1366.667	0.051501
1400	0.051509
1433.333	0.051519
1466.667	0.051529
1500	0.05154
1533.333	0.051552
1566.667	0.051564
1600	0.051578
1633.333	0.051592

366.6667	0.281656	4.702232
400	0.281468	4.702041
433.3333	0.28128	4.701828
466.6667	0.281091	4.701589
500	0.280903	4.701312
533.3333	0.280714	4.700985
566.6667	0.280525	4.700584
600	0.280337	4.700056
633.3333	0.280149	4.699081
666.6667	0.280211	4.700528
700	0.280492	4.703117
733.3333	0.280773	4.704439
766.6667	0.281055	4.705422
800	0.281336	4.706208
833.3333	0.281617	4.706861
866.6667	0.281898	4.707416
900	0.282179	4.707896
933.3333	0.28246	4.708317
966.6667	0.282741	4.708691
1000	0.283022	4.709025
1033.333	0.283303	4.709328
1066.667	0.283584	4.709604
1100	0.283865	4.709858
1133.333	0.284145	4.710092
1166.667	0.284426	4.710309
1200	0.284706	4.710513
1233.333	0.284987	4.710703
1266.667	0.285267	4.710884
1300	0.285548	4.711055
1333.333	0.285828	4.711218
1366.667	0.286109	4.711374
1400	0.286389	4.711524
1433.333	0.28667	4.71167
1466.667	0.286951	4.711811
1500	0.287231	4.711949
1533.333	0.287512	4.712085
1566.667	0.287793	4.712219
1600	0.288074	4.712352
1633.333	0.288356	4.712486

1666.667	0.051607
1700	0.051623
1733.333	0.05164
1766.667	0.051658
1800	0.051677
1833.333	0.051697
1866.667	0.051718
1900	0.05174
1933.333	0.051764
1966.667	0.051788

1666.667	0.288637	4.71262
1700	0.288919	4.712757
1733.333	0.289201	4.712898
1766.667	0.289483	4.713043
1800	0.289766	4.713197
1833.333	0.290049	4.71336
1866.667	0.290333	4.713538
1900	0.290617	4.713735
1933.333	0.290901	4.71396
1966.667	0.291186	4.714225

Table C-16 data for Fig.32

	Qr=5.024	Qr=3.298	Qr=2.34	Qr=1.502	Qr=1	Qr=0.666	Qr=0.303	Qr=0.110
1	1.00081	1.00148	1.00231	1.00381	1.00561	1.0077	1.01177	1.01554
2	1.00013	1.00062	1.00129	1.00256	1.00415	1.00604	1.0098	1.01333
3	0.99976	1.00001	1.00049	1.00151	1.00288	1.00456	1.00799	1.01127
4	0.99963	0.99963	0.99989	1.00065	1.00178	1.00324	1.00633	1.00936
5	0.99967	0.99943	0.99948	0.99996	1.00084	1.00208	1.00482	1.00759
6	0.99974	0.99938	0.99923	0.99942	1.00006	1.00106	1.00345	1.00596
7	0.99974	0.99944	0.99911	0.99903	0.99941	1.00018	1.00221	1.00445
8	0.99975	0.99929	0.99909	0.99876	0.9989	0.99944	1.00111	1.00308
9	0.99979	0.9993	0.99911	0.99861	0.99851	0.99882	1.00013	1.00183
10	0.99984	0.99933	0.99919	0.99855	0.99822	0.99831	0.99926	1.00069
11	0.99992	0.99938	0.99918	0.99855	0.99803	0.99791	0.99851	0.99967
12	1.00004	0.99945	0.99919	0.99859	0.99793	0.9976	0.99786	0.99876
13	1.00023	0.99954	0.99921	0.99859	0.99789	0.99738	0.99731	0.99795
14	1.00048	0.99968	0.99926	0.99859	0.99788	0.99724	0.99686	0.99723
15	1.00081	0.9999	0.99937	0.99862	0.9979	0.99717	0.99649	0.99661
16	1.00121	1.00018	0.99954	0.99867	0.9979	0.99712	0.9962	0.99608
17	1.0017	1.00055	0.99978	0.99875	0.99788	0.99709	0.99598	0.99563
18	1.00229	1.001	1.00011	0.99888	0.99789	0.99708	0.99583	0.99526
19	1.00296	1.00155	1.00052	0.9991	0.99793	0.99709	0.99573	0.99496
20	1.00374	1.00219	1.00103	0.9994	0.99803	0.99705	0.99566	0.99473
21	1.00463	1.00294	1.00164	0.99981	0.99822	0.99704	0.99561	0.99455
22	1.00563	1.00381	1.00237	1.00031	0.99851	0.99711	0.99557	0.99443
23	1.00675	1.00479	1.00321	1.00093	0.9989	0.99726	0.99555	0.99433
24	1.008	1.0059	1.00417	1.00168	0.99941	0.99753	0.99544	0.99425
25	1.00937	1.00713	1.00527	1.00256	1.00006	0.99792	0.99538	0.99419

26	1.01088	1.00851	1.0065	1.00357	1.00084	0.99846	0.99543	0.99414
27	1.01253	1.01002	1.00788	1.00474	1.00178	0.99915	0.99563	0.99411
28	1.01432	1.01169	1.00941	1.00606	1.00288	1.00001	0.99602	0.99434
29	1.01627	1.0135	1.0111	1.00754	1.00415	1.00106	0.99662	0.99436
30	1.01837	1.01548	1.01295	1.0092	1.00561	1.00231	0.99748	0.9948

Table C-17 data for Fig.33

1	1.00609
2	1.00532
3	1.00459
4	1.0039
5	1.00326
6	1.00267
7	1.00212
8	1.0016
9	1.00113
10	1.00069
11	1.0003
12	0.99993
13	0.9996
14	0.99931
15	0.99904
16	0.99881
17	0.9986
18	0.99842
19	0.99827
20	0.99814
21	0.99803
22	0.99795
23	0.99788
24	0.99783
25	0.9978
26	0.99777
27	0.99775
28	0.99774
29	0.99773
30	0.99772

Table C-18 data for Fig. 34

1	0.230136	4.456693
2	0.229947	4.45647
3	0.229757	4.456279
4	0.229568	4.45611
5	0.229379	4.455955
6	0.229191	4.455811
7	0.229002	4.455673
8	0.228814	4.45554
9	0.228625	4.45541
10	0.228437	4.455279
11	0.228249	4.455149
12	0.228061	4.455015
13	0.227873	4.454879
14	0.227686	4.454738
15	0.227498	4.45459
16	0.22731	4.454435
17	0.227122	4.454271
18	0.226934	4.454095
19	0.226746	4.453906
20	0.226558	4.4537
21	0.22637	4.453475
22	0.226182	4.453225
23	0.225994	4.452944
24	0.225806	4.452627
25	0.225618	4.452261
26	0.22543	4.451831
27	0.225242	4.451316
28	0.225053	4.450674
29	0.224865	4.449813
30	0.224677	4.448144

Table C-19 data for Fig.35

	Qhd
0	0.05166
33.33333	0.051629
66.66667	0.0516
100	0.051574
133.3333	0.051551
166.6667	0.051531
200	0.051513
233.3333	0.051497
266.6667	0.051484
300	0.051472
333.3333	0.051463
366.6667	0.051455
400	0.051449
433.3333	0.051444
466.6667	0.051441
500	0.051439
533.3333	0.051437
566.6667	0.051437
600	0.051436
633.3333	0.051437
666.6667	0.051437
700	0.051437
733.3333	0.051438
766.6667	0.051438
800	0.051439
833.3333	0.05144
866.6667	0.051441
900	0.051442
933.3333	0.051444

Table C-20 data for Fig.36

0	0.28373	4.703988
33.33333	0.283541	4.703788
66.66667	0.283352	4.703612
100	0.283163	4.703452
133.3333	0.282975	4.703302
166.6667	0.282786	4.703157
200	0.282598	4.703015
233.3333	0.282409	4.702871
266.6667	0.282221	4.702723
300	0.282033	4.70257
333.3333	0.281845	4.702407
366.6667	0.281656	4.702232
400	0.281468	4.702041
433.3333	0.28128	4.701828
466.6667	0.281091	4.701589
500	0.280903	4.701312
533.3333	0.280714	4.700985
566.6667	0.280525	4.700584
600	0.280337	4.700056
633.3333	0.280149	4.699081
666.6667	0.280211	4.700528
700	0.280492	4.703117
733.3333	0.280773	4.704439
766.6667	0.281055	4.705422
800	0.281336	4.706208
833.3333	0.281617	4.706861
866.6667	0.281898	4.707416
900	0.282179	4.707896
933.3333	0.28246	4.708317
966.6667	0.282741	4.708691

31	0.99772	31	0.224678	4.448122	966.6667	0.051445	1000	0.283022	4.709025
32	0.99772	32	0.224867	4.449791	1000	0.051447	1033.333	0.283303	4.709328
33	0.99773	33	0.225055	4.450651	1033.333	0.051449	1066.667	0.283584	4.709604
34	0.99775	34	0.225243	4.451293	1066.667	0.051452	1100	0.283865	4.709858
35	0.99777	35	0.225431	4.451809	1100	0.051455	1133.333	0.284145	4.710092
36	0.9978	36	0.225619	4.452238	1133.333	0.051459	1166.667	0.284426	4.710309
37	0.99783	37	0.225807	4.452604	1166.667	0.051463	1200	0.284706	4.710513
38	0.99788	38	0.225995	4.452922	1200	0.051468	1233.333	0.284987	4.710703
39	0.99795	39	0.226183	4.453202	1233.333	0.051473	1266.667	0.285267	4.710884
40	0.99803	40	0.226371	4.453452	1266.667	0.051479	1300	0.285548	4.711055
41	0.99814	41	0.226559	4.453677	1300	0.051486	1333.333	0.285828	4.711218
42	0.99827	42	0.226747	4.453883	1333.333	0.051493	1366.667	0.286109	4.711374
43	0.99842	43	0.226935	4.454072	1366.667	0.051501	1400	0.286389	4.711524
44	0.9986	44	0.227122	4.454248	1400	0.051509	1433.333	0.28667	4.71167
45	0.99881	45	0.22731	4.454412	1433.333	0.051519	1466.667	0.286951	4.711811
46	0.99904	46	0.227498	4.454567	1466.667	0.051529	1500	0.287231	4.711949
47	0.99931	47	0.227686	4.454714	1500	0.05154	1533.333	0.287512	4.712085
48	0.9996	48	0.227873	4.454856	1533.333	0.051552	1566.667	0.287793	4.712219
49	0.99993	49	0.228061	4.454992	1566.667	0.051564	1600	0.288074	4.712352
50	1.0003	50	0.228249	4.455125	1600	0.051578	1633.333	0.288356	4.712486
51	1.00069	51	0.228437	4.455256	1633.333	0.051592	1666.667	0.288637	4.71262
52	1.00113	52	0.228625	4.455386	1666.667	0.051607	1700	0.288919	4.712757
53	1.0016	53	0.228813	4.455517	1700	0.051623	1733.333	0.289201	4.712898
54	1.00212	54	0.229002	4.45565	1733.333	0.05164	1766.667	0.289483	4.713043
55	1.00267	55	0.22919	4.455787	1766.667	0.051658	1800	0.289766	4.713197
56	1.00327	56	0.229378	4.455931	1800	0.051677	1833.333	0.290049	4.71336
57	1.0039	57	0.229567	4.456085	1833.333	0.051697	1866.667	0.290333	4.713538
58	1.00459	58	0.229756	4.456254	1866.667	0.051718	1900	0.290617	4.713735
59	1.00532	59	0.229946	4.456445	1900	0.05174	1933.333	0.290901	4.71396
60	1.00609	60	0.230135	4.456668	1933.333	0.051764	1966.667	0.291186	4.714225

Table C-21 data for Fig. 38

1	0.776741
2	0.776755
3	0.776768
4	0.776779
5	0.776788

Table C-22 data for Fig.39

	TD=0.00001	TD=0.01	TD=0.1	TD=1	TD=7500
33	39.27136	42.67226	16.9668	9.410869	3.275071
67	39.27136	32.29891	13.8825	7.946439	2.701226
100	39.27136	27.67968	12.30938	7.234757	2.44334
133	39.27136	25.14709	11.20231	6.728581	2.262621
167	39.27136	23.74463	10.37078	6.340722	2.125448

6	0.776796	200	39.27136	22.99441	9.727516	6.03422	2.017732
7	0.776802	233	39.27136	22.6166	9.221685	5.788249	1.931676
8	0.776807	267	39.27136	22.44036	8.820479	5.589482	1.862357
9	0.77681	300	39.27136	22.36493	8.501582	5.428831	1.806458
10	0.776812	333	39.27136	22.33549	8.249345	5.299878	1.76166
11	0.776812	367	39.27136	22.32509	8.05259	5.19801	1.726308
12	0.77681	400	39.27136	22.32186	7.903294	5.119884	1.699215
13	0.776807	433	39.27136	22.32107	7.795754	5.063112	1.679534
14	0.776802	467	39.27136	22.32104	7.726059	5.026051	1.666687
15	0.776796	500	39.27136	22.32121	7.691761	5.007666	1.660309
16	0.776788	533	39.27136	22.32144	7.691678	5.007453	1.660225
17	0.776779	567	39.27136	22.32172	7.725801	5.025409	1.666436
18	0.776767	600	39.27136	22.32221	7.795299	5.062027	1.679111
19	0.776755	633	39.27136	22.32345	7.902605	5.118333	1.698612
20	0.776741	667	39.27136	22.32715	8.051613	5.195961	1.725515
21	0.776741	700	39.27136	22.338	8.248002	5.297287	1.760662
22	0.776748	733	39.27136	22.36787	8.499772	5.425638	1.805235
23	0.776755	767	39.27136	22.44366	8.818065	5.585612	1.860883
24	0.776762	800	39.27136	22.6201	9.218489	5.783605	1.929919
25	0.776768	833	39.27136	22.99783	9.723294	6.028677	2.015648
26	0.776774	867	39.27136	23.74743	10.36517	6.334116	2.122981
27	0.77678	900	39.27136	25.14845	11.19482	6.720669	2.259683
28	0.776785	933	39.27136	27.67828	12.29934	7.225209	2.439811
29	0.77679	967	39.27136	32.29235	13.86884	7.934734	2.696908
30	0.776794	1000	39.27136	42.65448	16.94682	9.395448	3.26929
31	0.776798	1033	39.27136	42.65448	16.94682	9.395448	3.26929
32	0.776802	1067	39.27136	32.29235	13.86884	7.934734	2.696908
33	0.776805	1100	39.27136	27.67828	12.29934	7.225209	2.439811
34	0.776808	1133	39.27136	25.14845	11.19482	6.720669	2.259683
35	0.77681	1167	39.27136	23.74743	10.36517	6.334116	2.122981
36	0.776812	1200	39.27136	22.99783	9.723294	6.028677	2.015648
37	0.776814	1233	39.27136	22.6201	9.218489	5.783605	1.929919
38	0.776815	1267	39.27136	22.44366	8.818065	5.585612	1.860883
39	0.776816	1300	39.27136	22.36787	8.499772	5.425638	1.805235
40	0.776816	1333	39.27136	22.338	8.248002	5.297287	1.760662
41	0.776816	1367	39.27136	22.32715	8.051613	5.195961	1.725515
42	0.776816	1400	39.27136	22.32345	7.902605	5.118333	1.698612
43	0.776815	1433	39.27136	22.32221	7.795299	5.062027	1.679111
44	0.776814	1467	39.27136	22.32172	7.725801	5.025409	1.666436

45	0.776812
46	0.77681
47	0.776808
48	0.776805
49	0.776802
50	0.776798
51	0.776794
52	0.77679
53	0.776785
54	0.77678
55	0.776774
56	0.776768
57	0.776762
58	0.776755
59	0.776748
60	0.776741

1500	39.27136	22.32144	7.691678	5.007453	1.660225
1533	39.27136	22.32121	7.691761	5.007666	1.660309
1567	39.27136	22.32104	7.726059	5.026051	1.666687
1600	39.27136	22.32107	7.795754	5.063112	1.679534
1633	39.27136	22.32186	7.903294	5.119884	1.699215
1667	39.27136	22.32509	8.05259	5.19801	1.726308
1700	39.27136	22.33549	8.249345	5.299878	1.76166
1733	39.27136	22.36493	8.501582	5.428831	1.806458
1767	39.27136	22.44036	8.820479	5.589482	1.862357
1800	39.27136	22.6166	9.221685	5.788249	1.931676
1833	39.27136	22.99441	9.727516	6.03422	2.017732
1867	39.27136	23.74463	10.37078	6.340722	2.125448
1900	39.27136	25.14709	11.20231	6.728581	2.262621
1933	39.27136	27.67968	12.30938	7.234757	2.44334
1967	39.27136	32.29891	13.8825	7.946439	2.701226
2000	39.27136	42.67226	16.9668	9.410869	3.275071

Table C-23 data for Fig. 40

	TD=0.00001	TD=0.01	TD=0.1	TD=1	TD=7500
33	26.28053	38.03089	15.53687	8.444895	2.767912
67	26.28053	27.72446	12.47729	7.147413	2.366708
100	26.28053	23.97061	10.93607	6.532717	2.181642
133	26.28053	22.44126	9.899682	6.109791	2.054533
167	26.28053	21.87923	9.164936	5.79976	1.961067
200	26.28053	21.70469	8.63634	5.56933	1.89131
233	26.28053	21.66015	8.259118	5.400144	1.839887
267	26.28053	21.65096	7.999521	5.280994	1.803547
300	26.28053	21.64952	7.836556	5.204884	1.780272
333	26.28053	21.64947	7.757896	5.167699	1.768877
367	26.28053	21.64962	7.757814	5.167517	1.768808
400	26.28053	21.64999	7.836299	5.204329	1.780064
433	26.28053	21.65174	7.999049	5.280043	1.803192
467	26.28053	21.66125	8.258361	5.398758	1.839374
500	26.28053	21.70608	8.635187	5.567447	1.890621
533	26.28053	21.88082	9.163221	5.797295	1.960178
567	26.28053	22.44277	9.89715	6.106617	2.053406
600	26.28053	23.97141	10.9323	6.528629	2.180218
633	26.28053	27.72327	12.47158	7.142094	2.364894

667	**26.28053**	**38.02413**	**15.5276**	**8.437483**	**2.765441**
700	**52.29498**	**45.11888**	**18.17456**	**10.25762**	**3.435044**
733	**52.29224**	**35.05787**	**15.00539**	**8.650589**	**2.892577**
767	**52.29224**	**30.23054**	**13.39054**	**7.86123**	**2.630982**
800	**52.29224**	**27.26747**	**12.23519**	**7.292801**	**2.442816**
833	**52.29224**	**25.37535**	**11.34898**	**6.850702**	**2.296281**
867	**52.29224**	**24.16268**	**10.64657**	**6.494899**	**2.178085**
900	**52.29224**	**23.39683**	**10.07842**	**6.202782**	**2.080794**
933	**52.29224**	**22.92616**	**9.612376**	**5.959801**	**1.999643**
967	**52.29224**	**22.64722**	**9.226291**	**5.755936**	**1.931367**
1000	**52.29224**	**22.48877**	**8.904379**	**5.583981**	**1.873622**
1033	**52.29224**	**22.40287**	**8.63503**	**5.438608**	**1.824675**
1067	**52.29224**	**22.35848**	**8.409552**	**5.315787**	**1.783219**
1100	**52.29224**	**22.3366**	**8.221342**	**5.212434**	**1.748257**
1133	**52.29224**	**22.32627**	**8.065328**	**5.126163**	**1.719014**
1167	**52.29224**	**22.32156**	**7.937604**	**5.055123**	**1.694891**
1200	**52.29224**	**22.31943**	**7.835159**	**4.997873**	**1.675422**
1233	**52.29224**	**22.31842**	**7.755697**	**4.953314**	**1.660252**
1267	**52.29224**	**22.31787**	**7.697511**	**4.920624**	**1.649113**
1300	**52.29224**	**22.3175**	**7.659387**	**4.899217**	**1.641816**
1333	**52.29224**	**22.31717**	**7.640551**	**4.888719**	**1.63824**
1367	**52.29224**	**22.31687**	**7.640626**	**4.888946**	**1.638326**
1400	**52.29224**	**22.31657**	**7.659615**	**4.899901**	**1.642073**
1433	**52.29224**	**22.31633**	**7.697906**	**4.921773**	**1.649544**
1467	**52.29224**	**22.31626**	**7.756283**	**4.954942**	**1.660862**
1500	**52.29224**	**22.31664**	**7.835968**	**5.000002**	**1.676218**
1533	**52.29224**	**22.31813**	**7.938683**	**5.05778**	**1.69588**
1567	**52.29224**	**22.32221**	**8.066735**	**5.129383**	**1.720207**
1600	**52.29224**	**22.33191**	**8.22315**	**5.216261**	**1.749668**
1633	**52.29224**	**22.35318**	**8.411855**	**5.320276**	**1.784864**
1667	**52.29224**	**22.39701**	**8.637941**	**5.443824**	**1.826574**
1700	**52.29224**	**22.48244**	**8.908042**	**5.590004**	**1.8758**
1733	**52.29224**	**22.6406**	**9.230882**	**5.762864**	**1.933854**
1767	**52.29224**	**22.9196**	**9.61812**	**5.967755**	**2.002475**
1800	**52.29224**	**23.3908**	**10.08564**	**6.211913**	**2.084017**
1833	**52.29224**	**24.15783**	**10.65566**	**6.505416**	**2.181767**
1867	**52.29224**	**25.37254**	**11.36046**	**6.862871**	**2.300504**
1900	**52.29224**	**27.26799**	**12.24973**	**7.306966**	**2.447689**
1933	**52.29224**	**30.23642**	**13.40908**	**7.877865**	**2.636654**

1967	52.29224	35.07261	15.02937	8.670458	2.899294
2000	52.29499	45.15083	18.2079	10.28314	3.443622

Table C-24 data for Fig. 41

TD= 0.10E-04, S>0	TD= 0.90E+4, S>0	TD= 0.10E-04, S=0	TD= 0.90E+4, S=0
0.84535	1.3	1.05297	1.45989
0.87242	1	1.04093	1.08077
0.90317	0.9	1.03129	0.92388
0.93804	0.9	1.02384	0.8463
0.97755	0.8	1.01833	0.81287
1.0223	0.8	1.01455	0.8124
1.07303	0.9	1.01228	0.84482
1.13057	0.9	1.01126	0.92109
1.19594	1.1	1.01126	1.07591
1.27035	1.5	1.01201	1.45079

Table C-25 data for Fig. 43

TD= 0.10E-04, S>0	TD= 0.90E+4, S>0	TD= 0.10E-04, S=0	TD= 0.90E+4, S=0
1.27035	1.507	1.01201	1.45079
1.19594	1.111	1.01126	1.07591
1.13057	0.948	1.01126	0.92109
1.07303	0.866	1.01228	0.84482
1.0223	0.829	1.01455	0.8124
0.97755	0.825	1.01833	0.81287
0.93804	0.852	1.02384	0.8463
0.90317	0.917	1.03129	0.92388
0.87242	1.045	1.04093	1.08077
0.84535	1.328	1.05297	1.45989

Table C-26 data for Fig. 45

0	0.1	1	10
1.00609	1.00424	1	1.00014
1.00532	1.0037	1	1.00012
1.00459	1.00319	1	1.0001
1.0039	1.00272	1	1.00009
1.00326	1.00227	1	1.00007
1.00267	1.00186	1	1.00006
1.00212	1.00147	1	1.00005
1.0016	1.00112	1	1.00004
1.00113	1.00079	1	1.00003
1.00069	1.00048	1	1.00002
1.0003	1.00021	1	1.00001
0.99993	0.99995	1	1
0.9996	0.99972	1	0.99999
0.99931	0.99952	1	0.99998
0.99904	0.99933	1	0.99998
0.99881	0.99917	1	0.99997
0.9986	0.99903	1	0.99997
0.99842	0.9989	1	0.99996
0.99827	0.99879	1	0.99996
0.99814	0.9987	1	0.99996
0.99803	0.99863	1	0.99996
0.99795	0.99857	1	0.99995
0.99788	0.99852	1	0.99995
0.99783	0.99849	1	0.99995
0.9978	0.99847	1	0.99995
0.99777	0.99845	1	0.99995
0.99775	0.99843	1	0.99995
0.99774	0.99842	1	0.99995
0.99773	0.99842	1	0.99995
0.99772	0.99841	1	0.99995
0.99772	0.99841	1	0.99995
0.99772	0.99842	1	0.99995
0.99773	0.99842	1	0.99995
0.99775	0.99843	1	0.99995
0.99777	0.99845	1	0.99995
0.9978	0.99847	1	0.99995

Table C-27 data for Fig. 46

0	0.1	1	10
1.56496	1.50283	1.20338	1.20338
1.30873	1.28339	1.13053	1.13053
1.18993	1.17681	1.08733	1.08733
1.10608	1.10066	1.05417	1.05417
1.04204	1.04191	1.02719	1.02719
0.9915	0.99517	1.00476	1.00476
0.95095	0.95742	0.98596	0.98596
0.91817	0.92673	0.9702	0.9702
0.89166	0.90179	0.95706	0.95706
0.87037	0.88167	0.94622	0.94622
0.85353	0.86571	0.93747	0.93747
0.8406	0.85344	0.93065	0.93065
0.8312	0.84449	0.92562	0.92562
0.82506	0.83864	0.9223	0.9223
0.82201	0.83573	0.92064	0.92064
0.82197	0.83569	0.92062	0.92062
0.82494	0.83852	0.92223	0.92223
0.831	0.84429	0.92549	0.92549
0.84031	0.85316	0.93047	0.93047
0.85315	0.86535	0.93725	0.93725
0.86989	0.88121	0.94594	0.94594
0.89107	0.90122	0.95671	0.95671
0.91747	0.92605	0.96979	0.96979
0.95011	0.95662	0.98549	0.98549
0.9905	0.99423	1.00421	1.00421
1.04086	1.0408	1.02655	1.02655
1.10468	1.09934	1.05345	1.05345
1.18826	1.17525	1.0865	1.0865
1.3067	1.28151	1.12957	1.12957
1.56229	1.5004	1.20227	1.20227
1.56235	1.5004	1.20227	1.20227
1.30675	1.28151	1.12957	1.12957
1.1883	1.17525	1.0865	1.0865
1.10472	1.09934	1.05345	1.05345
1.04089	1.0408	1.02655	1.02655
0.99053	0.99423	1.00421	1.00421

0.99783	0.99849	1	0.99995
0.99788	0.99852	1	0.99995
0.99795	0.99857	1	0.99995
0.99803	0.99863	1	0.99996
0.99814	0.9987	1	0.99996
0.99827	0.99879	1	0.99996
0.99842	0.9989	1	0.99996
0.9986	0.99903	1	0.99997
0.99881	0.99917	1	0.99997
0.99904	0.99933	1	0.99998
0.99931	0.99952	1	0.99998
0.9996	0.99972	1	0.99999
0.99993	0.99995	1	1
1.0003	1.00021	1	1.00001
1.00069	1.00048	1	1.00002
1.00113	1.00079	1	1.00003
1.0016	1.00112	1	1.00004
1.00212	1.00147	1	1.00005
1.00267	1.00186	1	1.00006
1.00327	1.00227	1	1.00007
1.0039	1.00272	1	1.00009
1.00459	1.00319	1	1.0001
1.00532	1.0037	1	1.00012
1.00609	1.00424	1	1.00014

0.95013	0.95662	0.98549	0.98549
0.91748	0.92605	0.96979	0.96979
0.89108	0.90122	0.95671	0.95671
0.86989	0.88121	0.94594	0.94594
0.85315	0.86535	0.93725	0.93725
0.84031	0.85316	0.93047	0.93047
0.83099	0.84429	0.92549	0.92549
0.82493	0.83852	0.92223	0.92223
0.82196	0.83569	0.92062	0.92062
0.822	0.83573	0.92064	0.92064
0.82505	0.83864	0.9223	0.9223
0.83119	0.84449	0.92562	0.92562
0.84059	0.85344	0.93065	0.93065
0.85351	0.86571	0.93747	0.93747
0.87035	0.88167	0.94622	0.94622
0.89164	0.90179	0.95706	0.95706
0.91815	0.92673	0.9702	0.9702
0.95093	0.95742	0.98596	0.98596
0.99148	0.99517	1.00476	1.00476
1.04202	1.04191	1.02719	1.02719
1.10606	1.10066	1.05417	1.05417
1.18991	1.17681	1.08733	1.08733
1.30871	1.28339	1.13053	1.13053
1.56494	1.50283	1.20338	1.20338

Table C-28 data for Fig. 47

skin	TD=0.10E-04	TD=0.75E+04
1	0.50374	0.88896
0.966667	0.51762	0.84789
0.933333	0.5323	0.82709
0.9	0.54785	0.81286
0.866667	0.56435	0.80266
0.833333	0.58189	0.7955
0.8	0.60058	0.79088
0.766667	0.62051	0.78848
0.733333	0.64184	0.78814
0.7	0.6647	0.78977
0.666667	0.68926	0.79332

Table C-29 data for Fig. 48

skin	TD=0.10E-04	TD=0.75E+04	TD=0.10E-04 zero skin	TD=0.75E+04 zero skin
0	2.51132	2.26116	1.00609	1.56496
0.033333	2.19157	1.77003	1.00532	1.30873
0.066667	1.944	1.54312	1.00459	1.18993
0.1	1.74666	1.38724	1.0039	1.10608
0.133333	1.58567	1.27094	1.00326	1.04204
0.166667	1.45185	1.18031	1.00267	0.9915
0.2	1.33885	1.10817	1.00212	0.95095
0.233333	1.24217	1.04947	1.0016	0.91817
0.266667	1.15851	1.00085	1.00113	0.89166
0.3	1.08541	0.96044	1.00069	0.87037
0.333333	1.02099	0.92689	1.0003	0.85353

0.633333	0.71574	0.79881
0.6	0.74434	0.80631
0.566667	0.77535	0.81594
0.533333	0.80907	0.82785
0.5	0.84589	0.84226
0.466667	0.88623	0.85948
0.433333	0.93065	0.87987
0.4	0.97977	0.90393
0.366667	1.0344	0.93228
0.333333	1.0955	0.96577
0.3	1.1643	1.00548
0.266667	1.24236	1.05292
0.233333	1.33166	1.11015
0.2	1.43483	1.18013
0.166667	1.55535	1.26727
0.133333	1.69801	1.37855
0.1	1.86951	1.52632
0.066667	2.07957	1.73854
0.033333	2.34282	2.18259
0.033333	2.34282	2.18259
0.066667	2.07957	1.73854
0.1	1.86951	1.52632
0.133333	1.69801	1.37855
0.166667	1.55535	1.26727
0.2	1.43483	1.18013
0.233333	1.33166	1.11015
0.266667	1.24236	1.05292
0.3	1.1643	1.00548
0.333333	1.0955	0.96577
0.366667	1.0344	0.93228
0.4	0.97977	0.90393
0.433333	0.93065	0.87987
0.466667	0.88623	0.85948
0.5	0.84589	0.84226
0.533333	0.80907	0.82785
0.566667	0.77535	0.81594
0.6	0.74434	0.80631
0.633333	0.71574	0.79881
0.666667	0.68926	0.79332

0.366667	0.96379	0.89769	0.99993	0.8406
0.4	0.91266	0.87345	0.9996	0.8312
0.433333	0.86668	0.85294	0.99931	0.82506
0.466667	0.82512	0.83556	0.99904	0.82201
0.5	0.78737	0.82113	0.99881	0.82197
0.533333	0.75292	0.80924	0.9986	0.82494
0.566667	0.72136	0.79956	0.99842	0.831
0.6	0.69234	0.79213	0.99827	0.84031
0.633333	0.66557	0.78671	0.99814	0.85315
0.666667	0.64079	0.78318	0.99803	0.86989
0.7	0.61779	0.78166	0.99795	0.89107
0.733333	0.59638	0.78212	0.99788	0.91747
0.766667	0.57641	0.78457	0.99783	0.95011
0.8	0.55774	0.78935	0.9978	0.9905
0.833333	0.54023	0.79667	0.99777	1.04086
0.866667	0.52379	0.807	0.99775	1.10468
0.9	0.50833	0.82148	0.99774	1.18826
0.933333	0.49375	0.84261	0.99773	1.3067
0.966667	0.47998	0.88432	0.99772	1.56229
0.966667	0.47998	0.88432	0.99772	1.56235
0.933333	0.49375	0.84261	0.99772	1.30675
0.9	0.50833	0.82148	0.99773	1.1883
0.866667	0.52379	0.807	0.99775	1.10472
0.833333	0.54023	0.79667	0.99777	1.04089
0.8	0.55774	0.78935	0.9978	0.99053
0.766667	0.57641	0.78457	0.99783	0.95013
0.733333	0.59638	0.78212	0.99788	0.91748
0.7	0.61779	0.78166	0.99795	0.89108
0.666667	0.64079	0.78318	0.99803	0.86989
0.633333	0.66557	0.78671	0.99814	0.85315
0.6	0.69234	0.79213	0.99827	0.84031
0.566667	0.72136	0.79956	0.99842	0.83099
0.533333	0.75292	0.80924	0.9986	0.82493
0.5	0.78737	0.82113	0.99881	0.82196
0.466667	0.82512	0.83556	0.99904	0.822
0.433333	0.86668	0.85294	0.99931	0.82505
0.4	0.91266	0.87345	0.9996	0.83119
0.366667	0.96379	0.89769	0.99993	0.84059
0.333333	1.02099	0.92689	1.0003	0.85351

0.7	0.6647	0.78977
0.733333	0.64184	0.78814
0.766667	0.62051	0.78848
0.8	0.60058	0.79088
0.833333	0.58189	0.7955
0.866667	0.56435	0.80266
0.9	0.54785	0.81286
0.933333	0.5323	0.82709
0.966667	0.51762	0.84789
1	0.50374	0.88896

0.3	1.08541	0.96044	1.00069	0.87035
0.266667	1.15851	1.00085	1.00113	0.89164
0.233333	1.24217	1.04947	1.0016	0.91815
0.2	1.33885	1.10817	1.00212	0.95093
0.166667	1.45185	1.18031	1.00267	0.99148
0.133333	1.58567	1.27094	1.00327	1.04202
0.1	1.74666	1.38724	1.0039	1.10606
0.066667	1.944	1.54312	1.00459	1.18991
0.033333	2.19157	1.77003	1.00532	1.30871
9.71E-17	2.51132	2.26116	1.00609	1.56494

Table C-30 data for Fig. 50

	TD=0.10E-04 HW	TD=0.75E+04 HW	TD=0.10E-04 U-shape	TD=0.75E+04 U-shape
0	0.37711	0.69921	0.50302	0.88859
33.33333	0.38288	0.68976	0.51689	0.84755
66.66667	0.38882	0.68514	0.53156	0.82677
100	0.39496	0.68218	0.54711	0.81255
133.3333	0.40131	0.68027	0.5636	0.80236
166.6667	0.40787	0.67913	0.58114	0.79522
200	0.41466	0.67864	0.59982	0.7906
233.3333	0.42169	0.67872	0.61976	0.78821
266.6667	0.42897	0.6793	0.64108	0.78788
300	0.4365	0.68033	0.66395	0.78952
333.3333	0.44433	0.68182	0.68852	0.79307
366.6667	0.45244	0.68371	0.715	0.79857
400	0.46086	0.68599	0.74362	0.80608
433.3333	0.46962	0.68869	0.77464	0.81572
466.6667	0.47873	0.69176	0.80839	0.82764
500	0.4882	0.69521	0.84523	0.84207
533.3333	0.49807	0.69907	0.88562	0.85929
566.6667	0.50836	0.70331	0.93008	0.8797
600	0.51908	0.70795	0.97927	0.90377
633.3333	0.53029	0.71301	1.03398	0.93215
666.6667	0.542	0.71849	1.09519	0.96566
700	0.55425	0.7244	1.16413	1.00541
733.3333	0.56709	0.73078	1.24237	1.05289

766.6667	0.58055	0.73764	1.33191	1.11018
800	0.59466	0.74499	1.43538	1.18025
833.3333	0.6095	0.75289	1.55633	1.26751
866.6667	0.62512	0.76134	1.69956	1.37896
900	0.64156	0.77038	1.87185	1.52701
933.3333	0.65892	0.78007	2.08304	1.7397
966.6667	0.67726	0.79044	2.34796	2.18513
1000	0.69665	0.80152	2.34796	2.18513
1033.333	0.71722	0.81341	2.08304	1.7397
1066.667	0.73906	0.82615	1.87185	1.52701
1100	0.76226	0.83979	1.69956	1.37896
1133.333	0.78702	0.85447	1.55633	1.26751
1166.667	0.81345	0.87024	1.43538	1.18025
1200	0.84172	0.88719	1.33191	1.11018
1233.333	0.87208	0.90551	1.24237	1.05289
1266.667	0.90473	0.92529	1.16413	1.00541
1300	0.93991	0.94668	1.09519	0.96566
1333.333	0.978	0.96994	1.03398	0.93215
1366.667	1.01933	0.99524	0.97927	0.90377
1400	1.06429	1.02284	0.93008	0.8797
1433.333	1.1135	1.05312	0.88562	0.85929
1466.667	1.16748	1.08639	0.84523	0.84207
1500	1.22695	1.1231	0.80839	0.82764
1533.333	1.29291	1.16388	0.77464	0.81572
1566.667	1.36638	1.20935	0.74362	0.80608
1600	1.44868	1.26034	0.715	0.79857
1633.333	1.54167	1.31803	0.68852	0.79307
1666.667	1.64742	1.38372	0.66395	0.78952
1700	1.76871	1.45917	0.64108	0.78788
1733.333	1.90949	1.54695	0.61976	0.78821
1766.667	2.07459	1.6502	0.59982	0.7906
1800	2.27086	1.77353	0.58114	0.79522
1833.333	2.5085	1.92391	0.5636	0.80236
1866.667	2.8016	2.11169	0.54711	0.81255
1900	3.17205	2.35485	0.53156	0.82677
1933.333	3.65606	2.69259	0.51689	0.84755
1966.667	4.31411	3.30865	0.50302	0.88859

Table C-31
data for
Fig. 51

0	11855	11843.69	3.333333
55	8900	8907.53	0.601504
165	6130	6141.019	0.780952
357	4750	4756.524	0.544974
420	4750	4756.524	0.5
609	3170	3186.59	0.453125
640	3170	3186.59	0.8
745	1944	1950.08	1.5
787	1944	1950.08	2.05
920	750	800	3
921	550		
935	0		

Table C-32
data for
Fig. 53

X-Values	PI=1000 STBD/psi	PI=2000 STBD/psi
200	1965.68	1968.675
400	1970.596	1974.849
600	1974.522	1979.297
800	1977.682	1982.536
1000	1980.238	1984.904
1200	1982.313	1986.628
1400	1984.001	1987.868
1600	1985.371	1988.737
1800	1986.482	1989.32
2000	1987.376	1989.685
2200	1988.089	1989.888
2400	1988.65	1989.978
2600	1989.083	1990
2800	1989.408	
3000	1989.644	
3200	1989.807	
3400	1989.91	
3600	1989.968	
3800	1989.994	
4000	1990	

Table C-33
data for
Fig. 52

X-Values	PI=2000 STBD/psi, PDD=10.032 psi	PI=1000 STBD/psi, PDD=10.022 psi
0	8.719	6.209193
200	6.174125	4.915141
400	4.447912	3.926565
600	3.238885	3.159657
800	2.367795	2.556256
1000	1.724532	2.075287
1200	1.239726	1.687297
1400	0.868937	1.370878
1800	0.365211	0.893895
2000	0.2027	0.712962
2200	0.089488	0.560987
2400	0	0.433099
2600		0.325679
2800		0.23607
3000		0.162368
3200		0.103251

Table C-34
data for
Fig. 54

X-Values	PI=2000 STBD/psi, PDD=10.032 psi	PI=1000 STBD/psi, PDD=10.022 psi
0	8.719	6.209193
200	6.174125	4.915141
400	4.447912	3.926565
600	3.238885	3.159657
800	2.367795	2.556256
1000	1.724532	2.075287
1200	1.239726	1.687297
1400	0.868937	1.370878

3400		0.057856
3600		0
3800		
4000		

1600	0.583525	1.110299
1800	0.365211	0.893895
2000	0.2027	0.712962
2200	0.089488	0.560987
2400	0	0.433099
2600		0.325679
2800		0.23607
3000		0.162368
3200		0.103251
3400		0.057856
3600		0
3800		
4000		

Table C-35
data for
Fig. 55

X-Values	flow profile	Pressure profile
200	16320.4	1968.205
400	13696.85	1973.765
600	11464.91	1977.681
800	9507.345	1980.424
1000	7738.463	1982.311
1200	6094.584	1983.561
1400	4528.239	1984.337
1600	3004.697	1984.765
1800	1500	1984.953
2000	500	1986
2200	1500	1984.953
2400	3004.697	1984.765
2600	4528.239	1984.337
2800	6094.584	1983.561
3000	7738.463	1982.311
3200	9507.345	1980.424
3400	11464.91	1977.681
3600	13696.85	1973.765
3800	16320.4	1968.205
4000	19499.94	1960.267

Table C-36
data for
Fig. 56

X-Values	PI=1000 STBD/psi, PDD=15.05 psi
0	7.937354
200	5.559947
400	3.91607
600	2.743786
800	1.886808
1000	1.250025
1200	0.775349
1400	0.428024
1600	0.188456
1800	0
2000	0
2200	0
2400	0.188456
2600	0.428024
2800	0.775349
3000	1.250025
3200	1.886808
3400	2.743786
3600	3.91607
3800	5.559947

NOMENCLATURE

A = sensitivity matrix
a = constant, or drainage dimension along x-direction, ft [m]
B = formation volume factor, rb/stb, [res m3/st m3]
b = constant, or drainage dimension along y-direction, ft [m]
CD = dimensionless wellbore storage coefficient
Cs = wellbore storage coefficient, bbl/psi
c = constant, or drainage dimension along z-direction, ft [m]
ct = total compressibility, 1/psi
c1~c4 = constants
E = residual (error) vector
Fw = additional pressure loss due to friction in the wellbore
f = Fanning friction factor, or function, or frequency, 1/sec
G = Green's function
I = unit matrix
J = objective function, or productivity index, stb/day/psi
k = permeability, md [m2]
ka = geometric average permeability in the plane normal to wellbore direction, md[m2]
LwD = dimensionless wellbore length
Lw = effective wellbore length, ft [m]
M= total number of nodes on wellbore
N = total number of nodes on outer boundaries, or sample number
NRe, = Reynolds number
P = pressure, psi, [pa]
pav = average reservoir pressure, psi [pa]
PD = dimensionless pressure
Pe = pressure at boundary, psi [pa]
Pi = initial reservoir pressure, psi [pa]
Pw = measured pressure response, psi [pa]
Pwf,h = flowing pressure at the heel, psi [pa]
$P_{wf,r}$ = pressure response without considering pressure loss in wellbore, psi [pa]
p δ □= constant-rate pressure response, psi [pa]
q = surface rate, stb/day [m3/s, or ft3/hr]
q_D = dimensionless after flow rate
q_h = flux (flow rate per unit length of wellbore), stb/day/ft [m3/s/m]
q_{hD} = dimensionless flux
q_r = reference flow rate, stb/day [m3/s, or ft3/hr]
q_{sf} = sandface flow rate, stb/day [m3/s, or ft3/hr]
q_t = total flow rate from well, stb/day [m3/s, or ft3/hr]
q_v = flow rate per unit volume, stb/day/ft3 [m3/s/m3]
R = a point in 3D space located at R(x, y, z)

r = radius, ft [m], or derivative of dimensionless sandface flow rate, 1/hr [1/s]
r_{eD} = dimensionless drainage radius, ft [m]
r_w = wellbore radius, ft [m]
r_{wD} = dimensionless wellbore radius
s = Laplace domain variable, or skin factor
sf = skin factor
t = time, hr [s]
t_D = dimensionless time
u = temperature, oC
V = reservoir volume, ft3 [m3]
X = frequency-domain function
x = time-domain function, or coordinate in x-direction
xe = length of drainage volume, ft [m]
x' = x-coordinate of well axis
y = coordinate in y-direction, or observed set of data
y' = y-coordinate of well axis
z = coordinate in z-direction
z' = z-coordinate of well axis
α = diffusivity, m2/s
β = estimated parameter vector
δ = Diract delta function
Δ = difference
ε = infinitesimal, absolute roughness
η = diffusivity, ft2/hr [m2/s]
φ = porosity, or basis function
λ = transmissivity ratio
μ = viscosity, cp [pa-s]
θ, θ' = polar angle
ρ = fluid density, lbm/ft3 [kg/m3], correlation coefficient
σ = standard deviation
ω = storativity ratio
Ω = 3D domain
Ω_1 = source domain
ψ = basis function
ξ = basis function
ζ = basis function
∇ = gradient
∇^2 = Laplace operator

Subscripts
cal = calculated

d = discrete
e = element
f = frequency domain
integ = numerical integral
m = measured
x = x-direction
y = y-direction
z = z-direction

Superscripts

-1 = inverse Fourier transform
T = transpose

REFERENCES

1. Colebrook, C.F. and White, C.M., “Experiments with Fluid friction roughened pipes.”, Proceedings of the Royal Society of London. Series A, Mathematical and Physical Sciences 161 (906): 367–381.

2. Gringarten, A. C. and Ramey, H. J., Jr.:"The Use of Source and Green's Functions in Solving Unsteady-Flow Problems in Reservoirs", SPEJ, October 1973, 285-296

3. Cinco, H., Miller, F.G., and Ramey, H.J. Jr.: "Unsteady-State Pressure Distribution Created by a Directionally Drilled Well," JPT (Nov. 1975) 1392.

4. Jain, A.K.: “Accurate Explicit Equation for Friction Factor,” Journal of Hydraulics Div. ASCE, pp.674, 1976. 19.

5. Goode and Thambynayagam.:” Pressure Drawdown and Buildup Analysis of Horizontal Wells in Anisotropic Media,” paper SPE 14250 presented at the 1985 SPE Annual Technical Conference and Exhibition held in Las Vegas, Sept. 22-25.

6. M.D. Clonts and H.J. Ramey Jr.:” Pressure Transient Analysis for Wells with Horizontal Drainholes,” paper SPE 15116 presented at the 56th California Regional Meeting of the Society of Petroleum Engineers held in Oakland, CA, April 2-4, 1986.

7. Ozkan, E., Raghavan, R., and Joshi, S.D.,:” Horizontal Well Pressure Analysis” SPE 16378, Presented at the SPE California Regional Meeting, Ventura California, April 8-10, 1987.

8. Renard, G.I. and Duppy, J.M.: “Influence of Formation Damage on the Flow Efficiency of Horizontal Wells,” SPE paper 19414, Presented at the Formation Damage Control Symposium, Lafayette, Louisiana. February 22-23, 1990.

9. Dikken, B.J.: “Pressure Drop in Horizontal Wells and Its Effects on Production Performance,” JPT pp.1426-1433, November 1990.

10. Folefac, A.N., Archer, J.S., Issa, R.I., and Arshad, A.M.: “Effects of Pressure Drop Along Horizontal Wellbores on Well Performance,” SPE Paper 23094, Presented at the Offshore Europe Conference, Abordeen, September 3-6, 1991.

11. Ozkan, E., Sarica, C., Haciislamoglu, M., and Raghavan, R.: ‘‘The Influence of Pressure Drop Along the Wellbore on Horizontal Well Productivity,’’ paper SPE 25502 available from SPE, Richardson, Texas 1993.
12. M.M. Kamal, I.M. Buhidma, SA Smith and W.R. Jones.:” Pressure-Transient Analysis for a Well With Multiple Horizontal Sections,” paper SPE 26444 presented at the 68th Annual Technical

Conference and Exhibition of the Society of Petroleum Engineers held in Houston, Texas, 3-6 October 1993.

13. Su, Z. and Gudmundsson, J.S.: "Friction Factor of Perforation Roughness in Pipes," paper SPE 26521 presented at the 1993 SPE Annual Technical Conference and Exhibition, Houston, 3–6 October.
14. Turban Yildiz and Erdal Ozkan.:" Transient Pressure Behavior of Selectively Completed Horizontal Wells," paper SPE 28388 presented at the 69th SPE Annual Technical Conference and Exhibition held in New Orleans, LA, U.S.A.,25-28 September 1994.
15. Novy, R.A.: "Pressure Drops in Horizontal Wells: When Can They Be Ignored?" SPE Reservoir
16. Engineering, pp. 29-35, February 1995.
17. Ozkan, E., Sarica, C., Haciislamoglu, M. and Raghavan, R.: "Effect of Conductivity on Horizontal Well Pressure Behavior," SPE Advanced Technology Series, Vol. 3, No. 1, pp 85-94, 1995.
18. Ozkan, E., Sarica, C., Haciislamoglu, M. and Raghavan, R.: "Supplement to SPE 24683: Effect of Conductivity on Horizontal Well Pressure Behavior," paper SPE 30230, 1995.
19. Ouyang, L-B., Arbabi, S., and Aziz, K.: ''General Wellbore Flow Model for Horizontal, Vertical, and Slanted Well Completions,'' paper SPE 36608 presented at the 1996 SPE Annual Technical Conference and Exhibition, Denver, 6–9 October.
20. X.Y. Kong, X. Z. Xu and D.T. Lu.:" Pressure Transient Analysis for Horizontal Well and Multi-Branched Horizontal Wells," paper SPE 37069 presented at the 1996 SPE International Conference on Horizontal Well Technology held in Calgary Canada, 18-20 November 1996.
21. Kuchuk, F.J. and Tarek Habashy: "Pressure Behavior of Laterally Composite Reservoirs," SPEFE, March 1997.
22. Erdal Ozkan and R. Raghavan.:"Estimation of Formation Damage in Horizontal Wells," paper SPE 37511 presented at the 1997 SPE Production Operations Symposium held in Oklahoma city, Oklahoma, 9-11 March 1997.
23. Penmatcha, V.R., Arbabi, S., and Aziz, K.: "Effects of Pressure Drop in Horizontal Wells and Optimum Well Length," SPE Paper 37494, presented at 1997 SPE Production Operations Symposium, Oklahoma City, Oklahoma, March 9-11.
24. Al Qahtani, Abdullah and Habib, Menour: "New Correlations for Optimizing Horizontal Wells Completions," Paper SPE 37768, presented at the 1997 Middle East Oil Show in Bahrain, March 15-18, 1997.
25. Turban Yildiz and Erdal Ozkan.:" Transient Pressure Behavior of Dual-Lateral Wells," paper SPE 38670 presented at the 1997 SPE Annual Technical Conference and Exhibition held in San Antonio, TX, 5-8 October.
26. Koichi Suzuki,:" Influence of Wellbore Hydraulics on Horizontal Well Pressure Transient Behavior," SPE Formation Evaluation, Vol. 12, No. 3, pp 175-181, 1997.

27. Ouyang, L.-B. and Aziz, K.: "A Simplified Approach to Couple Wellbore Flow and Reservoir Inflow for Arbitrary Well Configuration," paper SPE 48936 presented at the SPE Annual Technical Conference and Exhibition, New Orleans, Sept. 27-30, 1998.
28. Alkhonifer J., and Ershaghi, I.: 'Detection of Channel Sands and Vertical Shale Continuity Using a new Approach in Interference Analysis of Parallel Horizontal Wells,' SPE 53928 presented at the SPE Latin American and Caribbean Petroleum Engineering Conference held in Caracas, Venezuela, April 1999
29. Y. Ding. :"Transient Pressure Solution in the Presence of Pressure Drop in the Wellbore," paper SPE 56614 presented at the 1999 SPE Annual Technical Conference and Exhibition held in Houston, Texas, 3-6 October 1999.
30. Erdal Ozkan, Turhan Yildiz and Rajagopal Raghavan.:"Pressure-Transient Analysis of Perforated Slant and Horizontal Wells," paper SPE 56421 presented at the 1999 SPE Annual Technical Conference and Exhibition held in Houston, Texas, 3–6 October 1999.
31. Al Qahtani, Abdullah M.: "Evaluation of Horizontal Wells Performance Using Coiled Tubing Logging," Paper SPE 57539, presented at the 1999 SPE/IADC Middle East Drilling Technology Conference held in Abu Dhabi, UAE, 8-10 November 1999.
32. Turhan Yildiz. :"Multilateral Pressure-Transient Response 2000," paper SPE 65479 at the 2000 SPE/Petroleum Society of CIM International Conference on Horizontal Well Technology held in Calgary, Alberta, Canada, 6-8 November 2000.
33. Cho, H. and Shah, S.N.: "Prediction of Specific Productivity Index of Long Horizontal Wells", SPE Paper 67237 presented at the SPE Production and Operation Symposium held in Oklahoma City, Oklahoma 24-27 March 2001.
34. K. Furui, D. Zhu, A.D. Hill, :"A Rigorous Formation Damage Skin Factor and Reservoir Inflow Model for a Horizontal Well," paper SPE 74698 presented at the International Symposium and Exhibition on Formation Damage Control, 20-21 February 2002, Lafayette, Louisiana
35. Belhouchet Toufik, Djebbar Tiab,and Sarfraz Jokhio,:" Effect of Non-Uniform Skin on Finite Conductivity Horizontal Well," SPE 80926 presented at the SPE Production and Operations Symposium, 22 - 25 March 2003, Oklahoma City, Oklahoma
36. N. Mohannadi, E. ozkan, H. Kazemi,:" Pressure-Transient Responses of Horizontal and Curved Wells in Anticlines and Domes," paper SPE 84378 presented at the SPE Annual Technical Conference and Exhibition, 5-8 October 2003, Denver, Colorado
37. Abdeihafid Fahem, Djebbar Tiab, Sarfraz Jokhio and Jalal Owayed.:"Transient Pressure Behaviors of Dual Lateral Wells," paper SPE 83971 presented at Offshore Europe 2003 held in Aberdeen, UK, 2-5 September 2003.
38. Al-Khamis, M., Ozkan, E., and Raghavan, R.: "Analysis of Interference Tests with Horizontal Wells" paper SPE 84292 presented at the SPE Annual Technical Conference and Exhibition held in Denver, Colorado, Oct 2003.
39. Yula Tang, SPE, Turhan Yildiz, and Erdal Ozkan, :"Effects of Formation Damage and High-Velocity Flow on the Productivity of Perforated Horizontal Wells," SPE Reservoir Evaluation & Engineering , Vol. 8, No. 4, pp 315-324, 2005.
40. A.M. Al-Otaibi, and Erdal Ozkan,:" Interpretation of Skin Effect from Pressure Transient Tests in Horizontal Wells," paper SPE 93296 presented at the SPE Middle East Oil and Gas Show and Conference, Mar 12 - 15, 2005 2005, Kingdom of Bahrain
41. F. Medeiros, Jr., E. Ozkan and H. Kazemi.:"A Semi analytical, Pressure-Transient Model for

Horizontal and Multilateral Wells in Composite, Layered, and Compartmentalized Reservoirs," paper SPE 102834 presented at the 2006 SPE Annual Technical Conference and Exhibition held in San Antonio, Texas, U.S.A., 24–27 September 2006.
42. Dimitris Krinis, Naseem Dawood and Adeyinka Soremi:" Horizontal Well Performance Optimization using Linearized Inflow Control Device ," paper SPE 117213 presented at the Abu Dhabi International Petroleum Exhibition and Conference, 3-6 November,2008 Abu Dhabi, UAE
43. R.R. Ibatullin, N.G. Ibragimov, R.S. Khisamov, A.T. Zaripov, and M.I. Amerkhanov.:" A Novel Technology of Formation Stimulation involves Bi-wellhead Horizontal Wells," paper SPE 120413 presented in the 2009 SPE Middle East Oil and Gas Show and Conference, Bahrain, 15–18 March 2009.
44. M. Brown,and E. Ozkan, R. Raghavan, and H. Kazemi.: "Practical Solutions for Pressure Transient Responses of Fractured Horizontal Wells in Unconventional Reservoirs," paper SPE 125043 presented at the SPE Annual Technical Conference and Exhibition held in New Orleans, Louisiana, USA, 4–7 October 2009.
45. B.D. Poe Jr. and A. Erkal.:"Transient Behavior of Horizontal Wells with Inflow Control Devices for Inflow Profile Modification," paper SPE 132219 presented at the International Oil and Gas Conference and Exhibition in China, 8-10 June 2010, Beijing, China.
46. P. Q. Lian1, L. S. Cheng and J. Y. Cui: "A new computation model of fractured horizontal well coupling with reservoir," Int. J. of Numerical Methods. Fluids September 2010; 67:1047–1056.
47. Zhijun, S., Yongzhe, Z., Hongjun, Q. and Jianlin, L.: "Research and Application of Drilling Technology of Extended-reach Horizontally-intersected well Used to Extract Coalbed Methane," Earth and Planetary Science, 2011.
48. Zhonglan Tian, Ruichen Shen, Lei Qiao,:" One New Needle Technology of Remote Intersection between Two Wells and Application in Chinese Coalbed Methane Basin," paper SPE 155892 presented at IADC/SPE Asia Pacific Drilling Technology Conference and Exhibition, 9-11 July, 2012 Tianjin, China.

Curriculum Vitae

Personal Data

Name **Abdullah Mubarak Al Qahtani**
Nationality Saudi Arab
Marital Status Married
Current Address Box 671 Dhahran 31311 Saudi Arabia.
Tel.: +966 50 880 9000
E-mail: abdullah.qahtani@gmail.com

Academic and Professional Background

1988-2010 Worked in various departments in Saudi Aramco with major experience in production engineering, artificial lifting, pressure transient testing, and well design and modeling.
1997 Earned an MS degree in Petroleum Engineering from King Fahd University of Petroleum and Minerals.
1988 graduated with B.S. degree in Petroleum Engineering from King Fahd University of Petroleum and Minerals.

Publications

1. SPE 37112 Effect of Length and Distribution of Perforated Intervals on Horizontal Wells Rates
2. SPE 37768 New Correlations for Optimizing Horizontal Wells Completions
3. SPE 64718 Field Application of The X-Plot Technique Helps Predict Water Cut.
4. SPE 57539 Evaluation Of Horizontal Wells Performance Using Coiled Tubing Logging
5. SPE 68141 A New Technique and Field Application for Determining Reservoir Characteristics from Well Performance Data
6. SPE 81490 The E_c-Factor: A New Correlation For Optimizing Completion Efficiency
7. SPE 81520 A New Approach for Estimating Well Productivity and Reservoir Pressure Using Surface Performance Data.
8. SPE 80520 A New Method for Evaluating Stimulation Treatments in Carbonate Reservoirs in Saudi Arabia.
9. SPE 136935 Flow Simulation in Inflow Control Valves Using Lattice Boltzmann Modeling.
10. SPE 136942 Field Application of Composite Reservoir Model on Non-Unit Mobility Flow
11. SPE 136931 A Comparative Study Between Empirical Correlations and Mechanistic Models of Vertical Multiphase Flow
12. SPE 164443 From Empirical To Micro-scale Modeling Of Multiphase Flow; Bridging The Gap Of R&D
13. SPE 164377 Artificial Lifting of High Productivity Wells: A Production Optimization Scheme

Local Publications
Sand Production Control: Theory and Practice.

Teaching Experience
Conducted in-house courses for petroleum and non-petroleum engineers in the company.

Recognitions:
Was recognized twice for creative contribution and innovation on business line level.

Areas of Expertise

Well flow analysis, Nodal analysis and flow in pipes, artificial lifting, PVT modeling, fluid flow in porous media, well productivity improvement, etc

Research Experience

Horizontal well completion and productivity optimization, perforation design optimization, artificial lift design and optimization and multiphase modeling.

Computer Skills

Numerical analysis
Nonlinear regression analysis

Programming Proficiency

VB/VBA
Shell scripting
Fortran77

Language Proficiency

Fluent in spoken and written English.

Professional Affiliations

Society of Petroleum Engineers